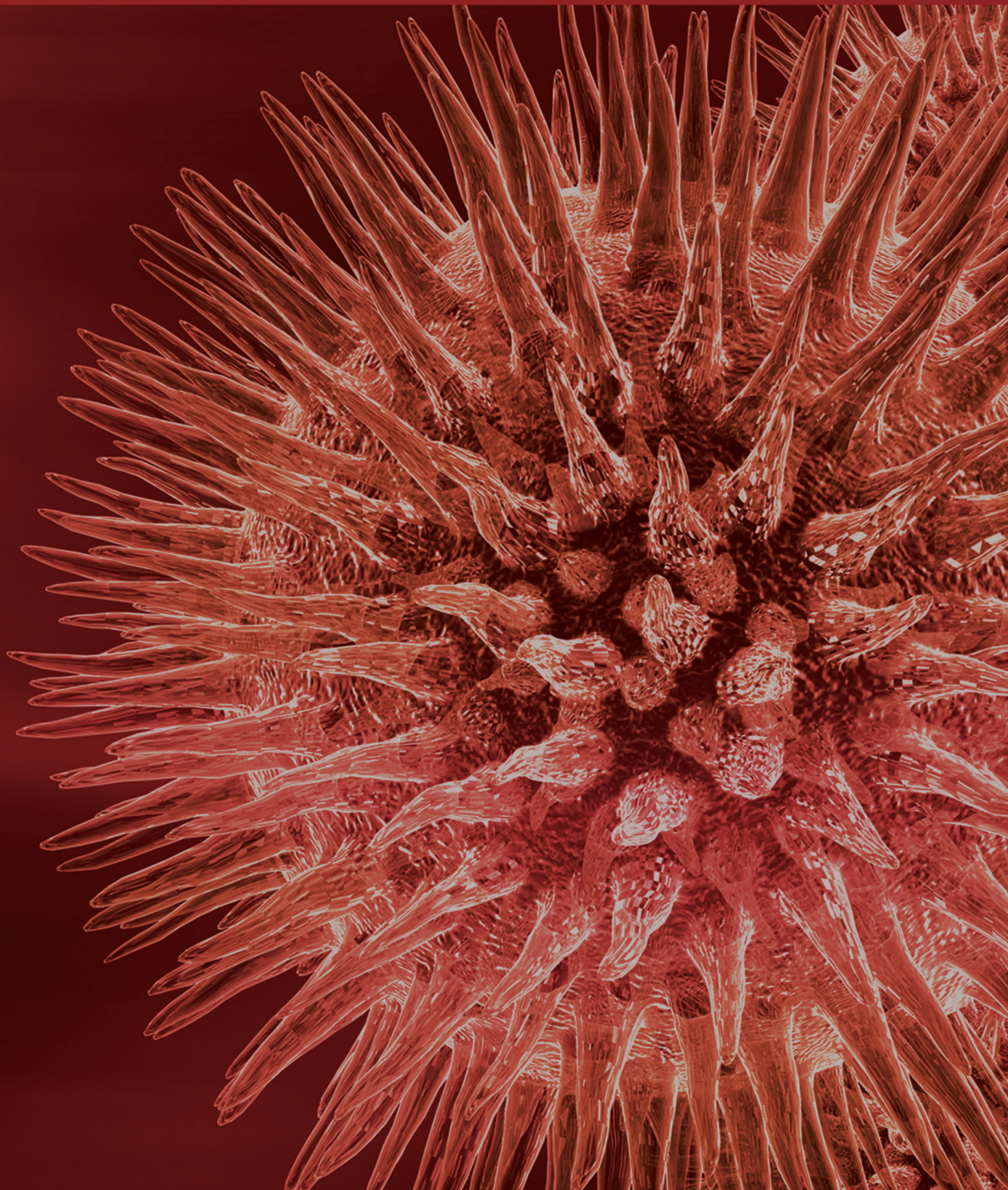


# PLP-Dependent Enzymes

Guest Editors: Alessandro Paiardini, Barbara Cellini,  
Ashley M. Buckle, and Roberto Contestabile





---

## **PLP-Dependent Enzymes**

## **PLP-Dependent Enzymes**

Guest Editors: Alessandro Paiardini, Roberto Contestabile,  
Ashley M. Buckle, and Barbara Cellini



---

Copyright © 2014 Hindawi Publishing Corporation. All rights reserved.

This is a special issue published in “BioMed Research International.” All articles are open access articles distributed under the Creative Commons Attribution License, which permits unrestricted use, distribution, and reproduction in any medium, provided the original work is properly cited.



## Contents

**PLP-Dependent Enzymes**, Alessandro Paiardini, Roberto Contestabile, Ashley M. Buckle, and Barbara Cellini  
Volume 2014, Article ID 856076, 2 pages

**Vitamin B6-Dependent Enzymes in the Human Malaria Parasite *Plasmodium falciparum*: A Druggable Target?**, Thales Kronenberger, Jasmin Lindner, Kamila A. Meissner, Flávia M. Zimbres, Monika A. Coronado, Frank M. Sauer, Isolmar Schettert, and Carsten Wrenger  
Volume 2014, Article ID 108516, 11 pages

**The Pyridoxal 5'-Phosphate (PLP)-Dependent Enzyme Serine Palmitoyltransferase (SPT): Effects of the Small Subunits and Insights from Bacterial Mimics of Human hLCB2a HSN1 Mutations**, Ashley E. Beattie, Sita D. Gupta, Lenka Frankova, Agne Kazlauskaitė, Jeffrey M. Harmon, Teresa M. Dunn, and Dominic J. Campopiano  
Volume 2013, Article ID 194371, 13 pages

**Characterization of C-S Lyase from *C. diphtheriae*: A Possible Target for New Antimicrobial Drugs**, Alessandra Astegno, Alejandro Giorgetti, Alessandra Allegrini, Barbara Cellini, and Paola Dominici  
Volume 2013, Article ID 701536, 13 pages

**Asymmetry of the Active Site Loop Conformation between Subunits of Glutamate-1-semialdehyde Aminomutase in Solution**, Barbara Campanini, Stefano Bettati, Martino Luigi di Salvo, Andrea Mozzarelli, and Roberto Contestabile  
Volume 2013, Article ID 353270, 10 pages

**Protein Homeostasis Defects of Alanine-Glyoxylate Aminotransferase: New Therapeutic Strategies in Primary Hyperoxaluria Type I**, Angel L. Pey, Armando Albert, and Eduardo Salido  
Volume 2013, Article ID 687658, 15 pages

**Structure-Based Mechanism for Early PLP-Mediated Steps of Rabbit Cytosolic Serine Hydroxymethyltransferase Reaction**, Martino L. Di Salvo, J. Neel Scarsdale, Galina Kazanina, Roberto Contestabile, Verne Schirch, and H. Tonie Wright  
Volume 2013, Article ID 458571, 13 pages

**Extremophilic SHMTs: From Structure to Biotechnology**, Sebastiana Angelaccio  
Volume 2013, Article ID 851428, 10 pages

**Interaction of Human Dopa Decarboxylase with L-Dopa: Spectroscopic and Kinetic Studies as a Function of pH**, Riccardo Montioli, Barbara Cellini, Mirco Dindo, Elisa Oppici, and Carla Borri Voltattorni  
Volume 2013, Article ID 161456, 10 pages

## Editorial

# PLP-Dependent Enzymes

**Alessandro Paiardini,<sup>1</sup> Roberto Contestabile,<sup>1</sup> Ashley M. Buckle,<sup>2</sup> and Barbara Cellini<sup>3</sup>**

<sup>1</sup> *Dipartimento di Scienze Biochimiche, Sapienza Università di Roma, 00185 Roma, Italy*

<sup>2</sup> *Department of Biochemistry and Molecular Biology, Monash University, Clayton, VIC 3800, Australia*

<sup>3</sup> *Section of Biological Chemistry, Department of Life Sciences and Reproduction, University of Verona, Strada Le Grazie 8, 37134 Verona, Italy*

Correspondence should be addressed to Alessandro Paiardini; [alessandro.paiardini@uniroma1.it](mailto:alessandro.paiardini@uniroma1.it)

Received 10 December 2013; Accepted 10 December 2013; Published 15 January 2014

Copyright © 2014 Alessandro Paiardini et al. This is an open access article distributed under the Creative Commons Attribution License, which permits unrestricted use, distribution, and reproduction in any medium, provided the original work is properly cited.

The main focus of this special issue is on structural, functional, and biomedical studies on pyridoxal-5'-phosphate (PLP-) dependent enzymes. The unparalleled catalytic versatility of PLP, the active form of vitamin B6, originates from its unique electron-sinking properties, which stabilize reaction intermediates, thus lowering the activation barrier during catalysis. At least five different protein scaffolds arose during evolution to bind PLP and harness its catalytic functionality. The role of the apoenzyme scaffolds is to assist in the proper orientation of the substrate's reacting groups relative to the  $\pi$ -electrons of PLP, to promote reactivity and control reaction specificity. In addition, the active site residues interacting with the leaving groups provide either stabilizing or destabilizing interactions to direct catalysis [1].

As a consequence, PLP-dependent enzymes are unrivaled in the variety of reactions they catalyze and the highly diverse metabolic pathways they are involved in, including the conversion of amino acids, one-carbon units, biogenic amines, tetrapyrrolic compounds, and amino sugars. These biocatalysts play also a key role in sulfur assimilation and incorporation in cysteine, biotin, and S-adenosyl methionine.

The consequence of their widespread occurrence and crucial importance is that a number of them are current drug targets. For example, inhibitors of  $\gamma$ -aminobutyric acid aminotransferase are used in the treatment of epilepsy [2], serine hydroxymethyltransferase has been identified as a target for cancer therapy [3], and inhibitors of L-DOPA decarboxylase are used in the treatment of Parkinson's disease [4]. Genetic defects affecting PLP enzymes have been also implicated in

a number of diseases, including Primary hyperoxaluria type 1, which is caused by mutations in alanine-glyoxylate aminotransferase [5, 6]. Finally, several PLP enzymes are autoantigens in autoimmune disease, for example, glutamate decarboxylase in type I diabetes [7] and SLA/LP in autoimmune hepatitis [8].

This special issue is therefore devoted to the unique and intriguing features of this group of enzymes. Detailed biochemical characterizations of several members of this clan, for example, C-S lyase, glutamate-1-semialdehyde aminomutase, serine hydroxymethyltransferase, and L-DOPA decarboxylase, are described. An original paper, describing the impact of pathogenic mutations of the enzyme serine palmitoyltransferase on its structure and activity, is also provided. Moreover, a review focusing on the role of alanine-glyoxylate aminotransferase homeostasis in the basic mechanisms of primary hyperoxaluria is included. Recent developments and ideas in the field of PLP-dependent enzymes, with a special emphasis given to applied aspects of this research area, have been summarized. The new insights coming from these studies will be hopefully translated into clinically useful agents for innovative therapies to counteract diseases involving PLP enzymes.

*Alessandro Paiardini  
Roberto Contestabile  
Ashley M. Buckle  
Barbara Cellini*

## References

- [1] A. C. Eliot and J. F. Kirsch, "Pyridoxal phosphate enzymes: mechanistic, structural, and evolutionary considerations," *Annual Review of Biochemistry*, vol. 73, pp. 383–415, 2004.
- [2] A. Sarup, O. M. Larsson, and A. Schousboe, "GABA transporters and GABA-transaminase as drug targets," *Current Drug Targets: CNS & Neurological Disorders*, vol. 2, no. 4, pp. 269–277, 2003.
- [3] F. Daidone, R. Florio, S. Rinaldo et al., "In silico and in vitro validation of serine hydroxymethyltransferase as a chemotherapeutic target of the antifolate drug pemetrexed," *European Journal of Medicinal Chemistry*, vol. 46, no. 5, pp. 1616–1621, 2011.
- [4] F. Daidone, R. Montioli, A. Paiardini et al., "Identification by virtual screening and in vitro testing of human DOPA decarboxylase inhibitors," *PLoS ONE*, vol. 7, no. 2, Article ID e31610, 2012.
- [5] E. Oppici, K. Fodor, A. Paiardini et al., "Crystal structure of the S187F variant of human liver alanine:aminotransferase associated with primary hyperoxaluria type I and its functional implications," *Proteins*, vol. 81, no. 8, pp. 1457–1465, 2013.
- [6] E. Oppici, A. Roncador, R. Montioli, S. Bianconi, and B. Cellini, "Gly161 mutations associated with primary hyperoxaluria type I induce the cytosolic aggregation and the intracellular degradation of the apo-form of alanine:glyoxylate aminotransferase," *Biochimica et Biophysica Acta*, vol. 1832, no. 12, pp. 2277–2288, 2013.
- [7] G. Fenalti and A. M. Buckle, "Structural biology of the GAD autoantigen," *Autoimmunity Reviews*, vol. 9, no. 3, pp. 148–152, 2010.
- [8] A. Paiardini and S. Pascarella, "Structural mimicry between SLA/LP and Rickettsia surface antigens as a driver of autoimmune hepatitis: insights from an in silico study," *Theoretical Biology and Medical Modelling*, vol. 10, article 25, 2013.

## Review Article

# Vitamin B6-Dependent Enzymes in the Human Malaria Parasite *Plasmodium falciparum*: A Druggable Target?

Thales Kronenberger,<sup>1</sup> Jasmin Lindner,<sup>1</sup> Kamila A. Meissner,<sup>1</sup> Flávia M. Zimbres,<sup>1</sup>  
Monika A. Coronado,<sup>2</sup> Frank M. Sauer,<sup>1</sup> Isolmar Schettert,<sup>3</sup> and Carsten Wrenger<sup>1</sup>

<sup>1</sup> Unit for Drug Discovery, Department of Parasitology, Institute of Biomedical Science, University of São Paulo, Avenida Professor Lineu Prestes 1374, 05508-000 São Paulo, SP, Brazil

<sup>2</sup> Multi User Center for Biomolecular Innovation, Department of Physics, São Paulo State University, UNESP/IBILCE, C. Postal 136, 15054-000 São José do Rio Preto, SP, Brazil

<sup>3</sup> Laboratory of Genetics and Molecular Cardiology, Heart Institute (InCor), Avenida Doctor Eneas de Carvalho Aguiar 44, 05403-000 São Paulo, SP, Brazil

Correspondence should be addressed to Carsten Wrenger; [cwrenger@icb.usp.br](mailto:cwrenger@icb.usp.br)

Received 17 May 2013; Revised 24 October 2013; Accepted 28 November 2013; Published 9 January 2014

Academic Editor: Ashley M. Buckle

Copyright © 2014 Thales Kronenberger et al. This is an open access article distributed under the Creative Commons Attribution License, which permits unrestricted use, distribution, and reproduction in any medium, provided the original work is properly cited.

Malaria is a deadly infectious disease which affects millions of people each year in tropical regions. There is no effective vaccine available and the treatment is based on drugs which are currently facing an emergence of drug resistance and in this sense the search for new drug targets is indispensable. It is well established that vitamin biosynthetic pathways, such as the vitamin B6 *de novo* synthesis present in *Plasmodium*, are excellent drug targets. The active form of vitamin B6, pyridoxal 5-phosphate, is, besides its antioxidative properties, a cofactor for a variety of essential enzymes present in the malaria parasite which includes the ornithine decarboxylase (ODC, synthesis of polyamines), the aspartate aminotransferase (AspAT, involved in the protein biosynthesis), and the serine hydroxymethyltransferase (SHMT, a key enzyme within the folate metabolism).

## 1. Introduction

Malaria is a devastating infectious disease, which causes serious problems in tropical and subtropical areas. According to the World Health Organization (WHO), the population of more than 100 countries is exposed to malaria parasites [1]. The causative agent of malaria is belonging to the genus *Plasmodium*, which can affect almost all vertebrates; however, only five species have been reported to be infective for humans, *P. falciparum*, *P. vivax*, *P. ovale*, *P. malariae*, and *P. knowlesi* [2]. The transmission of the parasite occurs via a blood meal of the *Anopheles* vector. Thereby, sporozoites are transmitted to the vertebrate host and the comprehensive life cycle of the pathogen is initiated [3]. In the past, several attempts to control the disease have been undertaken to exterminate the vector with insecticide. However, due to spreading drug resistance, these insecticides lost their efficacy [4]. A similar situation is present for the treatment of patients, since

an effective vaccine is not yet available and the medication of malaria is solely based on drugs [5, 6].

The folate (vitamin B9) metabolism is a validated drug target in several infectious diseases and its biosynthesis is not present in humans. Folate is an essential cofactor in enzymatic reactions transferring one-carbon (C1) groups [7, 8] and prominent antimalarials such as pyrimethamine and cycloguanil (inhibitors of the dihydrofolate reductase) and the sulfa drugs against the dihydropteroate synthase are well characterised within the vitamin B9 metabolism [7, 8]. However—among others—resistance is also rising against this metabolic pathway. Currently, there is a move towards artemisinin-based combination therapies (ACTs) [9, 10].

As already indicated above, due to the fact that currently no effective vaccine is available and the parasite's speed in developing resistance against almost all chemotherapeutic compounds is alarming, there is an urgent need to discover



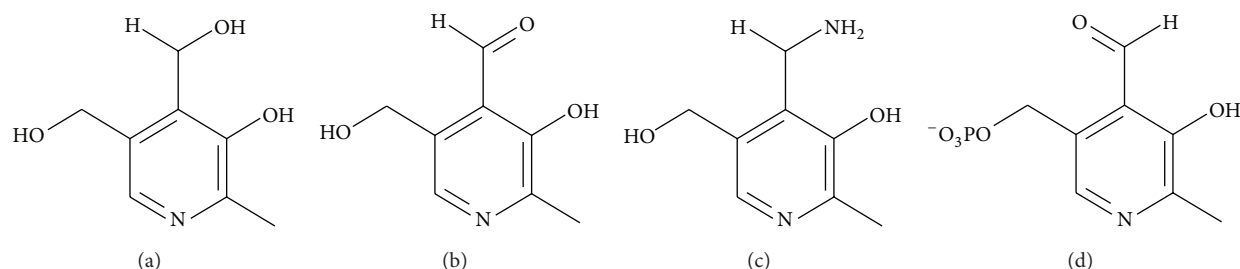


FIGURE 1: Chemical structures of vitamin B6: (a) pyridoxine, (b) pyridoxal, (c) pyridoxamine, and (d) its active form pyridoxal 5-phosphate.

novel drug-targets, which are subsequently exploitable for the design of new therapeutics against the malaria pathogen [11, 12]. In the search for novel antimalarials, attention has been drawn on selective interference with the parasite's metabolism without harming the human host [13]. In this sense promising drug targets are vitamin biosynthetic pathways.

Vitamins are molecules which have a variety of functions in nature. They act as antioxidants, as precursors in electron carrying processes, or are involved in enzymatic reactions by acting as cofactors in metabolic pathways such as the vitamins of the B-family [14]. Mammals generally depend on the uptake of vitamins, unlike other groups, such as bacteria, plants, and fungi which can synthesize them *de novo*. Some apicomplexan parasites possess also vitamin biosynthetic pathways which represent attractive drug targets to interfere with [7, 13].

So far, three vitamin biosynthetic pathways have been identified in malaria parasites [7, 13]. Besides the occurrence of the biosynthesis for folate (vitamin B9) and the thiamine (vitamin B1) biosynthesis, *Plasmodium* possesses also a vitamin B6 biosynthetic pathway. Vitamin B6 is designated for six vitamers: pyridoxine (PN), pyridoxamine (PM), pyridoxal (PL), and their respective phosphorylated forms. The different molecules differentiate in their substitutions at the 4th position of the pyridine ring (Figure 1). However, pyridoxal 5-phosphate (PLP) is the only active form of the enzymatic cofactor which is mainly involved in decarboxylation and transamination reactions [15].

Up to now, two different vitamin B6 biosynthesis pathways are described: (i) the 1-deoxy-D-xylulose 5-phosphate (DOXP)-dependent pathway is found in some proteobacteria and is leading to pyridoxine 5-phosphate [16–18]; (ii) the second pathway, the DOXP-independent pathway, is found in plants, fungi, and the apicomplexan parasites *Plasmodium* and *Toxoplasma gondii* [19–21].

Historically, the DOXP-independent pathway was identified in plants and ascribed to oxidative stress response [22, 23]. Afterwards, the analysis of this pathway discovered the biosynthesis of PLP, which is mediated by an enzyme complex (PLP-synthase) composed of a core of 12 Pdx1 (also known as SNZ1 in yeast) individually surrounded by 12 Pdx2 (called SNO1 in yeast) [24, 25]. The reaction mechanism has already been studied in some detail, starting with the deamination of glutamine to glutamate which is catalysed by Pdx2, subsequently, the ammonia group is channelled to Pdx1, where it is combined with the two other substrates, ribose

5-phosphate and glyceraldehyde 3-phosphate, leading to the active cofactor [24, 26]. This complex has already been tested for its druggability by performing *in silico* screens in order to dock compounds into the active site. Identified compounds were further employed in *in vitro* assays using recombinantly expressed enzymes. The best compound derived from this screen was 4-phospho-D-erythronhydrazide, which revealed an  $IC_{50}$ -value of  $10\ \mu\text{M}$  in cell culture experiments [27].

Moreover, besides the well-established function of vitamin B6 in acting as a cofactor, the molecule is also involved in the combat against reactive oxygen species (ROS), in particular against singlet oxygen [22, 28]. This additional mode of action is especially of relevance for the intraerythrocytic stage of the human malaria parasite, because *Plasmodium* is permanently exposed to ROS during proliferation within the erythrocytes due to the oxidative environment of its host cell which is accompanied by the parasite-driven haemoglobin degradation [29, 30].

Additionally, the parasite's genome encodes also for an interconversion pathway which consists of the pyridoxal kinase (PdxK) and a phosphatase [4, 7]. The latter reveals a broad substrate spectrum and therefore it is questionable whether this enzyme is solely responsible for the dephosphorylation of B6 vitamers [20, 31]. The PdxK catalyses the phosphorylation of pyridoxal but also accepts the other B6 vitamers as substrate [20, 32]. The presence of both—biosynthetic and interconversion—pathways remains still for elucidation since the parasite is able to generate PLP via two pathways which would obviously emphasise an uptake of B6 vitamers [4].

In *P. falciparum*, the PdxK enzyme was already exploited as drug target by channelling prodrugs into the parasite's metabolism. Pyridoxyl-tryptophan chimeras were converted into their respective phosphorylated forms by the PdxK. Subsequently, these molecules were shown to interfere with PLP-dependent enzymes by inhibiting their catalyses and hence the growth of the parasite [32].

## 2. PLP-Dependent Enzymes

PLP-dependent enzymes are characterised by their broad range of enzymatic activities and their participations in different metabolic pathways [15, 52]. They are mainly concentrated within the amino-acid metabolism [53]. Besides the glycogen phosphorylases, which follow a different mechanism [54, 55], PLP-dependent enzymes bind PLP during catalysis covalently to the respective substrate by acting as an electrophilic

TABLE 1: Different classes of PLP-dependent enzymes according to [15, 33].

Group number	Enzyme class/activity	Representative enzymes
1	Aminotransferases and the amino-acid decarboxylases	Serine hydroxymethyltransferase (SHMT) and the aspartate aminotransferase (AspAT, prototype)
2	Replacement and elimination of C <sub>β</sub> -groups	Serine and threonine dehydratases and the tryptophan synthase (prototype)
3	Interconversion of L- and D-amino acids with a common folding (alpha/beta) <sub>8</sub>	Alanine racemase
4	Alanine aminotransferase	D-Alanine aminotransferase
5	Glycogen phosphorylase	Glycogen phosphorylase
6	5,6-Aminomutase	D-Lysine 5,6-aminomutase
7	2,3-Aminomutase	Lysine 2,3-aminomutase

stabilizer of the carbanion intermediate [56]. In the past, a few attempts have been undertaken to classify PLP-dependent enzymes according to their activities and evolutionary history by splitting them into four major classes [57, 58]. Due to their conservation in the nature, it has been suggested that PLP-dependent enzymes derived from a common ancestor before division into the three kingdoms of life occurred [57].

Afterwards, this classification was refined by analysing genomic and structural information [15, 33] which led to the sorting of PLP-dependent enzymes into seven groups (Table 1).

Kappes and collaborators suggested that, because of the existing metabolic diversity, PLP-dependent enzymes in protozoan parasites would have potential to be good drug targets [59]. Most of the enzymes found (at least 2/3) belong to group I, followed by the less expressive group II, while the groups IV and V are rare and the groups VI and VII are almost inexistent. Recent genome database analyses of different parasites identified a minimal set of enzymes that are highly abundant which includes the serine hydroxymethyltransferase (SHMT), the aspartate aminotransferase (AspAT), the alanine transaminase, the branched-chain amino-acid transaminase, and the cysteine desulfurase [59].

Moreover, the comparison of all available genomes of free-living organisms revealed that only two EC-classified enzymes are always present: the AspAT (EC 2.6.1.1) and the SHMT (EC 2.1.2.1), which underlines the fundamental importance of these enzymes [15].

Additionally, several other PLP-dependent enzymes have already been exploited as drug targets such as the  $\gamma$ -aminobutyric acid GABA aminotransferase by the drug vigabatrin for treatment of epilepsy [60], the alanine racemase in microbicides [61], or the ornithine decarboxylase (ODC) in cancer research [62]. In particular, the ODC was also subject to drug discovery approaches against protozoan parasites but not limited as outlined below to the aspartate aminotransferase (AspAT) and the serine hydroxymethyltransferase (SHMT). However, the occurrence of PLP-dependent enzymes in the malaria parasite is not restricted to these three proteins as shown in Table 2.

### 3. Ornithine Decarboxylase (ODC)

As already outlined above, vitamin B6-dependent enzymes play central roles not only in the metabolism of amino acids

but also in the polyamine synthesis. Polyamines are simply structured aliphatic nitrogenous bases containing an essential role in cell growth, proliferation, and differentiation due to their stabilizing effect on macromolecules such as nucleic acids, proteins, and lipids. Their function is considered to be based on reversible ionic interactions with the negatively charged macromolecules [63–65].

The ornithine decarboxylase (ODC) is a PLP-dependent enzyme (Figure 2) which acts as a key regulator in the polyamine biosynthesis by decarboxylating ornithine to the polyamine putrescine—the first step in this synthesis. In contrast to ornithine, the other precursor of the polyamine synthesis, S-adenosylmethionine (AdoMet), is synthesized from methionine and ATP by the enzyme AdoMet synthase. AdoMet is also used to generate the polyamines spermidine and spermine. *P. falciparum* possesses a unique polyamine biosynthesis due to the bifunctional organisation of its key enzymes, S-adenosylmethionine decarboxylase (AdoMetDC) and ornithine decarboxylase (ODC) [42, 66]. Thereby, both enzymes appear as the bifunctional AdoMetDC/ODC whose organisation was discussed as an advantage in substrate channelling [66].

There are more bifunctional proteins known in *P. falciparum* such as the dihydrofolate reductase-thymidylate synthase (DHFR-TS) which is also present in other protozoa [67, 68], the dihydro-6-hydroxymethylpterin pyrophosphokinase-dihydropteroate synthase (PPPK-DHPS) [69], the glucose-6-phosphate dehydrogenase/6-phosphogluconolactonase [70], and the guanylate cyclase/adenylate cyclase [71].

Among others, this unique organisation of the *Pf*ODC has been discussed to be an attractive drug target [72]. As the amino acid sequence of *Pf*ODC shares about 39% identity to the human homologue, complications in rational drug design of *Pf*ODC-specific lead compounds could be a crucial issue [39]. Generally, there are three different strategies of inhibitor design. A formerly used strategy for designing inhibitors of vitamin B6-dependent enzymes is based on coenzyme-substrate conjugates that cannot be processed by the enzyme in their reduced form [73].

Another—already validated—strategy is the use of substrate analogues in order to inhibit enzyme catalysis like the specific ODC inhibitor difluoromethylornithine (DFMO), originally designed as an anticancer agent. DFMO blocks the erythrocytic schizogony of *P. falciparum* in cell culture at the

TABLE 2: PLP-dependent enzymes in *Plasmodium*.

EC-number	EC-name	PlasmoDB number	Annotation according to PlasmoDB	Pathway	Inhibitors	References
2.1.2.1	Glycine hydroxymethyltransferase	PFL1720w	Serine hydroxymethyltransferase	Folate metabolism	1843U89, AG331, AG337, D1694, GRI, pemetrexed, pyrimethamine, WR99210, methotrexate, glycine (competitively)	[34, 35]
2.3.1.37	5-Aminolevulinate synthase	PFL2210w	ALA synthase (aminolevulinate synthase)	Tetrapyrrole biosynthesis	Aminomalonate, Ethanolamine, Hemin	[36]
2.6.1.1	Aspartate aminotransferase	PFB0200c	Aspartate aminotransferase	Amino acid and pyrimidine metabolism	Inhibited by his own N-terminal peptide	[37]
2.6.1.13	Ornithine aminotransferase	PFF0435w	Ornithine aminotransferase	Arginine metabolism	L-canaline	[38]
2.6.1.57	Aromatic amino-acid transaminase	PFB0200c	Aspartate aminotransferase	Amino acid and pyrimidine metabolism	—	—
4.1.1.17	Ornithine decarboxylase	PF10_0322	S-Adenosylmethionine decarboxylase/ornithine decarboxylase (bifunctional)	Polyamine biosynthesis	Alpha-difluoromethylornithine, alpha-difluoroornithine, CGP52622A, CGP54619A, putrescine (feedback control)	[39–44]
4.1.3.38	<i>p</i> -Aminobenzoic acid synthetase	PFI1100w	<i>p</i> -Aminobenzoic acid synthetase, putative	Folate biosynthesis	—	—
2.6.1.7	3-Hydroxykynurenine transaminase		Present in the insect vector: <i>Anopheles</i>	Xanthurenic acid is needed by the parasite for proliferation/development	—	[45]
Putative PLP-dependent enzymes						
2.3.1.50	Serine C-Palmitoyltransferase	PF14_0155	Serine C-Palmitoyltransferase	Sphingolipid metabolism	—	—
2.6.1.42	Branched-chain amino-acid aminotransferase	PF14_0557	“Conserved <i>Plasmodium</i> protein”	Pantothenate and CoA biosynthesis	—	—
2.8.1.7	Cysteine desulfurase	PF07_0068, MAL7PI.150	Cysteine desulfurase, putative	Iron-sulfur cluster synthesis	—	—
4.1.1.18	Lysine decarboxylase	PFD0285c, PFD0670c	Lysine decarboxylase, putative	Polyamine metabolism	—	—

micromolar level (Table 2) and reduces the parasitemia in *Plasmodium berghei*-infected mice [47, 48, 74, 75]. DFMO, a derivative of ornithine, inhibits the enzyme irreversibly by an alkylation of its active site. A combination of DFMO and bis(benzyl)polyamines revealed a curative effect in rodent malaria [76]. Moreover, DFMO reveals a more prominent role due to its effectiveness against *Trypanosoma brucei gambiense*, the agent of the West African Sleeping Sickness [77–79]. Only marginal effects of DFMO have been observed against the apicomplexan relatives of *P. falciparum*, *Cryptosporidium* sp. [80] and *Toxoplasma gondii* [50].

Furthermore, two decades ago, a series of potent ODC inhibitors were synthesized. These compounds belong to the group of 3-amino-oxy-1-propanamine (APA) [81, 82], such

as CGP52622A and CGP54619A (Figure 2), which reversibly inhibit the *Pf*ODC with  $IC_{50}$ -values at the nanomolar range (Table 3). APA itself had an  $IC_{50}$ -value of 1  $\mu$ M revealing a 1000-fold stronger antiparasmodial effect than DFMO ( $IC_{50}$  value of 1.3 mM) (Table 3). However, APA and its analogues failed as drug candidates in the mouse model [83].

Another interesting PLP-mimicking compound is the cyclic pyridoxyl-tryptophan methyl ester PT3 which inhibits in its phosphorylated form (PPT3) the proliferation of *P. falciparum* at the cellular level ( $IC_{50}$ -value of 14  $\mu$ M) without harming human cells [32]. Two further compounds of this chemical group, PPHME and PPT5, act as inhibitors of the plasmodial ODC with  $IC_{50}$ -values of 58  $\mu$ M and 64  $\mu$ M, respectively [32] (Figure 2).

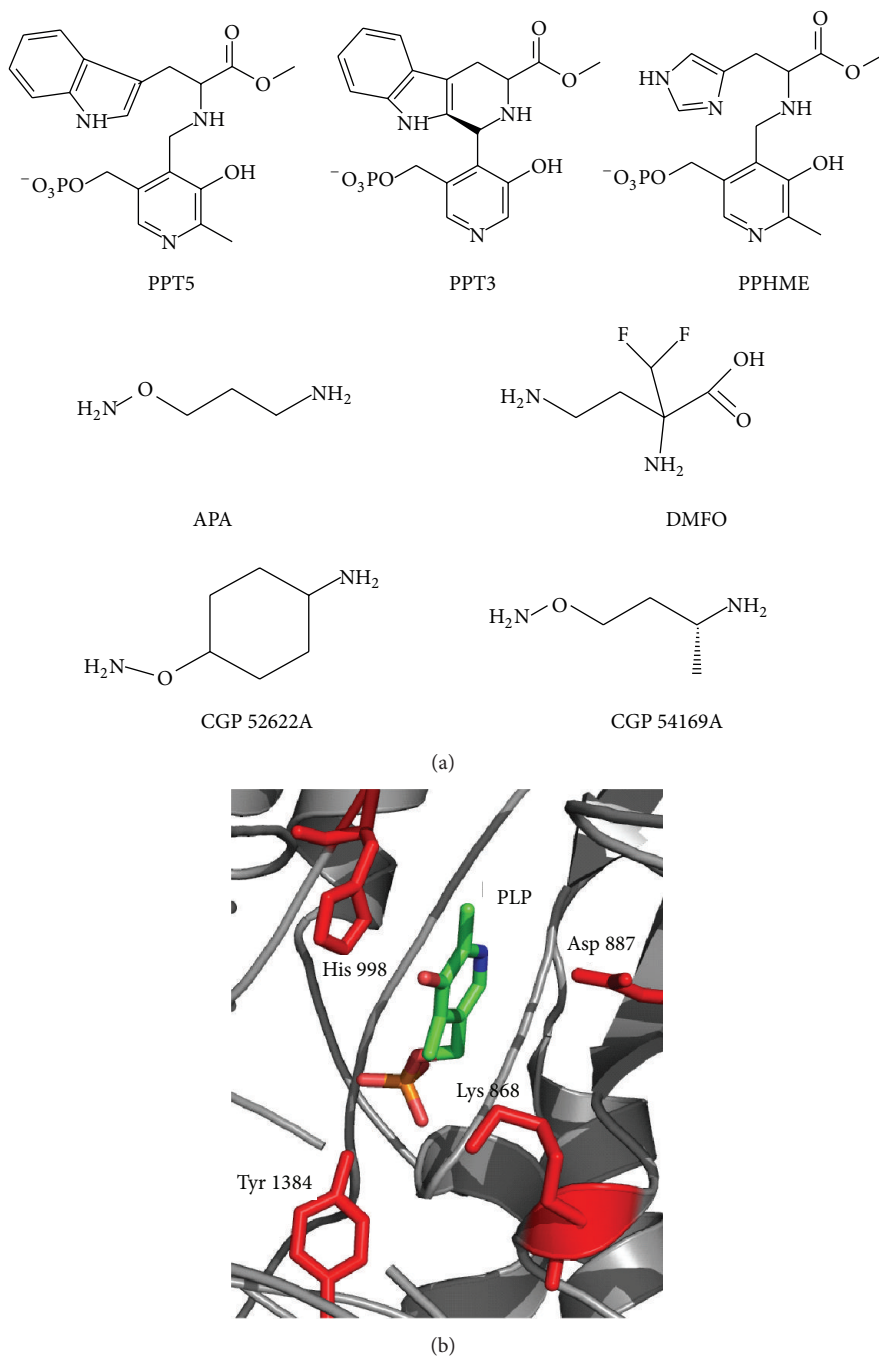


FIGURE 2: Comparison of the active site of the human and plasmodial ornithine decarboxylases (ODC). (a) Structures of ODC inhibitors tested against *Plasmodium*. (b) A structural homology model of the positions of the *P. falciparum* ODC active site (the respective residues are illustrated in red; amino acid numbering refers to the bifunctional protein) as well as the bound cofactor PLP.

#### 4. The *P. falciparum* Aspartate Aminotransferase (AspAT)

Aspartate aminotransferases are involved in three different metabolic pathways. AspAT is responsible for the reversible catalysis of L-aspartate (Asp) into oxaloacetate (OAA) and  $\alpha$ -ketoglutarate (2OG) into L-glutamate (Glu) [37]. Bulusu and collaborators [84] highlighted that AspAT also acts together with the fumarate hydratase (FH) and the malate-quinone

oxidoreductase (MQO) in the conversion of fumarate to aspartate. The enzyme has also been described to accept  $\alpha$ -ketomethylthiobutyrate as substrate in order to generate methionine [85]. Like all other aminotransferases, AspAT is structurally classified as a PLP-dependent enzyme of the subgroup I as outlined previously (Table 1) [86].

In the malaria parasite, AspAT is localised in the cytosol and reveals a homodimeric structure with two joint active site regions formed by both subunits [87–89]. Special



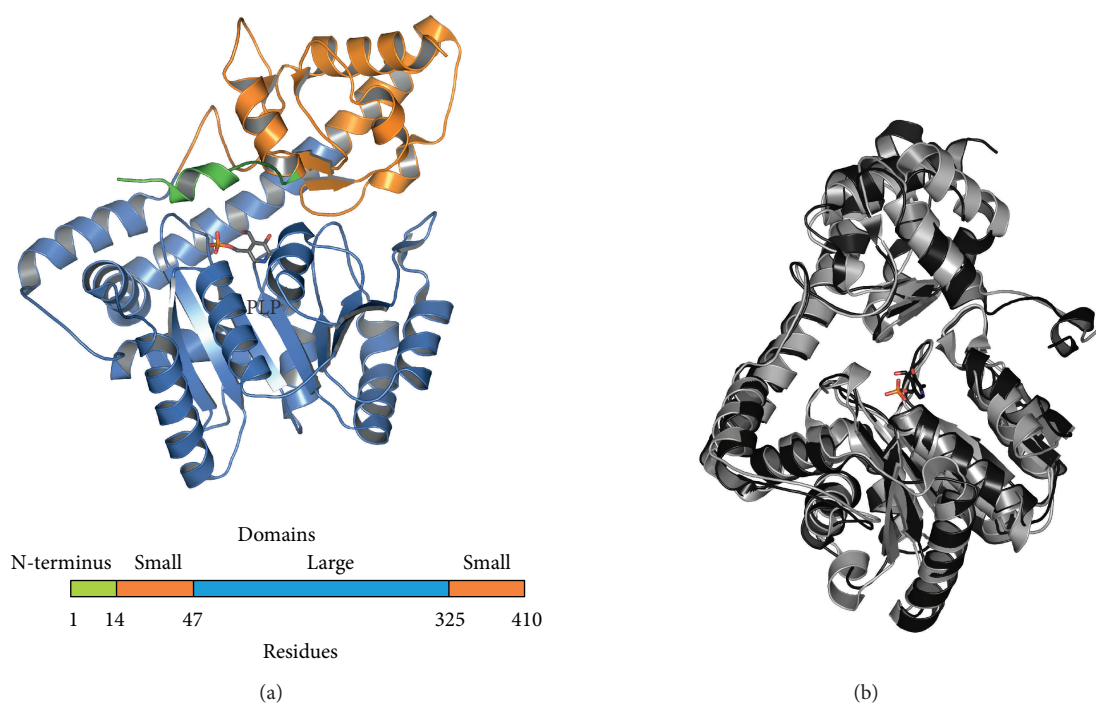


FIGURE 3: Three-dimensional structures of the AspATs. (a) The 3D structure of *Pf*AspAT (PDB code: 3K7Y) highlighting the three major domains and the N-terminus (green) as additionally shown in the scheme below. (b) Comparison between the human AspAT (grey, PDB code: 3HLM) and the *P. falciparum* counterpart (dark grey). The respective N-terminal region is illustrated in black and the cofactor PLP in colour.

TABLE 3: Comparison of the kinetic and inhibitory properties of ornithine decarboxylases.

	<i>P. falciparum</i> *	<i>M. musculus</i>	<i>T. gondii</i>	<i>T. brucei</i>	References
Molecular mass (kDa)	86.4	50–54	14	90	[41, 46]
$K_m$ -value of L-ornithine ( $\mu$ M)	47.3	30–200	—	161	[41, 47, 48]
$K_i$ -value of putrescine ( $\mu$ M)	50.4	600	0.92	—	[41, 49]
$K_i$ -value of DFMO ( $\mu$ M)	87.6	39	0.025	220	[41, 50, 51]
$K_i$ -value of CGP52622A (nM)	20.4	—	—	—	[41]
$K_i$ -value of CGP54619A (nM)	7.9	—	—	—	[41]
IC <sub>50</sub> -value of putrescine ( $\mu$ M)	157	—	—	—	[41]
IC <sub>50</sub> -value of CGP52622A (nM)	63.5	25	—	—	[41]
IC <sub>50</sub> -value of CGP54619A (nM)	25	10	—	—	[41]

\*Data derived from the *rPf* hinge-ODC [41].

attention has been drawn on the plasmodial AspAT (PDB code 3K7Y) which possesses a N-terminal-extended region that is required for the dimerisation process (Figure 3) [37]. This was already used for binding of the N-terminal AspAT peptide to the N-terminal protein domain of the other *Pf*AspAT monomer which prevents the formation of the homodimer. Interestingly, the plasmodial N-terminal region differs significantly from its human counterpart, so that the plasmodial peptide did not affect the human AspAT [37]. Furthermore, activity assays using *P. falciparum* protein extracts and the recombinantly expressed N-terminal *Pf*AspAT peptide have been performed which prevented AspAT activity suggesting that the malaria parasite possesses

no other enzyme that can compensate for the respective catalysis [37, 89].

## 5. Serine Hydroxymethyltransferase (SHMT)

As mentioned before, the folate metabolism in *P. falciparum* is a verified drug target and enzymatic reactions catalysed, for example, by the dihydrofolate reductase (DHFR) are already exploited by the classic antimalarials pyrimethamine and cycloguanil [90]. Another enzymatic step within the folate metabolism is carried out by the serine hydroxymethyltransferase (SHMT), catalysing the transfer of one-carbon units from serine to tetrahydrofolate to generate 5,10-methylene

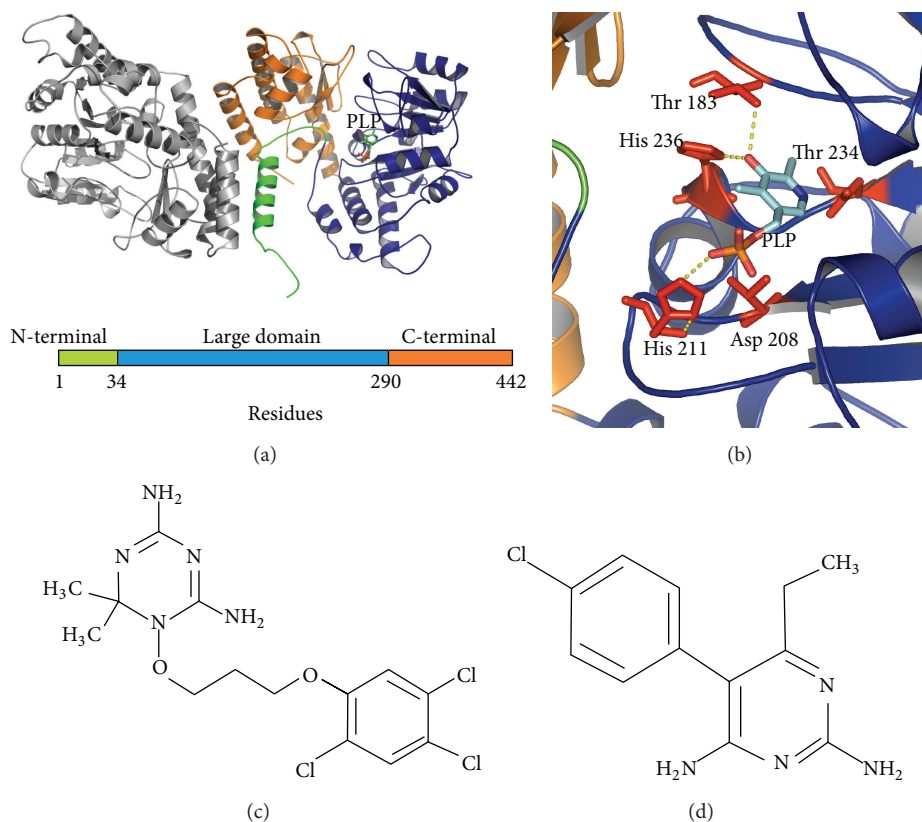


FIGURE 4: Model of the plasmodial SHMT and their active site residues. (a) Homology model of the SHMT of *P. falciparum* highlighting the three major domains: N-terminal (green), the core and active site (blue), and the C-terminal domain (orange). (b) The conserved residues Asp208, His211, Thr234, His236 and the *Plasmodium*-specific Thr183 residue are illustrated within the active site of the *Pf*SHMT as well as its embedded cofactor. Chemical structures of validated inhibitors of the folate metabolism (c) WR99210 and (d) pyrimethamine.

tetrahydrofolate and glycine; this  $\alpha$ -elimination catalysis is PLP-dependent, thereby belonging to the subgroup I [91].

The folate metabolism is of particular interest because it is involved in the pyrimidine biosynthesis which is required for the DNA synthesis. Since the SHMT is part of the folate metabolism, its transcription profile is increased in the S-phase of the DNA replication [92]. Due to the importance of this enzyme, SHMT is considered as a potential drug target in cancer research [93, 94]. In this sense, inhibitors against tumour cells have already been developed, which are intended to mimic nucleosides in order to be subsequently incorporated into the DNA, thereby leading to its fragmentation [95]. The SHMT of *P. falciparum* has been analysed for its functionality by complementation assays in *Escherichia coli* [96]. Moreover, activity assays using the recombinantly expressed *Pf*SHMT showed that the enzyme accepts in addition to the natural substrate—unlike its mammal counterpart—D-serine. This lack of stereospecificity has also been observed for the respective *P. vivax* enzyme [97]. Further, the plasmodial enzyme can be also inhibited competitively by glycine and serine [34].

Since the substrates of SHMT and DHFR are structurally similar (Figure 4), pyrimethamine, a potent inhibitor of the plasmodial DHFR, has also been tested on the recombinant SHMT, however, only with a marginal effect ( $IC_{50}$ -value in

the midmicromolar range) [35]. The comparison between the active site of the human enzyme and the plasmodial one showed a high degree of similarity as illustrated in Figure 4 [98], but, in contrast to the mammalian SHMT, which reveals a homotetrameric structure, the structural conformation of the plasmodial protein pointed towards a homodimeric appearance due to the lack of amino acid residues proposed to be involved in tetramerisation (like the His 135 and a poly-K sequence within the N-terminal domain) [98].

Despite all the similarities between the human and the malaria SHMT, the plasmodial enzyme possesses some peculiarities in the regulation of the folate metabolism such as binding to its own RNA [35], thus inhibiting protein translation [99].

Recently, a second open reading frame encoding for a potential mitochondrial SHMT (PF14\_0534, mSHMT) has been identified in *P. falciparum*. However, in comparison to other SHMTs, the active site of the plasmodial mSHMT does not reveal preserved amino acid residues [35, 100].

## 6. Druggable PLP-Dependent Enzymes in the Malaria Vector

Within the life cycle of *P. falciparum*, the necessity of PLP-dependent enzymes is not only restricted to the parasite. In

order to complete its life cycle, sexual forms of the parasite have to be taken up via the blood meal of the *Anopheles* vector to enter the mosquito gut [3]. Subsequently, the gametogenesis is induced in the mosquito stage by *Anopheles* derived triggers [101]. One of these molecules, that has been described to play a role in this event, is xanthurenic acid (XA) [101]. XA is generated by a transamination reaction of 3-hydroxykynurenine (3-HK) which is catalysed by the PLP-dependent *A. gambiae* 3-HK transaminase (AgHKT), an enzyme classified to the subgroup I. This reaction is necessary to prevent accumulation of the 3-HK, which can become a toxic molecule if it undergoes spontaneous oxidation and thereby generates ROS [45, 101]. The three-dimensional structure of the recombinant AgHKT was solved as a homodimer with a PLP molecule located in its active site [58, 86]. Currently, there are no inhibitors known to target the AgHKT, although structural information would enable *in silico* based drug-design [45]. Selective interference with the mosquito HKT would prevent the synthesis of XA and thereby offers the opportunity to block the life cycle of the malaria parasite in the mosquito stage.

## 7. Conclusion

Although the mortality of malaria infections is declining, the disease, of which malaria tropica (caused by *P. falciparum*) is the most fatal form, belongs still to the most important infectious disease to man. Due to the increasing level of resistance against the current chemotherapeutics, there is an urgent need to discover novel drugs which should have the ability to selectively interfere with the proliferation of this human pathogen. In this sense, the unique plasmodial cofactor metabolism becomes an attractive drug target due to the variety of cofactor-dependent enzymes. In particular, PLP-dependent enzymes are widely distributed in the metabolism of *P. falciparum* and responsible for plenty of essential catalyses such as the reactions carried out by the ODC, AspAT, or SHMT as outlined in this minireview. Hence, drug discovery towards inhibition of cofactor-binding would not only target single enzymes; moreover, the entire family of PLP-dependent proteins would be affected. This would certainly lead to the death of the parasite. However, the respective PLP-dependent host enzymes have to be taken into account. Therefore, the selective impairment of the malaria specific vitamin B6 biosynthesis should be considered.

## Conflict of Interests

The authors declare that there is no conflict of interests regarding the publication of this paper.

## Authors' Contribution

Thales Kronenberger, Jasmin Lindner, Kamila A. Meissner, and Flávia M. Zimbres contributed equally to this work.

## Acknowledgments

This work was financially supported by the Grants nos. 2009/54325-2, 2010/20647-0, 2011/13706-3, 2011/19703-6,

2012/12807-3, 2012/12790-3, and 2013/10288-1 from the Fundação de Amparo a Pesquisa do Estado de São Paulo (FAPESP). The authors would also like to acknowledge the CAPES/DAAD support within the UNIBRAL Programme entitled "INFECTBIO-USP-WWU" (348/2013).

## References

- [1] (WHO), WHO, Geneva, Switzerland, 2011.
- [2] S. Sabbatani, S. Fiorino, and R. Manfredi, "The emerging of the fifth malaria parasite (*Plasmodium Knowlesi*). A public health concern?" *Brazilian Journal of Infectious Diseases*, vol. 14, no. 3, pp. 299–309, 2010.
- [3] B. M. Greenwood, D. A. Fidock, D. E. Kyle et al., "Malaria: progress, perils, and prospects for eradication," *Journal of Clinical Investigation*, vol. 118, no. 4, pp. 1266–1276, 2008.
- [4] J. M. Cohen, D. L. Smith, C. Cotter et al., "Malaria resurgence: a systematic review and assessment of its causes," *Malaria Journal*, vol. 11, article 122, 2012.
- [5] D. G. Heppner, "The malaria vaccine—status quo 2013," *Travel Medicine and Infectious Disease*, vol. 11, pp. 2–7, 2013.
- [6] E. M. Riley and V. A. Stewart, "Immune mechanisms in malaria: new insights in vaccine development," *Nature Medicine*, vol. 19, pp. 168–178, 2013.
- [7] T. Kronenberger, I. Schetttert, and C. Wrenger, "Targeting the vitamin biosynthesis pathways for the treatment of malaria," *Future Medicinal Chemistry*, vol. 5, no. 7, pp. 769–779, 2013.
- [8] A. Nzila, S. A. Ward, K. Marsh, P. F. G. Sims, and J. E. Hyde, "Comparative folate metabolism in humans and malaria parasites (part I): pointers for malaria treatment from cancer chemotherapy," *Trends in Parasitology*, vol. 21, no. 6, pp. 292–298, 2005.
- [9] J. N. Burrows, "Antimalarial drug discovery: where next?" *Future Medicinal Chemistry*, vol. 4, no. 18, pp. 2233–2235, 2012.
- [10] A. Bhattarai, A. S. Ali, S. P. Kachur et al., "Impact of artemisinin-based combination therapy and insecticide-treated nets on malaria burden in Zanzibar," *PLoS Medicine*, vol. 4, no. 11, article e309, 2007.
- [11] P. Oliaro, "Mode of action and mechanisms of resistance for antimalarial drugs," *Pharmacology and Therapeutics*, vol. 89, no. 2, pp. 207–219, 2001.
- [12] I. B. Müller and J. E. Hyde, "Antimalarial drugs: modes of action and mechanisms of parasite resistance," *Future Microbiology*, vol. 5, no. 12, pp. 1857–1873, 2010.
- [13] I. B. Müller, J. E. Hyde, and C. Wrenger, "Vitamin B metabolism in *Plasmodium falciparum* as a source of drug targets," *Trends in Parasitology*, vol. 26, no. 1, pp. 35–43, 2010.
- [14] W. Friedrich, *Vitamins*, Walter de Gruyter, Berlin, Germany, 1988.
- [15] R. Percudani and A. Peracchi, "A genomic overview of pyridoxal-phosphate-dependent enzymes," *EMBO Reports*, vol. 4, no. 9, pp. 850–854, 2003.
- [16] T. B. Fitzpatrick, N. Amrhein, B. Kappes, P. Macheroux, I. Tews, and T. Raschle, "Two independent routes of de novo vitamin B6 biosynthesis: not that different after all," *Biochemical Journal*, vol. 407, no. 1, pp. 1–13, 2007.
- [17] H. M. Lam, E. Tancula, W. B. Dempsey, and M. E. Winkler, "Suppression of insertions in the complex *pdxJ* operon of *Escherichia coli* K-12 by *lon* and other mutations," *Journal of Bacteriology*, vol. 174, no. 5, pp. 1554–1567, 1992.



- [18] B. B. Roa, D. M. Connolly, and M. E. Winkler, "Overlap between *pdxA* and *ksgA* in the complex *pdxA-ksgA-apaG-apaH* operon of *Escherichia coli* K-12," *Journal of Bacteriology*, vol. 171, no. 9, pp. 4767–4777, 1989.
- [19] J. Knöckel, I. B. Müller, B. Bergmann, R. D. Walter, and C. Wrenger, "The apicomplexan parasite *Toxoplasma gondii* generates pyridoxal phosphate de novo," *Molecular and Biochemical Parasitology*, vol. 152, no. 1, pp. 108–111, 2007.
- [20] C. Wrenger, M. Eschbach, I. B. Müller, D. Warnecke, and R. D. Walter, "Analysis of the vitamin B6 biosynthesis pathway in the human malaria parasite *Plasmodium falciparum*," *The Journal of Biological Chemistry*, vol. 280, no. 7, pp. 5242–5248, 2005.
- [21] M. Gengenbacher, T. B. Fitzpatrick, T. Raschle et al., "Vitamin B6 biosynthesis by the malaria parasite *Plasmodium falciparum*: biochemical and structural insights," *The Journal of Biological Chemistry*, vol. 281, no. 6, pp. 3633–3641, 2006.
- [22] M. Ehrenshaft, P. Bilski, M. Li, C. F. Chignell, and M. E. Daub, "A highly conserved sequence is a novel gene involved in de novo vitamin B6 biosynthesis," *Proceedings of the National Academy of Sciences of the United States of America*, vol. 96, no. 16, pp. 9374–9378, 1999.
- [23] M. Ehrenshaft, A. E. Jenns, K. R. Chung, and M. E. Daub, "SOR1, a gene required for photosensitizer and singlet oxygen resistance in *Cercospora* fungi, is highly conserved in divergent organisms," *Molecular Cell*, vol. 1, no. 4, pp. 603–609, 1998.
- [24] M. Strohmeier, T. Raschle, J. Mazurkiewicz et al., "Structure of a bacterial pyridoxal 5'-phosphate synthase complex," *Proceedings of the National Academy of Sciences of the United States of America*, vol. 103, no. 51, pp. 19284–19289, 2006.
- [25] J. Zhu, J. W. Burgner, E. Harms, B. R. Belitsky, and J. L. Smith, "A new arrangement of ( $\beta/\alpha$ )8 barrels in the synthase subunit of PLP synthase," *The Journal of Biological Chemistry*, vol. 280, no. 30, pp. 27914–27923, 2005.
- [26] I. B. Müller, J. Knöckel, M. R. Groves et al., "The assembly of the plasmodial PLP synthase complex follows a defined course," *PLoS ONE*, vol. 3, no. 3, Article ID e1815, 2008.
- [27] S. B. Reeksting, I. B. Müller, P. B. Burger et al., "Exploring inhibition of Pdx1, a component of the PLP synthase complex of the human malaria parasite *Plasmodium falciparum*," *Biochemical Journal*, vol. 449, no. 1, pp. 175–187, 2013.
- [28] J. Knöckel, I. B. Müller, S. Butzloff, B. Bergmann, R. D. Walter, and C. Wrenger, "The antioxidative effect of de novo generated vitamin B6 in *Plasmodium falciparum* validated by protein interference," *Biochemical Journal*, vol. 443, no. 2, pp. 397–405, 2012.
- [29] K. Becker, L. Tilley, J. L. Vennerstrom, D. Roberts, S. Rogerson, and H. Ginsburg, "Oxidative stress in malaria parasite-infected erythrocytes: host-parasite interactions," *International Journal for Parasitology*, vol. 34, no. 2, pp. 163–189, 2004.
- [30] S. Müller, "Redox and antioxidant systems of the malaria parasite *Plasmodium falciparum*," *Molecular Microbiology*, vol. 53, no. 5, pp. 1291–1305, 2004.
- [31] J. Knöckel, B. Bergmann, I. B. Müller, S. Rathaur, R. D. Walter, and C. Wrenger, "Filling the gap of intracellular dephosphorylation in the *Plasmodium falciparum* vitamin B1 biosynthesis," *Molecular and Biochemical Parasitology*, vol. 157, no. 2, pp. 241–243, 2008.
- [32] I. B. Müller, F. Wu, B. Bergmann et al., "Poisoning pyridoxal 5-phosphate-dependent enzymes: a new strategy to target the malaria parasite *Plasmodium falciparum*," *PLoS ONE*, vol. 4, no. 2, Article ID e4406, 2009.
- [33] A. Amadasi, M. Bertoldi, R. Contestabile et al., "Pyridoxal 5'-phosphate enzymes as targets for therapeutic agents," *Current Medicinal Chemistry*, vol. 14, no. 12, pp. 1291–1324, 2007.
- [34] S. Maenpuen, K. Sopitthummakun, Y. Yuthavong, P. Chaiyen, and U. Leartsakulpanich, "Characterization of *Plasmodium falciparum* serine hydroxymethyltransferase—a potential anti-malarial target," *Molecular and Biochemical Parasitology*, vol. 168, no. 1, pp. 63–73, 2009.
- [35] C. K. T. Pang, J. H. Hunter, R. Gujjar et al., "Catalytic and ligand-binding characteristics of *Plasmodium falciparum* serine hydroxymethyltransferase," *Molecular and Biochemical Parasitology*, vol. 168, no. 1, pp. 74–83, 2009.
- [36] S. Varadharajan, S. Dhanasekaran, Z. Q. Bonday, P. N. Rangarajan, and G. Padmanaban, "Involvement of  $\delta$ -aminolaevulinic synthase encoded by the parasite gene in de novo haem synthesis by *Plasmodium falciparum*," *Biochemical Journal*, vol. 367, no. 2, pp. 321–327, 2002.
- [37] C. Wrenger, I. B. Müller, A. J. Schifferdecker, R. Jain, R. Jordanova, and M. R. Groves, "Specific inhibition of the aspartate aminotransferase of *Plasmodium falciparum*," *Journal of Molecular Biology*, vol. 405, no. 4, pp. 956–971, 2011.
- [38] C. Gafan, J. Wilson, L. C. Berger, and B. J. Berger, "Characterization of the ornithine aminotransferase from *Plasmodium falciparum*," *Molecular and Biochemical Parasitology*, vol. 118, no. 1, pp. 1–10, 2001.
- [39] L. Birkholtz, F. Joubert, A. W. H. Neitz, and A. I. Louw, "Comparative properties of a three-dimensional model of *Plasmodium falciparum* ornithine decarboxylase," *Proteins*, vol. 50, no. 3, pp. 464–473, 2003.
- [40] L. M. Birkholtz, C. Wrenger, F. Joubert, G. A. Wells, R. D. Walter, and A. I. Louw, "Parasite-specific inserts in the bifunctional S-adenosylmethionine decarboxylase/ornithine decarboxylase of *Plasmodium falciparum* modulate catalytic activities and domain interactions," *Biochemical Journal*, vol. 377, no. 2, pp. 439–448, 2004.
- [41] T. Krause, K. Lüersen, C. Wrenger, T. W. Gilberger, S. Müller, and R. D. Walter, "The ornithine decarboxylase domain of the bifunctional ornithine decarboxylase/S-adenosylmethionine decarboxylase of *Plasmodium falciparum*: recombinant expression and catalytic properties of two different constructs," *Biochemical Journal*, vol. 352, no. 2, pp. 287–292, 2000.
- [42] C. Wrenger, K. Lüersen, T. Krause, S. Müller, and R. D. Walter, "The *Plasmodium falciparum* bifunctional ornithine decarboxylase, S-adenosyl-L-methionine decarboxylase, enables a well balanced polyamine synthesis without domain-domain interaction," *The Journal of Biological Chemistry*, vol. 276, no. 32, pp. 29651–29656, 2001.
- [43] A. C. van Brumelen, K. L. Olszewski, D. Willinski, M. Llinás, A. I. Louw, and L. Birkholtz, "Co-inhibition of *Plasmodium falciparum* S-Adenosylmethionine decarboxylase/ornithine decarboxylase reveals perturbation-specific compensatory mechanisms by transcriptome, proteome, and metabolome analyses," *The Journal of Biological Chemistry*, vol. 284, no. 7, pp. 4635–4646, 2009.
- [44] M. Williams, J. Sprenger, E. Human et al., "Biochemical characterisation and novel classification of monofunctional S-adenosylmethionine decarboxylase of *Plasmodium falciparum*," *Molecular and Biochemical Parasitology*, vol. 180, no. 1, pp. 17–26, 2011.
- [45] F. Rossi, S. Garavaglia, G. B. Giovenzana, B. Arcà, J. Li, and M. Rizzi, "Crystal structure of the *Anopheles gambiae* 3-hydroxykynurenine transaminase," *Proceedings of the National*



- Academy of Sciences of the United States of America*, vol. 103, no. 15, pp. 5711–5716, 2006.
- [46] M. A. Phillips, P. Coffino, and C. C. Wang, "Trypanosoma brucei ornithine decarboxylase: enzyme purification, characterization, and expression in *Escherichia coli*," *The Journal of Biological Chemistry*, vol. 263, no. 34, pp. 17933–17941, 1988.
- [47] Y. G. Assaraf, J. Golenser, D. T. Spira, and U. Bachrach, "Polyamine levels and the activity of their biosynthetic enzymes in human erythrocytes infected with the malarial parasite, *Plasmodium falciparum*," *Biochemical Journal*, vol. 222, no. 3, pp. 815–819, 1984.
- [48] Y. G. Assaraf, C. Kahana, D. T. Spira, and U. Bachrach, "*Plasmodium falciparum*: purification, properties, and immunochemical study of ornithine decarboxylase, the key enzyme in polyamine biosynthesis," *Experimental Parasitology*, vol. 67, no. 1, pp. 20–30, 1988.
- [49] S. H. Seabra, R. A. DaMatta, F. G. de Mello, and W. de Souza, "Endogenous polyamine levels in macrophages is sufficient to support growth of *Toxoplasma gondii*," *Journal of Parasitology*, vol. 90, no. 3, pp. 455–460, 2004.
- [50] F. Derouin and C. Chastang, "Enzyme immunoassay to assess effect of antimicrobial agents on *Toxoplasma gondii* in tissue culture," *Antimicrobial Agents and Chemotherapy*, vol. 32, no. 3, pp. 303–307, 1988.
- [51] M. Dixon and E. C. Webb, *Enzymes*, Academic Press, New York, NY, USA, 1979.
- [52] S. D. Copley, "Enzymes with extra talents: moonlighting functions and catalytic promiscuity," *Current Opinion in Chemical Biology*, vol. 7, no. 2, pp. 265–272, 2003.
- [53] R. A. John, "Pyridoxal phosphate-dependent enzymes," *Biochimica et Biophysica Acta*, vol. 1248, no. 2, pp. 81–96, 1995.
- [54] A. J. Romo and H. W. Liu, "Mechanisms and structures of vitamin B6-dependent enzymes involved in deoxy sugar biosynthesis," *Biochimica et Biophysica Acta*, vol. 1814, no. 11, pp. 1534–1547, 2011.
- [55] D. Palm, H. W. Klein, R. Schinzel, M. Buehner, and E. J. M. Helmreich, "The role of pyridoxal 5'-phosphate in glycogen phosphorylase catalysis," *Biochemistry*, vol. 29, no. 5, pp. 1099–1107, 1990.
- [56] J. F. Kirsch, G. Eichele, G. C. Ford et al., "Mechanism of action of aspartate aminotransferase proposed on the basis of its spatial structure," *Journal of Molecular Biology*, vol. 174, no. 3, pp. 497–525, 1984.
- [57] P. K. Mehta and P. Christen, "The molecular evolution of pyridoxal-5'-phosphate-dependent enzymes," *Advances in Enzymology and Related Areas of Molecular Biology*, vol. 74, pp. 129–184, 2000.
- [58] P. Christen and P. K. Mehta, "From cofactor to enzymes. The molecular evolution of pyridoxal-5'-phosphate-dependent enzymes," *Chemical Records*, vol. 1, no. 6, pp. 436–447, 2001.
- [59] B. Kappes, I. Tews, A. Binter, and P. Macheroux, "PLP-dependent enzymes as potential drug targets for protozoan diseases," *Biochimica et Biophysica Acta*, vol. 1814, no. 11, pp. 1567–1576, 2011.
- [60] P. Storici, D. de Biase, F. Bossa et al., "Structures of  $\gamma$ -aminobutyric acid (GABA) aminotransferase, a pyridoxal 5'-phosphate, and [2Fe-2S] cluster-containing enzyme, complexed with  $\gamma$ -ethynyl-GABA and with the antiepilepsy drug vigabatrin," *The Journal of Biological Chemistry*, vol. 279, no. 1, pp. 363–373, 2004.
- [61] G. F. Stamper, A. A. Morollo, and D. Ringe, "Reaction of alanine racemase with 1-aminoethylphosphonic acid forms a stable external aldimine," *Biochemistry*, vol. 29, no. 20, pp. 10438–10445, 1998.
- [62] F. Wu and H. Gehring, "Structural requirements for novel coenzyme-substrate derivatives to inhibit intracellular ornithine decarboxylase and cell proliferation," *FASEB Journal*, vol. 23, no. 2, pp. 565–574, 2009.
- [63] C. W. Tabor and H. Tabor, "Polyamines," *Annual Review of Biochemistry*, vol. 53, pp. 749–790, 1983.
- [64] C. W. Tabor and H. Tabor, "Polyamines in microorganisms," *Microbiological Reviews*, vol. 49, no. 1, pp. 81–99, 1985.
- [65] H. M. Wallace, A. V. Fraser, and A. Hughes, "A perspective of polyamine metabolism," *Biochemical Journal*, vol. 376, no. 1, pp. 1–14, 2003.
- [66] S. Müller, A. Dădara, K. Lüersen et al., "In the human malaria parasite *Plasmodium falciparum*, polyamines are synthesized by a bifunctional ornithine decarboxylase, S-adenosylmethionine decarboxylase," *The Journal of Biological Chemistry*, vol. 275, no. 11, pp. 8097–8102, 2000.
- [67] K. M. Ivanetich and D. V. Santi, "Bifunctional thymidylate synthase-dihydrofolate reductase in protozoa," *FASEB Journal*, vol. 4, no. 6, pp. 1591–1597, 1990.
- [68] D. J. Bzik, W. B. Li, T. Horii, and J. Inselburg, "Molecular cloning and sequence analysis of the *Plasmodium falciparum* dihydrofolate reductase-thymidylate synthase gene," *Proceedings of the National Academy of Sciences of the United States of America*, vol. 84, no. 23, pp. 8360–8364, 1987.
- [69] T. Triglia and A. F. Cowman, "Primary structure and expression of the dihydropteroate synthetase gene of *Plasmodium falciparum*," *Proceedings of the National Academy of Sciences of the United States of America*, vol. 91, no. 15, pp. 7149–7153, 1994.
- [70] J. L. Clarke, D. A. Scopes, O. Sodeinde, and P. J. Mason, "Glucose-6-phosphate dehydrogenase-6-phosphogluconolactonase: a novel bifunctional enzyme in malaria parasites," *European Journal of Biochemistry*, vol. 268, no. 7, pp. 2013–2019, 2001.
- [71] D. J. Carucci, A. A. Witney, D. K. Muhia et al., "Guanylyl cyclase activity associated with putative bifunctional integral membrane proteins in *Plasmodium falciparum*," *The Journal of Biological Chemistry*, vol. 275, no. 29, pp. 22147–22156, 2000.
- [72] I. B. Müller, R. Das Gupta, K. Lüersen, C. Wrenger, and R. D. Walter, "Assessing the polyamine metabolism of *Plasmodium falciparum* as chemotherapeutic target," *Molecular and Biochemical Parasitology*, vol. 160, no. 1, pp. 1–7, 2008.
- [73] J. S. Heller, E. S. Canellakis, D. L. Bussolotti, and J. K. Coward, "Stable multisubstrate adducts as enzyme inhibitors. Potent inhibition of ornithine decarboxylase by N (5'-phosphopyridoxyl) ornithine," *Biochimica et Biophysica Acta*, vol. 403, no. 1, pp. 197–207, 1975.
- [74] A. J. Bitonti, P. P. McCann, and A. Sjoerdsma, "*Plasmodium falciparum* and *Plasmodium berghei*: effects of ornithine decarboxylase inhibitors on erythrocytic schizogony," *Experimental Parasitology*, vol. 64, no. 2, pp. 237–243, 1987.
- [75] M. R. Hollingdale, P. P. McCann, and A. Sjoerdsma, "*Plasmodium berghei*: inhibitors of ornithine decarboxylase block exoerythrocytic schizogony," *Experimental Parasitology*, vol. 60, no. 1, pp. 111–117, 1985.
- [76] A. J. Bitonti, J. A. Dumont, T. L. Bush et al., "Bis(benzyl)polyamine analogs inhibit the growth of chloroquine-resistant human malaria parasites (*Plasmodium falciparum*) in vitro and

- in combination with  $\alpha$ -difluoromethylornithine cure murine malaria," *Proceedings of the National Academy of Sciences of the United States of America*, vol. 86, no. 2, pp. 651–655, 1989.
- [77] C. J. Bacchi, H. C. Nathan, S. H. Hutner, P. P. McCann, and A. Sjoerdsma, "Polyamine metabolism: a potential therapeutic target in trypanosomes," *Science*, vol. 210, no. 4467, pp. 332–334, 1980.
- [78] C. Burri and R. Brun, "Efornithine for the treatment of human African trypanosomiasis," *Parasitology Research*, vol. 90, supplement 1, pp. S49–S52, 2003.
- [79] A. Sjoerdsma and P. J. Schechter, "Efornithine for African sleeping sickness," *The Lancet*, vol. 354, no. 9174, p. 254, 1999.
- [80] H. W. Moon, A. Schwartz, M. J. Welch, P. P. McCann, and P. L. Runnels, "Experimental fecal transmission of human cryptosporidia to pigs, and attempted treatment with an ornithine decarboxylase inhibitor," *Veterinary Pathology*, vol. 19, no. 6, pp. 700–707, 1982.
- [81] H. Mett, J. Stanek, J. A. Lopez-Ballester et al., "Pharmacological properties of the ornithine decarboxylase inhibitor 3-aminooxy-1-propanamine and several structural analogues," *Cancer Chemotherapy and Pharmacology*, vol. 32, pp. 39–45, 1993.
- [82] J. Stanek, J. Frei, H. Mett, P. Schneider, and U. Regenass, "2-Substituted 3-(aminooxy)propanamines as inhibitors of ornithine decarboxylase: synthesis and biological activity," *Journal of Medicinal Chemistry*, vol. 35, no. 8, pp. 1339–1344, 1992.
- [83] R. Das Gupta, T. Krause-Ihle, B. Bergmann et al., "3-Aminooxy-1-aminopropane and derivatives have an antiproliferative effect on cultured *Plasmodium falciparum* by decreasing intracellular polyamine concentrations," *Antimicrobial Agents and Chemotherapy*, vol. 49, no. 7, pp. 2857–2864, 2005.
- [84] V. Bulusu, V. Jayaraman, and H. Balaram, "Metabolic fate of fumarate, a side product of the purine salvage pathway in the intraerythrocytic stages of *Plasmodium falciparum*," *The Journal of Biological Chemistry*, vol. 286, no. 11, pp. 9236–9245, 2011.
- [85] L. C. Berger, J. Wilson, P. Wood, and B. J. Berger, "Methionine regeneration and aspartate aminotransferase in parasitic protozoa," *Journal of Bacteriology*, vol. 183, no. 15, pp. 4421–4434, 2001.
- [86] P. K. Mehta, T. I. Hale, and P. Christen, "Aminotransferases: demonstration of homology and division into evolutionary subgroups," *European Journal of Biochemistry*, vol. 214, no. 2, pp. 549–561, 1993.
- [87] R. Jain, R. Jordanova, I. B. Müller, C. Wrenger, and M. R. Groves, "Purification, crystallization and preliminary X-ray analysis of the aspartate aminotransferase of *Plasmodium falciparum*," *Acta Crystallographica F*, vol. 66, no. 4, pp. 409–412, 2010.
- [88] D. Liu, E. Pozharski, B. W. Lepore et al., "Inactivation of *Escherichia coli* L-aspartate aminotransferase by (S)-4-amino-4,5-dihydro-2-thiophenecarboxylic acid reveals 'A tale of two mechanisms,'" *Biochemistry*, vol. 46, no. 37, pp. 10517–10527, 2007.
- [89] C. Wrenger, I. B. Müller, A. M. Silber, R. Jordanova, V. S. Lamzin, and M. R. Groves, "Aspartate aminotransferase—bridging carbohydrate and energy metabolism in *Plasmodium falciparum*," *Current Drug Metabolism*, vol. 13, no. 3, pp. 332–336, 2012.
- [90] A. Nzila, "The past, present and future of antifolates in the treatment of *Plasmodium falciparum* infection," *Journal of Antimicrobial Chemotherapy*, vol. 57, no. 6, pp. 1043–1054, 2006.
- [91] V. Schirch and D. M. E. Szebenyi, "Serine hydroxymethyltransferase revisited," *Current Opinion in Chemical Biology*, vol. 9, no. 5, pp. 482–487, 2005.
- [92] N. Nirmalan, P. Wang, P. F. G. Sims, and J. E. Hyde, "Transcriptional analysis of genes encoding enzymes of the folate pathway in the human malaria parasite *Plasmodium falciparum*," *Molecular Microbiology*, vol. 46, no. 1, pp. 179–190, 2002.
- [93] S. Agrawal, A. Kumar, V. Srivastava, and B. N. Mishra, "Cloning, expression, activity and folding studies of serine hydroxymethyltransferase: a target enzyme for cancer chemotherapy," *Journal of Molecular Microbiology and Biotechnology*, vol. 6, no. 2, pp. 67–75, 2003.
- [94] H. G. Eichler, R. Hubbard, and K. Snell, "The role of serine hydroxymethyltransferase in cell proliferation: DNA synthesis from serine following mitogenic stimulation of lymphocytes," *Bioscience Reports*, vol. 1, no. 2, pp. 101–106, 1981.
- [95] A. Yoshioka, S. Tanaka, O. Hiraoka et al., "Deoxyribonucleoside triphosphate imbalance. 5-fluorodeoxyuridine-induced DNA double strand breaks in mouse FM3A cells and the mechanism of cell death," *The Journal of Biological Chemistry*, vol. 262, no. 17, pp. 8235–8241, 1987.
- [96] S. Alfadhli and P. K. Rathod, "Gene organization of a *Plasmodium falciparum* serine hydroxymethyltransferase and its functional expression in *Escherichia coli*," *Molecular and Biochemical Parasitology*, vol. 110, no. 2, pp. 283–291, 2000.
- [97] K. Sopitthummakhun, S. Maenpuen, Y. Yuthavong, U. Leartsakulpanich, and P. Chaiyen, "Serine hydroxymethyltransferase from *Plasmodium vivax* is different in substrate specificity from its homologues," *FEBS Journal*, vol. 276, no. 15, pp. 4023–4036, 2009.
- [98] T. C. França, P. G. Pascutti, T. C. Ramalho, and J. D. Figueroa-Villar, "A three-dimensional structure of *Plasmodium falciparum* serine hydroxymethyltransferase in complex with glycine and 5-formyl-tetrahydrofolate. Homology modeling and molecular dynamics," *Biophysical Chemistry*, vol. 115, no. 1, pp. 1–10, 2005.
- [99] E. Chu, C. H. Takimoto, D. Voeller, J. L. Grem, and C. J. Allegra, "Specific binding of human dihydrofolate reductase protein to Dihydrofolate reductase messenger RNA in vitro," *Biochemistry*, vol. 32, no. 18, pp. 4756–4760, 1993.
- [100] E. Salcedo, P. F. G. Sims, and J. E. Hyde, "A glycine-cleavage complex as part of the folate one-carbon metabolism of *Plasmodium falciparum*," *Trends in Parasitology*, vol. 21, no. 9, pp. 406–411, 2005.
- [101] G. E. Garcia, R. A. Wirtz, J. R. Barr, A. Woolfitt, and R. Rosenberg, "Xanthurenic acid induces gametogenesis in *Plasmodium*, the malaria parasite," *The Journal of Biological Chemistry*, vol. 273, no. 20, pp. 12003–12005, 1998.

## Research Article

# The Pyridoxal 5'-Phosphate (PLP)-Dependent Enzyme Serine Palmitoyltransferase (SPT): Effects of the Small Subunits and Insights from Bacterial Mimics of Human hLCB2a HSN1 Mutations

Ashley E. Beattie,<sup>1</sup> Sita D. Gupta,<sup>2</sup> Lenka Frankova,<sup>3</sup> Agne Kazlauskaitė,<sup>1</sup> Jeffrey M. Harmon,<sup>4</sup> Teresa M. Dunn,<sup>2</sup> and Dominic J. Campopiano<sup>1</sup>

<sup>1</sup> EastChem School of Chemistry, The University of Edinburgh, West Mains Road, Edinburgh EH9 3JJ, UK

<sup>2</sup> Department of Biochemistry and Molecular Biology, Uniformed Services University of the Health Sciences, Bethesda, MD 20184-4779, USA

<sup>3</sup> The Edinburgh Cell Wall Group, Institute of Molecular Plant Sciences, School of Biological Sciences, The University of Edinburgh, Daniel Rutherford Building, Edinburgh EH9 3JH, UK

<sup>4</sup> Department of Pharmacology, Uniformed Services University of the Health Sciences, Bethesda, MD 20184-4779, USA

Correspondence should be addressed to Dominic J. Campopiano; [dominic.campopiano@ed.ac.uk](mailto:dominic.campopiano@ed.ac.uk)

Received 12 June 2013; Accepted 22 July 2013

Academic Editor: Roberto Contestabile

Copyright © 2013 Ashley E. Beattie et al. This is an open access article distributed under the Creative Commons Attribution License, which permits unrestricted use, distribution, and reproduction in any medium, provided the original work is properly cited.

The pyridoxal 5'-phosphate (PLP)-dependent enzyme serine palmitoyltransferase (SPT) catalyses the first step of *de novo* sphingolipid biosynthesis. The core human enzyme is a membrane-bound heterodimer composed of two subunits (hLCB1 and hLCB2a/b), and mutations in both hLCB1 (e.g., C133W and C133Y) and hLCB2a (e.g., V359M, G382V, and I504F) have been identified in patients with hereditary sensory and autonomic neuropathy type I (HSAN1), an inherited disorder that affects sensory and autonomic neurons. These mutations result in substrate promiscuity, leading to formation of neurotoxic deoxysphingolipids found in affected individuals. Here we measure the activities of the hLCB2a mutants in the presence of ssSPTa and ssSPTb and find that all decrease enzyme activity. High resolution structural data of the homodimeric SPT enzyme from the bacterium *Sphingomonas paucimobilis* (*Sp* SPT) provides a model to understand the impact of the hLCB2a mutations on the mechanism of SPT. The three human hLCB2a HSN1 mutations map onto *Sp* SPT (V246M, G268V, and G385F), and these mutant mimics reveal that the amino acid changes have varying impacts; they perturb the PLP cofactor binding, reduce the affinity for both substrates, decrease the enzyme activity, and, in the most severe case, cause the protein to be expressed in an insoluble form.

## 1. Introduction

Sphingolipids (SLs) are membrane components found in all eukaryotes, some prokaryotes, and viruses. SLs and their downstream metabolites (such as ceramide) play important roles in mediating cell-stress response and cell proliferation and in regulating the cell cycle and apoptosis [1–3]. Deficiencies in SL metabolism have been implicated in several diseases that include cancer and diabetes, as well as neurodegenerative disorders such as Alzheimer's [4, 5]. The first enzyme of the

*de novo* sphingolipid biosynthetic pathway present in all SL-producing organisms is the pyridoxal 5'-phosphate- (PLP-) dependent serine palmitoyltransferase ((SPT) EC 2.3.1.50) [6]. It catalyses the condensation of L-serine with palmitoyl coenzyme-A to generate 3-ketodehydrosphinganine (KDS) that forms the sphingoid base backbone of all SLs. The 3D structure of the soluble, homodimeric SPT from the SL-producing organism *S. paucimobilis* (*Sp* SPT) was published by our group in 2007. It is a member of the PLP superfamily (fold type I) and contains three domains: N-terminal, central,



and C-terminal [7]. Based on extensive structural and biochemical analyses of this enzyme, a working SPT mechanism involves the formation of a number of key intermediates (Figure 1) [7]. An initial PLP-bound internal aldimine (covalently attached to Lys265) is displaced by L-serine to generate a PLP:L-serine external aldimine. Binding of the C16 acyl-CoA thioester allows formation of a carbanion/quinonoid nucleophile by deprotonation of the external aldimine. After Claisen-like condensation, a  $\beta$ -keto acid is formed which subsequently loses CO<sub>2</sub> to generate a PLP:KDS product aldimine which is then released from the enzyme, and the SPT returns to its PLP-bound internal aldimine form. We and others have investigated the catalytic roles of conserved active site SPT residues in this mechanism [8–11].

Eukaryotic SPT is a membrane-bound enzyme which contains two core subunits, LCB1 and LCB2 in yeast [12–14] and SPTLC1 and SPTLC2/3 in mammals [15–17]. For clarity we have adopted the nomenclature hLCB1, hLCB2a/b for the human subunits [18]. The hLCB1 and hLCB2 subunits display relatively high sequence homology to each other, but a comparison with other PLP-binding enzymes revealed that only the hLCB2a contains key catalytic residues including the lysine that binds PLP [19, 20]. In contrast, hLCB1 lacks these residues but contains other residues predicted to be involved in catalysis leading to the working hypothesis that the hLCB1/hLCB2a heterodimer has a single active site. Hornemann and colleagues suggested that the eukaryotic SPT may in fact be a higher order complex [21], and indeed recent results lend weight to that hypothesis. Also, the same group recently identified a second hLCB2 isoform, hLCB2b, also known as SPTLC3 with 68% sequence identity to hLCB2a that is predominantly expressed in the placenta and prefers shorter chain acyl-CoAs (C12 and C14) to generate short-chain SLs [22]. We identified two highly-related isoforms of a third “small subunit” in humans (ssSPTa and ssSPTb) which were shown to be crucial for maximal enzyme activity [18]. These are functionally orthologous to a previously-characterised small subunit (Tsc3p) discovered in yeast [23]. These ssSPTs can increase the catalytic activity of the hLCB1/hLCB2 complex up to 100 fold, and also influence the chain-length specificity of the acyl-CoA substrate, and, thus, impact directly on the concentrations and chemical nature of the SL pool. This complexity was further increased by the recent discovery of other components of a so-called SPOTS complex in yeast that is composed of LCB1/LCB2/Tsc3p, an ORM protein(s), and a phosphoinositide phosphatase, Sac1 [24, 25]. These ORM and Sac1 components are thought to play a role in modulating SPT activity and flux through the SL pathway by a phosphorylation-dependent mechanism [25–28].

Since SLs and ceramides are essential elements of cellular membranes that also play important roles in cell signalling, homozygous LCB1/LCB2 mutations that cause complete loss of SPT activity would be assumed to be lethal. However, there are very rare gain-of-function SPT mutations that have been identified and their genetic lineage has been studied [29–33]. These SPT mutations lead to hereditary sensory neuropathies (HSAN1) whose clinical outcomes include progressive distal sensory loss and severe ulcerations of the limbs. What causes the neuronal breakdown has been the subject of interesting

debate. As well having an impact on the basal SPT activity, a new hypothesis suggests that the SPT mutations associated with HSAN1 lead to an enzyme lacking exquisite substrate specificity for L-serine. Penno and colleagues discovered that tissue from HSAN1 patients contains high levels of L-alanine and glycine-derived deoxy-SLs that have been shown to be toxic to HEK293 cells [32]. Four missense mutations in the hLCB1 subunit associated with HSAN1 (C133W, C133Y, V144D, and G387A) were among the first to be identified (Table 1) and have shown to have a negative effect on the SPT enzyme and sphingolipid production [29, 30, 34, 35]. Another mutation at residue C133 (C133R) was identified in a patient with a mild phenotype, but its impact on SPT activity has not been characterized [36]. The multisubunit, membrane-bound nature of the eukaryotic SPT has prevented a detailed structural and mechanistic analysis of the impact of the HSAN1 causing mutations on the enzyme. To gain insight into and explore the molecular basis of the HSAN1 genotype we have used the *Sp* SPT isoform as a model system. Both cysteine mutations were previously engineered into the *Sp* SPT (as N100W and N100Y) in our group [10]. These mutations result in a compromised SPT enzyme, severely impacting PLP binding, reducing affinity for the L-serine substrate, and causing catastrophic effects on catalytic activity. More recently, two more hLCB1 mutations (S331F and A352V) were identified. The S331F mutation resulted in symptoms far more severe than those associated with the more common HSAN1 mutations. Furthermore, a second mutation at amino acid position Ser331 (S331Y) is linked to a distinct syndrome phenotype [37, 38]. Interestingly, for the first time, three different mutations (V359M, G382V, and I504F) were recently identified in the hLCB2a subunit by Rothier et al. [39]. They found that each mutation lowered the activity of the hLCB1/hLCB2a heterodimer and was also able to generate varying levels of deoxy-SLs. This group also modelled the three hLCB2a mutations onto the bacterial *Sp* SPT (V246M, G268V, and G385F) paving the way for the biochemical analysis that we describe here (Figure 2). In this report, we have studied the influence of the human small subunits on the activity of the HSAN1 hLCB2a mutations. As well as this, we have also characterised the bacterial mutant mimics using enzyme kinetics, spectroscopy, and molecular modelling to provide insight into the impact they have on PLP cofactor binding, catalytic activity, and/or substrate binding.

## 2. Materials and Methods

**2.1. Chemicals and Molecular Biology Materials.** Plasmids and competent cells were purchased from Novagen. All buffers and reagents were from Sigma. Palmitoyl-CoA was purchased from Avanti Lipids.

### 2.2. Methods

**2.2.1. Analysis of Human SPT Wild Type and HSAN1 Mutant Activity in the Presence of the ssSPTa and ssSPTb Subunits.** The construction of yeast mutant strains lacking *lcb1*, *lcb2*, and *tsc3* was described previously [18, 31]. Yeast microsomes were prepared, and expression of recombinant human forms



TABLE 1: Overview of currently known hLCB1 and hLCB2a HSN1 related mutations.

Mutant	Sp SPT residue	Location in Sp SPT	Clinical features	Reference
<b>hSPT1</b>				
C133Y	N100	Active site	Sensory neuropathy, ulceromutilations, and lancinating pains.	[29, 30]
C133W	N100	Active site	Sensory neuropathy, ulceromutilations, and lancinating pains.	[29, 30]
C133R	N100	Active site	Sensory neuropathy.	[36]
V144D	D121	Surface exposed	Sensory neuropathy, ulceromutilations, and lancinating pains.	[30]
S331F	H278	Surface exposed	Ulcerations, mental retardation, hypotonia, severe growth and mental retardation, vocal cord paralysis, and gastroesophageal reflux.	[33, 37]
S331Y	H278	Surface exposed	As S331F.	[38]
A352V	S308	Not surface exposed	Sensory neuropathy, ulceromutilations, and lancinating pains.	[33, 37]
G387A	E343	Surface exposed	No disease associated.	[40, 41]
<b>hSPT2</b>				
V359M	V246	Not surface exposed	Sensory neuropathy, ulceromutilations.	[39]
G382V	G268	Active Site	Sensory neuropathy, ulceromutilations.	[39]
I504F	G385	Surface exposed	Sensory neuropathy, ulcerations, osteomyelitis, and anhidrosis.	[39]
A182P	T79	Not surface exposed	Sensory neuropathy.	[42]

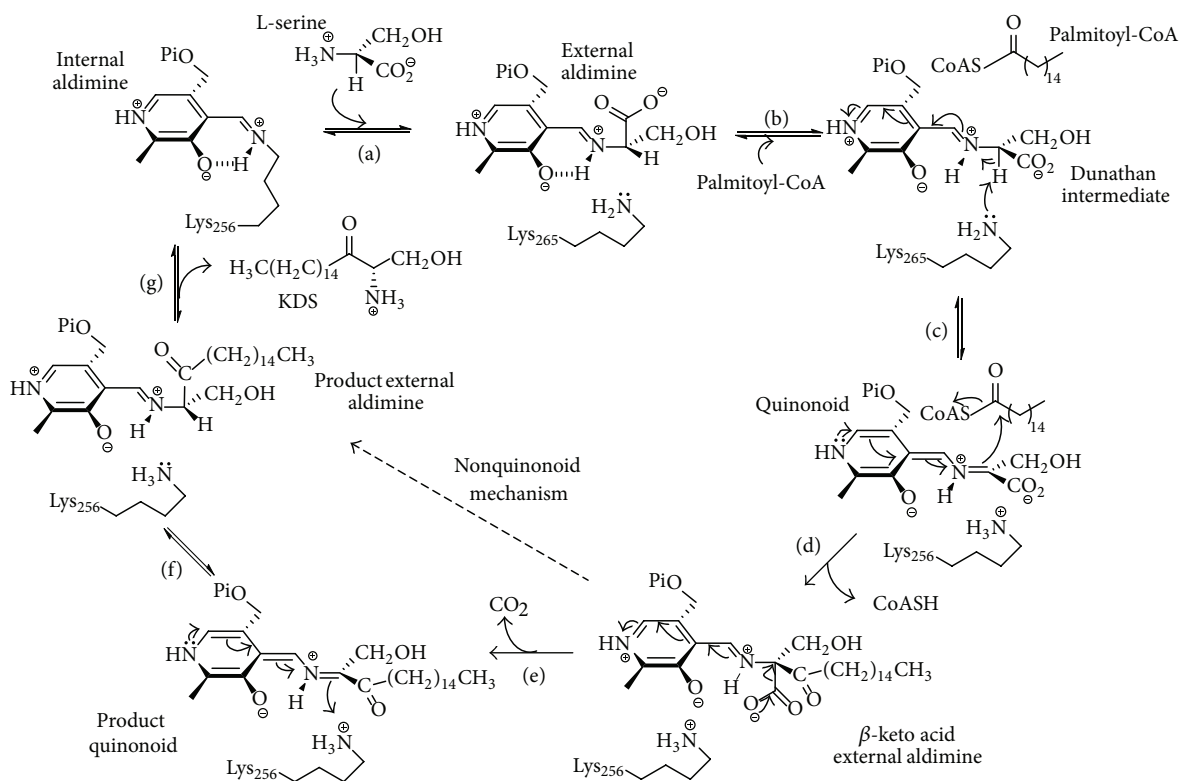


FIGURE 1: Proposed SPT mechanism. (a) Transamination of internal aldimine by incoming L-serine to form PLP-L-serine external aldimine intermediate; (b) binding of palmitoyl-CoA causes conformational change and deprotonation of external aldimine by Lys265 to form quinonoid/carbanion intermediate; (c) quinonoid/carbanion attack of the thioester; (d) formation of  $\beta$ -keto acid and CoASH release; (e) release of  $\text{CO}_2$  to form KDS product quinonoid; (f) reprotonation of KDS; (g) transamination to release KDS and restore the internal aldimine with PLP-bound to Lys265.

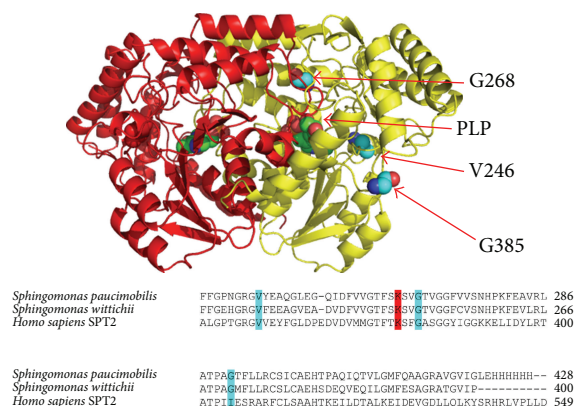


FIGURE 2: High resolution structure of *Sp* SPT homodimer PLP-L-serine external aldimine showing the position of the three hLCB2a HSN1 related mutations (PDB:2W8J). Each monomer is coloured (red and yellow). Sequence alignment of bacterial *Sp* SPT (Uniprot code: Q93UV0) with bacterial *Sw* SPT (Uniprot code: A5VD79) and human hLCB2a (Uniprot code: O15270). The key catalytic lysine residue (K265) involved in the formation of the internal aldimine is coloured red, and the HSN1 mutant mimics (V246M, G268V, and G385F) are coloured cyan.

of each subunit, hLCB1, hLCB2a, ssSPTa, or ssSPTb, was visualised by immunoblotting using antibodies directed against hLCB1, hLCB2a, and the HA epitope as previously described [18]. Yeast microsomal SPT activity was assayed by measuring [<sup>3</sup>H] serine incorporation into long chain bases as previously described [18].

**2.2.2. Bacterial SPT Gene Cloning and Mutagenesis.** The plasmid (pET 28a/*Sp* SPT) that we use to express *S. paucimobilis* SPT in *E. coli* was available at the start of this study and contains a six-histidine tag at the C-terminus [10]. This was used as a template, and all HSN1 mutations were made using the Liu and Naismith [43] mutagenesis protocol with the following primers:

5'CGGCATGTACGAGGCGCAAG 3' (V246M forward)

5'TCGTACATGCCGCGCCGTTG 3' (V246M reverse)

5'GGTCGTCACAGTCGGCGGCTTC 3' (G268V forward)

5'ACTGTGACGACCGATTGGAG 3' (G268V reverse)

5'CGGCCCTTACCTTCCTGCTG 3' (G385F forward)

5'AAGGTGAAGGCCGGGGTC 3' (G385F reverse).

The bases mutated are shown in bold and italic. The isolated mutants were verified by DNA sequencing and mass spectrometry analysis of the purified enzyme.

**2.2.3. Cloning and Expression of *Sphingomonas paucimobilis* SPT (*Sp* SPT) and HSN1 Mutant Mimics.** The *Sp* SPT enzyme was prepared as previously described [10]. A single colony pET28a *Sp* SPT was grown overnight at 37°C in LB selected with kanamycin (30 µg/mL) using *E. coli* BL21 (DE3) cells. The culture was diluted 1:100 into fresh LB/kanamycin solution and grown to an OD<sub>600</sub> of 0.6. Expression was induced with the addition of 0.1 mM isopropyl-β-D-1-thiogalactopyranoside (IPTG) and grown at 30°C, 200 rpm. Harvested cells were resuspended in lysis buffer, 20 mM potassium phosphate, pH 7.5, 150 mM NaCl, 10 mM imidazole, 25 µM PLP, and a protease inhibitor cocktail (Roche). Cells were lysed by sonication on ice (Soniprep 150, 15 cycles of 30 seconds on followed by 30 seconds off). The lysate was centrifuged for 25 minutes at 16,000 rpm. The resulting supernatant was incubated with preequilibrated Ni resin (Ni-NTA Superflow, Qiagen) for 1 hour at 4°C. The protein eluted with 300 mM imidazole and was further purified by gel filtration (S200 HR, GE Healthcare) using 20 mM potassium phosphate, pH 7.5, 150 mM NaCl, and 25 µM PLP buffer.

**2.2.4. Spectroscopic and Kinetic Measurements of Bacterial SPTs.** All UV-visible spectra were recorded on Cary 50 UV-visible spectrophotometer (Varian) and analysed using Cary WinUV software (Varian). Prior to all UV-visible spectroscopies and assays, SPT was dialysed against fresh buffers containing 250 µM PLP to ensure that the enzyme was in the PLP bound, holoform. Excess PLP was removed on a PD-10 (Sephadex G-25M) desalting column (GE Healthcare). For UV-visible assays the concentration of enzyme was 40 µM, and the spectrophotometer was blanked with 20 mM potassium phosphate (pH 7.5) containing 150 mM NaCl at 25°C. Quartz cuvettes from NSG Precision Cells, Type 18-BM, with a light path of 10 mm and a sample volume of 500 µL were used, and the spectra were collected from 800 nm to 200 nm. The release of CoASH from C16-CoASH during KDS formation was used to measure SPT activity as previously described [10]. Assays were performed on a 200 µL scale on a 96-well format in a Biotek Synergy HT plate reader. Kinetic constants were calculated using Michaelis-Menten kinetics and using GraphPad Prism 6 software.

**2.2.5. Bacterial SPT Enzyme Activity by Measuring KDS Formation.** SPT activity was also monitored by incorporation of [<sup>14</sup>C] L-serine into [<sup>14</sup>C]-KDS by a modification of a published method [10]. A final enzyme concentration of 25 µM SPT (in 20 mM potassium phosphate buffer, pH 7.5, and 150 mM NaCl) was incubated with 20 mM U-<sup>14</sup>C L-serine (7400 Bq, 0.2 µCi, PerkinElmer) and 250 µM palmitoyl-CoA in a final volume of 1 mL. The reaction was incubated at 37°C for 20 minutes, and then the reaction was quenched by the addition of NH<sub>4</sub>OH (final concentration 0.4 M). This was then extracted with an equal volume of CHCl<sub>3</sub>:CH<sub>3</sub>OH (2:1, v:v). The sample was centrifuged at 13,000 rpm for 5 minutes, and the aqueous phase was discarded. The organic phase was left to evaporate at 50°C. The resulting lipid residue was resuspended in 15 µL of CHCl<sub>3</sub>:CH<sub>3</sub>OH (2:1, v:v) and

spotted onto a Silica Gel 60 F<sub>254</sub> TLC plate. Separation was carried out with a mobile phase of CHCl<sub>3</sub>:CH<sub>3</sub>OH (2:1, v:v). The TLC plate was scanned with an AR-2000 imaging scanner and [<sup>14</sup>C]-labelled products quantified using the Laura 4 software (LabLogic).

**2.2.6. Determination of Dissociation Constants, Substrate and Product Quinonoid Detection, and SPT Activity Assays.** Binding assays typically contained 40 μM enzyme in 20 mM potassium phosphate (pH 7.5). Varying amounts of L-serine (0–40 mM) were added, and after addition of the substrate, the reaction mixture was allowed to equilibrate for 15 min at 25°C. The  $K_d$  values were calculated from plots of Δ425 versus L-serine concentrations by fitting to a hyperbolic saturation curve using Sigma Plot software

$$\Delta A_{\text{obs}} = \frac{\Delta A_{\text{max}} [\text{serine}]}{K_d + [\text{serine}]}, \quad (1)$$

where ΔA<sub>obs</sub> represents the observed change in absorbance at 425 nm, ΔA<sub>max</sub> is the maximal absorbance change, [serine] represents L-serine concentration, and the  $K_d$  is the dissociation constant. Also, the formation of the quinonoid intermediate was followed. In this case, 50 mM L-serine and 1.5 mM S-(2-oxoheptadecyl)-CoA were mixed to the enzyme (40 μM) [10, 32], and the reactants were allowed to equilibrate for 15 min at 25°C (data not shown).

### 3. Results

**3.1. Enzymatic Activity of Wild Type and HSAN1 hLCB2a Mutant SPT.** In the report of the hLCB2a-causing HSAN1 mutants (V359M, G382V, and I504F), Rotthier et al. expressed mutant hLCB2a subunits in human embryonic kidney (HEK 293) cells and measured microsomal SPT activity [39]. They noted that each mutation reduced enzyme activity (above background) by different amounts (~40–100% activity) compared with wild type. In 2009, Han and colleagues discovered small subunits of SPT (ssSPTa and ssSPTb) that when coexpressed with hLCB1 and hLCB2a increased human SPT activity by 50–100-fold [18]. These small subunit activators appear to play the same role as the small yeast protein Tsc3p also discovered by Gable and colleagues nearly ten years earlier [23]. To investigate the effect of the small subunits on the new HSAN1-associated hLCB2a mutants, we expressed each of the human mutant genes in yeast cells which had had the endogenous subunits of SPT knocked out. This strain, which completely lacks SPT activity, is not viable unless supplemented with a long chain base or a competent, active SPT complex. The yeast microsomes expressing wild-type hLCB1/hLCB2a in the absence of either small subunit displayed very low activity (<5 pmoles serine incorporated/min/mg protein) as predicted (Figure 3). Similarly, coexpression of each of the three HSAN1 hLCB2a mutants (V359M, G382V, and I504F) along with hLCB1 resulted in low activity, with G382V barely detectable above background mirroring the results reported by Rotthier and colleagues. Their activity values are in CPM (<sup>14</sup>C)/μg protein so they are difficult to be compared with ours in

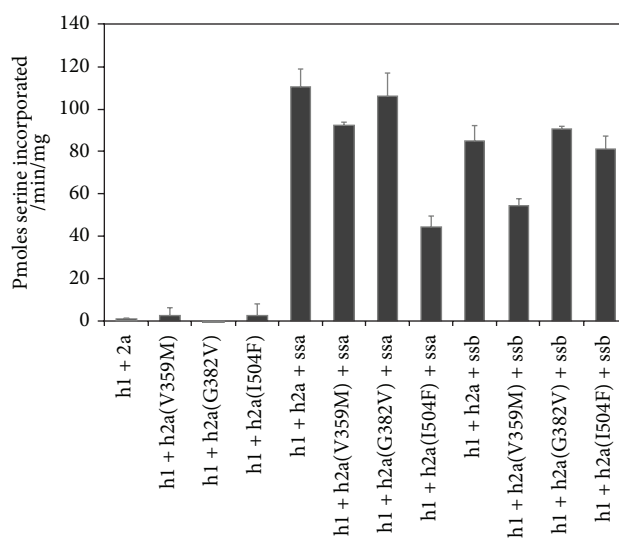


FIGURE 3: SPT activity in yeast microsomes expressing hLCB1 (h1) + hLCB2a (h2a, wt, or HSAN1 mutants) in the presence or absence of the small subunits ssSPTa (ssa) or ssSPTb (ssb).

absolute terms. When we coexpressed wild-type hLCB1 and hLCB2a in the presence of either ssSPTa or ssSPTb, the activity was indeed increased by 50–100-fold. Heterodimers containing the V359M and G382V mutant hLCB2a subunits were similarly activated by ssSPTa. In contrast heterodimers containing the I504 mutant hLCB2a subunit were activated to a lesser extent. When ssSPTb was expressed, heterodimers containing the G382V and I504F mutant hLCB2a subunits were activated to the same extent as wild-type heterodimers, but heterodimers containing the V359M mutant subunit were less well activated. Our interpretation of these data is that each of the new hLCB2a mutants had a small impact on SPT activity and that each mutant enzyme is still activated by the presence of the activating small subunits. The small impact of these new mutants is in contrast to the C133W, C133Y, and V144D mutations in hLCB1 but is similar to what was observed in the recently reported S331F mutation in hLCB1 [44].

**3.2. Expression and Purification of HSAN1 hLCB2a Mutant Mimics.** The three hLCB2a mutations that cause HSAN1 were individually introduced into the *Sp* SPT gene sequence (Figure 2), and the three mutant proteins were expressed using established protocols [10]. Two of the three mutants (*Sp* SPT V246M and G385F) were soluble. In contrast, the G268V mutant was found to be insoluble, and several attempts were made to improve the solubility of the protein (such as changing expression cell lines, induction at lower temperature, and different IPTG concentrations (data not shown)); however the majority of the protein remained in the cell pellet suggesting that this particular HSAN1 hLCB2a mutation leads to substantial protein misfolding of the bacterial mimic. The other two mutants (*Sp* SPT V246M and G385F) were obtained in milligram quantities and purified via nickel affinity chromatography as previously described for the wild-type SPT [10]. Both V246M and G385F behaved as



dimers by size exclusion chromatography (molecular weights ~90 kDa) and displayed elution profiles similar to wild-type SPT (data not shown).

**3.3. Spectroscopic Properties of WT SPT and HSAN1 Mutant Mimics.** Formation and breakdown of many of the intermediates within the SPT mechanism (Figure 1) can be monitored by UV-visible spectroscopy due to the yellow colour of the PLP-bound enzyme. Initial analysis of the *Sp* SPT V246M (Figure 4(b)) and G385F (Figure 4(c)) by UV-visible spectroscopy revealed that both HSAN1 mutants display spectra similar to wild-type SPT, with two absorbance maxima at around 335 and 420 nm (Figure 4(a)). These peaks are characteristic of the holo-, PLP-bound internal aldimine form of the enzyme, arising from the two tautomeric forms (enolimine and ketoenamine resp.) of PLP. These results confirm that both mutants were purified with the PLP cofactor covalently bound in the enzyme active site as an imine to Lys265. However, on closer inspection it is clear that there are subtle differences in the spectral profile of SPT G385F compared with the wild-type enzyme. In contrast to the wild-type SPT, the UV-visible spectrum of SPT G385F shows a significant blue shift with maximum absorbance values of 330 nm and 410 nm (Figure 4(c)). This suggests that mutation at position 385 has had an impact on the way the PLP cofactor binds at the active site.

The internal aldimine/PLP-bound form of SPT can be displaced with increasing concentrations of the substrate L-serine to form a SPT:PLP-L-serine external aldimine which can be easily monitored by observing the change in absorbance at 425 nm. Analysis of the wild-type SPT and both mutants led to the determination of the apparent L-serine dissociation constants ( $K_d^{\text{ser}}$ , Table 2). Binding studies were also carried out with L-alanine and glycine (data not shown). At physiological concentrations, L-serine was able to form the external aldimine in wild type and both mutant forms of SPT. Wild-type SPT binds L-serine with a  $K_d^{\text{ser}}$  of 1.1 mM (as obtained previously, Raman et al. [10]), and a similar  $K_d^{\text{ser}}$  value of 1.5 mM was obtained for the V246M mutant. This analysis supports the initial observation (based on UV-visible data) that PLP is bound in the same environment as that of the wild-type enzyme. In contrast, a  $K_d^{\text{ser}}$  of 4.7 mM was obtained for mutant G385F, a ~4-fold increase in comparison to the wild-type SPT, suggesting that this mutation has had some impact on both PLP and substrate binding. We have shown previously that the wild-type bacterial SPT is unable to use glycine or L-alanine as substrates to allow formation of deoxy-SLs to appreciable levels, and neither the V246M nor G385F mutant binds to L-alanine or glycine (data not shown).

**3.4. Kinetic Analysis and KDS Formation of SPT WT and HSAN1 Mutant Mimics.** In order to ascertain the effect that each of the HSAN1 hLCB2a mutant mimics has on enzyme catalysis, Michaelis-Menten kinetic analyses were performed for the wild-type V246M and G385F enzymes using a DTNB assay that monitors formation of the CoASH product (Figure 1). The wild-type SPT bound L-serine and palmitoyl-CoA (C16-CoA) with  $K_m$  values of 1.6 mM and 35.6  $\mu\text{M}$ ,

respectively (Table 2). The enzyme turned over with a  $k_{\text{cat}}$  of  $1.14 \text{ s}^{-1}$  and efficiency ( $k_{\text{cat}}/K_m$ ) of  $712 \text{ M}^{-1} \text{ s}^{-1}$  for L-serine and  $32022 \text{ M}^{-1} \text{ s}^{-1}$  for the acyl-CoA—all in good agreement with published values [10]. In contrast, we measured lower  $k_{\text{cat}}/K_m$  values of 176 and  $136 \text{ M}^{-1} \text{ s}^{-1}$  for L-serine (4- and 5-fold) and 3437 and  $7854 \text{ M}^{-1} \text{ s}^{-1}$  for C16-CoA (9- and 4-fold lower) and for the V246M and G385F mutants, respectively (Table 2). In addition, we monitored product KDS formation directly by using incorporation of  $^{14}\text{C}$  L-serine. Both mutants were less active and displayed 84% (V246M mutant) and 15% (G385F) KDS production relative to the wild-type SPT enzyme.

**3.5. Substrate Quinonoid Formation in SPT WT and HSAN1 Mutants.** The ability of the wild-type enzyme and mutants to generate a key carbanion/quinonoid species was tested using the C16-CoA thioether analogue, S-(2-oxoheptadecyl)-CoA. Addition of the analogue to the PLP-L-serine external aldimine form of the wild-type SPT led to the appearance of a peak at ~495 nm which is thought to be the substrate quinonoid [45]. Under the same conditions, both V246M and G385F generate a quinonoid peak confirming that these mutants can catalyse formation of this key intermediate (data not shown).

**3.6. Modelling the Structural Impact of HSAN1 Mutations.** Unfortunately, neither of the SPT V246M nor G385F HSAN1 mutant mimics crystallised (under the same conditions as wild type [7, 10] or by screening for new conditions). Therefore, to rationalise the impact that each of the HSAN1 hLCB2a mutations has on the structures of these altered enzymes, modelling was carried out based upon the crystal structure of holo-SPT (PDB:2JG2) [7] and the SPT:PLP-L-serine external aldimine complex (PDB:2W8J) [10]. It is worth noting that the PLP-binding site is at the subunit interface between the two monomers, and the active site is formed by residues from both subunits. We used the “mutagenesis” tool within PyMol [46] to replace the wild-type side chain with each mutant side chain and applied the default conformational constraints to produce a structural model. We chose to highlight interactions that were within 5 Å of each mutant residue of interest. The amide backbone of G268 makes polar contacts with the side chain of S97 and the backbone of F263 and most importantly the backbone of the crucial K265 residue involved in PLP binding (Figure 5). The model predicts that these polar contacts to S97 and F263 are maintained after inclusion of the isopropyl side chain of the G268V mutant; however, it loses the polar contact with the K265 residue. In addition to this, several new interactions are predicted to occur within 5 Å of the V268 mutant side chain in comparison to G268. The most interesting/important of these is the additional contact made with the backbone of M78 (from the same subunit) that leads to a severe steric clash with the side chain of V268. This interaction is not present in the wild-type structure and suggests that the bulky hydrophobic valine residue cannot be accommodated at this position. This structural change may well be the cause of the observed detrimental effect on protein solubility.

Position G385 is shown to be on the surface of SPT and solvent exposed (Figure 6). Mutation of this residue to F385



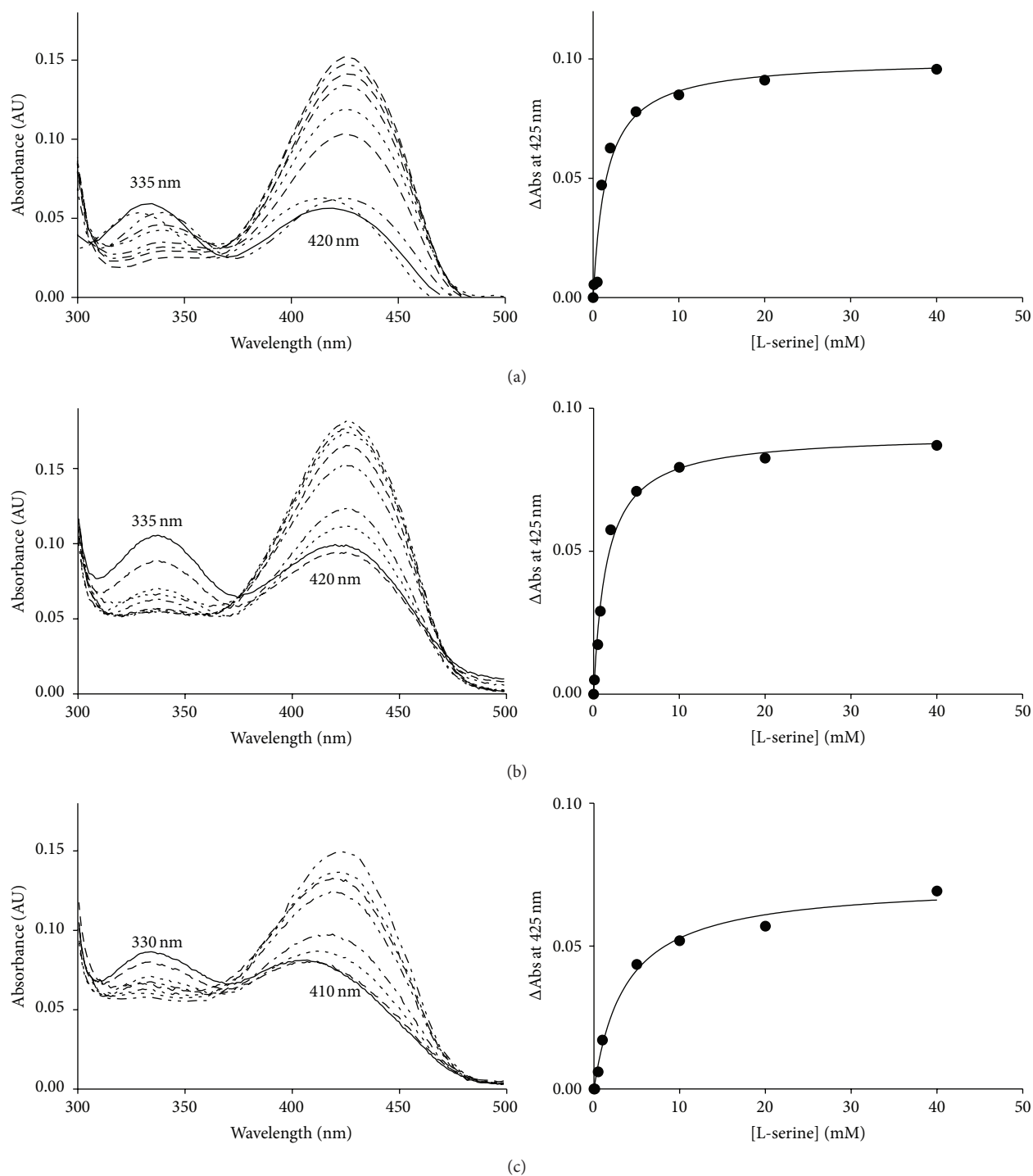


FIGURE 4: UV-visible analysis of *Sp* SPT wild-type and mutant mimics. Absorbance spectra of (a) *Sp* SPT wild type, (b) SPT V246M, and (c) SPT G385F. In the wild-type spectrum (a), the enolimine (335 nm) and ketoenamine (420 nm) forms of the external aldimine are shown. The solid line in each spectrum is the holoform of the enzyme (40  $\mu$ M SPT, 20 mM potassium phosphate buffer (pH 7.5), and 150 mM NaCl, 25°C). Increasing concentrations of L-serine were added (0, 0.5, 1, 2, 5, 10, 20, and 40 mM; dotted and dashed lines), and the spectrum was recorded after 15 minutes.

may result in this hydrophobic side chain preferring a buried hydrophobic pocket. G385 resides in an important, conserved SPT motif 379-PPATPAGTFLLR-390 that is known to undergo conformational change during the catalytic cycle.

Residue R378 is known to bind the carboxylate of the L-serine substrate in the PLP-L-serine external aldimine complex and to do so undergoes large movement brought about by the structural changes of the PPATP loop [10]. Mutation

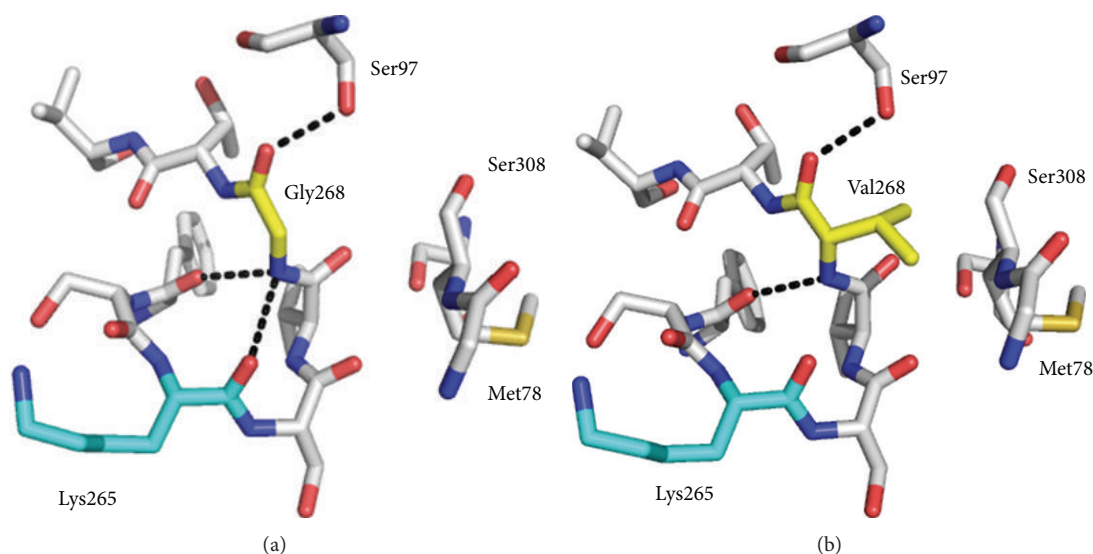


FIGURE 5: Structural models of the HSAN1 mutant mimic *Sp* SPT G268V using the *Sp* SPT PLP-L-serine external aldimine structure (PDB:2W8J). (a) Wild-type *Sp* SPT highlighting interactions within 5 Å of G268. (b) Mutated residue Val 268 showing new interactions within 5 Å. The models and figures were generated using PyMol software.

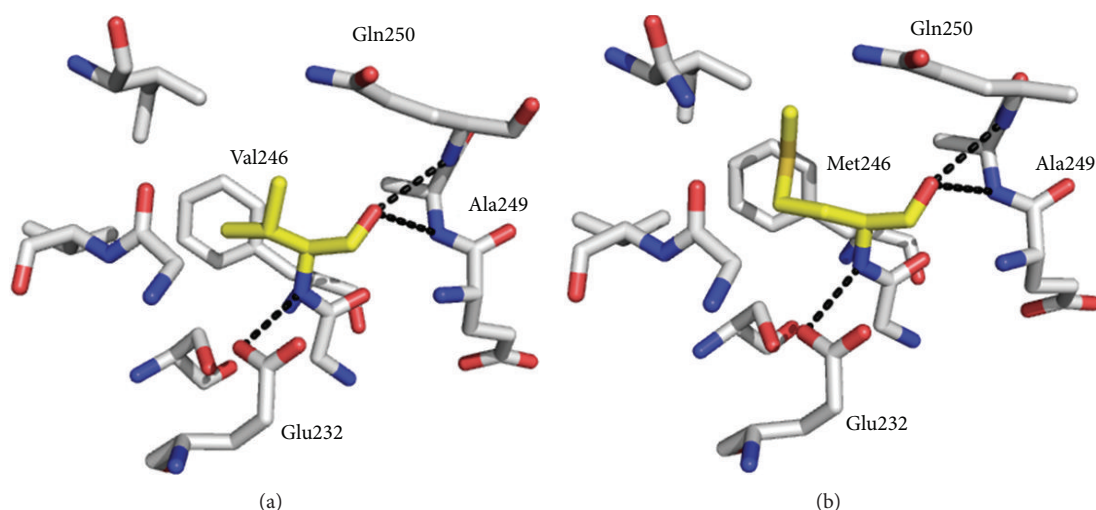


FIGURE 6: Structural models of HSAN1 mutant mimic *Sp* SPT V246M mutation using the *Sp* SPT-L-serine external aldimine structure (PDB:2W8J). (a) Wild-type V246. (b) Mutation of residue 246 to a methionine. Residue 246 is shown in yellow. The models and figures were generated using PyMol software.

of R378 impacts both substrate binding and catalysis; our model suggests that the introduction of F385 would alter the conformational flexibility of the enzyme. This is indeed the case since we observed a ~5-fold decrease in efficiency ( $k_{\text{cat}}/K_m^{\text{L-ser}}$ ) of the G385F mutant compared with wild type (Table 2).

The side chain of residue V246 is in a hydrophobic pocket in close proximity to F239 and V204, and the amide backbone makes polar contacts with the side chain of E232 and the backbone amides of A249 and Q250 (Figure 7). In the model, mutation of this residue to a methionine does not cause any severe alterations or clashes, and the M246 side chain is accommodated in the same pocket. Nevertheless, this mutation does have some impact on the palmitoyl-CoA

binding by reducing the  $K_m$  by ~4-fold and ( $k_{\text{cat}}/K_m^{\text{PCoA}}$ ) approximately by 9-fold.

#### 4. Discussion

HSANs are a rare group of disorders of the peripheral nervous system (PNS) [47]. They arise through a series of diverse genetic mutations and present a broad range of clinical symptoms. Overall, HSANs lead to neurodegeneration of the PNS, and the current working hypothesis is that HSAN1 is caused by mutations in subunits of SPT that impact the structure and function of the enzyme [29–31, 34, 48]. An appreciation of the complexity of the eukaryotic SPT enzyme has increased over the past 4–5 years with the identification of

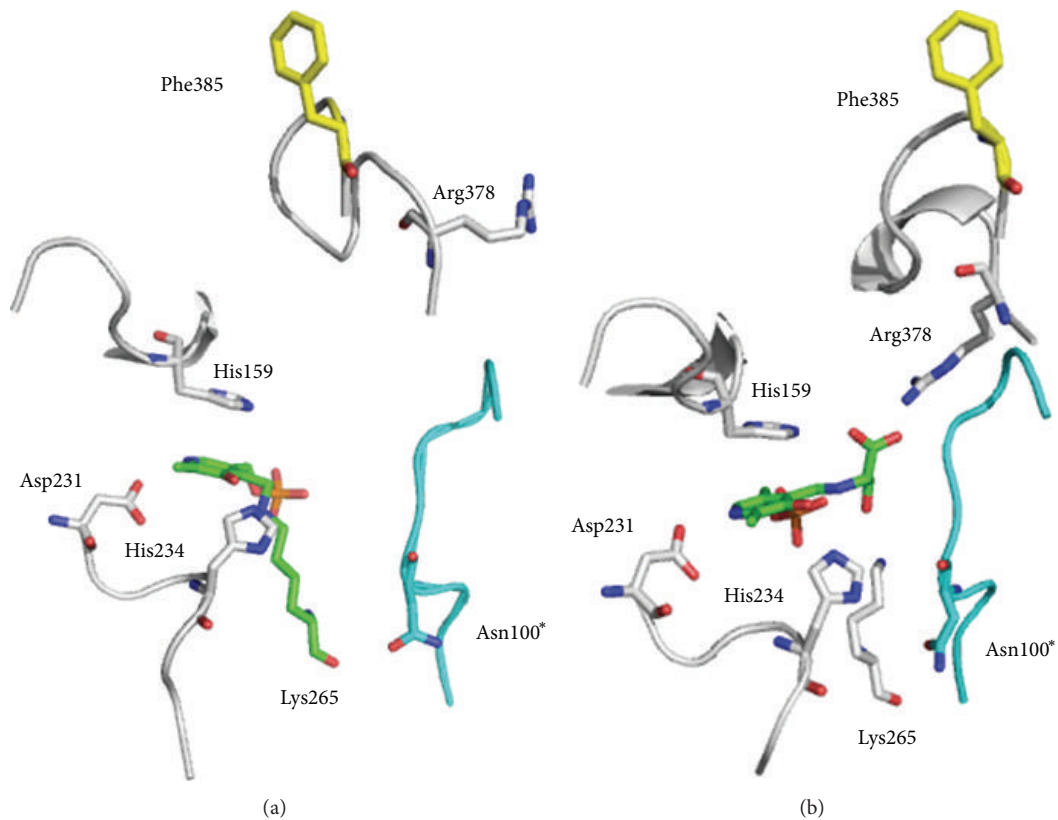


FIGURE 7: Structural models of the *Sp* SPT G385F mutant mimic. (a) *Sp* SPT holostructure (PDB:2JG2) and the L-serine external aldimine structure (PDB:2W8J). Residues from monomer one are shown in white, residues from monomer two are shown in teal, the PLP cofactor is shown in green, and the mutated glycine to phenylalanine residue is shown in yellow. The models and figures were generated using PyMol software.

TABLE 2: Kinetic parameters of wild-type *Sp* SPT and mutants.

Enzyme	$k_{\text{cat}} \times 10^{-2}$ (s <sup>-1</sup> )	$K_m^{\text{L-ser}}$ (mM)	$K_m^{\text{PCoA}}$ (μM)	$k_{\text{cat}}/K_m^{\text{L-ser}}$ (M <sup>-1</sup> s <sup>-1</sup> )	$k_{\text{cat}}/K_m^{\text{PCoA}}$ (M <sup>-1</sup> s <sup>-1</sup> )	$K_d^{\text{L-ser}}$ (mM)
SPT WT	114 ± 2.0	1.6 ± 0.09	35.6 ± 2.0	712	32022	1.1 ± 0.1
SPT V246M	44 ± 1.2	2.5 ± 0.2	128.0 ± 10.0	176	3437	1.5 ± 0.1
SPT G385F	41 ± 2.0	3.0 ± 0.5	52.2 ± 8.0	136	7854	4.7 ± 0.1
SPT G268V	—	—	—	—	—	—

new regulatory subunits (such as the small subunits ssSPTa and ssSPTb and the ORMs), but at its heart it requires the homologous subunits hLCB1 and hLCB2a which come together to form a heterodimeric core [24–26]. It is thought that, since hLCB2 contains residues that are conserved amongst other PLP-binding enzymes, it is essential for the covalent attachment of PLP and SPT catalyses, whereas hLCB1, which lacks the conserved residues, plays important roles in catalysis and regulation [6]. Mutations that knock out SPT activity all together are lethal emphasizing the importance of *de novo* SL biosynthesis. However, linkage analysis of patients/families with HSAN1 led to the identification of disease-causing mutations in the hLCB1 subunits of SPT [29, 30]. More recently additional disease-causing mutations have been found in hLCB1 [33, 36–38] as well as in the hLCB2a subunit [39]. Importantly, it was discovered that,

while mutations such as C133W and C133Y in hLCB1 greatly-reduced SPT activity, the pathophysiology of HSAN1 is most probably due to a gain of function that results in the ability to utilize alanine and/or glycine as substrates [29, 30]. Patients with the hLCB1 C133W/C133Y mutations generate deoxy-SLs (1-deoxy and 1-deoxymethyl) that are present in high concentrations compared to normal individuals. This was subsequently confirmed in mouse models of the disease [32, 49]. It is thought that these neurotoxic deoxy-SLs are built up over time to such concentrations that they lead to nerve damage and breakdown. Since these deoxy-SLs cannot be phosphorylated (to sphingosine 1-phosphate (S1P)), they cannot be degraded by the S1P lyase and accumulate in cells. The thinking is that different HSAN1 mutant SPTs (where either the hLCB1 or hLCB2a proteins are altered) have differing impacts on the activity with L-serine as a substrate, but where

there is a decrease, it is still above the threshold required for cell survival. More importantly, these mutations have differing influences on the promiscuity of the mutant enzyme such that it can also accept other amino acid substrates. A discussion of this interesting model by SPT experts at a symposium organised by a family afflicted by the disease (Deater Symposium, Boston, April 2008) also suggested that a potentially simple HSAN1 “cure (treatment)” would be increasing dietary serine thereby increasing the intracellular pool of L-serine to increase the ratio of serine/alanine thereby reducing the synthesis of the toxic deoxy-SLs. Indeed, this appears to be the case with the recent success of early clinical trials of oral L-serine supplementation that reduced deoxy-SL levels in serum and also led to an improvement in motor and sensory performance in mice [50].

Rotthier and colleagues presented data that the new HSAN1 hLCB2a mutants (V359M, G382V, and I504F) reduce SPT activity when expressed in HEK293 cells. They also measured the deoxy-SL levels in HEK293 cells and the lymphoblasts derived from HSAN1 patients carrying the G382V and I504F mutations. In both cases deoxy-SL levels were very high in agreement with the toxic SL hypothesis. We also wanted to measure the impact of the small subunits on the HSAN1 hLCB2a mutants. As well as activating basal SPT activity, the small subunits modulate the acyl-CoA chain-length specificity of the SPT [18]. We found that coexpression of either ssSPTa or ssSPTb increased basal activity of wild-type heterodimers and those containing all three hLCB2a mutants to varying degrees. In our recent paper we studied the kinetics of SPT containing the hLCB1<sup>C133W</sup> HSAN1 mutant subunit and found that it had similar affinity for L-serine as did wild-type SPT [31]. Surprisingly, the same was true for L-alanine indicating that the major impact of the C133W mutation is to enhance activation of the amino acid substrate for condensation with the acyl-CoA substrate. A similar kinetic analysis has not yet been done for the hLCB2a mutants. We do not discuss the ability of these new HSAN1 mutants to use glycine and/or L-alanine as substrates here as it requires a more detailed kinetic analysis of nine variables; the four subunits (SPT1/2 and ssSPTa/b) with five substrates (L-serine, glycine, L-alanine, and C14 and C16 acyl-CoAs), are the subject of current work. However, we felt that valuable insights would be gained by using the soluble bacterial SPT as a model to make mutant mimics. We previously studied the hLCB1 C133W mutant by mapping this residue to N100 of the *S. paucimobilis* SPT [10]. The side chain of N100 is close to but not in the active site of SPT, which lies at the subunit interface of the soluble bacterial homodimer. Nevertheless, it does contact the amide backbone of the key, conserved active site lysine (K265) that binds the PLP as an internal aldimine, and is also thought to act as the base that removes the proton from C- $\alpha$  of L-serine (Figure 1). Replacement of N100 with either the bulky tryptophan or tyrosine residue found in C133W and C133Y might be expected to be disruptive to the structure and activity of the homodimeric enzyme. Indeed, when we made the N100W and N100Y mutants, we noted that PLP binding was altered, and both the binding constants ( $k_m$ ) and catalytic activities ( $k_{cat}$ ) were lowered significantly compared to the

wild type. Moreover, we determined the crystal structure of the N100Y mutant in its PLP-L-serine external aldimine form, and a number of structural changes were observed; a key residue (Arg378) that binds the L-serine carboxylate was in the “swung out” conformation, the important PPATP loop was in a twisted conformation, and the side chain of the mutant mimic Y100 residue was now impacting the opposite subunit. This study revealed that mutations in one subunit can impact the overall structure and activity of the dimer and provided us with some insights as to how HSAN1 causing mutations may affect the human hLCB1/hLCB2a complex [10].

Two of the three new hLCB2a HSAN1 causing mutations (V359M and G382V) are found at residues that are strictly conserved in LCB2s from human, mouse, fly, rat, zebra fish, yeast, and bacterial SPT [39]. The third, I504, is less highly conserved; in fly (*Drosophila melanogaster*) it is a methionine, and in bacterial *Sp* SPT enzyme it is a glycine. The HSAN1 causing mutations in hLCB2a (V359M, G382V, and I504F) correspond to bacterial *Sp* SPT mutations V246M, G268V and G385F, respectively (Figure 2). G268 is three residues away from the essential active site residue K265 and in the 3D structure makes contact with the backbone of this residue. It was not surprising that introduction of G268V resulted in a drastic reduction in protein solubility, presumably due to misfolding during recombinant expression. Modelling studies reveal that this residue is also near to the side chain of residue N100 from the opposite subunit of the homodimer that we discussed above (Figure 5). In mutating G268 to valine, polar contacts to the K265 residue are lost. A plausible explanation for the misfolding of the G268V mutant is that it disrupts the polar contacts with the key lysine residue. The global fold of the protein could also be adversely affected by an apparent steric clash between the side chain of valine in position 268 and the backbone of Met78 (Figure 5(b)). In the initial report of the holo-*Sp* SPT structure by Yard et al., active site residues were identified, and G268 was also identified as an essential active site residue which hydrogen bonds with the backbone oxygen of K265 [7]. The G268V model predicts that this H-bond is lost and is therefore not surprising that this mutation has such a detrimental impact on the bacterial enzyme (Figure 5(b)).

In contrast to the G268V mutant, modelling studies do not give us clear insight as to the structural basis for the HSAN1 phenotype in the V246M or G385F mutants. These mutations appear to be more subtle. However, analysis of the PLP cofactor binding and enzyme kinetics of these two mutant mimics does provide some clue as to why these changes would cause alterations of the hLCB2a subunit that would lead to the HSAN1 phenotype. For the V246M mutant, structural models show that the V246 residue is far from the PLP active site, and polar contacts with E232, A249, and Q250 are retained after mutating the residue to a methionine (Figure 6). The UV-visible spectrum of this mutant is very similar to wild-type SPT and suggests that the PLP is bound in a similar orientation to the wild-type enzyme (Figure 4). The apparent  $K_d^{L-ser}$  is unchanged by the incorporation of the HSAN1 mutation, suggesting that, in this case, the key



L-serine external aldimine intermediate is formed in the same way as in the native SPT (Figure 1). However, this mutation does have a detrimental effect on the observed catalytic rate and efficiency, which again are 3-fold and 9-fold lower than wild-type enzyme (Table 2). This V246M mutant mimic also displays a significantly higher  $K_m$  for the acyl-CoA thioester substrate, suggesting that binding of this substrate is compromised at least subtly in this mutant. This is useful information about a residue potentially involved in binding the second substrate since, to date, we still do not have a structure of the *Sp* SPT PLP complex with palmitoyl-CoA bound.

In the structure of *Sp* SPT, residue G385 is surface-exposed (Figure 7). For the G385F mutant it is plausible that replacing glycine with the large, hydrophobic phenylalanine residue may lead it to adopt an alternative conformation. This has the potential to substantially affect the architecture of the surrounding structure, such as the important PPATP loop which undergoes large conformational changes during the catalytic mechanism. However, without crystallographic data for this mutant, it is impossible to confidently propose any effect of a potential realignment at this position. In the case of G385F, UV-visible analysis suggests that PLP binding is altered and that the cofactor is in a different environment compared to the wild-type enzyme. Furthermore, the apparent  $K_d^{L-ser}$  was ~5 times higher for this mutant indicating that serine binding is affected by this mutation (Table 2). Both the catalytic rate and catalytic efficiency are also significantly reduced (3-fold and 4-fold, resp.) demonstrating that catalysis is also impaired.

## 5. Conclusion

Our results have shed light on how the three recently-discovered HSN1 causing hLCB2a mutants affect the SPT complex in the presence of the activating small subunits (ssSPTa and ssSPTb). To explore the impact of these mutations on PLP binding, SPT structure, and activity, we also use mutants of the soluble homodimeric bacterial SPT as human SPT mimics to reveal that each mutant has a different impact on the enzyme. These range from subtle alterations to how PLP sits within the SPT active site, lowering substrate binding and catalytic activity through to a complete loss of solubility all brought about by a single change. New SPT mutations that result in HSN1 are being discovered periodically; for example, another on the hLCB2a subunit, A182P, was recently characterised that had reduced SPT activity, a higher preference for L-alanine, and increased plasma deoxy-SLs levels [42]. Exactly how these HSN1 mutations cause the human hLCB1/hLCB2a/ssSPT complex to lose its exquisite specificity for L-serine and also accept L-alanine and glycine to form deoxy-SLs will require in-depth structural and kinetic analyses of the purified wild-type and mutant SPT complexes.

## Abbreviations

SPT: Serine palmitoyltransferase  
PLP: Pyridoxal 5'-phosphate

SL: Sphingolipid  
LCB: Long chain base  
*Sp*: *Sphingomonas paucimobilis*  
HSAN1: Hereditary sensory and autonomic neuropathy type I  
ss: Small subunit  
AU: Absorbance unit.

## Acknowledgments

The authors thank the School of Chemistry, University of Edinburgh, and the Derek Stewart Charitable Trust for Ph.D. Student Funding (Ashley E. Beattie). Sita D. Gupta is supported by NIH Grant R01NS072446 (to Teresa M. Dunn) and USUHS Grants R071KD (to Teresa M. Dunn) and CO75PI (to Jeffrey M. Harmon). Work on the structure and mechanism of SPT in Dominic J. Campopiano's lab is supported by the BBSRC (BB/I013687/1), and the UK-USA collaboration is supported by BBSRC United States Partnering Award (BB/G53045X/1). Lenka Frankova thanks the Leverhulme Foundation for a Research Grant (F00158/CI). The authors thank Drs. David Clarke, Ken Gable, Gongshe Han, and Somashekarappa Niranjanakumari and Mr. John Wadsworth for helpful discussions.

## References

- [1] A. H. Futerman and Y. A. Hannun, "The complex life of simple sphingolipids," *EMBO Reports*, vol. 5, no. 8, pp. 777–782, 2004.
- [2] H. Fyrt and J. D. Saba, "An update on sphingosine-1-phosphate and other sphingolipid mediators," *Nature Chemical Biology*, vol. 6, no. 7, pp. 489–497, 2010.
- [3] A. H. Merrill Jr., "De novo sphingolipid biosynthesis: a necessary, but dangerous, pathway," *Journal of Biological Chemistry*, vol. 277, no. 29, pp. 25843–25846, 2002.
- [4] T. Kolter and K. Sandhoff, "Sphingolipid metabolism diseases," *Biochimica et Biophysica Acta*, vol. 1758, no. 12, pp. 2057–2079, 2006.
- [5] G. van Echten-Deckert and J. Walter, "Sphingolipids: critical players in Alzheimer's disease," *Progress in Lipid Research*, vol. 51, no. 4, pp. 378–393, 2012.
- [6] J. Lowther, J. H. Naismith, T. M. Dunn, and D. J. Campopiano, "Structural, mechanistic and regulatory studies of serine palmitoyltransferase," *Biochemical Society Transactions*, vol. 40, no. 3, pp. 547–554, 2012.
- [7] B. A. Yard, L. G. Carter, K. A. Johnson et al., "The structure of serine palmitoyltransferase; gateway to sphingolipid biosynthesis," *Journal of Molecular Biology*, vol. 370, no. 5, pp. 870–886, 2007.
- [8] H. Ikushiro, H. Hayashi, and H. Kagamiyama, "A water-soluble homodimeric serine palmitoyltransferase from *Sphingomonas paucimobilis* EY2395T strain: purification, characterization, cloning, and overproduction," *Journal of Biological Chemistry*, vol. 276, no. 21, pp. 18249–18256, 2001.
- [9] J. Lowther, G. Charmier, M. C. Raman, H. Ikushiro, H. Hayashi, and D. J. Campopiano, "Role of a conserved arginine residue during catalysis in serine palmitoyltransferase," *FEBS Letters*, vol. 585, no. 12, pp. 1729–1734, 2011.
- [10] M. C. C. Raman, K. A. Johnson, B. A. Yard et al., "The external aldimine form of serine palmitoyltransferase: structural, kinetic

- and spectroscopic analysis of the wild-type enzyme and HSAN1 mutant mimics," *Journal of Biological Chemistry*, vol. 284, no. 25, pp. 17328–17339, 2009.
- [11] Y. Shiraiwa, H. Ikushiro, and H. Hayashi, "Multifunctional role of His159 in the catalytic reaction of Serine palmitoyltransferase," *Journal of Biological Chemistry*, vol. 284, no. 23, pp. 15487–15495, 2009.
  - [12] R. Buede, C. Rinker-Schaffer, W. J. Pinto, R. L. Lester, and R. C. Dickson, "Cloning and characterization of LCB1, a Saccharomyces gene required for biosynthesis of the long-chain base component of sphingolipids," *Journal of Bacteriology*, vol. 173, no. 14, pp. 4325–4332, 1991.
  - [13] M. M. Nagiec, J. A. Baltisberger, G. B. Wells, R. L. Lester, and R. C. Dickson, "The LCB2 gene of Saccharomyces and the related LCB1 gene encode subunits of serine palmitoyltransferase, the initial enzyme in sphingolipid synthesis," *Proceedings of the National Academy of Sciences of the United States of America*, vol. 91, no. 17, pp. 7899–7902, 1994.
  - [14] C. Zhao, T. Beeler, and T. Dunn, "Suppressors of the Ca<sup>2+</sup>-sensitive yeast mutant (csg2) identify genes involved in sphingolipid biosynthesis. Cloning and characterization of SCS1, a gene required for serine palmitoyltransferase activity," *Journal of Biological Chemistry*, vol. 269, no. 34, pp. 21480–21488, 1994.
  - [15] T. Hornemann, S. Richard, M. F. Rütli, Y. Wei, and A. von Eckardstein, "Cloning and initial characterization of a new subunit for mammalian serine-palmitoyltransferase," *Journal of Biological Chemistry*, vol. 281, no. 49, pp. 37275–37281, 2006.
  - [16] M. M. Nagiec, R. L. Lester, and R. C. Dickson, "Sphingolipid synthesis: identification and characterization of mammalian cDNAs encoding the Lcb2 subunit of serine palmitoyltransferase," *Gene*, vol. 177, no. 1-2, pp. 237–241, 1996.
  - [17] B. Weiss and W. Stoffel, "Human and murine serine-palmitoyl-CoA transferase—cloning, expression and characterization of the key enzyme in sphingolipid synthesis," *European Journal of Biochemistry*, vol. 249, no. 1, pp. 239–247, 1997.
  - [18] G. Han, S. D. Gupta, K. Gable et al., "Identification of small subunits of mammalian serine palmitoyltransferase that confer distinct acyl-CoA substrate specificities," *Proceedings of the National Academy of Sciences of the United States of America*, vol. 106, no. 20, pp. 8186–8191, 2009.
  - [19] K. Hanada, T. Hara, and M. Nishijima, "Purification of the serine palmitoyltransferase complex responsible for sphingoid base synthesis by using affinity peptide chromatography techniques," *Journal of Biological Chemistry*, vol. 275, no. 12, pp. 8409–8415, 2000.
  - [20] S. Yasuda, M. Nishijima, and K. Hanada, "Localization, topology, and function of the LCB1 subunit of serine palmitoyltransferase in mammalian cells," *Journal of Biological Chemistry*, vol. 278, no. 6, pp. 4176–4183, 2003.
  - [21] T. Hornemann, Y. Wei, and A. von Eckardstein, "Is the mammalian serine palmitoyltransferase a high-molecular-mass complex?" *Biochemical Journal*, vol. 405, no. 1, pp. 157–164, 2007.
  - [22] T. Hornemann, A. Penno, M. F. Rütli et al., "The SPTLC3 subunit of serine palmitoyltransferase generates short chain sphingoid bases," *Journal of Biological Chemistry*, vol. 284, no. 39, pp. 26322–26330, 2009.
  - [23] K. Gable, H. Slife, D. Bacikova, E. Monaghan, and T. M. Dunn, "Tsc3p is an 80-amino acid protein associated with serine palmitoyltransferase and required for optimal enzyme activity," *Journal of Biological Chemistry*, vol. 275, no. 11, pp. 7597–7603, 2000.
  - [24] D. K. Breslow, S. R. Collins, B. Bodenmiller et al., "Orm family proteins mediate sphingolipid homeostasis," *Nature*, vol. 463, no. 7284, pp. 1048–1053, 2010.
  - [25] S. Han, M. A. Lone, R. Schneter, and A. Chang, "Orm1 and Orm2 are conserved endoplasmic reticulum membrane proteins regulating lipid homeostasis and protein quality control," *Proceedings of the National Academy of Sciences of the United States of America*, vol. 107, no. 13, pp. 5851–5856, 2010.
  - [26] D. K. Breslow and J. S. Weissman, "Membranes in balance: mechanisms of sphingolipid homeostasis," *Molecular Cell*, vol. 40, no. 2, pp. 267–279, 2010.
  - [27] M. Liu, C. Huang, S. R. Polu, R. Schneter, and A. Chang, "Regulation of sphingolipid synthesis through Orm1 and Orm2 in yeast," *Journal of Cell Science*, vol. 125, part 10, pp. 2428–2435, 2012.
  - [28] F. M. Roelants, D. K. Breslow, A. Muir, J. S. Weissman, and J. Thorner, "Protein kinase Ypk1 phosphorylates regulatory proteins Orm1 and Orm2 to control sphingolipid homeostasis in Saccharomyces cerevisiae," *Proceedings of the National Academy of Sciences of the United States of America*, vol. 108, no. 48, pp. 19222–19227, 2011.
  - [29] K. Bejaoui, C. Wu, M. D. Scheffler et al., "SPTLC1 is mutated in hereditary sensory neuropathy, type 1," *Nature Genetics*, vol. 27, no. 3, pp. 261–262, 2001.
  - [30] J. L. Dawkins, D. J. Hulme, S. B. Brahmabhatt, M. Auer-Grumbach, and G. A. Nicholson, "Mutations in SPTLC1, encoding serine palmitoyltransferase, long chain base subunit-1, cause hereditary sensory neuropathy type 1," *Nature Genetics*, vol. 27, no. 3, pp. 309–312, 2001.
  - [31] K. Gable, S. D. Gupta, G. Han, S. Niranjanakumari, J. M. Harmon, and T. M. Dunn, "A disease-causing mutation in the active site of serine palmitoyltransferase causes catalytic promiscuity," *Journal of Biological Chemistry*, vol. 285, no. 30, pp. 22846–22852, 2010.
  - [32] A. Penno, M. M. Reilly, H. Houlden et al., "Hereditary sensory neuropathy type 1 is caused by the accumulation of two neurotoxic sphingolipids," *Journal of Biological Chemistry*, vol. 285, no. 15, pp. 11178–11187, 2010.
  - [33] A. Rothier, A. Penno, B. Rautenstrauss et al., "Characterization of two mutations in the SPTLC1 subunit of serine palmitoyltransferase associated with hereditary sensory and autonomic neuropathy type I," *Human Mutation*, vol. 32, no. 6, pp. E2211–E2225, 2011.
  - [34] K. Bejaoui, Y. Uchida, S. Yasuda et al., "Hereditary sensory neuropathy type 1 mutations confer dominant negative effects on serine palmitoyltransferase, critical for sphingolipid synthesis," *Journal of Clinical Investigation*, vol. 110, no. 9, pp. 1301–1308, 2002.
  - [35] K. Gable, G. Han, E. Monaghan et al., "Mutations in the yeast LCB1 and LCB2 genes, including those corresponding to the hereditary sensory neuropathy type I mutations, dominantly inactivate serine palmitoyltransferase," *Journal of Biological Chemistry*, vol. 277, no. 12, pp. 10194–10200, 2002.
  - [36] B. Rautenstrauss, B. Neitzel, C. Muench, J. Haas, E. Holinski-Feder, and A. Abicht, "Late onset hereditary sensory neuropathy type 1 (Hsn1) caused by a novel P.C133r missense mutation in Sptlc1," *Journal of the Peripheral Nervous System*, vol. 14, pp. 124–125, 2009.
  - [37] A. Rothier, J. Baets, E. De Vriendt et al., "Genes for hereditary sensory and autonomic neuropathies: a genotype-phenotype correlation," *Brain*, vol. 132, part 10, pp. 2699–2711, 2009.

- [38] M. Auer-Grumbach, H. Bode, T. R. Pieber et al., "Mutations at Ser331 in the HSN type I gene SPTLC1 are associated with a distinct syndromic phenotype," *European Journal of Medical Genetics*, vol. 56, no. 5, pp. 266–269, 2013.
- [39] A. Roththier, M. Auer-Grumbach, K. Janssens et al., "Mutations in the SPTLC2 subunit of serine palmitoyltransferase cause hereditary sensory and autonomic neuropathy type I," *American Journal of Human Genetics*, vol. 87, no. 4, pp. 513–522, 2010.
- [40] T. Hornemann, A. Penno, S. Richard et al., "A systematic comparison of all mutations in hereditary sensory neuropathy type I (HSAN I) reveals that the G387A mutation is not disease associated," *Neurogenetics*, vol. 10, no. 2, pp. 135–143, 2009.
- [41] K. Verhoeven, K. Coen, E. De Vriendt et al., "SPTLC1 mutation in twin sisters with hereditary sensory neuropathy type I," *Neurology*, vol. 62, no. 6, pp. 1001–1002, 2004.
- [42] S. M. Murphy, D. Ernst, Y. Wei et al., "Hereditary sensory and autonomic neuropathy type 1 (HSAN1) caused by a novel mutation in SPTLC2," *Neurology*, vol. 80, no. 23, pp. 2106–2111, 2013.
- [43] H. Liu and J. H. Naismith, "An efficient one-step site-directed deletion, insertion, single and multiple-site plasmid mutagenesis protocol," *BMC Biotechnology*, vol. 8, article 91, 2008.
- [44] J. M. Harmon, D. Bacikova, K. Gable et al., "Topological and functional characterization of the ssSPTs, small activating subunits of serine palmitoyltransferase," *Journal of Biological Chemistry*, vol. 288, no. 14, pp. 10144–10153, 2013.
- [45] H. Ikushiro, S. Fujii, Y. Shiraiwa, and H. Hayashi, "Acceleration of the substrate C $\alpha$  deprotonation by an analogue of the second substrate palmitoyl-CoA in serine palmitoyltransferase," *Journal of Biological Chemistry*, vol. 283, no. 12, pp. 7542–7553, 2008.
- [46] W. L. DeLano, *The PyMol Molecular Graphics System*, DeLano Scientific, San Carlos, Calif, USA, 2002.
- [47] A. Roththier, J. Baets, V. Timmerman, and K. Janssens, "Mechanisms of disease in hereditary sensory and autonomic neuropathies," *Nature Reviews Neurology*, vol. 8, no. 2, pp. 73–85, 2012.
- [48] G. A. Nicholson, J. L. Dawkins, I. P. Blair, M. Auer-Grumbach, S. B. Brahmabhatt, and D. J. Hulme, "Hereditary sensory neuropathy type I: haplotype analysis shows founders in southern England and Europe," *American Journal of Human Genetics*, vol. 69, no. 3, pp. 655–659, 2001.
- [49] F. S. Eichler, T. Hornemann, A. McCampbell et al., "Overexpression of the wild-type SPT1 subunit lowers desoxysphingolipid levels and rescues the phenotype of HSAN1," *Journal of Neuroscience*, vol. 29, no. 46, pp. 14646–14651, 2009.
- [50] K. Garofalo, A. Penno, B. P. Schmidt et al., "Oral L-serine supplementation reduces production of neurotoxic deoxysphingolipids in mice and humans with hereditary sensory autonomic neuropathy type 1," *Journal of Clinical Investigation*, vol. 121, no. 12, pp. 4735–4745, 2011.

## Research Article

# Characterization of C-S Lyase from *C. diphtheriae*: A Possible Target for New Antimicrobial Drugs

Alessandra Astegno,<sup>1</sup> Alejandro Giorgetti,<sup>1</sup> Alessandra Allegrini,<sup>1</sup>  
Barbara Cellini,<sup>2</sup> and Paola Dominici<sup>1</sup>

<sup>1</sup> Department of Biotechnology, University of Verona, 15 Strada Le Grazie, 37134 Verona, Italy

<sup>2</sup> Department of Life Sciences and Reproduction, University of Verona, 8 Strada Le Grazie, 37134 Verona, Italy

Correspondence should be addressed to Paola Dominici; [paola.dominici@univr.it](mailto:paola.dominici@univr.it)

Received 5 June 2013; Accepted 16 July 2013

Academic Editor: Alessandro Paiardini

Copyright © 2013 Alessandra Astegno et al. This is an open access article distributed under the Creative Commons Attribution License, which permits unrestricted use, distribution, and reproduction in any medium, provided the original work is properly cited.

The emergence of antibiotic resistance in microbial pathogens requires the identification of new antibacterial drugs. The biosynthesis of methionine is an attractive target because of its central importance in cellular metabolism. Moreover, most of the steps in methionine biosynthesis pathway are absent in mammals, lowering the probability of unwanted side effects. Herein, detailed biochemical characterization of one enzyme required for methionine biosynthesis, a pyridoxal-5'-phosphate (PLP-) dependent C-S lyase from *Corynebacterium diphtheriae*, a pathogenic bacterium that causes diphtheria, has been performed. We overexpressed the protein in *E. coli* and analyzed substrate specificity, pH dependence of steady state kinetic parameters, and ligand-induced spectral transitions of the protein. Structural comparison of the enzyme with cystalysin from *Treponema denticola* indicates a similarity in overall folding. We used site-directed mutagenesis to highlight the importance of active site residues Tyr55, Tyr114, and Arg351, analyzing the effects of amino acid replacement on catalytic properties of enzyme. Better understanding of the active site of *C. diphtheriae* C-S lyase and the determinants of substrate and reaction specificity from this work will facilitate the design of novel inhibitors as antibacterial therapeutics.

## 1. Introduction

The emergence of resistance to antibacterial agents is a pressing concern for human health. New drugs to combat this problem are therefore in great demand. Acquired bacterial resistance has caused several antibiotics to become useless or, at best, compromised in their ability to counteract bacterial infection [1]. The potential of amino acid biosynthesis as an antimicrobial target has been validated both chemically and biochemically [2]. Methionine represents a key amino acid in prokaryotes and it is an attractive antimicrobial target because of its important role in cell metabolism. Methionine, in the form of S-adenosylmethionine, is the methyl donor for a number of essential biochemical reactions. The biosynthesis of methionine is therefore of vital importance to microbial growth. This has been validated by the fact that several natural products, including 2-amino-5-hydroxy-4-oxopentanoic acid [3], azoxybacilin [4], and rhizoctin [5],

target important enzymes for methionine biosynthesis and have antimicrobial properties. Moreover, most of the steps in the methionine biosynthesis pathway are unique to bacteria and plants.

We have studied one of the enzymes required for methionine biosynthesis, namely, NCBI protein NP\_940074, which has been annotated as a pyridoxal-5'-phosphate (PLP-) dependent C-S lyase from *Corynebacterium diphtheriae*, a pathogenic bacterium that causes diphtheria. The threat of diphtheria, even in countries with good coverage in childhood immunization programs by vaccination, has not disappeared and outbreaks in many European countries have revealed a phenomenon of decreasing immunity to diphtheria among adults [6]. The treatment of diphtheria patients is based on administration of antibiotics to eliminate the corynebacteria from the site of infection, thus stopping ongoing toxin production with or without additional treatment with specific immunoglobulins [7]. Thus, while diphtheria



antitoxin (DAT) contributes to reducing the case fatality rates of infections due to this microorganism, it is unlikely, in the foreseeable future, that it will substantially reduce the world's consumption of antimicrobial agents. This highlights the importance of the development of new antibacterial drugs.

C-S lyase catalyzes the  $\alpha,\beta$ -elimination of sulfur-containing amino acids, such as L-cystathionine (L-Cth), to generate ammonia, pyruvate, and homocysteine, the penultimate step in methionine biosynthesis transsulfuration pathway. The crystal structure of *C. diphtheriae* C-S lyase has been determined by X-ray crystallography at 1.99 Å resolution (PDB code: 3FDB, Joint Center for Structural Genomics, <http://www.jcsg.org/>). According to its folding pattern, the enzyme belongs to the fold type I family of the PLP-dependent enzymes [8]. The commonly known fold type I PLP-dependent enzymes have an aromatic amino acid residue located at the *re* face of the PLP-Lys internal aldimine and stacking with the pyridine ring of PLP. The structure shows that a conserved binding site for PLP which is covalently linked to Lys222 has a stacking interaction with Tyr114 and H-bond interaction with Asn160, Asp188, and His191. There is one molecule in each asymmetric unit (PDB code: 3FDB). Although the crystal structure has been solved, no protein characterization and structure-based design studies have been reported to date.

The availability of the protein in purified form has allowed us to obtain an insight into the biochemical properties of the enzyme by thorough characterization of its kinetic and spectral properties. With increasing resistance of bacteria to common antibiotics, C-S lyase appears to be an interesting novel target for the development of specific inhibitors against the pathogen *C. diphtheriae*.

## 2. Materials and Methods

**2.1. Chemicals.** PLP, L-cystathionine, L-cystine, L-cysteine, L-djenkolic acid, L-serine, aminoethyl-L-cysteine, O-acetyl-L-serine, L-homoserine, L-methionine, phenylhydrazine hydrochloride, NADH, pyruvate, rabbit muscle L-lactic dehydrogenase, 5,5'-dithiobis-(2-nitrobenzoic acid), isopropyl  $\beta$ -D-thiogalactoside, and the gel filtration molecular mass marker kit were obtained from Sigma. Chromatographic columns were from GE Healthcare, synthetic oligonucleotides were from Invitrogen, and the QuikChange site-directed mutagenesis kit was from Stratagene. pSpeedET-NP\_940074 vector was obtained from DNASU/PSI: Biology-MR plasmid repository at the Biodesign Institute at Arizona State University [9, 10]. All other chemicals were the highest grade commercially available.

**2.2. Enzyme Purification.** Expression of the protein was carried out using the pSpeedET-NP\_940074 vector by growing freshly transformed *E. coli* BL21(DE3) cells in LB medium. Cell cultures were grown at 37°C with vigorous shaking to an OD of 0.6 at 600 nm. The temperature was then lowered to 23°C and, after induction with 0.5 mM isopropyl- $\beta$ -D-1-thiogalactopyranoside (IPTG), cells were grown for 16 h, harvested by centrifugation, resuspended in extraction buffer (20 mM sodium phosphate pH 7.5, 200 mM sodium

chloride, and 10 mM imidazole), and lysed by sonication. The cell debris was removed by centrifugation (20,000×g for 30 min) and the supernatant was loaded onto an Ni-affinity column equilibrated with 20 mM sodium phosphate at pH 7.5, 200 mM sodium chloride, and 10 mM imidazole. The imidazole concentration was increased stepwise, first to 30 mM to remove nonspecifically bounded proteins, and then to 500 mM to elute the enzyme. Monomer concentration was determined from the calculated extinction coefficient ( $\epsilon_{280\text{ nm}} = 65048\text{ M}^{-1}\text{ cm}^{-1}$ ; <http://web.expasy.org/protparam/>). PLP content of holoenzyme was determined by releasing the coenzyme in 0.1 M NaOH and by using  $\epsilon_{388\text{ nm}} = 6600\text{ M}^{-1}\text{ cm}^{-1}$ . The yield from a standard purification was approximately 25 mg/L culture. The protein was stable at -80°C for many months and freezing and thawing did not alter the activity of the isolated enzyme.

**2.3. Site-Directed Mutagenesis.** Point mutants were made on the wild type construct pSpeedET-NP\_940074 using the QuikChange site-directed mutagenesis kit (Stratagene), following the manufacturer's protocols. For each mutant, two synthetic oligonucleotide primers were designed, each was complementary to the opposite strands of the plasmid and contained the desired mutation. The coding region of all mutated plasmids was verified by DNA sequencing. *E. coli* strain BL21(DE3) cells were transformed and used for expression. The conditions for expression and purification of the mutants were as described for the wild type enzyme.

**2.4. Enzyme Activity Assays.** Activity was measured at 30°C on a Jasco-V560 UV-Vis spectrophotometer. The assay buffer was composed of 50 mM MOPS, 50 mM bicine, 50 mM proline pH 9.0, and 20  $\mu$ M PLP. Reactions were initiated by the addition of 1  $\mu$ M enzyme. The activity of C-S lyase toward L-Cth was detected via two spectrophotometric assays by using the reaction of 5,5'-dithiobis-(2-nitrobenzoic acid) (DTNB) with the free thiol of the L-homocysteine product ( $\epsilon_{412\text{ nm}} = 13600\text{ M}^{-1}\text{ cm}^{-1}$ ) and by monitoring pyruvate formation with the coupling enzyme NADH-dependent lactate dehydrogenase (LDH) which reduces the pyruvate product to lactate, with the concomitant conversion of NADH to NAD<sup>+</sup> ( $\epsilon_{340\text{ nm}} = 6200\text{ M}^{-1}\text{ cm}^{-1}$ ). The LDH assay was also employed to monitor C-S lyase activity toward other substrates.

Initial velocity data obtained by varying substrate concentrations were fitted to the hyperbolic form of the Michaelis-Menten equation

$$\frac{v}{E_t} = \frac{k_{\text{cat}}S}{(K_m + S)}. \quad (1)$$

In the case of deviations from hyperbolic kinetics, initial velocity data obtained by varying substrate concentrations were fitted to a nonhyperbolic curve to (2) that takes into account substrate inhibition, that is, binding of a second molecule of substrate to the ES complex to form an inactive ternary complex SES [11]:

$$\frac{v}{E_t} = \frac{k_{\text{cat}}}{1 + (K_m/S) + (S/K_i)}, \quad (2)$$

where  $E_t$  is the total enzyme concentration,  $k_{\text{cat}}$  is the maximum velocity,  $S$  is the substrate concentration,  $K_m$  is the

apparent Michaelis-Menten constant, and  $K_i$  is the dissociation constant for the inhibitory SES ternary complex.

**2.5. Evaluation of the pH Dependence.** The pH dependence for C-S lyase towards L-Cth and L-cysteine was determined using both DTNB and LDH assays in 50 mM MOPS, 50 mM bicine, 50 mM proline, and 20  $\mu$ M PLP. Kinetic measurements were carried out between pH 7.8 and 10.3. The values for  $\log k_{cat}/K_m$  as a function of pH were fitted to the appropriate equations:

$$\log Y = \log \frac{C}{1 + (H/K_A)}, \quad (3)$$

$$\log Y = \log \frac{C}{1 + (H/K_A) + (K_B/H)}, \quad (4)$$

where  $K_A$  and  $K_B$  represent the ionization constants for enzyme or reactant functional group,  $Y$  is the value of the parameter observed as a function of pH, and  $C$  is the pH-independent value of  $Y$ . All data were fitted to the previous equations using the Origin8 program (OriginLab).

**2.6. Spectroscopic Measurements.** Absorption measurements were carried out on a Jasco-V560 UV-Vis spectrophotometer, using 10  $\mu$ M enzyme in a buffer solution containing 50 mM MOPS, 50 mM bicine, and 50 mM proline pH 8.5.

Fluorescence spectra were obtained with a Jasco FP8200 spectrofluorometer using 5 nm bandwidths on both sides at a protein concentration varying from 1 to 10  $\mu$ M in a solution containing 20 mM Bis-Tris propane pH 8.5. Spectra of blanks, that is of samples containing all component except the lyase, were taken immediately prior to the measurements of samples containing protein. Blank spectra were subtracted from spectra of samples containing enzyme.

CD measurements were carried out on a Jasco J-710 spectropolarimeter using 1 mg/mL enzyme in a buffer solution containing 50 mM Tris-HCl pH 8.5. For near-UV and visible wavelengths, three automatically averaged spectra were recorded in a cuvette with a 1 cm path length at a scan speed of 50 nm/min.

**2.7. Preparation and Reconstitution of Apoenzyme.** The coenzyme PLP was removed as a phenylhydrazone following the protocol in [12]. After the removal of the cofactor, C-S lyase exhibited no residual activity and no absorption peak at 413 nm. Titration of the apoenzyme with PLP was carried out at equilibrium by measuring the fluorescence emission at 500 nm ( $\lambda_{exc} = 413$  nm) after incubation of apoprotein (5  $\mu$ M) with various concentrations of the cofactor (0–100  $\mu$ M) at 25°C for 15 min in 20 mM Bis-Tris propane pH 8.5. The increase in fluorescence emission at 500 nm was dependent on added PLP and the values were used to calculate the  $K_d^{PLP}$  according to a tight-binding hypothesis (5):

$$F_{500} = \Delta F_{max} \frac{e_0 + l_0 + K_d - \sqrt{[(e_0 + l_0 + K_d)^2 - 4e_0l_0]}}{2e_0}, \quad (5)$$

where  $e_0$  and  $l_0$  are the total concentrations of C-S lyase subunit and PLP, respectively,  $K_d$  is the equilibrium dissociation

constant for the encounter complex, and  $\Delta F_{max}$  represents the fluorescence change at 500 nm recorded in the presence of an excess of PLP over apoprotein. The reconstituted enzyme completely recovered its original activity.

**2.8. Size Exclusion Chromatography.** The molecular weight of recombinant enzyme was monitored by analytical size exclusion chromatography (Superdex 200 HR 10/30) using ÄKTA FPLC system (GE Healthcare). The chromatography was performed using 20 mM sodium phosphate buffer pH 7.2 and 150 mM NaCl as the mobile phase, at a flow rate of 0.1 mL/min. The calibration curve was determined with gel filtration molecular weight standards containing bovine thyroglobulin (669 kDa), apoferritin (443 kDa),  $\beta$ -amylase (200 kDa), alcohol dehydrogenase (150 kDa), bovine serum albumin (66 kDa), carbonic anhydrase (29 kDa), and cytochrome c (12.4 kDa). The curve was linear between 12.4 and 669 kDa.

**2.9. Structural Similarity Analysis.** The structure of the C-S lyase in complex with the PLP-aminoethoxyvinylglycine (AVG) was obtained by optimal superposition of the main chain of the C-S lyase (PDB code: 3FDB) and the structure of the cystalysin from *Treponema denticola* (PDB code: 1C7O) as in [13].

### 3. Results

Recombinant C-S lyase was purified as a His-tagged protein to greater than 99% purity as confirmed by SDS-PAGE; the size of the protein, calculated with a molecular size marker, was about 44 kDa that corresponds well to the molecular mass elucidated from the sequence information. As determined by gel filtration, an apparent molecular mass of 85 kDa was calculated for the native enzyme. Therefore, these results indicate that, as suggested by interface interaction, recombinant C-S lyase from *C. diphtheriae* is a homodimer.

**3.1. Spectral Properties of Recombinant C-S Lyase.** The visible absorption spectrum of the native enzyme is dominated by a band centered around 413 nm (Figure 1). This peak indicates that the predominant tautomer of the internal aldimine is the ketoenamine, and the imine nitrogen of the cofactor is protonated allowing the formation of an intramolecular hydrogen bond with the 3'-oxygen atom of PLP and the conjugation of the  $\pi$  system of the imine with the pyridine ring [14, 15].

The intensity of the band did not change in the pH range from 6 to 11, indicating a  $pK_a$  of the internal aldimine higher than 11. The observed ratio  $A_{280\text{ nm}}/A_{413\text{ nm}}$  was  $\sim 8$ . The stoichiometric ratio of PLP to enzyme was calculated from the  $A_{388\text{ nm}}$  of the free cofactor, which was released upon incubation of the native holoenzyme in 0.1 M NaOH. By this method, a PLP content of 2 mol/mol of the native dimer was found.

As shown in Figure 2(a), the CD spectrum of the enzyme displays a positive dichroic band at 415 nm whose intensity does not change with pH. The near-UV spectrum is characterized by pronounced negative dichroic bands in the aromatic region at 260–296 nm, which would indicate the

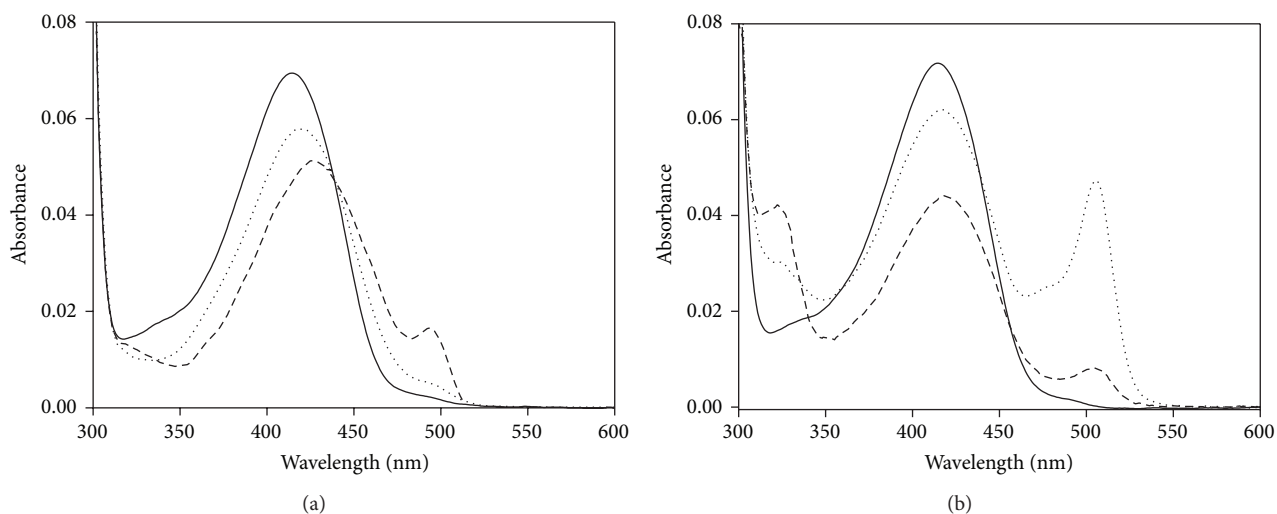


FIGURE 1: Absorption spectra of C-S lyase in the presence of substrates and substrate analogues. (a) Absorption spectra of 10  $\mu$ M C-S lyase in the absence (solid line) and presence of 100 mM L-serine (dashed line) and 100 mM O-acetyl-L-serine (dotted line). The spectra were subtracted from pyruvate absorbance. Pyruvate concentration was evaluated by a coupled LDH assay (see Section 2). (b) Absorption spectra of 10  $\mu$ M C-S lyase in the absence (solid line) and presence of 450 mM L-homoserine (dotted line) and 150 mM L-methionine (dashed line). All spectra were recorded in a solution containing 50 mM MOPS, 50 mM bicine, and 50 mM proline pH 8.5.

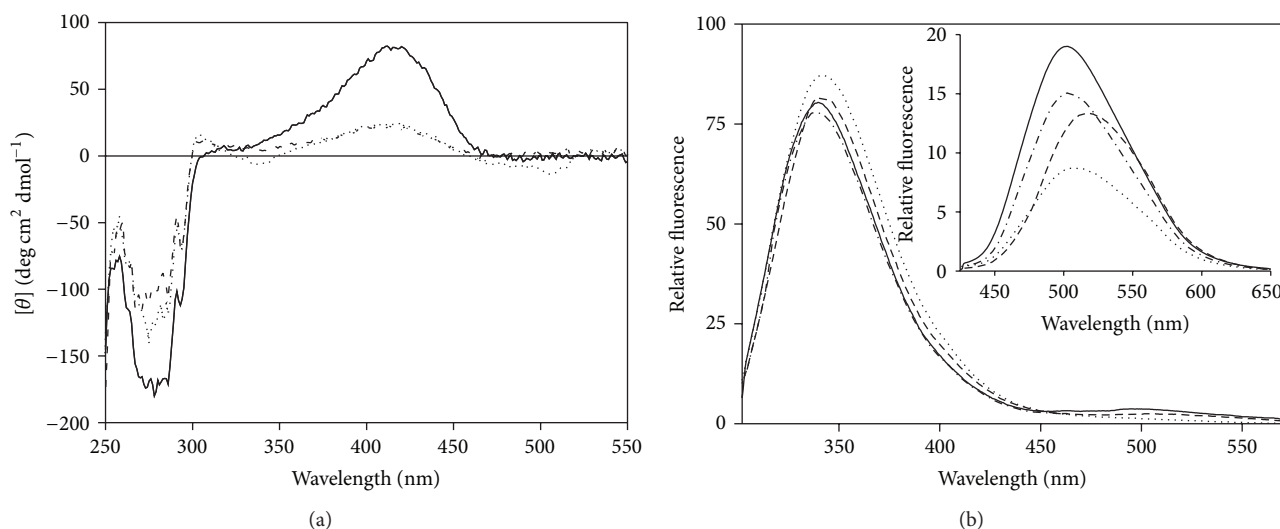


FIGURE 2: CD and fluorescence emission spectra of C-S lyase in the presence of substrates and substrate analogues. (a) CD spectra of enzyme (solid line) in the presence of 450 mM L-homoserine (dotted line) and 150 mM L-methionine (dashed line) in 50 mM Tris-HCl pH 8.5. (b) Fluorescence emission spectra of 1  $\mu$ M enzyme (solid line) in the presence of 150 mM L-methionine (dotted line), 100 mM L-serine (dashed line), and 100 mM O-acetyl-L-serine (dash dotted line) upon excitation at 295 nm. *Inset*: emission spectra of 10  $\mu$ M enzyme (solid line) in the presence of 100 mM O-acetyl-L-serine (dash dotted line), 100 mM L-serine (dashed line), and 150 mM L-methionine (dotted line) upon excitation at 418 nm. All spectra are recorded in 20 mM Bis-Tris-propane pH 8.5.

asymmetry of certain aromatic amino acids, most likely associated with the active site (Figure 2(a)).

The fluorescence emission spectra of C-S lyase recorded for the direct excitation at 295 nm of Trp residues exhibit a pronounced peak centered around 340 nm and a much lower intensity peak at around 500 nm (Figure 2(b)). The peak at 340 nm can be attributed to direct emission from Trp

residues, while the peak centered at 505 nm can be attributed to emission from PLP, resulting from an intramolecular energy-transfer process from the excited Trp residues to the cofactor [16, 17]. Direct excitation of the C-S lyase ketoenamine tautomer of PLP at 413 nm gives a single emission peak centered at 502 nm (Figure 2(b), inset), which is typical for emission from Schiff bases of PLP in a neutral, aqueous

environment [18, 19]. None of the fluorescence emission properties of the enzyme is affected by pH in the range from 5.7 to 10.2.

At pH 8.5 in 20 mM Bis-Tris propane, the excitation spectrum for the longer-wavelength emission of C-S lyase measured at 502 nm shows two bands. The peak of the shorter wavelength excitation band is located at 279 nm, and the peak of the longer-wavelength excitation band is located at 413 nm (data not shown).

The emission spectrum obtained for apo C-S lyase, when excited at 295 nm, exhibits a single peak centered at 345 nm, with a 4-fold increase in emission intensity and a 2 nm red shift compared to the holoenzyme (data not shown). The apoenzyme has no residual activity and does not exhibit either absorbance bands in the visible region or PLP emission fluorescence. Titration of apo C-S lyase with PLP resulted in an increase in the fluorescence emission at 500 nm; the values were plotted against PLP concentrations and used to calculate the  $K_d^{PLP}$  value for the enzyme by a theoretical curve fit of the experimental data using (5). The obtained  $K_d^{PLP}$  value was  $0.09 \pm 0.03 \mu\text{M}$ , indicating a tight binding of PLP to the enzyme.

**3.2. Steady-State Kinetic Studies.** Several sulfur- and nonsulfur containing amino acids were utilized as potential substrates for the enzyme. The enzyme showed maximum activity at pH 9 and 30°C, as determined in 50 mM MOPS, 50 mM bicine, and 50 mM proline. Table 1 shows that the enzyme has a relatively broad substrate specificity. L-Cth, L-djenkolate, and aminoethyl-L-cysteine were the most effective substrates. Cystine and L-cysteine, to a lesser extent, also acted as substrates. O-acetyl-L-serine and L-serine proved to be very poor substrates, whereas no activity could be detected with L-homocysteine, L-homoserine, or L-methionine. These latter inhibited, although to different extents, C-S lyase activity (data not shown), thus indicating their binding to the enzyme. The recombinant C-S lyase obeyed Michaelis-Menten kinetics with all substrates examined except for L-cysteine, for which substrate inhibition was observed. By using (2) (describing substrate inhibition, [11, 20]), initial velocity data obtained by varying L-cysteine concentrations fit a nonhyperbolic curve to yield  $K_m$  and  $K_i$  values of  $0.95 \pm 0.18$  and  $3.98 \pm 0.66 \text{ mM}$ , respectively.

**3.3. pH Dependence of Kinetic Parameters for C-S Lyase.** The pH dependence of the kinetic parameters for C-S lyase toward L-Cth and L-cysteine was determined, and the results are shown in Figures 3(a) and 3(b).  $\log k_{cat}$  is pH independent from 7.8 to 10.2 for both substrates. The  $\log k_{cat}/K_m$ —pH profile for L-Cth is bell shaped, consistent with the involvement of two ionizable groups, one with an apparent  $pK_a$  of  $8.05 \pm 0.07$  and the other with an apparent  $pK_a$  of  $9.90 \pm 0.07$  (Figure 3(a)). The  $\log k_{cat}/K_m$ —pH profile for L-cysteine exhibited a single  $pK_a$  of  $8.26 \pm 0.01$  for a group that must be deprotonated for activity (Figure 3(b)).

**3.4. Absorption, Fluorescence, and CD Spectral Changes of C-S Lyase with Substrates and Substrate Analogues.** Except

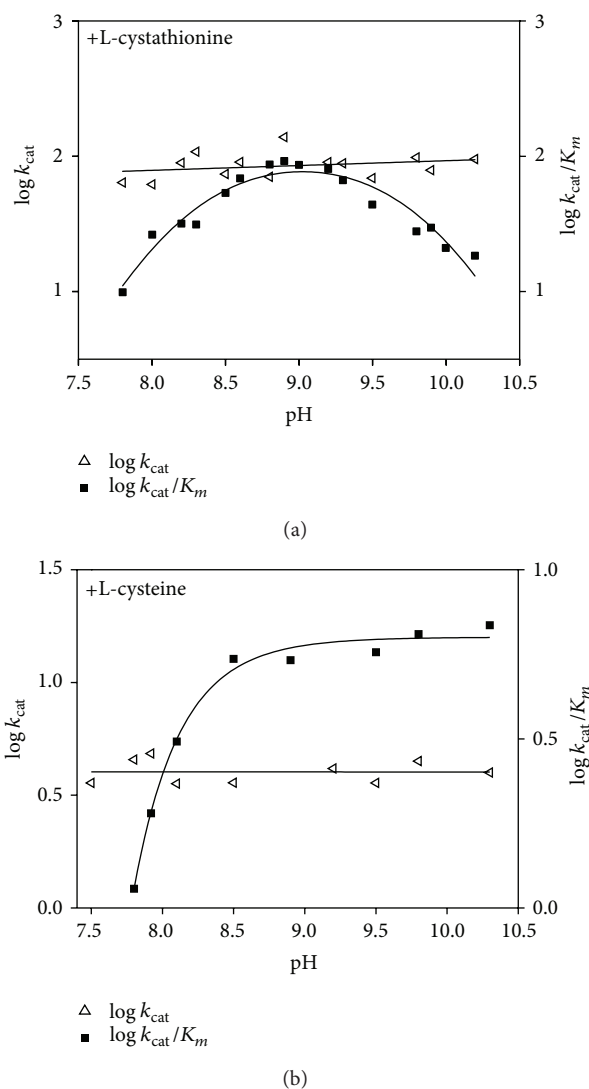


FIGURE 3: pH dependence of the kinetic parameters for C-S lyase reaction with L-Cth and L-cysteine.  $\log k_{cat}$  profile and  $\log k_{cat}/K_m$  profile for L-Cth (a) and L-cysteine (b). The points shown are experimentally determined values, while the curves are from fits to the data using (3) for  $\log k_{cat}/K_m$  for L-cysteine and (4) for  $\log k_{cat}/K_m$  for L-Cth.

for L-serine and O-acetyl-L-serine, the rate of reaction for the substrates tested (Table 1) was very high, and reaction of the enzyme with these substrates cannot be studied by conventional spectroscopy.

Addition of O-acetyl-L-serine to C-S lyase at pH 8.5 produces an immediate shift from 413 to 420 nm (Figure 1(a)). This shift is consistent with the conversion of internal to external aldimine (Figure 1(a)). A broad increase in the absorbance at wavelengths shorter than 350 nm hampers the accurate identification of specific bands and is likely due to the accumulation of reaction products, that is, pyruvate, which absorbs at 318 nm [21]. After subtraction of the contribution of pyruvate absorbance to the absorbance spectra of enzyme, the external aldimine is the only evident intermediate during



TABLE 1: Kinetic parameters for substrates in 50 mM MOPS, 50 mM bicine, and 50 mM proline pH 9.0 at 30 °C.

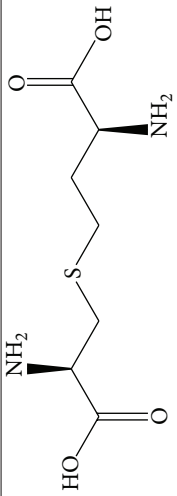
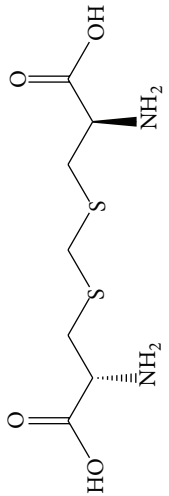
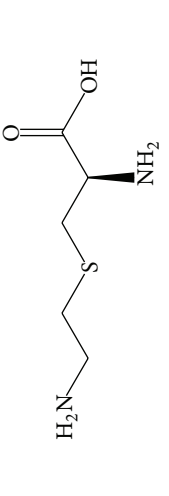
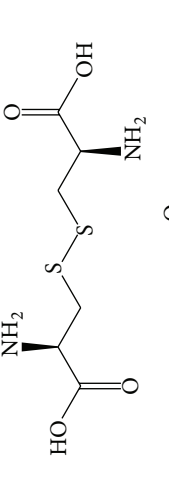
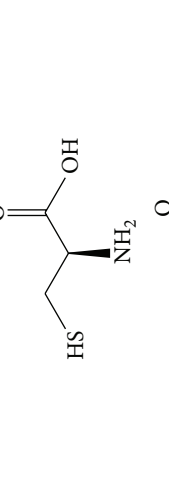
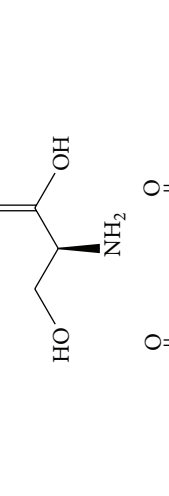
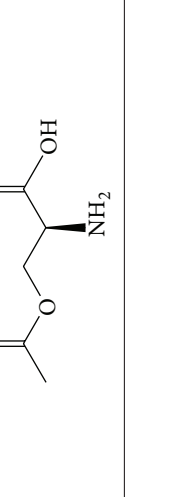
Substrate	$K_m$ (mM)	$k_{cat}$ (s <sup>-1</sup> )	$k_{cat}/K_m$ (mM <sup>-1</sup> s <sup>-1</sup> )	Structure
L-cystathionine	1.07 ± 0.22	92.67 ± 4.44	86.60 ± 21.46	
L-djenkolic acid	0.23 ± 0.087	49.11 ± 3.08	213.50 ± 94.14	
Aminoethyl-L-cysteine	1.29 ± 0.18	22.69 ± 0.75	17.59 ± 3.03	
L-cystine	1.14 ± 0.22	4.67 ± 0.25	4.10 ± 1.01	
L-cysteine	0.95 ± 0.18	4.36 ± 0.47	4.59 ± 1.85	
L-serine	8.28 ± 1.57	2.65 ± 0.13	0.32 ± 0.07	
O-acetyl-L-serine	11.21 ± 3.48	0.17 ± 0.018	0.015 ± 0.006	

TABLE 2: Kinetic parameters for C-S lyase wt and mutants using L-Cth in 50 mM MOPS, and 50 mM bicine, 50 mM proline pH 9.0 at 30°C.

Protein	$K_m$ (mM)	$k_{cat}$ (s <sup>-1</sup> )	Relative activity (%)
wt	1.07 ± 0.22	92.67 ± 4.44	100
Y114F	0.20 ± 0.01	1.20 ± 0.02	1.3
Y55F	0.62 ± 0.21	0.45 ± 0.01	0.5
R351A	n.d.*	n.d.*	—

\* n.d.: not detected.

steady-state conditions. On the other hand, binding of L-serine at pH 8.5 to the enzyme results in mixtures of external aldimine and quinonoid species absorbing at 428 and 495 nm, respectively (Figure 1(a)).

Binding of the substrate analogues L-methionine or L-homoserine at pH 8.5 to the enzyme results in mixtures of external aldimine ( $\lambda_{max}$  = 418 nm) and quinonoid species ( $\lambda_{max}$  = 505 nm). This equilibrium is attained immediately upon mixing (Figure 1(b)).

CD spectra of the PLP cofactor were obtained in the presence of L-methionine and L-homoserine (Figure 2(a)). The spectrum for unliganded enzyme exhibits a positive Cotton effect centered on the visible absorption band of the cofactor, as it has been found for many PLP enzymes including cystalysin [12] and O-acetylserine sulphydrylase [22] which catalyze reactions very similar to that catalyzed by C-S lyase. In the presence of saturating concentrations of L-methionine and L-homoserine, a positive Cotton effect is still evident, but with only 30% ellipticity relative to enzyme alone. The presence of L-homoserine gives a small negative dichroic signal centered around the visible absorption band of the quinonoid intermediate at 502 nm, and a modest negative dichroic band at 337 nm, mimicking what is observed in the visible spectrum.

Differences were also seen between the unliganded and liganded enzymes in the near-UV CD spectrum. Upon addition of ligands, a decrease of the negative dichroic signals in the Tyr spectral region was observed, which was more pronounced for L-methionine. Both these ligands have a pronounced effect on Trp residue(s) whose fine structure between 293 and 305 nm is clearly affected (Figure 2(a)).

Upon excitation at 295 nm, in the presence of L-serine, the cofactor emission band of C-S lyase exhibits a decrease in intensity compared to the internal aldimine emission spectrum (Figure 2(b)), while the Trp emission band is red shifted to 344 nm, maintaining almost the same intensity. The decrease in the emission band of the ketoenamine tautomer is confirmed by the direct excitation of the ketoenamine tautomer at 425 nm, which shows a decrease and a red shift to 517 nm compared to the emission of the internal aldimine (Figure 2(b), inset). When the enzyme was excited at 418 nm in the presence of O-acetyl-L-serine or L-methionine, the emission spectrum exhibited a quenching of the fluorescence emission at 500 nm, concomitant with a modest red shift to 504 or 506 nm, respectively (Figure 2(b), inset).

**3.5. Effects of Arg351, Tyr114, and Tyr55 Mutation on the Enzymatic Activity of C-S Lyase.** To identify the residues

involved in catalysis and/or substrate binding, we aligned the amino acid sequences of seven bacterial C-S lyases (Figure 4). The C-S lyases share similar sequences and exhibit identities to C-S lyase from *C. diphtheriae* ranging from 27% (cystalysin from *T. denticola*) to 54% (C-S lyase from *C. glutamicum*). The alignment indicates that 40 amino acids are strictly conserved, and structural comparison of C-S lyase with cystalysin indicates similarity in overall fold as well as in active site residues (Figure 5). Of the 20 residues bordering the active site and the cofactor, we focused on three amino acids that are invariant among all the enzymes of the transsulfuration pathway. The conserved tyrosines (Tyr55\* and Tyr114) and arginine (Arg351), located at the active site, were selected for point mutation based on structural analysis (Figure 5(b)). The effect of mutation on enzyme activity was examined (Table 2). Mutation of Tyr55 to Phe dramatically reduced enzymatic activity ( $k_{cat}$  = 0.45 s<sup>-1</sup>); this Tyr is located on the dimer interface, and its side chain directly interacts with the PLP of the other subunit. Mutant R351A reduced the activity below detectable levels. On the other hand, the Y114F mutant retained 1.3% of the turnover rate of wild type enzyme. Although Tyr114 and Arg351 are positioned near the dimer interface, there are no direct interactions with any residues of the other subunit.

**3.6. Structural Similarity Analysis.** Guided by structural superimposition and structural similarity analysis, interesting differences were found between cystalysin from *T. denticola* and C-S lyase from *C. diphtheriae* in the AVG adduct. Although the root mean square deviations (RMSD) between both structures are small, that is, 1.5 Å, there are important differences in the residues present in the binding cavity. Indeed, while in the cystalysin-AVG complex hydrophobic interactions are formed with Phe273 (cyan in Figure 5(b)), this residue is not conserved in C-S lyase, thus offering a larger binding cavity. On the other hand, there are two residues present in C-S lyase that are not conserved in cystalysin from *T. denticola*, that is, Asp88 and Lys230 (yellow in Figure 5(b)). Both these differences may dramatically affect the physicochemical properties of the binding cavity and allow the design of specific inhibitors.

## 4. Discussion

The enzymes of the bacterial transsulfuration pathway, cystathionine  $\gamma$ -synthase and cystathionine  $\beta$ -lyase, are attractive targets for the development of novel antimicrobial compounds because this pathway is unique to plants and bacteria.

<i>C. diphtheriae</i>	---MQFPSIEDLRARNTMKWTRY-----GQGVLPPLWVAESDFSTCPAVLQAITDAVQR	50
<i>C. glutamicum</i>	-----MADAVR	7
<i>C. halotolerans</i>	---MQFPSLDELKNRRTRKWTVY-----GDDVLPPLWIAESDFFTSPPVKQAIRDAVER	50
<i>C. glucuronolyticum</i>	---MKCPDLTLRRRTMKWTAF-----EPDVLPLWIAESDFATNPCTQALHQAIDE	50
<i>S. anginosus</i>	MSKYNFQTAPNRLSHHTYKWKET-----ETDPQLLPWIAEDMDFEVMPEVKQAIHDYAEQ	55
<i>S. mutans</i>	MGRYDFTTRPDLNQFTYKWKTS-----ENPELLQMWVADMDFLPVPEIKAEIINYGRE	55
<i>T. denticola</i>	-MIYDFTTKISRKNLGSCLKWDLMSYQNPVEGVNEVPLSVADMEFKNPPELIEGLKKYLDE	59
<i>C. diphtheriae</i>	EAFGYQPDGSLLSQATAEFYADRYGYQARPEWIFPIPDVVRGLYIAIDHFTPAQSKVIVP	110
<i>C. glutamicum</i>	EVFGYPPDATGLNDALTGFYERRYGFGNPESVFAIPDVVRGLKLAIEHFTKPGSAIIVP	67
<i>C. halotolerans</i>	ESFGYTPTSPLQALSDFYAGAYGWRPDPGMVAVPDVVRGLLLAITYMTRPGSPVVVP	110
<i>C. glucuronolyticum</i>	EQFGYPPAGNEVAEALSQFCQARYGWHVDPRIHLATDVMQALIAALRYIVPAG-PVVIP	109
<i>S. anginosus</i>	LVYGYTYASDELLQAVLDWEKSEHQYSFDKEDIVFVEGVVPAISIAIQAFTEGEAVLIN	115
<i>S. mutans</i>	HIFGYNFNDLYQAVIDWERKEHDYAVVKEDILFIDGVVPAISIALQAFSEKGDVAVLIN	115
<i>T. denticola</i>	TVLGYTGPTTEYKKTVKKMKDRHQWDIETDWIINTAGVPAVFNNAVREFTKPGDGWIII	119
<i>C. diphtheriae</i>	TPAYPPFFHLLSATQR-----EGIFIDATGGINLHDEVEKGFQAG-ARSILLCNPNPLGM	164
<i>C. glutamicum</i>	LPAYPPFIELPKVTGR-----QAIYIDAH-EYDLKEIEKAFADG-AGSLLFCNPHNPLGT	120
<i>C. halotolerans</i>	VPAYPPFLELPETADR-----EKVEVNAYDGLDLAEIEEAFRNG-AGSILLCSPNNPLGY	164
<i>C. glucuronolyticum</i>	TPSYPPFFACQSAGR-----EVVTIDGL---SLDAVEETFQDHHPAFILCSPHNPLGV	161
<i>S. anginosus</i>	SPVYPPFARSVRLNRRKLVNSLSKEENGLFQIDFEQLENDIVENDVKLYLLCNPHNPGGR	175
<i>S. mutans</i>	SPVYPPFARTIRLNDHRLVNSLQIINGRFEIDFEQLEKDIIDNNVKIYLLCSPHNPGGR	175
<i>T. denticola</i>	TPVYPPFMAIKNQRKIIIECELLEKDGYYTIDFEKLEKLSKDKNNKALLFCSPHNPGVR	179
<i>C. diphtheriae</i>	VFAPewLNELCDLAHRYDARVLVDEIHAPLVFDG-QHTVAAGVSDTAASVCITITAPSKA	223
<i>C. glutamicum</i>	VFSEYIRELTDIAAKYDARIIADEIHAPLVFYG-THVVAAGVSENAANTCITITATSKA	179
<i>C. halotolerans</i>	TLSEEFITDLVALADRYDARVLVDEIHAPLVFSG-RHIVAAGLENAKVCVTVTATSKA	223
<i>C. glucuronolyticum</i>	VHERDYLHLAELADRYDVRVLSDEIHAPLVYPGHHHCPTASVSDVASERTITFMSTSKG	221
<i>S. anginosus</i>	VWEREVLEQIGHLCQKHHVILVSDEIHQDLTLFGHEHVSFNTVSPDFKDFALVLSATKT	235
<i>S. mutans</i>	VWDNDLIKIAELCKKHGVILVSDEIHQDLALFNTHSLNTLDASYKDFITILSSATKT	235
<i>T. denticola</i>	VWKDELQKIKDIVLKSDDLMSWDEIHFDLIMPGEHTVFSIDEQLADKITITFTAPSKT	239
<i>C. diphtheriae</i>	WNIAGLKCAQIIFSNPSDAEHWQQLS-PVIKDGASTLGLIAEAAAYRYGTDFLNQEVAYL	282
<i>C. glutamicum</i>	WNTAGLKCAQIFFSGEADVAKWNLS-DITRDGVSILGLIAAETVYNEGEEFLDESIQIL	238
<i>C. halotolerans</i>	WNIAGLKCAQIIFTNPVDKETWGMKT-GVAKDGTSTIGVFAAAACYREGGDHLDEQLAYL	282
<i>C. glucuronolyticum</i>	WNVAGLSAQIILTNNDNDNAWGKLN-PSAVPPPSILGNVAATVCTYDTSFLDDEIAYL	280
<i>S. anginosus</i>	FNIAGTKNSAIIENPTLCAQFKHQQLVNNHHEVSSLGYIATETAYRYGKPLVALKAVL	295
<i>S. mutans</i>	FNIAGTKNSAIIQNESLRRKFQYRLANNQHEVPTVGMATQAAFYQYKGPWLEELKTVI	295
<i>T. denticola</i>	FNIAGMGMSNIIKNPDIRERFTKSRDITSGMPFTTLGYKACEICYKECGKWLDCIKVI	299
<i>C. diphtheriae</i>	KNNHDFLLHEIPKRIPGAKITPMQATYLMWIDFRDITIEG---SPSEFFIEKAKVAMNDG	339
<i>C. glutamicum</i>	KDNRDFAAAELEK--LGKVVYAPDSTYLMWLDFAGTKIEE---APSKILREEGKVMNDG	293
<i>C. halotolerans</i>	RGNRDWLVEELPKRVPLQVSNPEATYLMWLDGSGTVIGDLV-QPAAWLRNNAKVALNEG	341
<i>C. glucuronolyticum</i>	VENRDYLLTHLPEVLPGIGMSHPDATYLMWLDGSCILALRNNPQQVLAEKARVGLNAC	340
<i>S. anginosus</i>	EENIQFAVEYFAQEAPRLKVMKPGQTYLIWLDGSDYGLTDD--ALFTLLHDQAKVILNRG	353
<i>S. mutans</i>	EGNIKLVIKELEAKT-KIKVMEPEGTYLVWLDGSAIYAIQP--QLSEKLQNEAKVVLNDG	352
<i>T. denticola</i>	DKNQRIVKDFFEVNHPEIKAPLIEGTYLQWIDFRALKMDHK--AMEEFMIHKAQIFFDEG	357
<i>C. diphtheriae</i>	AWFGEDGTGFCRLNFATSREVLEEAIDRMKAVSHHT-----	376
<i>C. glutamicum</i>	AAFG-GFTTCARLNFACSRETLEELRRIASVL-----	325
<i>C. halotolerans</i>	TTFTGTGEYCARLNFATSRELEEGVRRMAEAVAQVDAED--	381
<i>C. glucuronolyticum</i>	TGFGAVHDGFARLNFCDRSTLAEMISRIGHTF-----	373
<i>S. anginosus</i>	SDYGSEGELHARLNIAPKSLVEEICKRIVCCLPK-----	388
<i>S. mutans</i>	AHFGKEGKYFARLNVATPKNTVQEALSRIISVFGK-----	387
<i>T. denticola</i>	YIFGDDGIGFERINLAAPSSVIQESLERLNKALKDLKNRHLK	399

FIGURE 4: Sequence alignment of C-S lyases. The target residues for mutational analysis are highlighted in gray. The arrow above the sequences indicates the PLP-binding lysine. The C-S lyases used in this alignment (UniProt accession numbers) and their sources are Q6NFZ9, *Corynebacterium diphtheriae* NCTC 13129; Q46061, *Corynebacterium glutamicum*; MINUD7, *Corynebacterium halotolerans*; COVUP4, *Corynebacterium glucuronolyticum*; A6BMJ3, *Streptococcus anginosus* IMU102; Q8DST5, *Streptococcus mutans*; Q56257, *Treponema denticola* ATCC 3540. All sequence alignments were carried out using the ClustalW program.

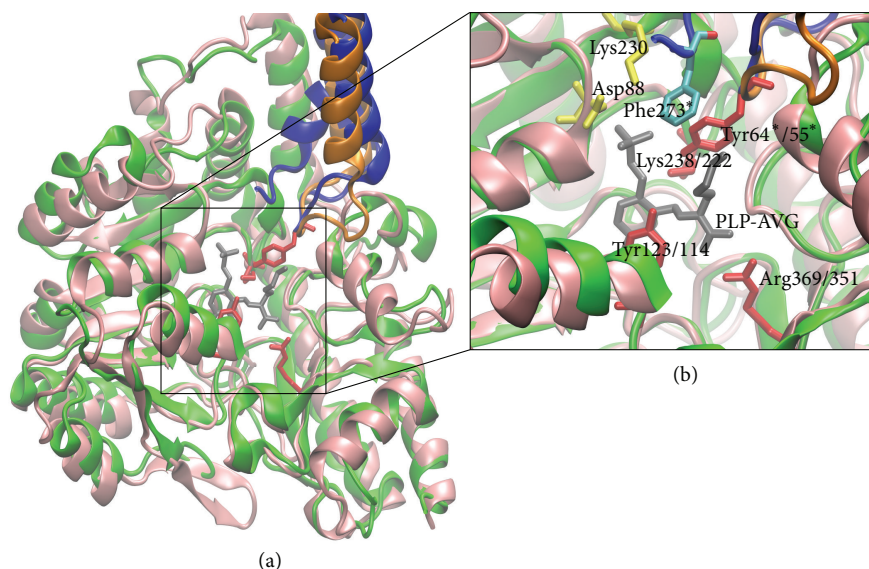


FIGURE 5: Superimposed structures of C-S lyase from *Corynebacterium diphtheriae* and cystalysin from *Treponema denticola*. (a) A subunit of C-S lyase (green) with a portion of chain B (orange) is superimposed with chains A and B of cystalysin (in pink and blue, resp.). (b) A close-up of the active site with the AVG inhibitor (in gray) is shown. Residues conserved in both proteins are shown in red. Phe273 is presented only in the chain B of cystalysin and is depicted in cyan, while residues Lys230 and Asp88 are presented only in C-S lyase and are shown in yellow. Residue numbers are indicated as cystalysin/C-S lyase. An asterisk (\*) indicates that the residues are present only in chain B.

Recent studies probing the active sites of these enzymes are providing information that will guide the design of novel therapeutics [2, 23]. As members of the  $\gamma$ -subfamily of fold-type I of PLP-dependent enzymes, they also represent a useful model system for studies exploring the molecular mechanisms that underlie specificity among enzymes dependent on this catalytically versatile cofactor. A thorough understanding of the mechanisms controlling substrate and reaction specificity is a necessary step to enable the engineering of PLP-dependent enzymes for biotechnological applications [24].

The structure of *C. diphtheriae* C-S lyase has been solved at 1.99 Å resolution (PDB code: 3FDB). We isolated the recombinant enzyme as a His-tagged protein at high yield and examined the spectral properties and steady state kinetic parameters of the purified enzyme, in addition to structural similarity analysis with cystalysin.

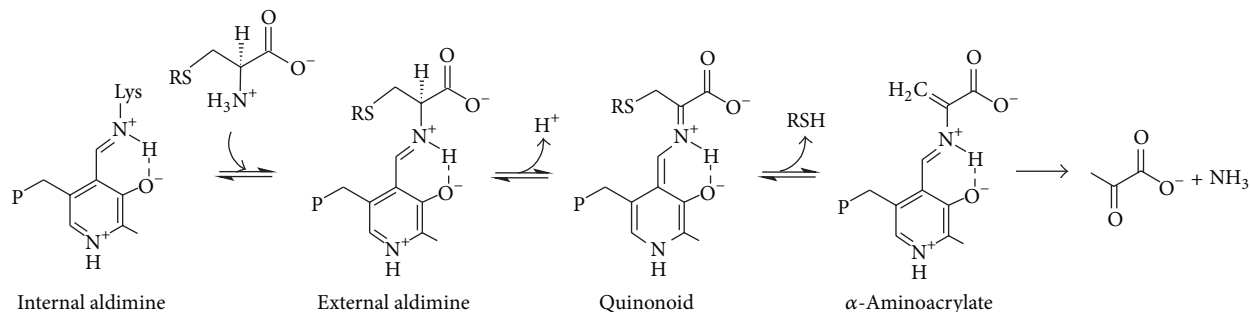
The internal aldimine absorbance spectra of C-S lyase exhibit a band centered at 413 nm (Figure 1(a)) which indicates that the predominant tautomer of the internal aldimine is the ketoenamine and that the imine nitrogen of the cofactor is protonated. This band is associated with a positive Cotton effect and gives rise to an emission maximum at about 500 nm. The enzyme spectrum is independent of pH from 6 to 11, indicating that the  $pK_a$  of the internal aldimine is higher than pH 11. In the structurally related enzyme cystalysin, a band at 320 nm was attributed to a substituted aldimine, a species stabilized with respect to the ketoenamine by alkaline pH [12]. Both cystalysin and C-S lyase are catalytically more competent at alkaline pH, where a remarkable portion of the coenzyme in cystalysin exists as inactive aldimine structure with a nucleophilic group. Interestingly, the spectrum of the

*C. diphtheriae* is pH independent; thus, this nucleophilic group is either missing or has a different location.

The apoenzyme showed no absorption in the visible range and no emission fluorescence due to PLP. When the intrinsic fluorescence emissions of holo- and apoenzyme were compared, it was evident that a substantial fraction (about 70%) of the Trp emission in the apoenzyme is quenched in the holoenzyme. Such quenching is concomitant with the appearance of the 500 nm emission indicative of energy transfer from Trp residue(s) to the internal Schiff base. The interaction between the apoenzyme and PLP is characterized by a dissociation constant of 0.09  $\mu$ M, which is indicative of very tight binding of the cofactor to the enzyme.

Conversion to the external aldimine upon addition of substrate or substrate analog is expected to involve a conformational change that causes, among other things, the exclusion of water molecules from the active site. Formation of the external aldimine with L-serine is accompanied by a bathochromic shift of the ketoenamine tautomer absorption band (15 nm; Figure 1(a)) compared to the same species with O-acetyl-L-serine, L-methionine, or L-homoserine (about 6 nm). This finding suggests a pronounced increase in the polarity of the microenvironment in the active site, likely due to a repositioning of charged or polar residues around the cofactor. Binding of L-serine to the enzyme results in mixtures of external aldimine and quinonoid species (Figure 1(a)).  $\alpha,\beta$ -Elimination mechanisms generally proceed via a quinonoid intermediate, in which the carbanion formed upon abstraction of the  $C\alpha$ -proton is stabilized by delocalization into the pyridinium ring of PLP. This transient intermediate with  $\lambda_{max} \sim 450$ –500 nm is detectable when



SCHEME 1: Key intermediate steps of  $\alpha,\beta$ -elimination reaction.

the elimination of the leaving group is slow, as might be expected for the hydroxyl group of L-serine [25]. The steady-state spectrum represents an intermediate whose formation is rate limiting or represents the sum of more than one intermediate if multiple steps are partially rate limiting [26]. Therefore, the presence of both the external aldimine and the substrate quinonoid in the steady-state spectrum of C-S lyase with L-serine indicates that the formation of these intermediates may be partially rate determining. In contrast, a quinonoid intermediate is not observed for the elimination of acetate from O-acetyl-L-serine as the acetate group of O-acetyl-L-serine does not require protonation and is a better leaving group than the hydroxyl group of the L-serine. Although L-methionine and L-homoserine bind to C-S lyase in an unproductive manner, they nonetheless give equilibrating mixtures of external aldimine and quinonoid species (Figure 1(b)). This implies that L-methionine or L-homoserine stops the reaction at the step involving the quinonoid intermediate. The effects of all amino acids tested on the CD and fluorescence spectra of C-S lyase consist, albeit to different extents, in a modest enhancement of intrinsic Trp fluorescence, quenching and red shift of the long wavelength PLP emission, and a change in the dissymmetry of bound cofactor and aromatic amino acids located near the active site (Figures 2(a) and 2(b)). Taken together, in terms of local perturbations these data can be interpreted as changes in the orientation of the PLP and in the relative orientations of an aromatic residue(s) and of cofactor upon binding of ligand.

The  $k_{\text{cat}}$  profile for the  $\alpha,\beta$ -elimination reaction of L-Cth or L-cysteine is pH independent. The  $k_{\text{cat}}/K_m$  versus pH profile for L-Cth is bell-shaped, with  $\text{p}K_a$  values of  $8.05 \pm 0.07$  ( $\text{p}K_{a1}$  acidic limb) and  $9.90 \pm 0.07$  ( $\text{p}K_{a2}$ , basic limb). The  $k_{\text{cat}}/K_m^{\text{L-Cth}}$ -pH profile decreased on the acid and basic sides with limiting slopes of 1 and -1, indicating that the ionization of the two groups is relevant to the enzymatic reaction, with one being protonated and the other unprotonated (Figure 3(a)).

The pH independence of the internal aldimine of C-S lyase indicates that this group cannot be assigned to one of those that titrates in the pH-activity profiles. The  $\text{p}K_a$  values of the R-NH<sub>2</sub> groups of L-Cth were determined by direct titration with NaOH as  $8.51 \pm 0.02$  and  $9.60 \pm 0.02$  at 25°C, which are within experimental error of those determined for the acidic and basic limb of the  $k_{\text{cat}}/K_m^{\text{L-Cth}}$  versus pH plot.

The basic limb ( $\text{p}K_{a2}$ ) of the  $k_{\text{cat}}/K_m^{\text{L-Cth}}$  versus pH profile was assigned to the  $\text{p}K_a$  of the R-amino group of L-Cth, since  $\text{p}K_{a2}$  was not present in the  $k_{\text{cat}}/K_m^{\text{L-cys}}$  profile (Figure 3(b)). The acidic limb ( $\text{p}K_{a1}$ ) can be assigned to the  $\alpha$ -amino group of L-Cth ( $\text{p}K_a = 8.54$ ), indicating that the substrate must bind in the deprotonated state. Alternatively, the  $\text{p}K_{a1}$  could reflect ionization of an enzyme group other than the imino moiety of the internal aldimine.

It is generally accepted that PLP-dependent  $\beta$ -eliminases, including  $\beta$ C-S lyases, have three key intermediate steps [8] (Scheme 1). Plausible catalytic mechanisms for the formation of intermediates have been reported for several  $\beta$ C-S lyases on the basis of structural and spectroscopic information [12, 27–30]. Contrary to their common intermediates, the quaternary structures (dimer and tetramer) and the active site residues of the  $\beta$ C-S lyase enzymes are somewhat different, possibly depending on their substrate specificity. When studying the  $\alpha,\beta$ -elimination reactions of sulfur containing amino acids in bacteria, determination of enzyme substrate specificity is crucial since it allows distinction between true cystathionine  $\beta$ -lyase activities involved in the synthesis of methionine and other C-S lyase activities. Thus, cystathionine  $\beta$ -lyase supports the cleavage of either L-Cth or djenkolate at high levels and shows low activity towards L-cystine. Conversely, C-S lyases are characterized by marginal cleavage of L-Cth and efficient synthesis of cysteine persulfide from L-cysteine [31, 32].

To define the substrate specificity of C-S lyase from *C. diphtheriae*, we examined the reaction of the enzyme with sulfur- and nonsulfur containing amino acids as well as with disulfidic amino acids (Table 1). Among the substrates tested, only L-cysteine exhibits substrate inhibition, similar to *T. denticola* cystalysin [12], C-DES from *Synechocystis* [33],  $\beta$ -cystathionase [31], and D-cysteine desulphydrase from *E. coli* [34].

Recombinant C-S lyase from *C. diphtheriae* showed a relatively broad substrate specificity toward sulfur-containing amino acids, as previously observed for the enzyme from *A. thaliana* [35], *E. coli* [31], *B. avium* [36], and *S. typhimurium* [37]. For all these enzymes, the highest rates of  $\beta$ -cleavage activity were obtained with L-Cth and djenkolate, whereas L-cystine and L-cysteine were poor substrates. In the case of L-cystine and L-cysteine, compared with L-Cth, substrate selectivity does not appear to derive from substrate binding,

since  $K_m$  values are similar, but rather from chemical steps that follow the binding (Table 1). Finally, no activity could be detected for the enzyme when either L-homocysteine or L-methionine was used as substrate ( $\gamma$ C-S linkages).

The present observations are in agreement with previous analysis of the substrate specificity of cystathionine  $\beta$ -lyase from *A. thaliana* [35] which showed the following: (1) all active substrates contain a C3 L- $\alpha$ -amino acid moiety; (2) the nature of the sulfur-containing bridge (thioether, thioacetal, or disulfide) influences the rate of the  $\alpha,\beta$ -elimination process; and (3) the length of the second moiety, and therefore the spatial separation of the two carboxyl groups of the substrate, has a critical role in the efficiency of cleavage. In light of these findings, *C. diphtheriae* should more properly be considered as a cystathionine  $\beta$ -lyase, rather than a C-S lyase, as annotated (NCBI protein NP\_940074). Interestingly, although both *C. diphtheriae* C-S lyase and cystalysin belong to fold type I, and share similar sequences (Figure 4) and structural similarity in overall fold and active site residues (Figure 5), they do not display desulfhydrase activity with similar substrate specificity. Cystalysin, in fact, displays a strong substrate preference for L-djenkolic acid and L-cystine over L-cysteine and, among sulfur-containing amino acids, the lowest  $\beta$ -cleavage activity was obtained with L-Cth [12]; its substrate specificity is similar to that of L-cysteine/cysteine C-S lyase (C-DES) from *Synechocystis*.

Based on structural and kinetic studies, a postulated catalytic mechanism with the intermediates has been proposed for cystalysin [38, 39] and *Streptococcus anginosus*  $\beta$ C-S lyase (Lcd) [40], the enzymes with the highest sequence identity to *C. diphtheriae* C-S lyase (Figure 5(a)) among structurally and enzymatically characterized  $\beta$ C-S lyases. The structural information on the intermediate complexes enabled us to select conserved residues for site-directed mutagenesis. Mutational analysis demonstrated the important roles of several active site residues, namely, Tyr55, Tyr114, and Arg351 (Figure 5(a)). In particular, Tyr114 recognizes the S  $\gamma$ -atom (or O  $\gamma$ -atom) of the substrate by the phenolic hydroxyl group and fixes PLP at the proper position by a stacking interaction throughout the  $\alpha,\beta$ -elimination reaction [27, 38].

Mutational analysis further revealed that Y114F retained only 1.3% of wt enzymatic activity (Table 2). On the basis of kinetic studies, Cellini et al. [38] concluded that Tyr64 of cystalysin (Tyr55 of *C. diphtheriae* C-S lyase) plays a role in the properly orienting Lys238 (Lys222). In agreement with structural observations, substitution of Tyr55 to Phe reduced the catalytic activity to 0.5% (Table 2), suggesting the importance of the phenolic hydroxyl group of this residue. In both Lcd external aldimine and  $\alpha$ -aminoacrylate forms, the guanidino group of Arg365 formed a salt bridge with the carboxyl moiety of the amino acid substrate bound to PLP [40]. This Arg is widely conserved among type I PLP-dependent enzymes and is supposed to act as a general  $\alpha$ -carboxylate docking site [41]. A similar salt bridge has been observed between the corresponding Arg and the carboxyl moiety of the coenzyme bound substrate in other PLP-dependent  $\beta$ -eliminases [28, 42] suggesting a common role of the Arg for substrate binding. Substitution of Arg351 with

Ala notably reduced catalytic activity toward L-Cth to below a detectable level (Table 2).

Although the residues involved in PLP and substrate binding are fully conserved, structural similarity analysis between cystalysin from *T. denticola* and C-S lyase from *C. diphtheriae* in the AVG adduct revealed subtle differences in the binding cavity. These involve just three amino acids, that is, two charged residues present in C-S lyase and not in cystalysin and *vice versa*, a Phe residue present in cystalysin and not in C-S lyase. Indeed, the availability of two charged residues and the lack of bulky hydrophobic one will dramatically affect the physicochemical properties of the binding cavity of C-S lyase. These elements can thus be exploited for rational design of novel and species specific inhibitors to be used in antibacterial therapeutics.

## Abbreviations

PLP:	Pyridoxal 5'-phosphate
DTNB:	5,5'-dithiobis-2-nitrobenzoate
LDH:	L-lactic dehydrogenase
L-Cth:	L-cystathionine
AVG:	L-aminoethoxyvinylglycine
$K_d^{PLP}$ :	Equilibrium dissociation constant for PLP
CD:	Circular dichroism
PDB:	Protein Data Bank
$k_{cat}$ :	Turnover rate
$K_m$ :	Michaelis constant

## References

- [1] A. Coates, Y. Hu, R. Bax, and C. Page, "The future challenges facing the development of new antimicrobial drugs," *Nature Reviews Drug Discovery*, vol. 1, no. 11, pp. 895–910, 2002.
- [2] L. J. Ejim, J. E. Blanchard, K. P. Koteva et al., "Inhibitors of bacterial cystathionine  $\beta$ -lyase: leads for new antimicrobial agents and probes of enzyme structure and function," *Journal of Medicinal Chemistry*, vol. 50, no. 4, pp. 755–764, 2007.
- [3] S. L. Jacques, I. A. Mirza, L. Ejim et al., "Enzyme-assisted suicide: molecular basis for the antifungal activity of 5-hydroxy-4-oxonorvaline by potent inhibition of homoserine dehydrogenase," *Chemistry and Biology*, vol. 10, no. 10, pp. 989–995, 2003.
- [4] Y. Aoki, M. Yamamoto, S. M. Hosseini-Mazinani, N. Koshikawa, K. Sugimoto, and M. Arisawa, "Antifungal azoxybacillin exhibits activity by inhibiting gene expression of sulfite reductase," *Antimicrobial Agents and Chemotherapy*, vol. 40, no. 1, pp. 127–132, 1996.
- [5] M. Kugler, W. Loeffler, C. Rapp, A. Kern, and G. Jung, "Rhizoctin A, an antifungal phosphono-oligopeptide of *Bacillus subtilis* ATCC 6633: biological properties," *Archives of Microbiology*, vol. 153, no. 3, pp. 276–281, 1990.
- [6] A. Galazka, "The changing epidemiology of diphtheria in the vaccine era," *Journal of Infectious Diseases*, vol. 181, supplement 1, pp. S2–S9, 2000.
- [7] K. S. Wagner, P. Stickings, J. M. White et al., "A review of the international issues surrounding the availability and demand for diphtheria antitoxin for therapeutic use," *Vaccine*, vol. 28, no. 1, pp. 14–20, 2009.
- [8] G. Schneider, H. Käck, and Y. Lindqvist, "The manifold of vitamin B6 dependent enzymes," *Structure*, vol. 8, no. 1, pp. R1–R6, 2000.

- [9] C. Y. Cormier, S. E. Mohr, D. Zuo et al., "Protein structure initiative material repository: an open shared public resource of structural genomics plasmids for the biological community," *Nucleic Acids Research*, vol. 38, no. 1, pp. D743–D749, 2010.
- [10] C. Y. Cormier, J. G. Park, M. Fiacco et al., "PSI: Biology-materials repository: a biologist's resource for protein expression plasmids," *Journal of Structural and Functional Genomics*, vol. 12, no. 2, pp. 55–62, 2011.
- [11] R. A. Copeland, "Kinetics of single-substrate enzyme reactions," in *Enzymes: A Practical Introduction to Structure, Mechanism, and Data Analysis*, pp. 109–145, John Wiley & Sons, New York, NY, USA, 2002.
- [12] M. Bertoldi, B. Cellini, T. Clausen, and C. B. Voltattorni, "Spectroscopic and kinetic analyses reveal the pyridoxal 5'-phosphate binding mode and the catalytic features of *Treponema denticola* cystalysin," *Biochemistry*, vol. 41, no. 29, pp. 9153–9164, 2002.
- [13] D. Raimondo, A. Giorgetti, F. Bernassola, G. Melino, and A. Tramontano, "Modelling and molecular dynamics of the interaction between the E3 ubiquitin ligase Itch and the E2 UbcH7," *Biochemical Pharmacology*, vol. 76, no. 11, pp. 1620–1627, 2008.
- [14] P. F. Cook and R. T. Wedding, "A reaction mechanism from steady state kinetic studies for O acetylserine sulphydrylase from *Salmonella typhimurium* LT-2," *The Journal of Biological Chemistry*, vol. 251, no. 7, pp. 2023–2029, 1976.
- [15] M. A. Becker, N. M. Kredich, and G. M. Tomkins, "The purification and characterization of O-acetylserine sulphydrylase-A from *Salmonella typhimurium*," *The Journal of Biological Chemistry*, vol. 244, no. 9, pp. 2418–2427, 1969.
- [16] G. B. Strambini, P. Cioni, A. Peracchi, and A. Mozzarelli, "Characterization of tryptophan and coenzyme luminescence in tryptophan synthase from *Salmonella typhimurium*," *Biochemistry*, vol. 31, no. 33, pp. 7527–7534, 1992.
- [17] G. D. McClure Jr. and P. F. Cook, "Product binding to the  $\alpha$ -carboxyl subsite results in a conformational change at the active site of O-acetylserine sulphydrylase-A: evidence from fluorescence spectroscopy," *Biochemistry*, vol. 33, no. 7, pp. 1674–1683, 1994.
- [18] M. Arrio-Dupont, "Fluorescence study of Schiff bases of pyridoxal. Comparison with L-aspartate aminotransferase," *Photochemistry and Photobiology*, vol. 12, no. 4, pp. 297–315, 1970.
- [19] M. Arrio-Dupont, "The effect of solvent on the fluorescence of Schiff bases of pyridoxal 5' phosphate," *Biochemical and Biophysical Research Communications*, vol. 44, no. 3, pp. 653–659, 1971.
- [20] P. H. Lodha and S. M. Aitken, "Characterization of the side-chain hydroxyl moieties of residues Y56, Y111, Y238, Y338, and S339 as determinants of specificity in *E. coli* cystathionine  $\beta$ -lyase," *Biochemistry*, vol. 50, no. 45, pp. 9876–9885, 2011.
- [21] B. Pioselli, S. Bettati, T. V. Demidkina, L. N. Zakomirdina, R. S. Phillips, and A. Mozzarelli, "Tyrosine phenol-lyase and tryptophan indole-lyase encapsulated in wet nanoporous silica gels: selective stabilization of tertiary conformations," *Protein Science*, vol. 13, no. 4, pp. 913–924, 2004.
- [22] K. D. Schnackerz, C. H. Tai, J. W. Simmons III, T. M. Jacobson, G. S. Rao, and P. F. Cook, "Identification and spectral characterization of the external aldimine of the O-acetylserine sulphydrylase reaction," *Biochemistry*, vol. 34, no. 38, pp. 12152–12160, 1995.
- [23] P. H. Lodha, A. F. Jaworski, and S. M. Aitken, "Characterization of site-directed mutants of residues R58, R59, D116, W340 and R372 in the active site of *E. coli* cystathionine  $\beta$ -lyase," *Protein Science*, vol. 19, no. 3, pp. 383–391, 2010.
- [24] M. L. di Salvo, R. Florio, A. Paiardini, M. Vivoli, S. D'Aguzzo, and R. Contestabile, "Alanine racemase from *Tolypocladium inflatum*: a key PLP-dependent enzyme in cyclosporin biosynthesis and a model of catalytic promiscuity," *Archives of Biochemistry and Biophysics*, vol. 529, no. 2, pp. 55–65, 2013.
- [25] S. Daum, C. H. Tai, and P. F. Cook, "Characterization of the S272A,D site-directed mutations of O-acetylserine sulphydrylase: involvement of the pyridine ring in the  $\alpha,\beta$ -elimination reaction," *Biochemistry*, vol. 42, no. 1, pp. 106–113, 2003.
- [26] G. A. Hunter and G. C. Ferreira, "Pre-steady-state reaction of 5-aminolevulinate synthase: evidence for a rate-determining product release," *The Journal of Biological Chemistry*, vol. 274, no. 18, pp. 12222–12228, 1999.
- [27] H. I. Krupka, R. Huber, S. C. Holt, and T. Clausen, "Crystal structure of cystalysin from *Treponema denticola*: a pyridoxal 5'-phosphate-dependent protein acting as a haemolytic enzyme," *EMBO Journal*, vol. 19, no. 13, pp. 3168–3178, 2000.
- [28] T. Clausen, J. T. Kaiser, C. Steegborn, R. Huber, and D. Kessler, "Crystal structure of the cystine C-S lyase from *Synechocystis*: stabilization of cysteine persulfide for FeS cluster biosynthesis," *Proceedings of the National Academy of Sciences of the United States of America*, vol. 97, no. 8, pp. 3856–3861, 2000.
- [29] T. Clausen, R. Huber, B. Laber, H. Pohlenz, and A. Messerschmidt, "Crystal structure of the pyridoxal-5'-phosphate dependent cystathionine  $\beta$ -lyase from *Escherichia coli* at 1.83 Å," *Journal of Molecular Biology*, vol. 262, no. 2, pp. 202–224, 1996.
- [30] U. Breiter, T. Clausen, S. Ehler, et al., "The three-dimensional structure of cystathionine  $\beta$ -lyase from *Arabidopsis* and its substrate specificity," *Plant Physiology*, vol. 126, no. 2, pp. 631–642, 2001.
- [31] C. M. Dwivedi, R. C. Ragin, and J. R. Uren, "Cloning, purification, and characterization of  $\beta$ -cystathionase from *Escherichia coli*," *Biochemistry*, vol. 21, no. 13, pp. 3064–3069, 1982.
- [32] M. Droux, S. Ravanel, and R. Douce, "Methionine biosynthesis in higher plants. II. Purification and characterization of cystathionine  $\beta$ -lyase from spinach chloroplasts," *Archives of Biochemistry and Biophysics*, vol. 316, no. 1, pp. 585–595, 1995.
- [33] T. Lang and D. Kessler, "Evidence for cysteine persulfide as reaction product of L-cyst(e)ine C-S-lyase (C-DES) from *Synechocystis*: analyses using cystine analogues and recombinant C-DES," *The Journal of Biological Chemistry*, vol. 274, no. 1, pp. 189–195, 1999.
- [34] T. Nagasawa, T. Ishii, H. Kumagai, and H. Yamada, "D-Cysteine desulfhydrase of *Escherichia coli*. Purification and characterization," *European Journal of Biochemistry*, vol. 153, no. 3, pp. 541–551, 1985.
- [35] S. Ravanel, D. Job, and R. Douce, "Purification and properties of cystathionine  $\beta$ -lyase from *Arabidopsis thaliana* overexpressed in *Escherichia coli*," *Biochemical Journal*, vol. 320, no. 2, pp. 383–392, 1996.
- [36] C. R. Gentry-Weeks, J. Spokes, and J. Thompson, " $\beta$ -cystathionase from *Bordetella avium*. Role(s) of lysine 214 and cysteine residues in activity cytotoxicity," *The Journal of Biological Chemistry*, vol. 270, no. 13, pp. 7695–7702, 1995.
- [37] L. J. Ejim, V. M. D'Costa, N. H. Elowe, J. C. Loredano-Osti, D. Malo, and G. D. Wright, "Cystathionine  $\beta$ -lyase is important for virulence of *Salmonella enterica* serovar typhimurium," *Infection and Immunity*, vol. 72, no. 6, pp. 3310–3314, 2004.
- [38] B. Cellini, M. Bertoldi, R. Montioli, and C. B. Voltattorni, "Probing the role of Tyr 64 of *Treponema denticola* cystalysin by site-directed mutagenesis and kinetic studies," *Biochemistry*, vol. 44, no. 42, pp. 13970–13980, 2005.

- [39] M. Bertoldi, B. Cellini, S. D'Aguzzo, and C. B. Voltattorni, "Lysine 238 is an essential residue for  $\alpha,\beta$ -elimination catalyzed by *Treponema denticola* cystalysin," *The Journal of Biological Chemistry*, vol. 278, no. 39, pp. 37336–37343, 2003.
- [40] Y. Kezuka, Y. Yoshida, and T. Nonaka, "Structural insights into catalysis by  $\beta$ C-S lyase from *Streptococcus anginosus*," *Proteins*, vol. 80, no. 10, pp. 2447–2458, 2012.
- [41] P. K. Mehta, T. I. Hale, and P. Christen, "Aminotransferases: demonstration of homology and division into evolutionary subgroups," *European Journal of Biochemistry*, vol. 214, no. 2, pp. 549–561, 1993.
- [42] D. Milić, T. V. Demidkina, N. G. Faleev, D. Matković-Čalogović, and A. A. Antson, "Insights into the catalytic mechanism of tyrosine phenol-lyase from X-ray structures of quinonoid intermediates," *The Journal of Biological Chemistry*, vol. 283, no. 43, pp. 29206–29214, 2008.



## Research Article

# Asymmetry of the Active Site Loop Conformation between Subunits of Glutamate-1-semialdehyde Aminomutase in Solution

Barbara Campanini,<sup>1</sup> Stefano Bettati,<sup>2,3</sup> Martino Luigi di Salvo,<sup>4</sup>  
Andrea Mozzarelli,<sup>1,3</sup> and Roberto Contestabile<sup>4</sup>

<sup>1</sup> Dipartimento di Farmacia, Università di Parma, Parco Area delle Scienze 23/A, 43124 Parma, Italy

<sup>2</sup> Dipartimento di Neuroscienze, Università di Parma, Via Volturno 39, 43125 Parma, Italy

<sup>3</sup> Istituto Nazionale di Biostrutture e Biosistemi, Viale Medaglie d'Oro 305, 00136 Roma, Italy

<sup>4</sup> Dipartimento di Scienze Biochimiche "A. Rossi-Fanelli", Sapienza Università di Roma, Piazzale Aldo Moro 5, 00185 Roma, Italy

Correspondence should be addressed to Roberto Contestabile; [roberto.contestabile@uniroma1.it](mailto:roberto.contestabile@uniroma1.it)

Received 15 May 2013; Accepted 27 June 2013

Academic Editor: Barbara Cellini

Copyright © 2013 Barbara Campanini et al. This is an open access article distributed under the Creative Commons Attribution License, which permits unrestricted use, distribution, and reproduction in any medium, provided the original work is properly cited.

Glutamate-1-semialdehyde aminomutase (GSAM) is a dimeric, pyridoxal 5'-phosphate (PLP)-dependent enzyme catalysing in plants and some bacteria the isomerization of L-glutamate-1-semialdehyde to 5-aminolevulinate, a common precursor of chlorophyll, haem, coenzyme B<sub>12</sub>, and other tetrapyrrolic compounds. During the catalytic cycle, the coenzyme undergoes conversion from pyridoxamine 5'-phosphate (PMP) to PLP. The entrance of the catalytic site is protected by a loop that is believed to switch from an open to a closed conformation during catalysis. Crystallographic studies indicated that the structure of the mobile loop is related to the form of the cofactor bound to the active site, allowing for asymmetry within the dimer. Since no information on structural and functional asymmetry of the enzyme in solution is available in the literature, we investigated the active site accessibility by determining the cofactor fluorescence quenching of PMP- and PLP-GSAM forms. PLP-GSAM is partially quenched by potassium iodide, suggesting that at least one catalytic site is accessible to the anionic quencher and therefore confirming the asymmetry observed in the crystal structure. Iodide induces release of the cofactor from PMP-GSAM, apparently from only one catalytic site, therefore suggesting an asymmetry also in this form of the enzyme in solution, in contrast with the crystallographic data.

## 1. Introduction

Chlorophyll, haem, coenzyme B<sub>12</sub>, and other tetrapyrrolic compounds share the same biosynthetic origin. They are assembled from four molecules of porphobilinogen, itself the product of the linkage of two 5-aminolevulinate (ALA) molecules [1]. In animals, yeast, and some bacteria, ALA is synthesised in the Shemin pathway, by the condensation of succinyl-CoA with glycine, followed by decarboxylation. The overall reaction is catalysed by ALA synthase, a pyridoxal 5'-phosphate-dependent enzyme [2]. Plants, green algae, and the majority of bacteria synthesise ALA in a completely different way. In these organisms, ALA is obtained through the

isomerisation of glutamate-1-semialdehyde (GSA), a compound deriving from glutamate [3]. This reaction is catalysed by glutamate-1-semialdehyde aminomutase (GSAM, EC 5.4.3.8), an enzyme belonging to fold type I PLP-dependent enzymes. The primary sequence and tertiary structure of GSAM are strongly related to the class III of aminotransferases [4]. GSAM is a potential target for safe selective herbicides and antibiotics because, while it carries out an essential role in the metabolism of plants and some pathogenic bacteria, it is absent in animals [5].

The mechanism of the aminomutase reaction catalysed by GSAM [6–8] is also closely analogous to that of the transamination reaction [9]. The exceptional feature of GSAM is

that, unlike aminotransferases, it catalyses an intramolecular exchange of the amino and carbonyl moieties, which are both present in the substrate. The catalytic cycle starts with GSA and the pyridoxamine 5'-phosphate (PMP) form of the enzyme and is completed without the need of a cognate amino acid substrate (Figure 1). A pivotal step in the mechanism is the isomerisation between the two aldimine intermediates that can be formed with either the 4 or the 5-amino group of the 4, 5-diaminovalerate (DAVA) intermediate. Whether this part of the reaction takes place through dissociation of DAVA (steps 3 and 4 in Figure 1) or formation of a geminal diamine intermediate (steps 3' and 4' in Figure 1) is unclear. Dissociation of DAVA appears mechanistically unnecessary, and even detrimental, although some dissociation has been found to occur to an extent governed by the concentration of the enzyme itself [10]. The PLP form of the enzyme is unable to catalyse the aminomutase reaction [10].

At the end of the purification procedure, dimeric GSAM from *Synechococcus* contains a mixture of PLP and PMP [7, 11]. This is invariably observed in GSAM purified from other sources [8, 12]. Preparations of native GSAM can be treated with substrate analogues that have either an amino or a carbonyl function and, therefore, react in a half-transamination reaction, converting the enzyme into either the PLP form or the PMP form [13]. Notably, crystallographic investigations on native GSAM from *Synechococcus* showed that the distribution of PLP and PMP was asymmetric within each enzyme dimer [14, 15]. Moreover, the two subunits showed asymmetry also in the mobility of a 19-residue loop (spanning residues 153–181), which has been shown to control access to the active site and limit the dissociation of the DAVA intermediate [16]. Crystallographic studies have been also carried out on the apoenzyme form and on double PLP or double PMP forms (containing the same form of cofactor in both subunits of the same dimer and obtained by adding either PLP or PMP to the apoenzyme) [15]. In the apo form, the active site loop is disordered in both subunits, whereas in the double PMP form, it is ordered and symmetrically opened. In the double PLP form, one loop is closed and the other is disordered (Table 1). It seems that the loop cannot be present in a closed conformation in both subunits at the same time. It is clear that the conformational state of the loop depends on the particular form of the cofactor present at the active site and is functional to the reaction trajectory of the aminomutase reaction catalysed by GSAM [15, 17]. When PMP is present at the active site, the loop is open, thus allowing substrate entry and product release. In contrast, when the active site contains PLP as internal aldimine and the intermediate DAVA, the loop is closed and access to the active site is obstructed by the short helical section of the loop residues 164–168 [15].

Since no studies on the structural and functional asymmetry of GSAM in solution have been reported in the literature, we investigated the effect of different fluorescence quenchers on the emission properties of the *Synechococcus* enzyme in solution, in order to ascertain the existence of a relationship between the form of the cofactor present at the active site and its accessibility.

## 2. Materials and Methods

**2.1. Materials.** GSA aminomutase from *Synechococcus* was expressed and purified as described previously [11]. All chemicals and buffers were purchased from Sigma-Aldrich (St. Louis, MO, USA) and were of the best available quality.

**2.2. Conversion of the Native Enzyme into the PLP and PMP Form.** Complete conversion of the enzyme into the PLP or PMP form was achieved using succinic semialdehyde and racemic 4, 5-diaminovalerate (DAVA), respectively, and followed by gel filtration. Succinic semialdehyde (20 mM) or DAVA (5 mM) was added to a solution (1 mL) of enzyme (60–300  $\mu$ M) in 100 mM Na-Tricine buffer, pH 7.9. Succinic semialdehyde or DAVA in the same buffer (1 mL, same concentrations) was loaded on a G-25 Sephadex column (45  $\times$  1 cm) and allowed to drain in before loading the enzyme. The column was equilibrated and eluted with 100 mM Na-Tricine, pH 7.9. The high molecular mass fraction was collected in the void volume well separated from small molecules.

**2.3. Absorbance and Fluorescence Spectroscopy.** PLP-GSAM and PMP-GSAM, stored as concentrated solutions in 100 mM Tricine pH 7.9, were diluted in 20 mM Tricine pH 7.9 for fluorescence and absorption spectroscopy experiments. Experiments were carried out at 25°C.

Absorption measurements were carried out using a Cary Scan 400 spectrophotometer (Varian Inc., Palo Alto, CA, USA). Temperature was maintained at  $25 \pm 0.5^\circ\text{C}$  with a circulating water bath.

The fluorescence emission of tryptophans and the four cofactor species under analysis were detected by exciting at 298 nm, 320 nm, 330 nm, 340 nm, and 420 nm, respectively, using a FluoroMax-3 fluorometer (HORIBA Jobin Yvon, Longjumeau Cedex, France) equipped with a thermostated cell holder. Excitation and emission slits were set at 3 nm except for excitation at 420 nm where 5 nm slits were used. Spectra were corrected for buffer contribution. The accessibility of the cofactor was assessed by fluorescence quenching. CsCl, KI, and acrylamide solutions were prepared in 20 mM Tricine, pH 7.9.  $\text{Na}_2\text{S}_2\text{O}_3$  at 0.01 mM concentration was added to KI solutions to prevent iodide oxidation. Fluorescence of either 6  $\mu$ M PLP-GSAM or 2  $\mu$ M PMP-GSAM was excited at 330 nm using 5 nm slits. Quenching data were analyzed with the Stern-Volmer equation [18]:

$$\frac{F_0}{F} = 1 + K_{\text{SV}} \cdot [\text{Q}], \quad (1)$$

where  $F_0$  is the fluorescence intensity in the absence of the quencher,  $F$  is the fluorescence at each given quencher concentration,  $K_{\text{SV}}$  is the Stern-Volmer constant, and  $[\text{Q}]$  is the concentration of the quencher.

**2.4. Time-Resolved Fluorescence Spectroscopy.** Fluorescence intensity decays were measured by the phase and modulation technique [19, 20] using an ISS GREG 200 fluorometer (ISS Inc., Champaign, IL, USA). PLP-GSAM fluorescence decays were measured at a protomer concentration of 48.8  $\mu$ M, upon

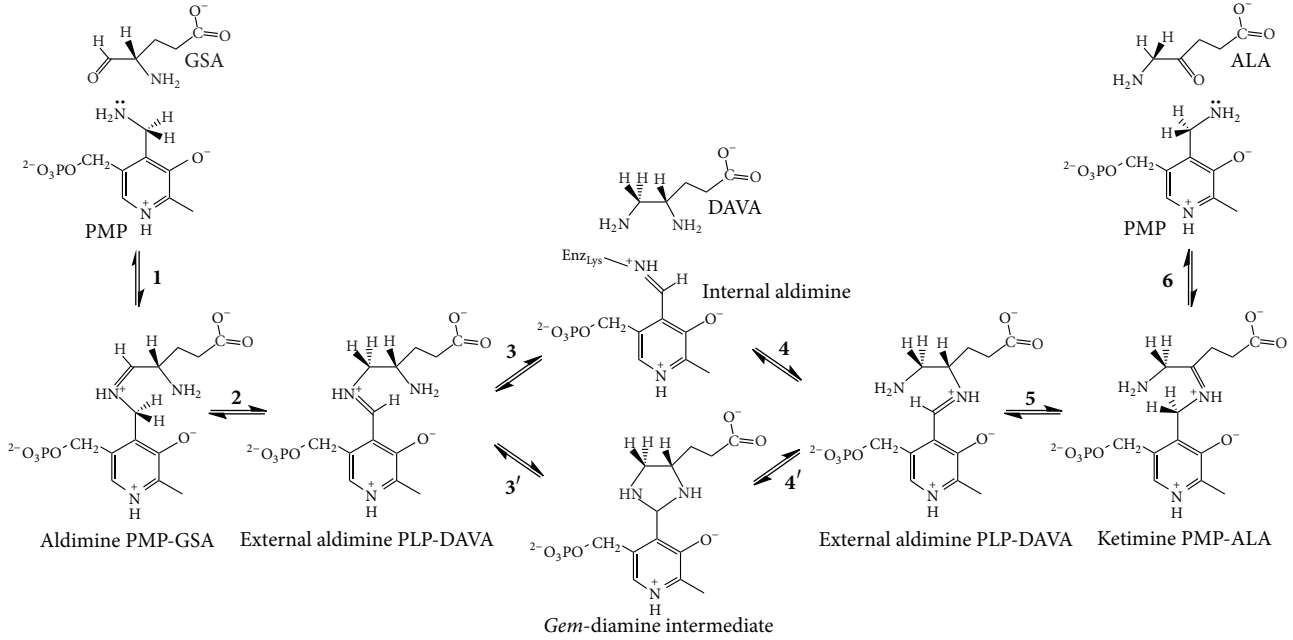


FIGURE 1: Proposed mechanism for the reaction catalysed by GSAM.

 TABLE 1: Conformation of the active site loop in different crystal forms of dimeric *Synechococcus* GSAM [15].

Enzyme form	Loop at subunit 1	Loop at subunit 2
apo-GSAM	Disordered	Disordered
PMP-GSAM	Ordered, open	Ordered, open
PLP-GSAM	Ordered, closed	Disordered

excitation at 330 nm performed using a 300 W xenon lamp and a Jobin Yvon monochromator with 16 nm band width. A *p*-bis [2-(phenoxazoyl)] benzene (POPOP) solution was used as a lifetime standard reference ( $\tau = 1.05$  ns). To eliminate polarization artifacts in the intensity decay, data were collected under magic angle conditions with the excitation light polarized normal to the laboratory plane,  $0^\circ$ , and the emission polarizer oriented at  $54.7^\circ$  [20]. Samples were equilibrated at  $25 \pm 0.5^\circ\text{C}$  using a jacketed cell holder and a circulating water bath. A set of 20 modulation frequencies, varied continuously in the 2 to 200 MHz range, was used. Data were fitted to a sum of discrete exponentials [21] with lifetime  $\tau_i$  and fractional intensity  $f_i$  by the Marquardt algorithm of the Globals Unlimited software (University of Illinois, Urbana, IL, USA) [22]. Frequency-independent standard error values of  $0.2^\circ$  for phase data and 0.004 for modulation data were routinely applied. The  $\chi^2$  minimization was the criterion used to select the best fits [19, 21]. The  $\tau_i$  and  $f_i$  values reported in Results and Discussion represent the average of three measurements on different samples.

Mean lifetimes  $\langle\tau\rangle$  were obtained from lifetimes  $\tau_i$  and fractional intensities  $f_i$  according to the equation [23]:

$$\langle\tau\rangle = \sum \alpha_i \cdot \tau_i, \quad (2)$$

where  $\alpha_i$ , the preexponential factor for a multiexponential decay law, was determined as

$$\alpha_i = \frac{f_i/\tau_i}{\sum f_i/\tau_i}. \quad (3)$$

### 3. Results and Discussion

#### 3.1. Spectroscopic Properties of PLP-GSAM and PMP-GSAM.

Two freshly prepared forms of the enzyme from *Synechococcus* were used: the PLP form (PLP-GSAM), obtained by treating the native enzyme with succinic-1-semialdehyde, and the PMP form (PMP-GSAM), obtained by the addition of DAVA [13]. The absorption spectra of equimolar solutions of PLP-GSAM and PMP-GSAM are shown in Figure 2. The absorption spectrum of PLP-GSAM shows, in addition to the band of aromatic amino acids centred at 278 nm, a major band centred at 418 nm, typical of the internal aldimine between PLP and the active site lysine, and a modest though measurable absorbance at about 330 nm that could be attributed to the enolimine tautomer of the internal aldimine or to traces of PMP bound to the active site of the enzyme. Several PLP-binding enzymes exhibit equilibrium between enolimine and ketoenamine tautomers of the Schiff base formed by the coenzyme with the active site lysine (internal aldimine) or with a bound amino acid or reaction intermediate (external aldimines). Ketoenamine tautomers absorb light at longer wavelength with respect to enolimine and are favored in more polar active sites [24]. PMP-GSAM shows a band at 340 nm attributed to PMP in the active site of the enzyme [6]. No absorption from the internal aldimine of PLP is discernible in the visible range of the spectrum. The absorption spectrum confirms that PMP-GSAM is pure with respect to the content of the cofactor.

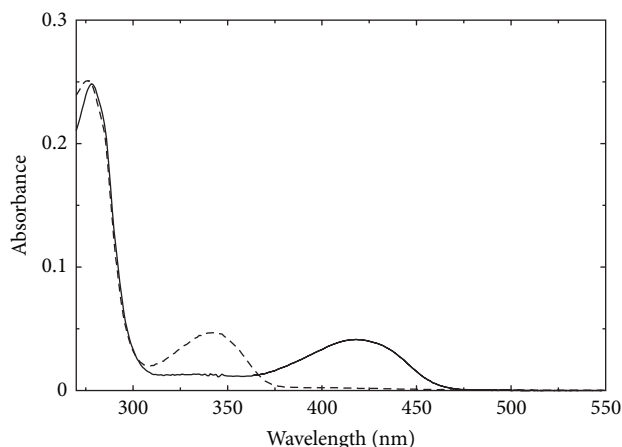


FIGURE 2: Absorption spectra of PLP-GSAM and PMP-GSAM. Absorption spectra of PLP-GSAM (solid line) and PMP-GSAM (dashed line) recorded on a solution containing  $7.1 \mu\text{M}$  protein in 20 mM Tricine, pH 7.9.

The intrinsic fluorescence of tryptophans and coenzyme has been previously exploited to investigate structural and dynamic features of some PLP-dependent enzymes and their modification upon binding of substrates, inhibitors, and regulatory molecules [25–30]. In GSAM, both PLP and PMP are fluorescent upon excitation in either the UV or visible range of the spectrum. At 298 nm, tryptophan fluorescence is selectively excited, with almost no contribution from the other aromatic side chains of tyrosine and phenylalanine. When excited at 298 nm, both PLP-GSAM and PMP-GSAM show an emission band centred at about 345 nm characteristic of direct tryptophan emission (Figure 3(a)). Emission from PMP-GSAM is slightly less intense than that of PLP-GSAM. GSAM has two tryptophans, Trp53 and Trp67. Trp67 is buried inside the protein structure at about  $10 \text{ \AA}$  from the cofactor, whereas Trp53 is exposed to the solvent far away from the active site. The distance between Trp67 and the coenzyme is compatible with Förster resonance energy transfer from the former to the latter [25, 31]. However, differently from what observed for other PLP-dependent enzymes like *O*-acetylserine sulphydrylase [25] or tryptophan synthase [32], the perpendicular spatial disposition of the two chromophores appears to hinder an efficient energy transfer, as demonstrated by the emission spectrum upon excitation at 298 nm where no bands around 500, attributable to coenzyme emission, are observed, except for a barely detectable shoulder in the case PLP-GSAM (Figure 3(a)).

Upon excitation at 420 nm, only PLP-GSAM yields a significant emission, with a band centered at 500 nm (Figure 3(b)). In agreement with absorption data, this observation further supports the notion that PMP-GSAM samples do not carry significant amounts of cofactor in the PLP form.

Both PMP-GSAM and PLP-GSAM show fluorescence emission upon excitation at around 330 nm (Figures 3(c) and 3(d)). The shape of PMP-GSAM emission spectrum does not depend on the excitation wavelength in the 320–340 nm range, and the emission intensity is maximum at

$\lambda_{\text{ex}} = 340 \text{ nm}$ , consistent with the absorbance spectrum (Figure 2). The emission spectra of PLP-GSAM for excitation at 320, 330, and 340 nm also show a broad band centred at about 390 nm, that could be due to the direct emission of the enolimine tautomer of PLP or to the presence of some fraction of subunits carrying a chromophore in the PMP form. If the latter was predominantly the case, we would expect fluorescence emission to parallel the behaviour of PMP-GSAM, with emission intensity increasing consistently from  $\lambda_{\text{ex}} = 320 \text{ nm}$  to  $\lambda_{\text{ex}} = 340 \text{ nm}$ . Moreover, the emission band of PLP-GSAM excited at 320 and 330 nm appears to have a slightly red-shifted (by 3–4 nm) peak wavelength with respect to PMP-GSAM, and is definitely more asymmetric, being broader on the low energy side of the emission spectrum (the ratio of emission intensity at 390 and 500 nm is about 5, compared to more than 20 for PMP-GSAM). Furthermore, differently from PMP-GSAM, when PLP-GSAM is excited at 340 nm, the main emission band is slightly decreased in intensity and is accompanied by a shoulder at about 500 nm (Figure 3(c)), most likely due to direct excitation of the high energy tail of the absorption band of PLP ketoenamine tautomer [30, 33, 34]. The presence of a discrete emission at around 500 nm could also originate from the ketoenamine tautomer that forms in the excited state following proton transfer from the  $3' \text{-OH}$  group to the imine nitrogen [35, 36]. This observation further supports the view that the absorption at around 330 nm arises from the enolimine tautomer of the internal aldimine rather than from a substituted aldimine, as previously pointed out for other PLP-dependent enzymes [35, 37].

The results of absorbance and fluorescence emission spectroscopic characterization clearly indicate that the PLP-GSAM and PMP-GSAM preparations used in this work are at least 90% pure with respect to the state of the bound cofactor.

**3.2. Fluorescence Quenching.** Fluorescence quenching is a powerful technique to assess the accessibility of fluorophores to the solvent. We have previously exploited this approach to investigate changes in cofactor accessibility of wild-type and mutant forms of another PLP-dependent enzyme, *O*-acetylserine sulphydrylase [38]. Quenchers that are commonly used in protein fluorescence are caesium (as chloride salt), iodide (as potassium salt), and acrylamide. The different polarity and charge of these molecules allow the application of fluorescence quenching to assess the accessibility of both apolar and polar sites. In fact, the polarity of the site entrance influences the access of the quencher independently of the steric accessibility of the site. The active site of GSAM is mainly edged by positively charged residues likely to hamper the access to the positively charged caesium ions [14]. Quenching experiments were carried out exciting the fluorescence of the cofactor at 330 nm. Both acrylamide and caesium chloride proved to be ineffective at quenching the cofactor fluorescence. In particular, whereas acrylamide does not show any effect on the emission intensity of the cofactor up to about 1 M, caesium chloride induces an increase, rather than a decrease, in the cofactor emission intensity of both PMP-GSAM and PLP-GSAM (Figure 4(a)). The same effect



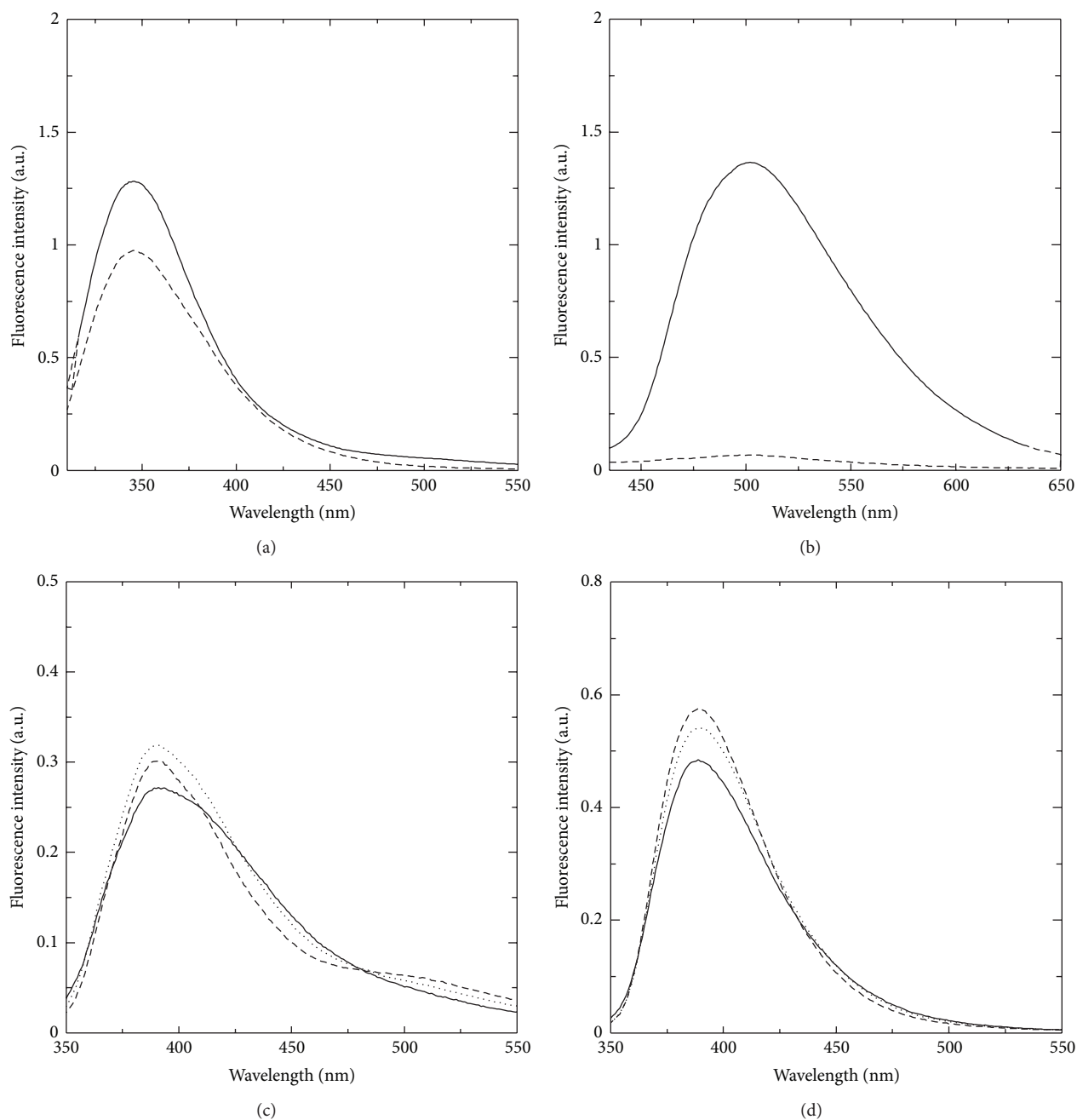


FIGURE 3: Fluorescence emission spectra of PLP-GSAM and PMP-GSAM. To allow direct comparison of the data, the reported spectra are normalized for protein concentration. Spectra were collected in 20 mM Tricine buffer, pH 7.9 solutions and were normalized to a protein concentration of 7  $\mu$ M. (a) Emission spectra of PLP-GSAM (solid line) and PMP-GSAM (dashed line) upon excitation at 298 nm with 3 nm emission and excitation slits. (b) Emission spectra of PLP-GSAM (solid line) and PMP-GSAM (dashed line) upon excitation at 420 nm with 5 nm emission and excitation slits. (c) Emission spectra of PLP-GSAM upon excitation at 320 nm (solid line), 330 nm (dotted line), and 340 nm (dashed line) with 3 nm emission and excitation slits. (d) Emission spectra of PMP-GSAM upon excitation at 320 nm (solid line), 330 nm (dotted line), and 340 nm (dashed line) with 3 nm emission and excitation slits.

is observed if caesium chloride is substituted by potassium chloride (Figure 4(a)) or potassium acetate (data not shown), suggesting a nonspecific effect of the ionic strength on the fluorescence quantum yield of the cofactor. The effect is more pronounced on PMP-GSAM, leading to a doubling of the signal at about 140 mM salt.

On the other hand, potassium iodide is effective in quenching the fluorescence of PLP-GSAM (Figure 4(b)), indicating that at least one catalytic site is in an open conformation, accessible to the anionic quencher. The linearity of data shown in Figure 4(b) demonstrates that the enolimine form of enzyme-bound PLP is exposed to a structurally

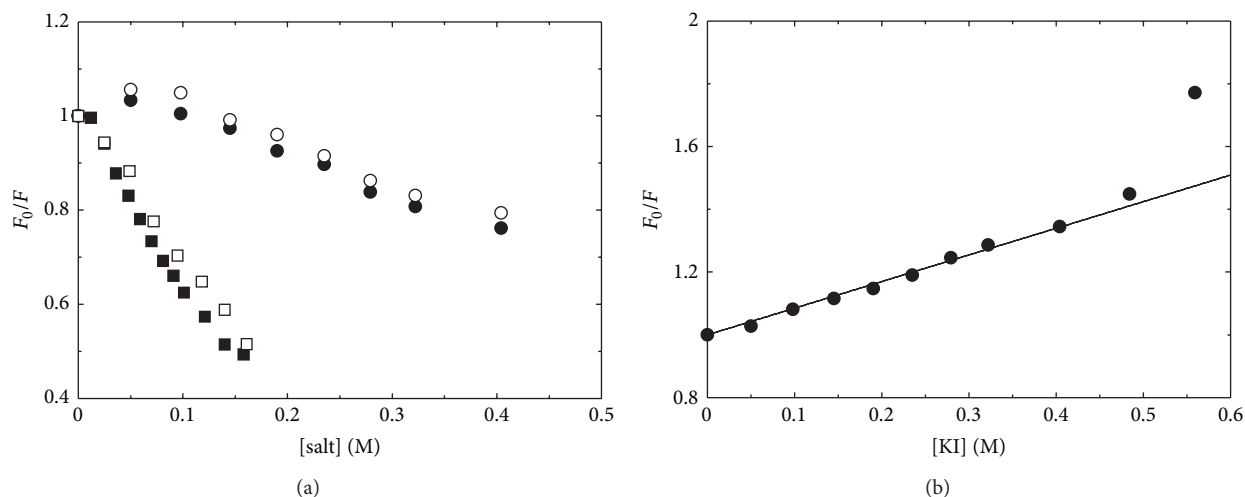


FIGURE 4: Dependence of fluorescence emission intensity on quencher concentration. (a) Dependence of the relative emission intensity at 384 nm, upon excitation at 330 nm, of PLP-GSAM (circles) and PMP-GSAM (squares) on caesium chloride (closed symbols) and potassium chloride (open symbols) concentration. (b) Stern-Volmer plot for the quenching of PLP-GSAM by iodide. The line through data points represents the fitting to (1).

homogeneous environment. The ionic radius of  $\text{Cs}^+$  is about  $1.6 \text{ \AA}$  whereas the ionic radius of  $\text{I}^-$  is about  $2.2 \text{ \AA}$ , so the differences in the accessibility to the active site cannot be ascribed to steric effects but rather to electrostatic repulsion between  $\text{Cs}^+$  and polar or positively charged groups at the active site entrance. The analysis of experimental data in Figure 4(b) according to (1) (Materials and Methods) gave a Stern-Volmer constant ( $K_{\text{SV}}$ ) value of  $0.84 \pm 0.01 \text{ M}^{-1}$ . Since the value of  $K_{\text{SV}}$  that we measured for quenching by iodide of free PLP in solution is  $2.61 \pm 0.07 \text{ M}^{-1}$ , in agreement with data present in the literature [39], it appears that the active site of PLP-GSAM is only partially accessible to the solvent. More significantly, the difference between the bimolecular quenching rate constants (i.e., the ratio between  $K_{\text{SV}}$  and the lifetime of the excited state [39–41]) of free PLP and PLP-GSAM complexes, that are the true measure of active site accessibility, should be larger than the difference between the Stern-Volmer constants, considering that the fluorescence lifetime of free PLP is expected to be significantly smaller than that of protein-bound PLP. The fluorescence lifetime decays of PLP-GSAM are well fitted by two discrete exponential components with lifetimes of  $8.6 \pm 0.2$  and  $1.40 \pm 0.05 \text{ ns}$  and fractional intensity of  $10.3 \pm 0.8\%$  and  $89.7 \pm 0.8\%$ , respectively, (data not shown). The mean lifetime, calculated as reported in Materials and Methods, is  $1.53 \text{ ns}$ . This value can be compared to those calculated from data reported in the literature [25] for free PLP in solution and PLP-L-valine, a model compound of PLP Schiff base, upon excitation at  $330 \text{ nm}$ :  $0.32 \text{ ns}$  and  $0.68 \text{ ns}$ , respectively. By considering the latter a better mimic of PLP bound to the enzyme as an internal aldimine, a ratio of about 7 can be calculated between the apparent bimolecular quenching rate constant of PLP-L-valine ( $3.84 \cdot 10^{-9} \text{ M}^{-1} \text{ s}^{-1}$ ) and PLP-GSAM ( $0.55 \cdot 10^{-9} \text{ M}^{-1} \text{ s}^{-1}$ ). These values are in good agreement with those previously reported for free coenzyme and the internal

aldimine of the PLP-dependent enzyme tryptophan synthase  $\alpha_2\beta_2$  complex ( $0.52 \cdot 10^{-9} \text{ M}^{-1} \text{ s}^{-1}$ ) [39], known to be in an “open” conformation [42].

At potassium iodide concentrations higher than  $0.5 \text{ M}$ , the Stern-Volmer plot of PLP-GSAM quenching by iodide shows an upward curvature (Figure 4(b)) that could be due to a static quenching component or to a conformational change in the protein structure that leads to a change in the accessibility of the active site to the quencher. For example, an upward curvature of the Stern-Volmer plot of the tetrameric PLP-dependent enzyme tryptophan synthase was attributed to subunit dissociation induced by potassium iodide [39].

Interestingly, the same iodide quenching experiment on PLP-GSAM, carried out following the fluorescence emission intensity upon excitation at  $420 \text{ nm}$ , gives only small changes in the relative fluorescence intensity (data not shown). This suggests that the fraction of PLP present in the ketoenamine form is less accessible by the anionic quencher. This could be due in principle to a closed conformation of the active site or to a different arrangement of polar and charged residues at the active entrance with respect to the enolimine tautomer.

All together, the results obtained with PLP-GSAM indicate, in agreement with the crystallographic data, a degree of structural asymmetry in the microenvironment surrounding the enzyme-bound PLP. This asymmetry might correspond to an asymmetric distribution of the ketoenamine (less accessible) and enolimine forms of PLP at the two active sites of the enzyme.

The dependence of the emission spectrum of PMP-GSAM on potassium iodide concentration is complex. The intensity of the emission upon excitation at  $330 \text{ nm}$  increases with increasing KI concentrations up to about  $250 \text{ mM}$  and then decreases with a red shift of the peak maximum (data not shown). Differently from what we observed on PLP-GSAM, the emission signal in the presence of KI is not stable with

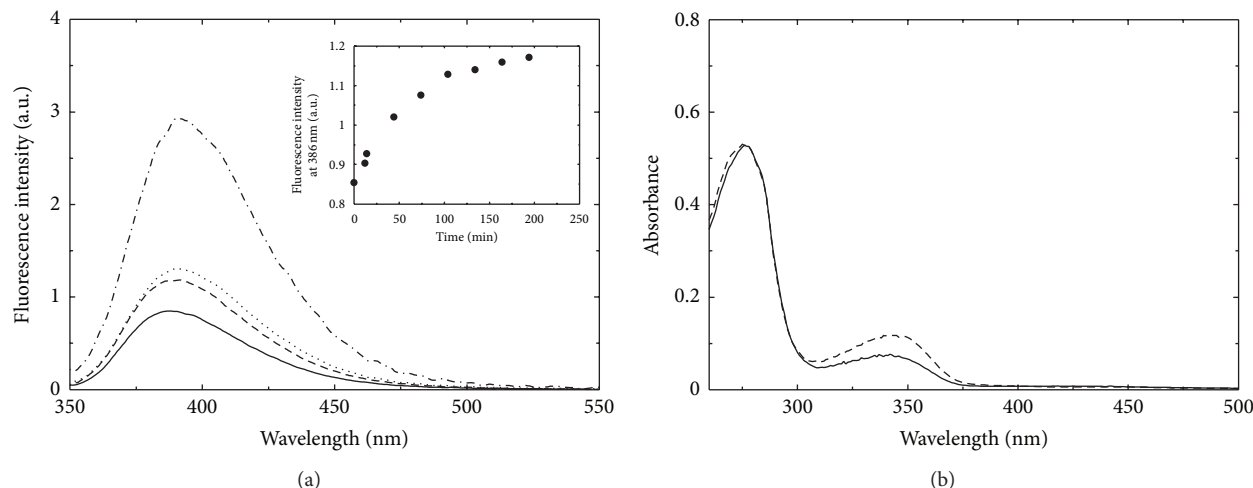


FIGURE 5: KI-induced release of the cofactor from PMP-GSAM. (a) Fluorescence emission spectra upon excitation at 330 nm of 2  $\mu$ M PMP-GSAM in the absence (solid line) and in the presence (dashed line) of 50 mM KI (after 195 minutes incubation). The emission spectra of 2  $\mu$ M PMP in Tricine (dashed-dotted line) and 1  $\mu$ M PMP in Tricine plus 1  $\mu$ M PMP-GSAM (dotted line) are shown for comparison. Inset: time course of the fluorescence emission intensity of 2  $\mu$ M PMP-GSAM ( $\lambda_{\text{ex}} = 330$  nm,  $\lambda_{\text{em}} = 386$  nm) after the addition of 50 mM KI. (b) Absorbance spectrum of a solution of PMP-GSAM before (solid line) and after (dashed line) treatment with 50 mM KI. The protein solution was mixed with a concentrated solution of KI to a final concentration of 50 mM and extensively dialyzed first against 50 mM KI in Tricine buffer pH 7.9 and then against KI-free buffer.

time, but, at low KI concentrations, it increases with time (Figure 5(a), inset). The fluorescence emission intensity of PMP free in solution is about 3 times higher than that of PMP bound to GSAM (Figure 5(a)). The increase of fluorescence emission caused by KI could thus be due to the release of the cofactor from the catalytic site, and the decrease and red-shifting of emission intensity at higher quencher concentration might be related to quenching of PMP free in solution. Indeed, the spectrum of 2  $\mu$ M PMP-GSAM after 195 minutes incubation in 50 mM KI nearly coincides with that calculated, adding the absorption of 1  $\mu$ M PMP in the presence of 50 mM KI to that of 1  $\mu$ M PMP-GSAM. This finding suggests that about 50% of the cofactor has been released from PMP-GSAM complex. This was confirmed by dialysis experiments in which a solution of PMP-GSAM containing 50 mM KI was first dialysed against 50 mM KI and then against KI-free buffer. After dialysis, the absorption peak of the cofactor was reduced by 1.6-fold (Figure 5(b)), further indicating that treatment with KI causes the release of about 50% PMP from PMP-GSAM. Other anions were previously shown to cause, at high concentration, the release of PMP from the active site, for example, GSAM from pea leaves treated with 0.2 M phosphate at acidic pH [43]. Interestingly, also in that case the release of PMP was not complete, about 44% of the theoretical amount.

Our results, showing that 50% of PMP dissociates from the enzyme at low KI concentration, suggest the release of PMP from only one active site and imply a structural asymmetry of the double PMP form of GSAM. This is in contrast with the previously published crystallographic data, showing that in the PMP-GSAM form, the active site loop is ordered and symmetrically opened in both subunits [15]. The asymmetry of PMP-GSAM in solution could be either

preexisting or be generated once a single PMP molecule has left the dimer. The preexisting asymmetry could originate from the different experimental protocols used to prepare PMP-GSAM: by addition of PMP to the apoenzyme (crystallographic data), or by the addition of DAVA to the native enzyme, that is typically purified as an asymmetric PLP/PMP form (this work). In our PMP-GSAM, one active site of the dimer may still contain the reaction product. Indeed, we previously observed some instability, upon prolonged storage, of the PLP- and PMP-GSAM preparations obtained by reacting native GSAM with substrate analogues undergoing half-transamination reaction. Although from the absorption spectra, they appear to contain only one or the other form of the cofactor when freshly prepared, they seem to slowly revert to a form containing both PLP and PMP (data not shown). Interestingly, in the characterisation of different spectral forms of GSAM by electrospray mass spectrometry, Brody et al. [44] reported that reduction with  $\text{NaBH}_4$  of the PLP form yielded two molecular species of different mass, suggesting that the cofactor was actually present also as PMP. The PMP form obtained by the same authors was also recognised to have a “barely detectable” absorption peak at 420 nm.

#### 4. Conclusion

The asymmetry of the active site loop conformation between subunits of dimeric glutamate-1-semialdehyde aminomutase in solution was investigated by fluorescence spectroscopy. Cationic and neutral quenchers are ineffective in quenching PMP-GSAM and PLP-GSAM fluorescence, likely due to the distribution of positive charges that characterizes the entrance of the active site of both enzyme forms. On the other

hand, KI quenches PLP-GSAM fluorescence, although only the fraction of coenzyme molecules present as the enolimine tautomer is significantly accessible to the solvent, clearly indicating an asymmetric structure of the active sites. These observations match the crystallographic data, which show an asymmetric conformation of the loop controlling access to the active site, so that when the enzyme is in the double PLP form, one loop is closed and the other is disordered [15]. Due to the known effect of environment polarity on the equilibrium between the enolimine and ketoenamine forms of PLP, it is tempting to assume that selective quenching of the enolimine arises from asymmetric loop closure stabilizing a different equilibrium of tautomers at the two active sites.

Comparatively low concentrations of KI cause the release of PMP from PMP-GSAM, apparently only from one subunit of the dimer. A possible interpretation of this result is that the double PMP-GSAM presents active site structural asymmetry, in contrast to previous crystallographic reports. Alternatively, this asymmetry may be generated once one PMP molecule has left the dimeric enzyme. This latter explanation is not in contrast with the crystallographic data and relies on the fact that communication between subunits of the GSAM dimer has been shown experimentally and has been proposed on the basis of structural and mechanistic considerations [15–17].

Other important examples of involvement of an active site gating loop in PLP-dependent catalysis are found in fold-type I decarboxylases, such as human isoforms of glutamate decarboxylase [45] and DOPA decarboxylase [46]. In these enzymes, an active site loop plays a pivotal role in controlling reaction specificity. In *O*-acetylserine sulphydrylase, the interaction of the substrate carboxylate with a substrate-binding loop, highly conserved from bacteria to plants, triggers the closure of the active site to favor catalysis through proper positioning of substrate-binding groups and exclusion of water molecules [47–49]. Indeed, the control of substrate and reaction specificity, and catalytic efficiency, through an equilibrium between “open” and “closed” states of the active site appears to be a common feature in PLP-dependent enzymes [50].

## Abbreviations

ALA:	5-Aminolevulinate
DAVA:	4,5-Diaminovalerate
GSA:	L-Glutamate-1-semialdehyde
GSAM:	Glutamate-1-semialdehyde aminomutase
PLP:	Pyridoxal 5'-phosphate
PLP-GSAM:	GSAM form with PLP bound to both subunits of the dimer
PMP:	Pyridoxamine 5'-phosphate
PMP-GSAM:	GSAM form with PMP bound to both subunits of the dimer.

## Acknowledgments

This work was partly supported by grants from the Italian Ministero dell'Istruzione, dell'Università e della Ricerca and

from Finanziamento Progetti di Ricerca 2011 of Sapienza University of Rome.

## References

- [1] P. M. Jordan and D. Shemin,  *$\delta$ -Aminolevulinic Acid Synthetase, in the Enzymes*, Academic Press, New York, NY, USA, 1972.
- [2] S. I. Beale and J. D. Weinstein, *Biosynthesis of Haem and Chlorophylls*, McGraw-Hill, New York, NY, USA, 1990.
- [3] C. G. Kannangara, S. P. Gough, P. Bruyant, J. K. Hooper, A. Kahn, and D. von Wettstein, “tRNA(Glu) as a cofactor in delta-aminolevulinate biosynthesis: steps that regulate chlorophyll synthesis,” *Trends in Biochemical Sciences*, vol. 13, pp. 139–143, 1988.
- [4] N. V. Grishin, M. A. Phillips, and E. J. Goldsmith, “Modeling of the spatial structure of eukaryotic ornithine decarboxylases,” *Protein Science*, vol. 4, pp. 1291–1304, 1995.
- [5] R. Contestabile, T. Jenn, M. Akhtar, D. Gani, and R. A. John, “Reactions of glutamate 1-semialdehyde aminomutase with R- and S-enantiomers of a novel, mechanism-based inhibitor, 2,3-diaminopropyl sulfate,” *Biochemistry*, vol. 39, no. 11, pp. 3091–3096, 2000.
- [6] M. A. Smith, C. G. Kannangara, B. Grimm, and D. Von Wettstein, “Characterization of glutamate-1-semialdehyde aminotransferase of *Synechococcus*. Steady-state kinetic analysis,” *European Journal of Biochemistry*, vol. 202, no. 3, pp. 749–757, 1991.
- [7] M. A. Smith, B. Grimm, C. G. Kannangara, and D. Von Wettstein, “Spectral kinetics of glutamate-1-semialdehyde aminomutase of *Synechococcus*,” *Proceedings of the National Academy of Sciences of the United States of America*, vol. 88, no. 21, pp. 9775–9779, 1991.
- [8] C. E. Pugh, J. L. Harwood, and R. A. John, “Mechanism of glutamate semialdehyde aminotransferase: roles of diamino- and dioxo-intermediates in the synthesis of aminolevulinate,” *Journal of Biological Chemistry*, vol. 267, no. 3, pp. 1584–1588, 1992.
- [9] P. Christen and D. E. Metzler, *Transaminases*, Wiley, New York, NY, USA, 1995.
- [10] R. J. Tyacke, J. L. Harwood, and R. A. John, “Properties of the pyridoxalimine form of glutamate semialdehyde aminotransferase (glutamate-1-semialdehyde 2,1-aminomutase) and analysis of its role as an intermediate in the formation of aminolaevulinate,” *Biochemical Journal*, vol. 293, part 3, pp. 697–701, 1993.
- [11] B. Grimm, A. J. Smith, C. G. Kannangara, and M. Smith, “Gabaculine-resistant glutamate 1-semialdehyde aminotransferase of *Synechococcus*: deletion of a tripeptide close to the NH<sub>2</sub> terminus and internal amino acid substitution,” *Journal of Biological Chemistry*, vol. 266, no. 19, pp. 12495–12501, 1991.
- [12] L. L. Ilag and D. Jahn, “Activity and spectroscopic properties of the *Escherichia coli* glutamate 1-semialdehyde aminotransferase and the putative active site mutant K265R,” *Biochemistry*, vol. 31, no. 31, pp. 7143–7151, 1992.
- [13] S. D'Aguzzo, I. N. Gonzales, M. Simmaco, R. Contestabile, and R. A. John, “Stereochemistry of the reactions of glutamate-1-semialdehyde aminomutase with 4,5-diaminovalerate,” *Journal of Biological Chemistry*, vol. 278, no. 42, pp. 40521–40526, 2003.
- [14] M. Hennig, B. Grimm, R. Contestabile, R. A. John, and J. N. Jansonius, “Crystal structure of glutamate-1-semialdehyde aminomutase: an  $\alpha$ 2-dimeric vitamin B6-dependent enzyme



- with asymmetry in structure and active site reactivity,” *Proceedings of the National Academy of Sciences of the United States of America*, vol. 94, no. 10, pp. 4866–4871, 1997.
- [15] J. Stetefeld, M. Jenny, and P. Burkhard, “Intersubunit signaling in glutamate-1-semialdehyde-aminomutase,” *Proceedings of the National Academy of Sciences of the United States of America*, vol. 103, no. 37, pp. 13688–13693, 2006.
- [16] R. Contestabile, S. Angelaccio, R. Maytum, F. Bossa, and R. A. John, “The contribution of a conformationally mobile, active site loop to the reaction catalyzed by glutamate semialdehyde aminomutase,” *Journal of Biological Chemistry*, vol. 275, no. 6, pp. 3879–3886, 2000.
- [17] J. L. Sorensen and J. Stetefeld, “Kinemage of action—proposed reaction mechanism of glutamate-1-semialdehyde aminomutase at an atomic level,” *Biochemical and Biophysical Research Communications*, vol. 413, no. 4, pp. 572–576, 2011.
- [18] M. R. Eftink and C. A. Ghiron, “Fluorescence quenching studies with proteins,” *Analytical Biochemistry*, vol. 114, no. 2, pp. 199–227, 1981.
- [19] E. Gratton and M. Limkeman, “A continuously variable frequency cross-correlation phase fluorometer with picosecond resolution,” *Biophysical Journal*, vol. 44, no. 3, pp. 315–324, 1983.
- [20] R. D. Spencer and G. Weber, “Measurements of subnanosecond fluorescence lifetimes with a cross-correlation phase fluorometer,” *Annals of the New York Academy of Sciences*, vol. 158, pp. 361–376, 1969.
- [21] D. M. Jameson and T. L. Hazlett, “Time resolved fluorescence in biology and biochemistry,” in *Biophysical and Biochemical Aspects of Fluorescence Spectroscopy*, T. G. Dewey, Ed., pp. 106–133, Plenum, New York, NY, USA, 1991.
- [22] J. M. Beechem and E. Gratton, “Time-resolved laser spectroscopy in biochemistry,” in *Proceedings of the SPIE*, International Society for Optical Engineering, Bellingham, Wash, USA, 1988.
- [23] M. R. Eftink, “The use of fluorescence methods to monitor unfolding transitions in proteins,” *Biophysical Journal*, vol. 66, no. 2 I, pp. 482–501, 1994.
- [24] E. J. Faeder and G. G. Hammes, “Kinetic studies of tryptophan synthetase. Interaction of L-serine, indole, and tryptophan with the native enzyme,” *Biochemistry*, vol. 10, no. 6, pp. 1041–1045, 1971.
- [25] S. Benci, S. Vaccari, A. Mozzarelli, and P. F. Cook, “Time-resolved fluorescence of O-acetylserine sulphydrylase,” *Biochimica et Biophysica Acta*, vol. 1429, no. 2, pp. 317–330, 1999.
- [26] E. Salsi, R. Guan, B. Campanini et al., “Exploring O-acetylserine sulphydrylase-B isoenzyme from *Salmonella typhimurium* by fluorescence spectroscopy,” *Archives of Biochemistry and Biophysics*, vol. 505, no. 2, pp. 178–185, 2011.
- [27] A. Mozzarelli and S. Bettati, “Exploring the pyridoxal 5'-phosphate-dependent enzymes,” *Chemical Record*, vol. 6, no. 5, pp. 275–287, 2006.
- [28] A. Chattopadhyay, M. Meier, S. Ivaninskii et al., “Structure, mechanism, and conformational dynamics of O-acetylserine sulphydrylase from *Salmonella typhimurium*: comparison of A and B isozymes,” *Biochemistry*, vol. 46, no. 28, pp. 8315–8330, 2007.
- [29] E. Salsi, B. Campanini, S. Bettati et al., “A two-step process controls the formation of the bienzyme cysteine synthase complex,” *Journal of Biological Chemistry*, vol. 285, no. 17, pp. 12813–12822, 2010.
- [30] E. Pennacchietti, T. M. Lammens, G. Capitani et al., “Mutation of His465 alters the pH-dependent spectroscopic properties of *Escherichia coli* glutamate decarboxylase and broadens the range of its activity toward more alkaline pH,” *Journal of Biological Chemistry*, vol. 284, no. 46, pp. 31587–31596, 2009.
- [31] P. J. R. Lakowicz, *Principles of Fluorescence Spectroscopy*, Plenum Press, New York, NY, USA, 1983.
- [32] S. Vaccari, S. Benci, A. Peracchi, and A. Mozzarelli, “Time-resolved fluorescence of tryptophan synthase,” *Biophysical Chemistry*, vol. 61, no. 1, pp. 9–22, 1996.
- [33] M. Arrio-Dupont, “Fluorescence study of Schiff bases of pyridoxal. Comparison with L-aspartate aminotransferase,” *Photochemistry and Photobiology*, vol. 12, no. 4, pp. 297–315, 1970.
- [34] E. Passera, B. Campanini, F. Rossi et al., “Human kynurenine aminotransferase II—reactivity with substrates and inhibitors,” *FEBS Journal*, vol. 278, no. 11, pp. 1882–1900, 2011.
- [35] M. T. Olmo, F. Sánchez-Jiménez, M. A. Medina, and H. Hayashi, “Spectroscopic analysis of recombinant rat histidine decarboxylase,” *Journal of Biochemistry*, vol. 132, no. 3, pp. 433–439, 2002.
- [36] S. Benci, S. Vaccari, A. Mozzarelli, and P. F. Cook, “Time-resolved fluorescence of O-acetylserine sulphydrylase catalytic intermediates,” *Biochemistry*, vol. 36, no. 49, pp. 15419–15427, 1997.
- [37] M. Bertoldi, B. Cellini, T. Clausen, and C. B. Voltattorni, “Spectroscopic and kinetic analyses reveal the pyridoxal 5'-phosphate binding mode and the catalytic features of *Treponema denticola* cystalysin,” *Biochemistry*, vol. 41, no. 29, pp. 9153–9164, 2002.
- [38] B. Campanini, S. Raboni, S. Vaccari et al., “Surface-exposed tryptophan residues are essential for O-acetylserine sulphydrylase structure, function, and stability,” *Journal of Biological Chemistry*, vol. 278, no. 39, pp. 37511–37519, 2003.
- [39] A. N. Lane, “The accessibility of the active site and conformation states of the beta 2 subunit of tryptophan synthase studied by fluorescence quenching,” *European Journal of Biochemistry*, vol. 133, no. 3, pp. 531–538, 1983.
- [40] M. R. Eftink and C. A. Ghiron, “Exposure of tryptophanyl residues in proteins. Quantitative determination by fluorescence quenching studies,” *Biochemistry*, vol. 15, no. 3, pp. 672–680, 1976.
- [41] M. R. Eftink and C. A. Ghiron, “Fluorescence quenching of indole and model micelle systems,” *Journal of Physical Chemistry*, vol. 80, no. 5, pp. 486–493, 1976.
- [42] S. Raboni, S. Bettati, and A. Mozzarelli, “Tryptophan synthase: a mine for enzymologists,” *Cellular and Molecular Life Sciences*, vol. 66, no. 14, pp. 2391–2403, 2009.
- [43] S. P. Nair, J. L. Harwood, and R. A. John, “Direct identification and quantification of the cofactor in glutamate semialdehyde aminotransferase from pea leaves,” *FEBS Letters*, vol. 283, no. 1, pp. 4–6, 1991.
- [44] S. Brody, J. S. Andersen, C. G. Kannangara, M. Meldgaard, P. Roepstorff, and D. Von Wettstein, “Characterization of the different spectral forms of glutamate 1-semialdehyde aminotransferase by mass spectrometry,” *Biochemistry*, vol. 34, no. 49, pp. 15918–15924, 1995.
- [45] G. Fenalti, R. H. P. Law, A. M. Buckle et al., “GABA production by glutamic acid decarboxylase is regulated by a dynamic catalytic loop,” *Nature Structural and Molecular Biology*, vol. 14, no. 4, pp. 280–286, 2007.
- [46] M. Bertoldi, M. Gonsalvi, R. Contestabile, and C. B. Voltattorni, “Mutation of tyrosine 332 to phenylalanine converts

- dopa decarboxylase into a decarboxylation-dependent oxidative deaminase,” *Journal of Biological Chemistry*, vol. 277, no. 39, pp. 36357–36362, 2002.
- [47] P. Burkhard, C.-H. Tai, C. M. Ristroph, P. F. Cook, and J. N. Jansonius, “Ligand binding induces a large conformational change in O-acetylserine sulphydrylase from *Salmonella typhimurium*,” *Journal of Molecular Biology*, vol. 291, no. 4, pp. 941–953, 1999.
- [48] H. Tian, R. Guan, E. Salsi et al., “Identification of the structural determinants for the stability of substrate and aminoacrylate external schiff bases in O-acetylserine sulphydrylase-A,” *Biochemistry*, vol. 49, no. 29, pp. 6093–6103, 2010.
- [49] A. Mozzarelli, S. Bettati, B. Campanini et al., “The multifaceted pyridoxal 5'-phosphate-dependent O-acetylserine sulphydrylase,” *Biochimica et Biophysica Acta*, vol. 1814, no. 11, pp. 1497–1510, 2011.
- [50] S. Raboni, R. Contestabile, F. Spyraakis et al., “Pyridoxal 5'-phosphate-dependent enzymes: catalysis, conformation and genomics,” in *Comprehensive Natural Products II Chemistry and Biochemistry*, El Sevier, Oxford, UK, 2010.

## Review Article

# Protein Homeostasis Defects of Alanine-Glyoxylate Aminotransferase: New Therapeutic Strategies in Primary Hyperoxaluria Type I

Angel L. Pey,<sup>1</sup> Armando Albert,<sup>2</sup> and Eduardo Salido<sup>3</sup>

<sup>1</sup> Departamento de Química-Física, Facultad de Ciencias, Universidad de Granada, Avenida Fuentenueva s/n, 18071 Granada, Spain

<sup>2</sup> Departamento de Cristalografía y Biología Estructural, Instituto de Química Física “Rocasolano”, Consejo Superior de Investigaciones Científicas, Serrano 119, 28006 Madrid, Spain

<sup>3</sup> Centre for Biomedical Research on Rare Diseases (CIBERER), University Hospital of the Canary Islands, and CIBICAN, University of La Laguna, 38320 Tenerife, Spain

Correspondence should be addressed to Eduardo Salido; [esalido@ull.es](mailto:esalido@ull.es)

Received 28 April 2013; Accepted 23 May 2013

Academic Editor: Barbara Cellini

Copyright © 2013 Angel L. Pey et al. This is an open access article distributed under the Creative Commons Attribution License, which permits unrestricted use, distribution, and reproduction in any medium, provided the original work is properly cited.

Alanine-glyoxylate aminotransferase catalyzes the transamination between L-alanine and glyoxylate to produce pyruvate and glycine using pyridoxal 5'-phosphate (PLP) as cofactor. Human alanine-glyoxylate aminotransferase is a peroxisomal enzyme expressed in the hepatocytes, the main site of glyoxylate detoxification. Its deficit causes primary hyperoxaluria type I, a rare but severe inborn error of metabolism. Single amino acid changes are the main type of mutation causing this disease, and considerable effort has been dedicated to the understanding of the molecular consequences of such missense mutations. In this review, we summarize the role of protein homeostasis in the basic mechanisms of primary hyperoxaluria. Intrinsic physicochemical properties of polypeptide chains such as thermodynamic stability, folding, unfolding, and misfolding rates as well as the interaction of different folding states with protein homeostasis networks are essential to understand this disease. The view presented has important implications for the development of new therapeutic strategies based on targeting specific elements of alanine-glyoxylate aminotransferase homeostasis.

## 1. Alanine-Glyoxylate Aminotransferase and Primary Hyperoxaluria Type I

Alanine-glyoxylate aminotransferase (AGT) is one of the aminotransferases that has raised most biomedical interest, since its deficiency causes primary hyperoxaluria type I (PH1), a rare inherited entity with unique features in terms of cellular and molecular biology of human disease. AGT, encoded by the *AGXT* gene, catalyzes the transamination between L-alanine and glyoxylate to produce pyruvate and glycine using pyridoxal 5'-phosphate (PLP) as cofactor.

As it has been the case for a number of advances in the understanding of the molecular basis of disease, the in-depth analysis of the pathogenesis of PH1 has shed light into a broader field, such as the subcellular compartmentalization

of enzymes or the effect of gene modifiers on phenotype and the synergy between mutations and common genetic polymorphisms.

**1.1. Role of AGT in Glyoxylate Metabolism.** Glyoxylate is a two-carbon keto-acid of intermediary metabolism, with glycine, glyoxal, hydroxyproline, and glycolate as its best known sources in humans. Glyoxylate is readily converted into oxalate by various dehydrogenases and oxidases, including lactate dehydrogenase (LDH). Oxalate is an end product of metabolism in mammals that has to be eliminated with the urine; otherwise, it tends to precipitate as tissue-damaging calcium oxalate. The relevance of glyoxylate detoxification to human health is underscored by the deleterious consequences of inherited mutations in genes coding for

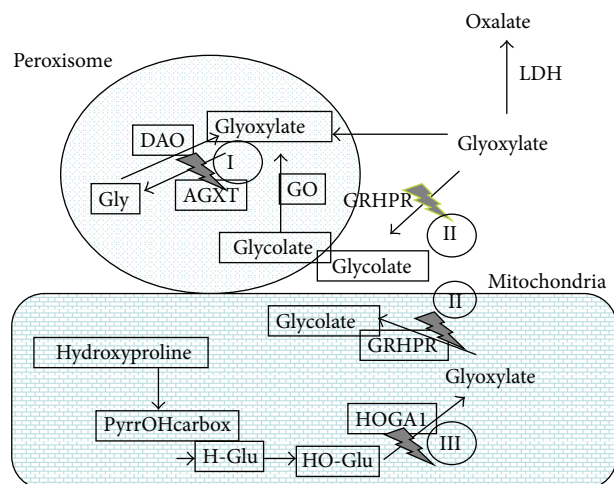


FIGURE 1: Summary of the glyoxylate metabolism in human hepatocytes. Simplified pathways involving glycine, glycolate, and hydroxyproline as the main sources of glyoxylate. Peroxisomal glyoxylate is detoxified by AGT, while mitochondrial and cytosolic glyoxylate is reduced to glycolate by GRHPR, preventing excessive oxidation to oxalate by LDH. Hydroxyproline metabolism results in the production of 4-hydroxy-2-oxoglutarate that is normally split into glyoxylate and pyruvate by HOGA1. PyrOHcarbox=pyrroline-5-carboxylate; H-Glu= 4-hydroxy-glutamate; HO-Glu=4-hydroxy-2-oxoglutarate. The three genetic defects currently known to cause PH are inherited with autosomal recessive pattern. The genes involved are alanine-glyoxylate aminotransferase (AGXT, at 2q37.3, MIM\*604285), for PH type I (PH1, MIM#259900), glyoxylate reductase/hydroxypyruvate reductase (GRHPR, at 9q12, MIM\*604296), for PH type II (PH2, MIM#260000), and 4-hydroxy-2-oxoglutarate aldolase (HOGA1 at 10q24.2, MIM\*613597), for PH type III (PH3, MIM#613616).

key enzymes in this pathway, AGXT being one of them (Figure 1). Human conditions characterized by high oxalate levels in urine are known as hyperoxalurias, and their genetic forms, termed primary hyperoxalurias (PH), are due to high oxalate production by hepatocytes deficient in one of these enzymes [1–3]. PH patients have urinary excretion levels  $>0.5 \text{ mmol/L/1.73 m}^2$  per day (typically  $>1 \text{ mmol/L/1.73 m}^2$ ), while normal oxalate excretion is below  $0.45 \text{ mmol/L/1.73 m}^2$ .

Since LDH is abundant in the hepatocyte cytosol and vertebrates do not have a functional glyoxylate shunt capable of using glyoxylate as a substrate for the tricarboxylic acid cycle, most of the glyoxylate generated must be metabolized within organelles such as the peroxisome and mitochondria in order to limit oxalate production. To further control the levels of oxalate produced, cytosolic glyoxylate reductase (GRHPR) competes with LDH for glyoxylate, reducing it to glycolate, a highly soluble two-carbon molecule.

Glyoxylate detoxification reflects the evolutionary origins of metabolic partitioning into the various subcellular organelles [5]. Thus, the subcellular distribution of the key enzymes of the glyoxylate detoxification pathway has been under evolutionary pressure and diet must have been an important component of such pressure, since glycolate is

abundant in vegetables while hydroxyproline is abundant in meat.

Human AGT is a hepatocyte-specific enzyme that is normally located in the peroxisomes only [6], making this organelle an efficient site for detoxification of glyoxylate either imported from the cytosol or mitochondria or produced in situ by either D-amino acid oxidase (DAO) or hydroxyacid oxidase (HAOI) (glycolate oxidase), using glycine or glycolate as substrate, respectively. The peroxisome membrane is permeable to glycolate, glyoxylate, and other small hydrophilic solutes, largely through the PMP2 channel [7]. Since AGT can tolerate high glyoxylate concentrations [8], the peroxisome, rich in AGT, plays a crucial role as glyoxylate detoxifying compartment that shields the surrounding cytoplasm from glyoxylate accumulation and secondary oxalate production.

Mitochondria also play an important role in glyoxylate metabolism [9, 10]. In humans, this role is based on their capacity to metabolize hydroxyproline [11], but in mammals with mitochondrial AGT this enzyme is also central to glyoxylate detoxification in this organelle. Collagen, containing ~15% hydroxyproline, is a major constituent of extracellular matrix and daily collagen turnover yields 300–450 mg hydroxyproline, accounting for the production of 180–240 mg glyoxylate [12, 13]. The last step of this pathway involves the cleavage of 4-hydroxy-2-oxoglutarate (2-keto-4-hydroxyglutarate) into glyoxylate and pyruvate by 4-hydroxy-2-oxoglutarate aldolase (HOGA1). The glyoxylate can then be converted to glycolate by GRHPR.

**1.2. Primary Hyperoxaluria Type I.** PH has an estimated prevalence of 1–3 per million population and an estimated incidence rate of ~1:100,000 live births per year in Europe [14–16], although the exact prevalence is unknown due to underdiagnosis. The most comprehensive attempts to estimate the true incidence of the disease [16] have resulted in higher incidence rates than previously reported. Higher rates have also been found in historically isolated populations, like the Canary Islands, due to founder effect [17]. Although PH accounts for less than 1% of children in end-stage renal disease (ESRD) registries of developed countries [18], almost 10% of Kuwaiti children and 13% of Tunisian children with ESRD have been reported to suffer PH [19, 20].

PH1, caused by deficient or mistargeted AGT [21], is the most common (around 80%) and the most severe PH type, usually resulting in ESRD at some point, although with a wide range of severity. At ESRD, the buildup of oxalate in the body (known as oxalosis) quickly results in bone, heart, skin, and retinal complications. Oxalosis is a life-threatening condition, unless liver-kidney transplantation is performed [14, 17, 22].

The interest in PH1 prompted the cloning of AGXT cDNA [23, 24], using probes from the orthologous rat gene [25]. The gene has 11 exons and spans ~10 kb [26], resulting in a 1.7 kb mRNA with a coding sequence of 1,176 bp. The gene product AGT is a homodimeric protein, each 43 kDa subunit containing 392 amino acids and holding one molecule of PLP as cofactor [27]. The main N-terminal domain contains



most of the catalytic active site, the cofactor-binding site, and the dimerization interface. The smaller C-terminal domain is known to interact with the peroxisomal receptor PEX5, targeting the dimer to the peroxisome. AGT, carrying a non-canonical peroxisomal targeting sequence (PTS1), is among the peroxisomal proteins with the weakest affinities for PEX5 [28]. An ancillary sequence surrounding amino acids 324–345 has been proposed to help the peroxisomal targeting of AGT [29]. A recently released crystal structure of the AGT in complex with the PTS1-binding domain of PEX5 (PDB: 3IMZ) also confirmed that residues 303–306 and 327–330 are largely buried upon binding. In fact, AGT binds to PEX5 with ~10-fold higher affinity than its PTS1 octapeptide, showing the functional role of this ancillary sequence in PEX5 binding [30].

The 3D structure of AGT (PDB: 1H0C) [27] has provided important information to better understand the function of the protein and the effect of changes in amino acid that account for a majority of the PH1 mutations (see Section 3 below).

More than 150 mutations have been described for *AGXT*, and they have been summarized recently [31]. Missense mutations are common, followed by small insertion/deletions (indels). Wild type *AGXT* comes in two polymorphic variants, the most frequent major haplotype (refseq NM\_000030) and the less frequent minor haplotype, carrying two single amino acid substitutions (p.P11L and p.I340M) among other genomic changes in strong linkage disequilibrium. Since these two polymorphisms are quite old, most of the individual PH1 mutations described are typically found in either the major or minor haplotype, but rarely in both, which is useful when searching for mutations in new PH1 cases [32]. The minor haplotype (simply defined by the refSNP rs34116584, p.Pro11Leu), with an allelic frequency of 0.1–0.2 in western countries and average heterozygosity around 0.2, does not cause PH1 by itself, but it is known to act synergistically with the deleterious effects of several common mutations [33, 34].

**1.3. Molecular Mechanisms of Disease.** *AGXT* mutations result in severe reductions of AGT enzymatic activity in the peroxisome, with a relatively wide range of residual activity, depending on the mutations present in both alleles [35]. Although AGT functions as a dimer, all the mutations described so far are related to loss of function, with recessive pattern of inheritance, without evidence of potential dominant negative effect.

Small indels are responsible for some PH1 cases due to AGT synthesis defects, most notably c.33dupC, the main mutation of the major haplotype, with the predicted consequence of early stop codon and nonsense mediated mRNA decay. We could also include in this category of synthesis defects most splicing mutations and occasional missense mutations leading to highly unstable protein that is degraded rapidly, such as p.S205P [36]. But the majority of PH1 alleles are missense mutations, with four potential molecular mechanisms involved: mitochondrial mistargeting, protein aggregation, catalytic defects, and enhanced turnover.

About a third of PH1 alleles involve the p.G170R substitution, in the minor haplotype, which is responsible for mitochondrial mistargeting of the gene product, becoming one of the best known examples of human mutations resulting in mistargeting as the main mechanism of disease [37–39]. In addition to p.G170R, p.F152I, also in the minor haplotype, was found to cause AGT mistargeting to the mitochondria instead of the peroxisome, depleting the latter organelle of its glyoxylate detoxifying capability.

The polymorphism p.P11L of the minor haplotype plays a crucial role for p.G170R to result in mitochondrial mistargeting [40], which has been associated to impaired folding efficiency to form functional dimers, therefore allowing mitochondrial import of mutant AGT [41].

Protein aggregation is a relatively frequent outcome of missense mutations in conformational diseases [42]. Several of the most frequent PH1 mutations of the minor haplotype, such as p.G41R [37] and p.I244T [34], are known to display protein aggregation. The p.P11L polymorphism was also found to play a crucial role for the I244T mutation to result in a conformationally unstable protein, prone to aggregation [34], while the p.G41R mutation disturbs the local interactions of the N-terminus, causing conformational instability as well [43].

Catalytic defects are a common mechanism of disease in inborn errors of metabolism involving enzyme-coding genes. Enzymatic characterization of several PH1 missense mutations (p.G82E, p.G41R, and p.F152I) have demonstrated significant alterations in their performance, including strong decreases in catalytic efficiency and reduced binding affinities for PLP and PMP cofactors [44].

Genotype-phenotype correlations have been described for some mutations of the *AGXT* gene [33, 45, 46], but the wide allelic heterogeneity limits this type of analysis to the most common mutations, unless large international registries are used. Significant environmental influences and the potential effect of genetic modifiers also play an important role to the point that siblings who share the same genotype could have very different clinical phenotypes [47].

## 2. Structure-Function Relationships of AGT

The crystal structure of AGT was solved at atomic resolution [27] to gain insights on the molecular and structural basis of the disease. AGT is a homodimer with each protomer folded into a large N-terminal domain (residues 22–282) and a smaller C-terminal domain (283–392). Most of the contacts within the dimer involve the large N-terminal domain. Besides, a long unstructured N-terminal tail (residues 1–21) grabs the subunits within the dimer (Figure 2(a)). This structure provided valuable information about the enzyme functioning and a framework to map the mutations of the AGT gene. This analysis showed that they are almost randomly scattered over the entire three-dimensional structure of the enzyme [30], making it difficult to establish general rules on the molecular consequences of these variants. However, the

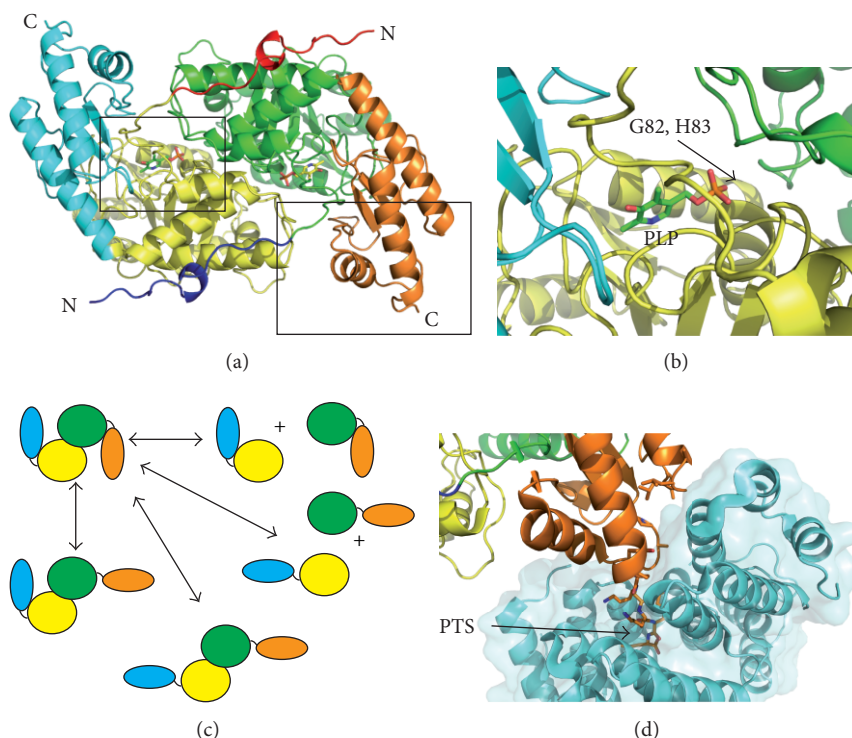


FIGURE 2: The structure of AGT. (a) A ribbon representation of the dimeric AGT structure (PDB code 1H0C) colored to highlight the domain organization. The black squares represent the zoomed sections shown in panels 1b and 1d. (b) A representation of the PLP binding site; G82 and H83 are in the vicinity of the cofactor. (c) A schematic representation of the possible “almost folded” AGT intermediates. (d) A representation of the AGT-Pep5x intermolecular interface. The molecular surface representation of Pep5p is also displayed and colored in cyan. Those AGT residues interacting with Pep5x are displayed in a stick representation.

available structural information resolves central questions on the knowledge about the basis of the disease.

The effect of mutations affecting the enzymatic properties of AGT can be rationalized in structural terms. p.G82E and p.H83R are well characterized to produce catalytic defects [8, 48]. The analysis of the structure reveals that both of them cluster in the vicinity of the active site. These changes involve bulkier side chains that hinder either cofactor or substrate binding (Figure 2(b)). By contrast, the attempts to rationalize the effect of variants leading to protein aggregation in terms of the structure have been unsuccessful since it is likely that either kinetic and/or thermodynamic changes are the main mechanism involved [48]. The modeling of these mutations on the structure reveals no significant changes since they often involve either conservative changes or solvent accessible residues. Consequently, it is not expected to induce large predictable conformational changes in AGT structure. This is well illustrated by the structural analysis of the G170R variant, which resulted in a nearly identical structure to the wild type [49]. In addition, the expression of many of these mutations yields unstable aggregated and/or partially unfolded products that cannot be crystallized.

The three-dimensional structure of the complex between the ring chaperonin GroEL and AGT-LTM variant provided evidence that the mutated enzyme is able to form nonnative folding intermediates that interact with the chaperone [50].

These intermediates consist of an “open” version of AGT protomer in which the small and the large domains are correctly folded (Figure 2(c)). Such intermediates may be prone to protein aggregation but they constitute a promising target for pharmacological chaperones.

The crystal structure of the AGT in complex with the PTS1-binding domain of Pep5p was determined to shed light into the mechanism of AGT import into peroxisomes [30]. The complex displays Pep5p-AGT-AGT-Pep5p stoichiometry and confirms that dimeric and perfectly folded AGT interacts with the receptor. On the AGT side, the complex buries completely those residues forming the PTS1 and some constituting the smaller C-terminal domain (Figure 2(d)). This suggests that those mutations affecting the surface properties of the interaction area will affect the import to peroxisomes.

### 3. Biophysical, Biochemical, and Cell Biology Approaches to Study AGT Deficiency and Protein Homeostasis Defects

Protein homeostasis controls the functional properties of proteins by minimizing the presence of misfolded protein states that may be damaging to cellular function [51, 52]. A complex and highly interacting and regulated network of pathways, involving over 800 different proteins, is in charge of protein homeostasis [53], regulating protein synthesis,

A simple model for protein homeostasis in PH1

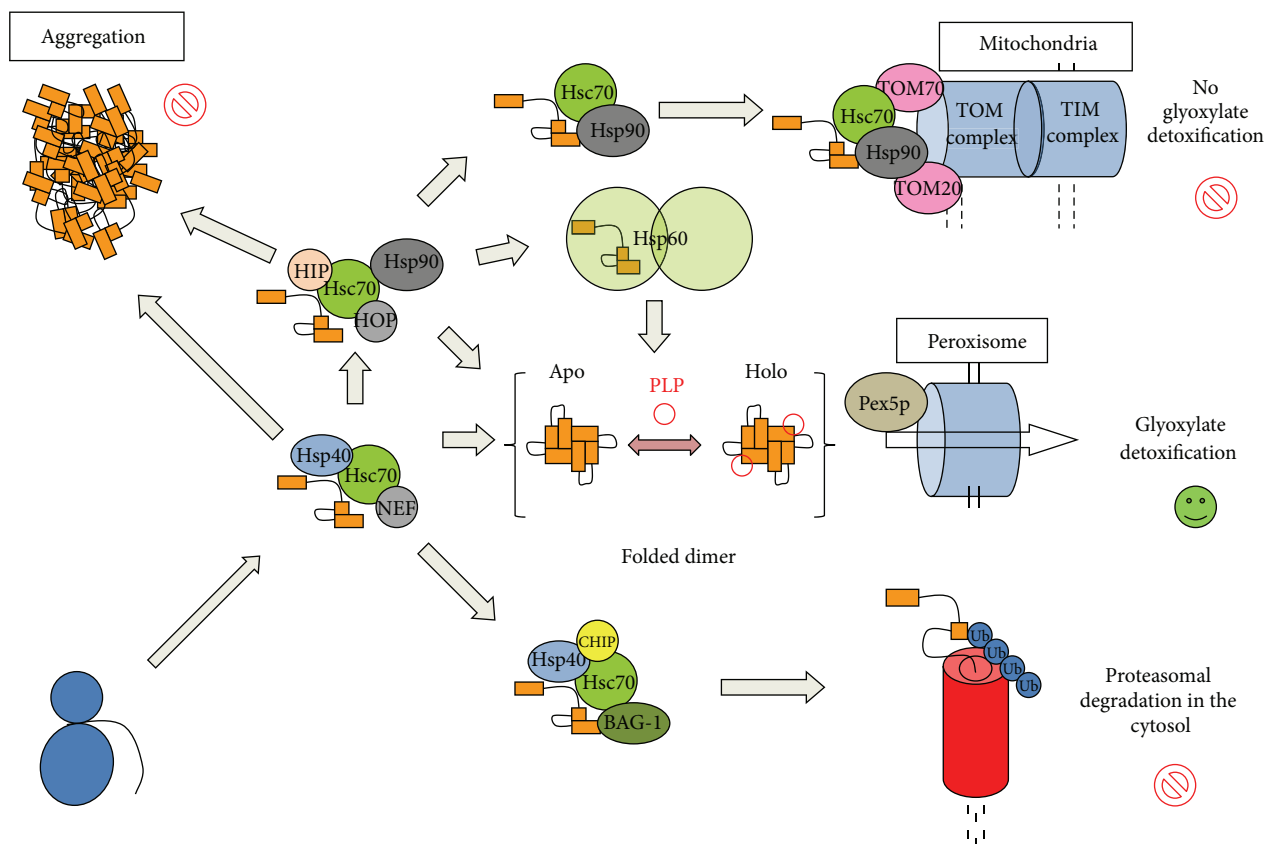


FIGURE 3: A simple scheme representing potentially important checkpoints in the folding and misfolding of human AGT. After ribosomal synthesis, the AGT monomer is maintained in a partially folded and soluble state upon interaction with Hsp40 chaperones allowing its engagement to the Hsp70 machinery. Correct folding may proceed through the transfer of the partially folded polypeptide to the Hsp90 and Hsp60 machineries leading to the folded holo-AGT dimer and peroxisomal import through the Pex5p import machinery. However, PH1 causing mutants to show enhanced interactions with Hsp70, Hsp60, and Hsp90 chaperone systems which may (i) delay correct folding eventually causing AGT aggregation; (ii) allow engaging the proteasomal degradation machinery mediated by CHIP and BAG-1 proteins; (iii) allow Hsp70/Hsp90 mediated presentation to the mitochondrial import machinery via TOM20 or TOM70 receptors. For further details and references, see the main text.

folding, trafficking, and degradation [51, 52]. Protein homeostasis defects are associated with aging and disorders of protein folding, including metabolic diseases, cancer, and neurodegenerative diseases [51, 52, 54]. In the context of protein homeostasis, intrinsic physicochemical properties of polypeptide chains such as thermodynamic stability, folding, unfolding, and misfolding rates as well as the interaction of different folding states with protein homeostasis networks are essential to understand protein folding and misfolding under physiological and pathological conditions [54]. In this section, we summarize the knowledge on protein homeostasis defects in PH1 to provide a comprehensive and integrated perspective of PH1 as a folding disease. The view presented has important implications for the development of new therapeutic strategies for PH1 based on targeting specific elements of AGT protein homeostasis (summarized in Figure 3).

**3.1. Stability of AGT Variants toward Chemical Denaturants, Temperature, and Proteases: Mechanistic Implications.** Several studies have addressed the unfolding of AGT, both wild type (WT) and PH1 mutants, by either chemical denaturants (guanidine, urea, and pH) [55–57] or temperature [44, 48, 56, 57]. The mechanistic studies derived from these studies are discussed in this section in some detail.

**3.1.1. Chemical Denaturation of AGT WT and Disease Causing Variants: Presence of Unfolding Intermediates.** Chemical unfolding by guanidium, urea, and mild acidic pH has been shown to irreversibly denature AGT at the experimental conditions used by different research groups [55–57]. We must note that the term *irreversible* is used here to indicate that removal of the denaturant does not provide the refolding yields required for applying equilibrium thermodynamic

analyses. However, we must also note that very mild refolding conditions have proved to enhance remarkably AGT refolding yields [58]. Therefore, we will not attempt to extract thermodynamic information from the biophysical studies discussed here, even though they may provide insight into partially folded states that could be relevant to understand the (un)folding pathways of AGT variants *in vitro* (and possibly intracellularly), the effect of PH1 mutants on folding of AGT and the role of molecular chaperones in AGT folding and misfolding.

Unfolding of holo- and apo AGT WT, minor AGT (LM, p.P11L-I340M) and LM-G170R (p.G170R in minor AGT - LM-, LRM for short) variants by guanidium hydrochloride and mild acidic pH have revealed the presence of a molten-globule-like unfolding intermediate (MG). This MG intermediate does not refold to the native state spontaneously and is able to interact with molecular chaperones in cell-free systems, suggesting that last folding steps of AGT may require help from molecular *chaperones in vitro* and intracellularly [57]. Interestingly, Hopper et al. [56] have shown that native state ligands such as PLP and AOA stabilize AGT WT and LM towards guanidium denaturation, even though the thermodynamic or kinetic basis of such stabilization and their relation with the partially unfolded states are unclear. Aggregation-prone unfolding intermediates are also observed in the urea induced denaturation of AGT, especially in the apo-forms and/or when the P11L polymorphism is present [55]. Indeed, the partially unfolded states found in the unfolding pathways of LRM variant might be related to its tendency for mitochondrial import [55], also explaining the strong interaction of this variant along its folding process with Hsp70 and Hsp90 chaperones in cell-free systems [57]. Additionally, aggregation of apo-AGT WT in refolding trials is prevented by the presence of the bacterial Hsp40 DnaJ in a concentration dependent manner (Figure 4), suggesting that binding to this chaperone is the first step to engage the Hsp70 machinery (Figure 3).

**3.1.2. Thermal Denaturation of AGT Variants: The Role of AGT Kinetic Stability in PH1.** Thermal denaturation of AGT variants has been monitored by multiple techniques, including activity, circular dichroism, differential scanning fluorimetry (DSF), and differential scanning calorimetry (DSC) [43, 44, 48, 55–57, 59, 60]. All these studies have shown that withdrawal of PLP has a dramatic effect in terms of stability, reducing 20–25°C AGT thermal stability. The denaturation of holoproteins is consistent with a single denaturation transition using multiple probes, while denaturation of apoproteins is sometimes described by a one or two thermal transitions, depending on the AGT variant and the technique monitoring denaturation [48, 55–57, 59, 60]. The presence of two denaturation events has been discussed as the uncoupled denaturation of the large and small domains [59]. However, we must note that enzyme inactivation coincides with the low  $T_m$  transition found by Far-UV CD and DSF [48, 56, 59, 60] and the single transition found by DSC [48, 57]. Moreover, kinetic analyses of DSC transitions based on a two-state denaturation model provide denaturation rates

at 37°C for apoproteins in excellent agreement with those obtained from inactivation kinetics, indicating that DSC based kinetic analyses monitor irreversible denaturation and inactivation of apo-proteins [48]. Almost all studies coincide in the destabilizing effect of the minor allele, while additional mutations further reduce AGT thermal stability [44, 48, 56, 57, 59, 60].

We have recently performed a thorough characterization of thermal denaturation of holo- and apoproteins by differential scanning calorimetry in AGT WT and eleven mutants and polymorphic variants found in PH1 patients [48, 57]. Denaturation of all AGT variants as apo- and holoproteins is described by a phenomenological two-state irreversible denaturation model. In this scenario, the stability of the native state is determined by the rate of irreversible denaturation  $k$ , that relates to the half-life for denaturation by  $t_{1/2} = \ln 2/k$  [2, 48, 57]. The value of  $k$  is determined by the height of the activation free energy that the native state must cross to reach the denaturation (rate-limiting) transition state (TS) [48, 57, 61]. Thermal denaturation of AGT mostly involves a dimeric TS, indicating that the kinetic stability of AGT enzymes is mainly dictated by the impact of mutations on the free energy of the dimeric native and TS states. Thus, dimer dissociation and monomer unfolding do not contribute to the AGT kinetic stability, because these steps must occur after the denaturation rate-limiting step [48]. The large kinetic stabilization exerted by PLP results from its preferential binding to the native state, increasing the denaturation free energy barrier by  $\sim 7 \text{ kcal}\cdot\text{mol}^{-1}$  [48, 57]. The temperature dependence of calorimetric enthalpies agrees well with the theoretical value for a dimer of this size, suggesting that holo- and apo-proteins unfold extensively and to a similar extent upon thermal denaturation, and possibly involving denaturation of both domains in AGT [48, 57].

Kinetic analyses of DSC traces provide a unique opportunity to compare denaturation rates among AGT variants spanning a wide range of stabilities (half-lives from minutes to years at physiological temperature). For instance, removal of PLP decreases (in WT and most of PH1 variants) AGT kinetic stability by 4–5 orders of magnitude [48, 57]. The presence of P11L and LM polymorphism reduces AGT kinetic stability by  $\sim 150$  and  $\sim 20$ -fold, while the presence of I340 M kinetically stabilizes AGT compared to AGT WT (Fabelo-Rosa, submitted). In general, PH1 causing mutants show similar stability to AGT LM as holo-proteins, with a remarkably high kinetic stability (half-lives in the range of years at 37°C), while they often reduce apo-AGT kinetic stability (and denature in a time scale of minutes-hours; [48, 57, 62]). Thus, PLP binding overstabilizes the AGT native state in some mutants [2] which might explain the PLP responsiveness found for some of them in PH1 patients [63, 64]. Therefore, targeting the cellular systems responsible for PLP bioavailability (enzymes involved in PLP recycling and delivery; [65]) may represent a pharmacological approach to overcome mutation induced protein destabilization in PH1.

**3.1.3. Resistance to Proteolysis: Effects of PH1 Mutations on Protein Flexibility and High-Energy States.** Proteolysis is an



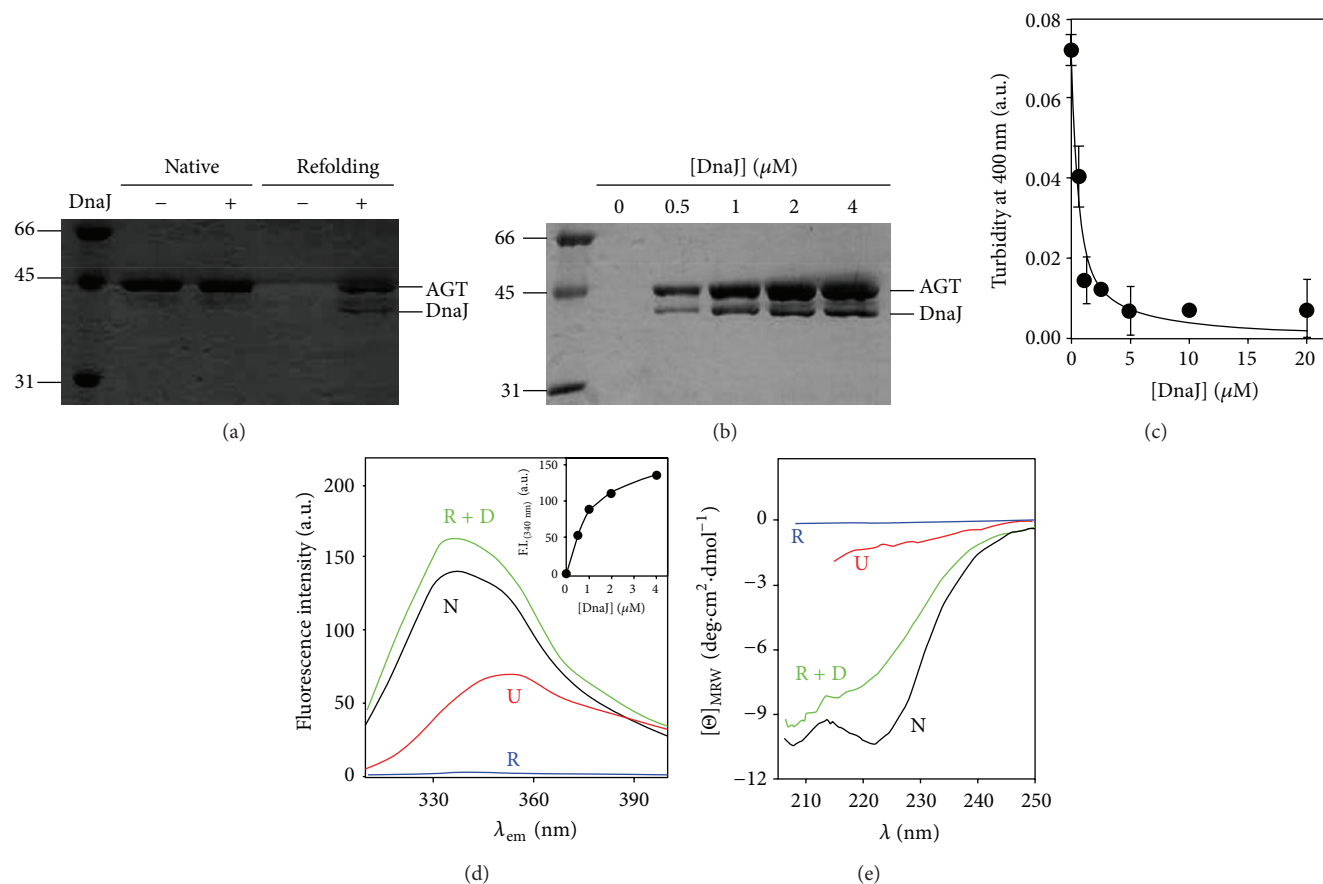


**FIGURE 4:** DnaJ prevents aggregation of a partially folded state of AGT. (a) IMAC-based copurification assay of his-tagged apo-AGTwt with DnaJ (1  $\mu$ M each), under native (no urea) and refolding (20-fold dilution from a 16 h incubated sample with 8 M urea) conditions; (b) DnaJ protein concentration dependence of its interaction with apo-AGTwt under refolding conditions (the same conditions as in (a)). (c) DnaJ protein concentration dependence of the maximal turbidity at 400 nm in the apo-AGTwt refolding (data are from three independent experiments); (d) and (e) solubility and conformational assays of Apo-AGTwt based on its intrinsic Trp-emission fluorescence ((d); exc.295 nm) or Far-UV CD (e) under different conditions: native (0 M urea; N), unfolded (8 M urea; U), and apo-AGTwt *refolded* in the absence (R) or presence of 4  $\mu$ M DnaJ (R + D). After urea-dilution, samples were incubated at 25°C for 30 min, centrifuged at 15000 rpm for 30 min, and the spectroscopic analyses were performed in the supernatants. The contribution from DnaJ to fluorescence is negligible due to the absence of Trp residues, while its contribution to Far-UV-CD spectra was subtracted from R + D. Inset: DnaJ protein concentration dependence of the Trp-fluorescence on the soluble fraction. A fitting to a hyperbolic function is shown, providing half-maximal fluorescence recovery at  $1.0 \pm 0.1 \mu$ M DnaJ. All the experiments were performed at 25°C in Na-Hepes 20 mM NaCl 200 mM pH 7.4 2 mM DTT using 1  $\mu$ M AGT (in protein subunit). DnaJ was purified according to [4].

excellent method to study protein flexibility and transient population of protein high energy states, as long as flexible or partially unfolded regions in the protein are accessible for binding and proteolytic cleavage [66]. Indeed, kinetics of proteolysis has provided information on protein high energy states present in native state ensembles which are not accessible for most of ensemble averaged-based biophysical methods [66]. Several studies have addressed the stability of AGT enzymes towards proteolysis using different proteases ([34, 43, 57, 67, 68] and Figure 5). Trypsin and proteinase K degradation have been applied to several PH1 mutants [34, 43, 68], showing that P11L polymorphism enhances protease sensitivity that is further exacerbated by additional mutations. In the case of LM-G41R, detailed characterization of proteolysis products in combination with molecular dynamic simulations supports that G41R mutation enhances

conformational fluctuations in the N-terminal region of AGT, thus accelerating cleavage by proteases [43, 68]. Interestingly, native state ligands and naturally occurring osmolytes are able to increase protease resistance in several PH1 mutants [68], suggesting that reshaping of the native state ensemble energetics by ligands may modulate the conformational fluctuations in some PH1 mutants. From a physiopathological viewpoint, studies in cell free systems on the proteasomal susceptibility also reveal that disease causing mutations enhance degradation [67].

AGT WT undergoes rapid cleavage by thermolysin leading to an active ~75 kDa dimer (referred here to as D\* state) [57]. The stability of this D\* state has been further characterized by a combination of thermolysin digestion and thermal scans for different holo-AGT enzymes (Figure 4). The apparent rate constants for proteolysis are extracted from

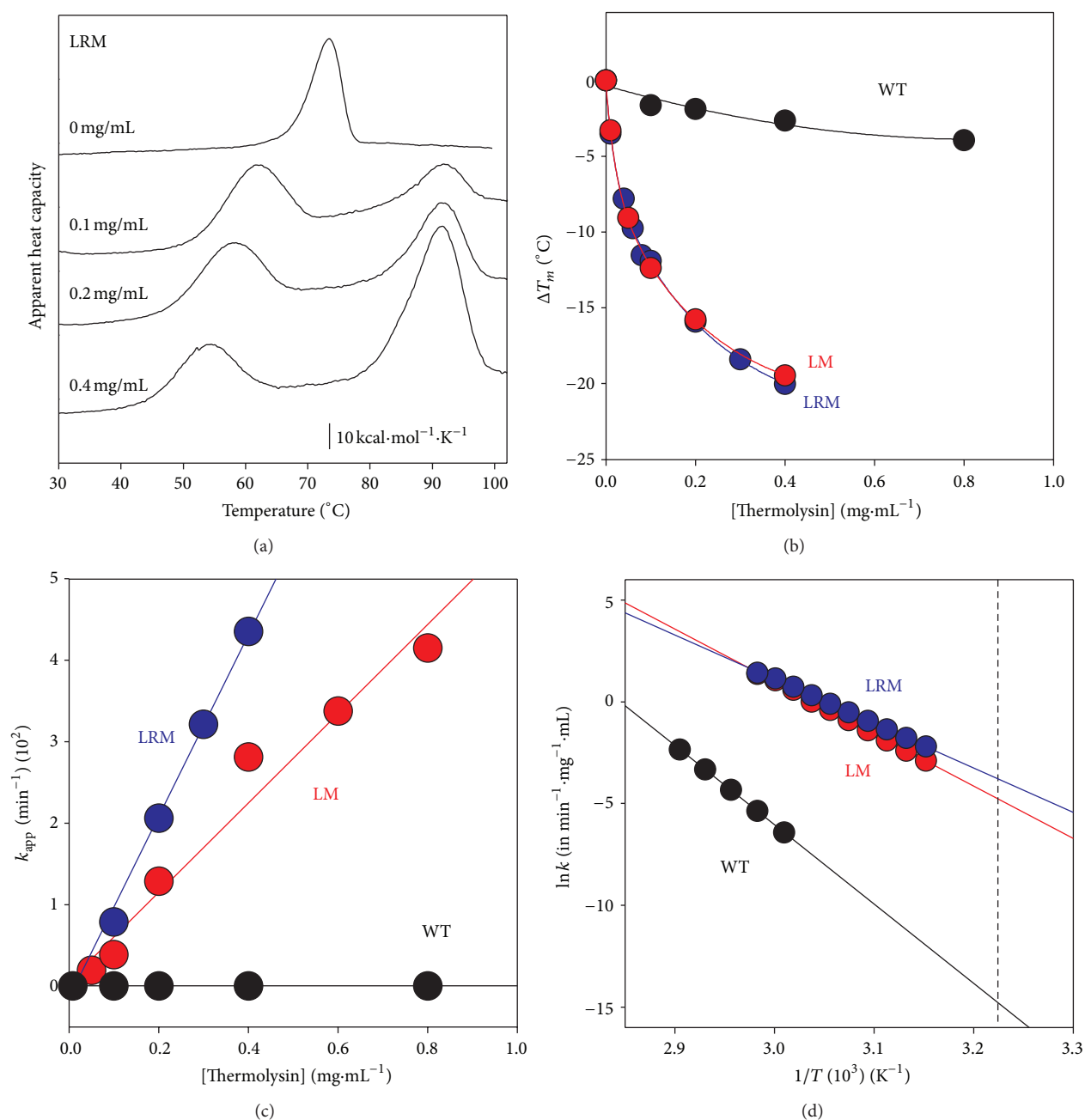


FIGURE 5: Temperature dependent proteolysis of AGT variants by thermolysin. (a) thermal scans of AGT-LRM (10  $\mu$ M in protein subunit) in the presence of different thermolysin concentrations (0–0.4 mg/mL). The high temperature transition ( $T_m \sim 90^{\circ}$ C) corresponds to thermolysin denaturation, which is thermostable. (b) Dependence of  $T_m$  downshift of thermal transitions of AGT variants by thermolysin. (c) Dependence of the apparent proteolysis rate constants on thermolysin concentration at 44  $^{\circ}$ C. The slope of these plots provides the second-order rate constants (plotted in (d)); (d) Arrhenius plots for the second-order rate constants for proteolysis. The vertical dashed line indicates 37  $^{\circ}$ C. Experiments were performed in Hepes 20 mM NaCl 200 mM CaCl $_2$  10 mM.

thermal scans at a given protease concentration in the temperature range of the transition [69]. The  $T_m$  value of LM and LM-G170R is shown to be more sensitive to the concentration of protease than that of WT AGT (Figure 4(b)). The apparent first-order rate constants for proteolysis (Figure 4(c)) indicate that proteolysis is  $\sim 6$  orders of magnitude slower for WT AGT than for the LM and LM-G170R, while LM-G170R

is degraded about twice faster than AGT LM. At 37  $^{\circ}$ C (Figure 4(d)), the half-lives against proteolysis (at 0.1 mg/mL protease) are 60-(WT),  $3.9 \cdot 10^4$ -(LM), and  $6.2 \cdot 10^4$ -fold (LM-G170R) lower than those determined in the absence of protease, suggesting that holo-AGT enzymes might be very sensitive to proteolysis despite their robustness towards thermal induced aggregation.

**3.2. Protein Homeostasis of AGT: Implications to Develop New Therapeutic Strategies.** Peroxisomal import of human AGT occurs upon direct interaction of the fully folded dimer with Pex5p in the cytosol. Multiple lines of evidence support that protein folding defects are implicated in AGT loss of function in PH1 [30, 48]. However, dissecting the protein homeostasis defects in PH1 represents a remarkable challenge, since the biomolecular interactions of partially folded states with the protein homeostasis network may involve over 200 different proteins in cytosolic folding ([53]; see Figure 3 for a very *simplistic* view in PH1). In this section, we do our best to gather the most relevant available information on the physiological folding and peroxisomal targeting, as well as those protein homeostasis defects alterations that may lead to AGT loss of function due to different mechanisms, including mitochondrial mistargeting, enhanced protein aggregation, and degradation.

**3.2.1. Peroxisomal and Mitochondrial Targeting of Human AGT.** The PTS1 of human AGT is suboptimal (-KKL versus the consensus-SKL; [41]), and its molecular recognition by Pex5 requires additional structural elements at the C-terminal domain [29, 30]. In fact, the interaction of AGT WT and Pex5p PTS1 binding domain (Pex5p-pbd) is of moderate affinity ( $K_d \sim 1.5\text{--}3.5\ \mu\text{M}$ ; [30, 48]) and decreases 10-fold for the isolated C-terminal PTS1 octapeptide [2, 28]. The low affinity of human AGT for its peroxisomal receptor may have several important implications to understand the evolutionary changes in AGT subcellular location and function [70, 71], the correct peroxisomal biogenesis [28], and the role of peroxisomal import in PH1 pathogenesis [30, 48].

AGT subcellular location seems to vary among species depending on a delicate balance between mitochondrial and peroxisomal import signaling pathways and the capacity of cytosolic protein homeostasis networks to fold AGT proteins [70, 71]. The presence of mitochondrial AGT in carnivores, peroxisomal AGT in herbivores, and both locations in omnivores suggest that subcellular location of AGT may have resulted from dietary selection pressure [72]. Additionally, the presence of a strong N-terminal mitochondrial targeting sequence (MTS) in AGT from *X. laevis* drives the mitochondrial localization of this enzyme, while the corresponding N-terminal MTS seems to be weak in human AGT [71]. The weak MTS in hAGT seems to be strengthened by additional natural variations associated with mitochondrial mistargeting, such as P11L polymorphism and the G170R, F152I and G41R mutations [38, 39, 73, 74]. Only the LM-G41R seems to be N-terminal cleaved upon mitochondrial import [38, 73], possibly because of the enhanced conformational fluctuations caused by the mutation next to the MTS [43], which suggests that the MTS is not generally cleaved upon import of hAGT as observed for many other MTS-containing proteins. Interestingly, proteins containing short MTS are known to be imported by a mechanism where unfolding is rate-limiting [75, 76], and thus, the low kinetic stability of LM-G170R, LM-F152I and LM-G41R as apo-proteins [43, 48, 57, 62] may speed up mitochondrial import of these mutants.

Besides the classical interaction between TOM20 mitochondrial receptors and N-terminal MTS, alternative mechanisms of mitochondrial import might be involved, such as presentation of internal targeting sequences in partially folded states to TOM20 or TOM70 receptors by molecular chaperones ([57, 77, 78]; see Figure 3). Enhanced interaction of misfolded/partially folded PH1 variants with molecular chaperones seems to be a common feature to many PH1 mutants [34, 48, 50, 57], and thus not only restricted to the mistargeting LM-F152I and LM-G170R variants. Some mutations, such as LM-I244T, have been studied by several groups using different cell lines (COS and CHO) for heterologous gene expression, different cell culture media and PLP concentrations. Consequently, significant differences in mutant outcomes have been observed, showing either peroxisomal aggregation [34] or mitochondrial mistargeting [73], further supporting the view that different AGT *load* and variable capabilities of protein homeostasis networks may have a large impact on the final fate of PH1 causing mutants. Dissection the molecular details of these protein homeostasis defects is thus required to develop specific therapeutic strategies targeting different PH1 molecular mechanisms, possibly involving the cooperation of multiple proteostasis elements (Figure 3) including Hsp60, Hsp70 and Hsp90 machineries [34, 48, 50, 57].

A recent study on PTS1 octapeptides from 42 human peroxisomal proteins has shown that these sequences range over four orders of magnitude on their affinity for Pex5p-pbd, and interestingly, the PTS1 corresponding to hAGT is the second weakest among this list [28]. A detailed analysis on protein expression levels for these peroxisomal proteins revealed a remarkable negative correlation between binding affinities and expression levels of cargo proteins, thus providing a mechanistic framework to generating a uniform population of Pex5p-cargo complexes necessary for proper peroxisomal biogenesis [28]. Pex5p-pbd binding studies of PH1 causing mutations G170R and V336D on the major allele [30] as well as some of the most common mutations on the minor allele, including G170R, I244T and F152I [48], revealed no changes in the molecular recognition of PH1 mutants by Pex5p, further supporting that folding defects are likely responsible for mitochondrial mistargeting and protein aggregation mechanisms in PH1.

**3.2.2. Folding Defects Are Common to Mitochondrial Mistargeting and Aggregation in PH1: Targeting Protein Homeostasis Networks as Pharmacological Strategies for PH1.** Early studies in liver samples from PH1 patients showed that the LM-G170R variant reduces the protein levels and activity and lead to mitochondrial mistargeting [39]. Further studies, expanded to LM-G41R/LM-F152I compound heterozygotes showed combined mitochondrial/peroxisomal location, intraperoxisomal aggregation and null activity [38]. The LM-F152I, LM-G170R and LM-I244T variants show reduced folding efficiency in both prokaryotic and eukaryotic systems [40, 48, 57, 73], while a milder effect is observed for LM polymorphic variant in these studies. These evidences clearly pointed to PH1 as conformational disease. However, up to

date, the molecular details of PH1 protein homeostasis defects are mostly unknown.

We have recently initiated a comparative study on several PH1 variants that shows a positive correlation between apo-AGT kinetic stability, interaction with molecular chaperones, and decrease solubility and total protein levels in transiently transfected CHO cells [48]. This seems to apply for either aggregation (LM-I244T) or mistargeting (LM-F152I and LM-G170R) mechanisms. Accordingly, a recent study has shown that human AGT is capable of complementing yeast strains lacking endogenous yeast AGT in glycine-free medium [56], while LM-F152I and specially LM-I244T, but not LM-G170R, reduced the complementation elicited by AGT LM. Complementation by PH1 mutants in this system closely correlated with steady-state expression levels, indicating that these mutants affect proper intracellular folding *in vivo*. More recently, using a novel stability reporter assay [60], a clear correlation between *in vivo* steady AGT levels and kinetic stability and yeast growth was found for LM-F152I, LM-G170R and LM-I244T. Overall, these expression studies support a link between intracellular folding efficiency and kinetic stability of apo-AGT variants associated to mistargeting and aggregation mechanisms.

As we have mentioned in Section 3.2.1, the intracellular fate of AGT mutants depends on the experimental conditions of *in vitro* expression (LM-I244T is an excellent example; [34, 48, 73]). An interesting possibility to explain these differences is that different capacities of the protein homeostasis networks might determine the phenotype at the molecular level (aggregation versus mistargeting), a phenomena that has been described for disease penetrance even among isogenic individuals in animal models of several folding diseases [79]. These differences in folding capability might explain different phenotypic outcomes even among siblings sharing a given phenotype [2], and also possibly, the different response to pyridoxine supplementation among PH1 patients with the same phenotype [63, 64].

**3.2.3. Interaction with Molecular Chaperones.** Protein folding intermediates are commonly observed for proteins larger than 100 aminoacids, and these intermediates often require substantial structural reorganization upon interaction with molecular chaperones to reach the native conformation [80]. As we describe in Section 3.1.1, human AGT is known to populate (un)folding intermediates upon chemical denaturation, and these intermediates do not generally reactivate [55, 57] and also stably interact with several types of molecular chaperones ([34, 50, 57]; Figure 3). Moreover, the strong interaction of several misfolding AGT mutants with molecular chaperones suggests that these chaperones might be important checkpoints in AGT folding and misfolding [34, 50, 57]. Thus, modulation of the interaction of partially folded states of AGT variants with molecular chaperones is a plausible approach for pharmacological intervention in PH1, as similarly described for other protein folding diseases [81–83].

An important question is whether WT and PH1 causing mutants populate different folding/unfolding intermediates,

or whether, kinetic/thermodynamic aspects of these folding intermediates and their interaction with the protein homeostasis networks [84–86] determine the final fate of AGT variants (mistargeting versus aggregation versus degradation). The structure/energetics of the TS for the rate limiting step of irreversible denaturation of WT and PH1 mutants is strikingly similar, suggesting a fine-tuning of the structure/energetics of this TS as determinant for the kinetic stability of PH1 mutants (unpublished observations). On the other hand, the structural properties of the chaperone competent MG state formed at mild acidic pH is similar for WT, LM and LM-G170R, but seems to accumulate in a Hsc70- or Hsp90-bound state upon expression in cell-free systems for LM-G170R [57]. Moreover, aggregation of AGT WT is prevented *in vitro* by its interaction along its folding pathway with Hsp40 in a partially folded state that resembles the acid-induced MG state (Figures 4(d)-4(e)), which may prevent AGT aggregation co- or post-translationally, thus delivering the polypeptide to the Hsc70 machinery [80, 86]. Hsc70 machinery may represent the first essential folding checkpoint, as the interaction of these chaperones with Hsp40 proteins and nucleotide exchange factors [86] would determine the partitioning between correct folding and peroxisomal import, mitochondrial import or degradation (Figure 3). Transfer of cargo AGT from Hsp70 to Hsp90 might also occur through the Hsc70-Hsp90 organizing protein (HOP; [86]). Moreover, we have also described that overexpression of bacterial Hsp60 (GroEL; [50]) increase the recovery of LM-I244T in *E. coli*, forming stable complexes with GroEL. The characterization of the bound AGT LM-I244T by cryo-electron microscopy shows that AGT monomers display folded N- and C-terminal domains in an open conformation [50]. Overall, these studies suggest that the last steps in AGT folding involve domain docking and acquisition of quaternary structure that are crucial for AGT conformation of PH1 mutant. Thus, pharmacological modulation of the proteostasis pathways involved may rescue AGT function in PH1 patients.

## 4. AGT as a Drugable Target for the Treatment of PH1

Once the diagnosis of PH1 is made, or even suspected, conservative measures should be initiated as soon as possible with the goal of preserving renal function. Once renal function is lost, the threat posed by progressive oxalate accumulation makes it necessary to perform liver and kidney transplantation, an aggressive treatment not free of difficulties, risks and limitations. Thus, current research aims at medical treatments for PH1.

High fluid intake has been proven to be effective in kidney stone diseases [87]. In PH, the recommended fluid intake is at least 3 L/m<sup>2</sup> per day, and special care should be taken in situations of fluid losses (diarrhea, vomiting, and fever) or limited oral hydration (surgery), where i.v. fluid administration might be necessary to keep high urine flow. In addition, alkalinization of the urine with alkali citrate is implemented to reduce urinary CaOx saturation.



Administration of pyridoxine hydrochloride was proposed as a conservative PH1-specific measure several decades ago. This form of treatment has been known to be associated with a decrease in urinary oxalate (UOx) in about 30% of PH1 patients [88, 89]. Since vitamin B6 is very safe, with a small risk of sensory neurotoxicity as the main side effect, a trial of pyridoxine treatment should be performed in most cases, and particularly in patients with missense mutations. If responsive, patients should be treated until liver transplantation is performed, even if they are in ESRD undergoing haemodialysis. The recommended starting dose is 5 mg/kg per day, increasing in 5 mg/kg steps to a maximum of 20 mg/kg body weight per day [90]. Responsiveness is currently defined by >30% decrease in UOx excretion after a test period of a minimum of 3 months at maximum dose [22, 91]. A subset of patients carrying one or two copies of G170R or F152I mutations have been shown to respond best to pyridoxine [63, 64].

In addition to the experimental data obtained in the last few years on the cellular and molecular consequences of various missense mutations, the empirical response of some PH1 patients to vitamin B6 treatment supports the view of AGT as a “drugable target” that deserves serious commitment to develop small molecules with enhanced chaperone capability or proteostatic effect.

As we describe in detail in Section 3.1.2, binding of PLP to AGT protein dramatically enhances its kinetic stability, particularly in variants of the minor haplotype, such as G170R and I244T [57]. The most relevant parameter to estimate the kinetic stability of properly folded cytosolic AGT dimers seems to be the half-life for irreversible denaturation of the apo-forms. Conversion of apo- to holo-AGT is a slow process that is catalyzed and regulated by specific enzyme systems [57, 65], and this conversion may trap the AGT in a folded and kinetically stable holo-form ready for peroxisomal import. This is especially relevant for PH1 missense mutations that are more destabilized in their apo-form than in their holo-form.

Building on this view of PLP as a natural kinetic stabilizer of AGT, it is reasonable to expect that pharmacological chaperones will be found that specifically bind to the AGT native state leading to thermodynamic and/or kinetic stabilizations. Ideally, they will have enhanced chaperone activity on mutant AGT variants, leading to more efficient conservative treatments for PH1. To move forward, a more precise understanding of the mechanism of PLP kinetic “overstabilization” of missense mutations is needed. The precise molecular details of this overstabilization are under investigation.

Nevertheless, since protein stabilization can be searched by high-throughput screening of chemical and virtual libraries [92, 93], the possibility exists that potential pharmacological chaperones are found empirically. In some cases, pharmacological chaperones resemble known protein ligands or inhibitors, and their stabilizing effect may be enhanced by structure-based approaches [93, 94]. Pharmacological chaperones have been shown to correct protein misfolding in several genetic diseases and it seems likely that missense PH1 mutations can benefit from this approach also. In addition, targeting cellular systems responsible for PLP bioavailability (enzymes involved in PLP recycling and delivery; [65]) may

represent a pharmacological approach to overcome mutation induced protein destabilization in PH1.

Chemical chaperones are small organic compounds which favor compact protein states over unfolded states through the so-called “solvophobic effect”, which involves destabilizing interactions of the water/chaperone mixture with the polypeptide backbone [95]. Their beneficial effect on mutant AGT has been demonstrated in vitro [34, 43], although the high concentrations required for protein stabilization and the lack of specificity of the stabilizing effect make them poor candidates to move forward into preclinical investigation.

In the future, the complexity of AGT intracellular homeostasis will also be better understood. The macromolecular assemblies that assist AGT expression, folding, stability, intracellular trafficking and degradation include key components that are also drugable targets for conservative treatment of PH1. AGT native state kinetic stability [57, 62] and interactions of partially folded states with molecular chaperones such as Hsp40/DnaJ, Hsp60/GroEL, Hsc70 and Hsp90 [34, 48, 50, 57] may be involved in the partition of AGT protein between correctly folded dimers and misfolding, with mitochondrial mistargeting, aggregation and degradation.

Pharmacological modulation of molecular chaperones is a promising therapeutic strategy in several conformational diseases [82]. However, the complexity of the molecular chaperone system in humans poses a significant challenge. The HSP70 machinery, for instance, includes at least 11 HSP70s, 41 J-proteins and 13 nucleotide exchange factors (NEFs) [86]. In addition, mammalian J-proteins and NEF proteins are structurally and functionally complex, displaying additional functions beyond the canonical model. J-proteins are known to be involved in shunting client proteins for degradation, remodeling and partially unfolding client proteins, while the BAG (BCL2-associated athanogene) family of NEFs are also known to target client proteins for proteasomal degradation [86]. Thus, finding the ideal target and modulating it pharmacologically in just the right direction is a formidable challenge. As a first step, an exhaustive biochemical and cellular definition on all these targets is needed, in order to determine those responsible for mitochondrial mistargeting, aggregation and degradation of mutant AGT.

## Conflict of Interests

The authors declare no conflict of interests.

## Acknowledgments

The authors thank Professor Arturo Muga for the DnaJ expression clone. This work was supported by the Spanish ministry of Science and Innovation (RYC2009-04147 and CSD2009-00088 to Angel L. Pey, SAF2011-23933 to Eduardo Salido, and CSD2006-00015 and BFU2011-25384 to Armando Albert), Junta de Andalucía (PI1CTS-7187 A.L.P.), and European Union (FP7-REGPOT-CT2012-31637-IMBRAIN to E.S.).

## References

- [1] B. Hoppe, "An update on primary hyperoxaluria," *Nature Reviews Nephrology*, vol. 8, pp. 467–475, 2012.
- [2] E. Salido, A. L. Pey, R. Rodriguez, and V. Lorenzo, "Primary hyperoxalurias: disorders of glyoxylate detoxification," *Biochimica et Biophysica Acta*, vol. 1822, no. 9, pp. 1453–1464, 2012.
- [3] C. J. Danpure, "Primary hyperoxalurias," in *The Metabolic and Molecular Bases of Inherited Disease*, C. R. Scriver, A. L. Beaudet, W. S. Sly et al., Eds., vol. 2, pp. 3323–3367, McGraw-Hill, New York, NY, USA, 8th edition, 2001.
- [4] M. Zylicz, T. Yamamoto, N. McKittrick, S. Sell, and C. Georgopoulos, "Purification and properties of the dnaJ replication protein of *Escherichia coli*," *The Journal of Biological Chemistry*, vol. 260, no. 12, pp. 7591–7598, 1985.
- [5] W. Martin, "Evolutionary origins of metabolic compartmentalization in eukaryotes," *Philosophical Transactions of the Royal Society B*, vol. 365, no. 1541, pp. 847–855, 2010.
- [6] R. J. A. Wanders and H. R. Waterham, "Biochemistry of mammalian peroxisomes revisited," *Annual Review of Biochemistry*, vol. 75, pp. 295–332, 2006.
- [7] A. Rokka, V. D. Antonenkov, R. Soininen et al., "Pxmp2 is a channel-forming protein in mammalian peroxisomal membrane," *PLoS ONE*, vol. 4, no. 4, Article ID e5090, 2009.
- [8] B. Cellini, M. Bertoldi, R. Montioli, A. Paiardini, and C. B. Voltattorni, "Human wild-type alanine:glyoxylate aminotransferase and its naturally occurring G82E variant: functional properties and physiological implications," *Biochemical Journal*, vol. 408, no. 1, pp. 39–50, 2007.
- [9] J. Knight and R. P. Holmes, "Mitochondrial hydroxyproline metabolism: implications for primary hyperoxaluria," *The American Journal of Nephrology*, vol. 25, no. 2, pp. 171–175, 2005.
- [10] J. Knight, J. Jiang, D. G. Assimos, and R. P. Holmes, "Hydroxyproline ingestion and urinary oxalate and glycolate excretion," *Kidney International*, vol. 70, no. 11, pp. 1929–1934, 2006.
- [11] E. Adams and L. Frank, "Metabolism of proline and the hydroxyprolines," *Annual Review of Biochemistry*, vol. 49, pp. 1005–1061, 1980.
- [12] R. P. Holmes and D. G. Assimos, "Glyoxylate synthesis, and its modulation and influence on oxalate synthesis," *Journal of Urology*, vol. 160, no. 5, pp. 1617–1624, 1998.
- [13] J. M. Phang, C. A. Hu, and D. Valle, "Disorders in proline and hydroxyproline metabolism," in *The Metabolic and Molecular Bases of Inherited Disease*, C. R. Scriver, A. Beaudet, W. Sly, D. Valle, and B. Childs, Eds., pp. 1821–1838, McGraw-Hill, New York, NY, USA, 2001.
- [14] P. Cochat, A. Deloraine, M. Rotily, F. Olive, I. Liponski, and N. Deries, "Epidemiology of primary hyperoxaluria type 1," *Nephrology Dialysis Transplantation*, vol. 10, supplement 8, pp. 3–7, 1995.
- [15] N. Kopp and E. Leumann, "Changing pattern of primary hyperoxaluria in Switzerland," *Nephrology Dialysis Transplantation*, vol. 10, no. 12, pp. 2224–2227, 1995.
- [16] C. S. van Woerden, J. W. Groothoff, R. J. A. Wanders, J. Davin, and F. A. Wijburg, "Primary hyperoxaluria type 1 in The Netherlands: prevalence and outcome," *Nephrology Dialysis Transplantation*, vol. 18, no. 2, pp. 273–279, 2003.
- [17] V. Lorenzo, A. Alvarez, A. Torres, V. Torregrosa, D. Hernández, and E. Salido, "Presentation and role of transplantation in adult patients with type 1 primary hyperoxaluria and the I244T AGXT mutation: single-center experience," *Kidney International*, vol. 70, no. 6, pp. 1115–1119, 2006.
- [18] J. Harambat, K. J. van Stralen, L. Espinosa et al., "Characteristics and outcomes of children with primary oxalosis requiring renal replacement therapy," *Clinical Journal of the American Society of Nephrology*, vol. 7, no. 3, pp. 458–465, 2012.
- [19] A. A. Al-Eisa, M. Samhan, and M. Naseef, "End-stage renal disease in Kuwaiti children: an 8-year experience," *Transplantation Proceedings*, vol. 36, no. 6, pp. 1788–1791, 2004.
- [20] A. Kamoun and R. Lakhoua, "End-stage renal disease of the Tunisian child: epidemiology, etiologies, and outcome," *Pediatric Nephrology*, vol. 10, no. 4, pp. 479–482, 1996.
- [21] C. J. Danpure and P. R. Jennings, "Peroxisomal alanine:glyoxylate aminotransferase deficiency in primary hyperoxaluria type 1," *FEBS Letters*, vol. 201, no. 1, pp. 20–24, 1986.
- [22] E. Leumann and B. Hoppe, "The primary hyperoxalurias," *Journal of the American Society of Nephrology*, vol. 12, no. 9, pp. 1986–1993, 2001.
- [23] K. Nishiyama, G. Berstein, T. Oda, and A. Ichiyama, "Cloning and nucleotide sequence of cDNA encoding human liver serine-pyruvate aminotransferase," *European Journal of Biochemistry*, vol. 194, no. 1, pp. 9–18, 1990.
- [24] Y. Takada, N. Kaneko, H. Esumi, P. E. Purdue, and C. J. Danpure, "Human peroxisomal L-alanine:glyoxylate aminotransferase. Evolutionary loss of a mitochondrial targeting signal by point mutation of the initiation codon," *Biochemical Journal*, vol. 268, no. 2, pp. 517–520, 1990.
- [25] T. Oda, T. Funai, and A. Ichiyama, "Generation from a single gene of two mRNAs that encode the mitochondrial and peroxisomal serine:pyruvate aminotransferase of rat liver," *The Journal of Biological Chemistry*, vol. 265, no. 13, pp. 7513–7519, 1990.
- [26] P. E. Purdue, M. J. Lumb, M. Fox et al., "Characterization and chromosomal mapping of a genomic clone encoding human alanine: glyoxylate aminotransferase," *Genomics*, vol. 10, no. 1, pp. 34–42, 1991.
- [27] X. Zhang, S. M. Roe, Y. Hou et al., "Crystal structure of alanine:glyoxylate aminotransferase and the relationship between genotype and enzymatic phenotype in primary hyperoxaluria type 1," *Journal of Molecular Biology*, vol. 331, no. 3, pp. 643–652, 2003.
- [28] D. Ghosh and J. M. Berg, "A proteome-wide perspective on peroxisome targeting signal 1(PTS1)-Pex5p affinities," *Journal of the American Chemical Society*, vol. 132, no. 11, pp. 3973–3979, 2010.
- [29] P. A. J. Huber, G. M. Birdsey, M. J. Lumb et al., "Peroxisomal import of human alanine:glyoxylate aminotransferase requires ancillary targeting information remote from its C terminus," *The Journal of Biological Chemistry*, vol. 280, no. 29, pp. 27111–27120, 2005.
- [30] K. Fodor, J. Wolf, R. Erdmann, W. Schliebs, and M. Wilmanns, "Molecular requirements for peroxisomal targeting of alanine-glyoxylate aminotransferase as an essential determinant in primary hyperoxaluria type 1," *PLoS Biology*, vol. 10, no. 4, Article ID e1001309, 2012.
- [31] E. L. Williams, C. Acquaviva, A. Amoroso et al., "Primary hyperoxaluria type 1: update and additional mutation analysis of the AGXT gene," *Human Mutation*, vol. 30, no. 6, pp. 910–917, 2009.
- [32] E. Williams and G. Rumsby, "Selected exonic sequencing of the AGXT gene provides a genetic diagnosis in 50% of patients with primary hyperoxaluria type 1," *Clinical Chemistry*, vol. 53, no. 7, pp. 1216–1221, 2007.

- [33] C. J. Danpure and G. Rumsby, "Molecular aetiology of primary hyperoxaluria and its implications for clinical management," *Expert Reviews in Molecular Medicine*, vol. 6, no. 1, pp. 1–16, 2004.
- [34] A. Santana, E. Salido, A. Torres, and L. J. Shapiro, "Primary hyperoxaluria type 1 in the Canary Islands: a conformational disease due to I244T mutation in the P11L-containing alanine:glyoxylate aminotransferase," *Proceedings of the National Academy of Sciences of the United States of America*, vol. 100, no. 12, pp. 7277–7282, 2003.
- [35] C. J. Danpure, P. R. Jennings, P. Fryer, P. E. Purdue, and J. Allsop, "Primary hyperoxaluria type 1: genotypic and phenotypic heterogeneity," *Journal of Inherited Metabolic Disease*, vol. 17, no. 4, pp. 487–499, 1994.
- [36] K. Nishiyama, T. Funai, S. Yokota, and A. Ichiyama, "ATP-dependent degradation of a mutant serine:pyruvate/alanine:glyoxylate aminotransferase in a primary hyperoxaluria type 1 case," *Journal of Cell Biology*, vol. 123, no. 5, pp. 1237–1248, 1993.
- [37] C. J. Danpure, P. J. Cooper, P. J. Wise, and P. R. Jennings, "An enzyme trafficking defect in two patients with primary hyperoxaluria type 1: peroxisomal alanine:glyoxylate aminotransferase rerouted to mitochondria," *Journal of Cell Biology*, vol. 108, no. 4, pp. 1345–1352, 1989.
- [38] C. J. Danpure, P. E. Purdue, P. Fryer et al., "Enzymological and mutational analysis of a complex primary hyperoxaluria type I phenotype involving alanine:glyoxylate aminotransferase peroxisome-to-mitochondrion mistargeting and intraperoxisomal aggregation," *The American Journal of Human Genetics*, vol. 53, no. 2, pp. 417–432, 1993.
- [39] P. E. Purdue, Y. Takada, and C. J. Danpure, "Identification of mutations associated with peroxisome-to-mitochondrion mistargeting of alanine:glyoxylate aminotransferase in primary hyperoxaluria Type I," *Journal of Cell Biology*, vol. 111, no. 6, pp. 2341–2351, 1990.
- [40] M. J. Lumb and C. J. Danpure, "Functional synergism between the most common polymorphism in human alanine:glyoxylate aminotransferase and four of the most common disease-causing mutations," *The Journal of Biological Chemistry*, vol. 275, no. 46, pp. 36415–36422, 2000.
- [41] C. J. Danpure, "Primary hyperoxaluria type 1: AGT mistargeting highlights the fundamental differences between the peroxisomal and mitochondrial protein import pathways," *Biochimica et Biophysica Acta*, vol. 1763, no. 12, pp. 1776–1784, 2006.
- [42] L. M. Luheshi and C. M. Dobson, "Bridging the gap: from protein misfolding to protein misfolding diseases," *FEBS Letters*, vol. 583, no. 16, pp. 2581–2586, 2009.
- [43] B. Cellini, R. Montioli, A. Paiardini et al., "Molecular defects of the glycine 41 variants of alanine glyoxylate aminotransferase associated with primary hyperoxaluria type I," *Proceedings of the National Academy of Sciences of the United States of America*, vol. 107, no. 7, pp. 2896–2901, 2010.
- [44] B. Cellini, R. Montioli, and C. B. Voltattorni, "Human liver peroxisomal alanine:glyoxylate aminotransferase: characterization of the two allelic forms and their pathogenic variants," *Biochimica et Biophysica Acta*, vol. 1814, no. 11, pp. 1577–1584, 2011.
- [45] D. Pirulli, M. Marangella, and A. Amoroso, "Primary hyperoxaluria: genotype-phenotype correlation," *Journal of Nephrology*, vol. 16, no. 2, pp. 297–309, 2003.
- [46] G. Rumsby, E. Williams, and M. Coulter-Mackie, "Evaluation of mutation screening as a first line test for the diagnosis of the primary hyperoxalurias," *Kidney International*, vol. 66, no. 3, pp. 959–963, 2004.
- [47] B. Hoppe, C. J. Danpure, G. Rumsby et al., "A vertical (pseudodominant) pattern of inheritance in the autosomal recessive disease primary hyperoxaluria type 1: lack of relationship between genotype, enzymic phenotype, and disease severity," *The American Journal of Kidney Diseases*, vol. 29, no. 1, pp. 36–44, 1997.
- [48] N. Mesa-Torres, I. Fabelo-Rosa, D. Riverol et al., "The role of protein denaturation energetics and molecular chaperones in the aggregation and mistargeting of mutants causing primary hyperoxaluria type I," *PLoS ONE*. In press.
- [49] S. Djordjevic, X. Zhang, M. Bartlam, S. Ye, Z. Rao, and C. J. Danpure, "Structural implications of a G170R mutation of alanine:glyoxylate aminotransferase that is associated with peroxisome-to-mitochondrion mistargeting," *Acta Crystallographica F*, vol. 66, no. 3, pp. 233–236, 2010.
- [50] A. Albert, C. Yunta, R. Arranz et al., "Structure of GroEL in complex with an early folding intermediate of alanine glyoxylate aminotransferase," *The Journal of Biological Chemistry*, vol. 285, no. 9, pp. 6371–6376, 2010.
- [51] W. E. Balch, R. I. Morimoto, A. Dillin, and J. W. Kelly, "Adapting proteostasis for disease intervention," *Science*, vol. 319, no. 5865, pp. 916–919, 2008.
- [52] E. T. Powers, R. I. Morimoto, A. Dillin, J. W. Kelly, and W. E. Balch, "Biological and chemical approaches to diseases of proteostasis deficiency," *Annual Review of Biochemistry*, vol. 78, pp. 959–991, 2009.
- [53] F. U. Hartl, A. Bracher, and M. Hayer-Hartl, "Molecular chaperones in protein folding and proteostasis," *Nature*, vol. 475, no. 7356, pp. 324–332, 2011.
- [54] R. I. Morimoto, "Proteotoxic stress and inducible chaperone networks in neurodegenerative disease and aging," *Genes and Development*, vol. 22, no. 11, pp. 1427–1438, 2008.
- [55] B. Cellini, A. Lorenzetto, R. Montioli, E. Oppici, and C. B. Voltattorni, "Human liver peroxisomal alanine:glyoxylate aminotransferase: different stability under chemical stress of the major allele, the minor allele, and its pathogenic G170R variant," *Biochimie*, vol. 92, no. 12, pp. 1801–1811, 2010.
- [56] E. D. Hopper, A. M. C. Pittman, M. C. Fitzgerald, and C. L. Tucker, "In vivo and in vitro examination of stability of primary hyperoxaluria-associated human alanine:glyoxylate aminotransferase," *The Journal of Biological Chemistry*, vol. 283, no. 45, pp. 30493–30502, 2008.
- [57] A. L. Pey, E. Salido, and J. M. Sanchez-Ruiz, "Role of low native state kinetic stability and interaction of partially unfolded states with molecular chaperones in the mitochondrial protein mistargeting associated with primary hyperoxaluria," *Amino Acids*, vol. 41, no. 5, pp. 1233–1245, 2011.
- [58] M. B. Coulter-Mackie, Q. Lian, and S. G. Wong, "Overexpression of human alanine:glyoxylate aminotransferase in *Escherichia coli*: renaturation from guanidine-HCl and affinity for pyridoxal phosphate co-factor," *Protein Expression and Purification*, vol. 41, no. 1, pp. 18–26, 2005.
- [59] E. Oppici, R. Montioli, A. Lorenzetto, S. Bianconi, C. B. Voltattorni, and B. Cellini, "Biochemical analyses are instrumental in identifying the impact of mutations on holo and/or apo-forms and on the region(s) of alanine:glyoxylate aminotransferase variants associated with primary hyperoxaluria type I," *Molecular Genetics and Metabolism*, vol. 105, no. 1, pp. 132–140, 2012.



- [60] A. M. Pittman, M. D. Lage, V. Poltoratsky et al., "Rapid profiling of disease alleles using a tunable reporter of protein misfolding," *Genetics*, vol. 192, no. 3, pp. 831–842, 2012.
- [61] J. M. Sanchez-Ruiz, "Protein kinetic stability," *Biophysical Chemistry*, vol. 148, no. 1–3, pp. 1–15, 2010.
- [62] B. Cellini, R. Montioli, A. Paiardini, A. Lorenzetto, and C. B. Voltattorni, "Molecular insight into the synergism between the minor allele of human liver peroxisomal alanine:glyoxylate aminotransferase and the F1521 mutation," *The Journal of Biological Chemistry*, vol. 284, no. 13, pp. 8349–8358, 2009.
- [63] C. G. Monico, S. Rossetti, J. B. Olson, and D. S. Milliner, "Pyridoxine effect in type I primary hyperoxaluria is associated with the most common mutant allele," *Kidney International*, vol. 67, no. 5, pp. 1704–1709, 2005.
- [64] C. S. van Woerden, J. W. Groothoff, F. A. Wijburg, C. Annink, R. J. A. Wanders, and H. R. Waterham, "Clinical implications of mutation analysis in primary hyperoxaluria type 1," *Kidney International*, vol. 66, no. 2, pp. 746–752, 2004.
- [65] M. L. di Salvo, R. Contestabile, and M. K. Safo, "Vitamin B6 salvage enzymes: mechanism, structure and regulation," *Biochimica et Biophysica Acta*, vol. 1814, no. 11, pp. 1597–1608, 2011.
- [66] C. Park and S. Marqusee, "Probing the high energy states in proteins by proteolysis," *Journal of Molecular Biology*, vol. 343, no. 5, pp. 1467–1476, 2004.
- [67] M. B. Coulter-Mackie and Q. Lian, "Consequences of missense mutations for dimerization and turnover of alanine:glyoxylate aminotransferase: study of a spectrum of mutations," *Molecular Genetics and Metabolism*, vol. 89, no. 4, pp. 349–359, 2006.
- [68] M. B. Coulter-Mackie and Q. Lian, "Partial trypsin digestion as an indicator of mis-folding of mutant alanine:glyoxylate aminotransferase and chaperone effects of specific ligands. Study of a spectrum of missense mutants," *Molecular Genetics and Metabolism*, vol. 94, no. 3, pp. 368–374, 2008.
- [69] G. Tur-Arlandis, D. Rodriguez-Larrea, B. Ibarra-Molero, and J. M. Sanchez-Ruiz, "Proteolytic scanning calorimetry: a novel methodology that probes the fundamental features of protein kinetic stability," *Biophysical Journal*, vol. 98, no. 6, pp. L12–L14, 2010.
- [70] C. J. Danpure, "Variable peroxisomal and mitochondrial targeting of alanine: glyoxylate aminotransferase in mammalian evolution and disease," *BioEssays*, vol. 19, no. 4, pp. 317–326, 1997.
- [71] J. D. Holbrook and C. J. Danpure, "Molecular basis for the dual mitochondrial and cytosolic localization of alanine:glyoxylate aminotransferase in amphibian liver cells," *The Journal of Biological Chemistry*, vol. 277, no. 3, pp. 2336–2344, 2002.
- [72] G. M. Birdsey, J. Lewin, J. D. Holbrook, V. R. Simpson, A. A. Cunningham, and C. J. Danpure, "A comparative analysis of the evolutionary relationship between diet and enzyme targeting in bats, marsupials and other mammals," *Proceedings of the Royal Society B*, vol. 272, no. 1565, pp. 833–840, 2005.
- [73] S. Fargue, J. Lewin, G. Rumsby, and C. J. Danpure, "Four of the most common mutations in primary hyperoxaluria type 1 unmask the cryptic mitochondrial targeting sequence of alanine:glyoxylate aminotransferase encoded by the polymorphic minor allele," *The Journal of Biological Chemistry*, vol. 288, no. 4, pp. 2475–2484, 2013.
- [74] P. E. Purdue, J. Allsop, G. Isaya, L. E. Rosenberg, and C. J. Danpure, "Mistargeting of peroxisomal L-alanine:glyoxylate aminotransferase to mitochondria in primary hyperoxaluria patients depends upon activation of a cryptic mitochondrial targeting sequence by a point mutation," *Proceedings of the National Academy of Sciences of the United States of America*, vol. 88, no. 23, pp. 10900–10904, 1991.
- [75] A. Matouschek, A. Azem, K. Ratliff, B. S. Glick, K. Schmid, and G. Schatz, "Active unfolding of precursor proteins during mitochondrial protein import," *EMBO Journal*, vol. 16, no. 22, pp. 6727–6736, 1997.
- [76] A. J. Wilcox, J. Choy, C. Bustamante, and A. Matouschek, "Effect of protein structure on mitochondrial import," *Proceedings of the National Academy of Sciences of the United States of America*, vol. 102, no. 43, pp. 15435–15440, 2005.
- [77] J. C. Young, N. J. Hoogenraad, and F. U. Hartl, "Molecular chaperones Hsp90 and Hsp70 deliver preproteins to the mitochondrial import receptor Tom70," *Cell*, vol. 112, no. 1, pp. 41–50, 2003.
- [78] H. Yamamoto, K. Fukui, H. Takahashi et al., "Roles of Tom70 in import of presequence-containing mitochondrial proteins," *The Journal of Biological Chemistry*, vol. 284, no. 46, pp. 31635–31646, 2009.
- [79] M. O. Casanueva, A. Burga, and B. Lehner, "Fitness trade-offs and environmentally induced mutation buffering in isogenic *C. elegans*," *Science*, vol. 335, no. 6064, pp. 82–85, 2012.
- [80] F. U. Hartl and M. Hayer-Hartl, "Converging concepts of protein folding in vitro and in vivo," *Nature Structural and Molecular Biology*, vol. 16, no. 6, pp. 574–581, 2009.
- [81] D. W. Neef, M. L. Turski, and D. J. Thiele, "Modulation of heat shock transcription factor 1 as a therapeutic target for small molecule intervention in neurodegenerative disease," *PLoS Biology*, vol. 8, no. 1, Article ID e1000291, 2010.
- [82] D. S. T. Ong and J. W. Kelly, "Chemical and/or biological therapeutic strategies to ameliorate protein misfolding diseases," *Current Opinion in Cell Biology*, vol. 23, no. 2, pp. 231–238, 2011.
- [83] B. Calamini, M. C. Silva, F. Madoux et al., "Small-molecule proteostasis regulators for protein conformational diseases," *Nature Chemical Biology*, vol. 8, no. 2, pp. 185–196, 2012.
- [84] S. Prakash and A. Matouschek, "Protein unfolding in the cell," *Trends in Biochemical Sciences*, vol. 29, no. 11, pp. 593–600, 2004.
- [85] A. J. McClellan, S. Tam, D. Kaganovich, and J. Frydman, "Protein quality control: chaperones culling corrupt conformations," *Nature Cell Biology*, vol. 7, no. 8, pp. 736–741, 2005.
- [86] H. H. Kampinga and E. A. Craig, "The HSP70 chaperone machinery: J proteins as drivers of functional specificity," *Nature Reviews Molecular Cell Biology*, vol. 11, no. 8, pp. 579–592, 2010.
- [87] L. Borghi, T. Meschi, F. Amato, A. Briganti, A. Novarini, and A. Giannini, "Urinary volume, water and recurrences in idiopathic calcium nephrolithiasis: a 5-year randomized prospective study," *Journal of Urology*, vol. 155, no. 3, pp. 839–843, 1996.
- [88] D. A. Gibbs and R. W. Watts, "The action of pyridoxine in primary hyperoxaluria," *Clinical science*, vol. 38, no. 2, pp. 277–286, 1970.
- [89] R. W. E. Watts, N. Veall, P. Purkiss, M. A. Mansell, and E. F. Haywood, "The effect of pyridoxine on oxalate dynamics in three cases of primary hyperoxaluria (with glycolic aciduria)," *Clinical Science*, vol. 69, no. 1, pp. 87–90, 1985.
- [90] B. Hoppe, K. Latta, C. von Schnakenburg, and M. J. Kemper, "Primary hyperoxaluria—the German experience," *The American Journal of Nephrology*, vol. 25, no. 3, pp. 276–281, 2005.
- [91] B. Hoppe, B. B. Beck, and D. S. Milliner, "The primary hyperoxalurias," *Kidney International*, vol. 75, no. 12, pp. 1264–1271, 2009.



- [92] A. L. Pey, M. Ying, N. Cremades et al., "Identification of pharmacological chaperones as potential therapeutic agents to treat phenylketonuria," *Journal of Clinical Investigation*, vol. 118, no. 8, pp. 2858–2867, 2008.
- [93] J. Underhaug, O. Aubi, and A. Martinez, "Phenylalanine hydroxylase misfolding and pharmacological chaperones," *Current Topics in Medicinal Chemistry*, vol. 12, no. 22, pp. 2534–2545, 2012.
- [94] S. Connelly, S. Choi, S. M. Johnson, J. W. Kelly, and I. A. Wilson, "Structure-based design of kinetic stabilizers that ameliorate the transthyretin amyloidoses," *Current Opinion in Structural Biology*, vol. 20, no. 1, pp. 54–62, 2010.
- [95] D. W. Bolen and G. D. Rose, "Structure and energetics of the hydrogen-bonded backbone in protein folding," *Annual Review of Biochemistry*, vol. 77, pp. 339–362, 2008.

## Research Article

# Structure-Based Mechanism for Early PLP-Mediated Steps of Rabbit Cytosolic Serine Hydroxymethyltransferase Reaction

Martino L. Di Salvo,<sup>1</sup> J. Neel Scarsdale,<sup>2</sup> Galina Kazanina,<sup>2</sup> Roberto Contestabile,<sup>1</sup> Verne Schirch,<sup>3</sup> and H. Tonie Wright<sup>3</sup>

<sup>1</sup> Dipartimento di Scienze Biochimiche, Sapienza Università di Roma, 00185 Roma, Italy

<sup>2</sup> Center for the Study of Biological Complexity and Institute for Structural Biology and Drug Discovery, Richmond, VA 23284-2030, USA

<sup>3</sup> Department of Biochemistry and Institute of Structural Biology and Drug Discovery, Virginia Commonwealth University, Richmond, VA 23219, USA

Correspondence should be addressed to Martino L. Di Salvo; [martino.disalvo@uniroma1.it](mailto:martino.disalvo@uniroma1.it)

Received 6 June 2013; Accepted 26 June 2013

Academic Editor: Alessandro Paiardini

Copyright © 2013 Martino L. Di Salvo et al. This is an open access article distributed under the Creative Commons Attribution License, which permits unrestricted use, distribution, and reproduction in any medium, provided the original work is properly cited.

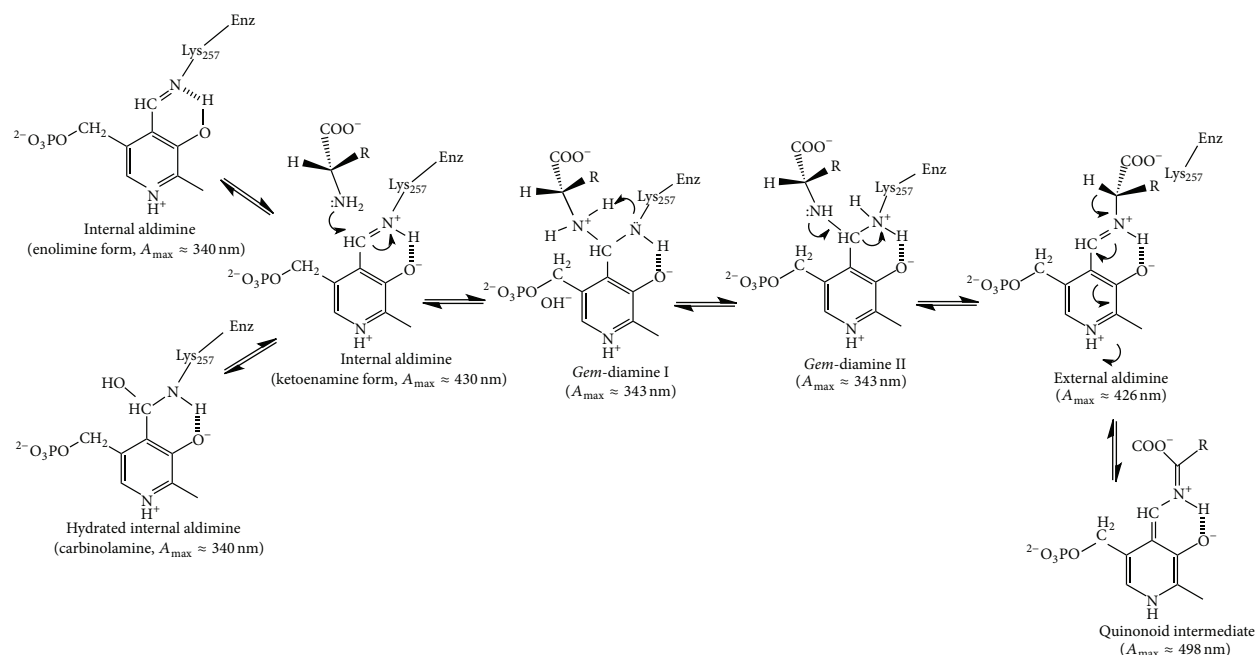
Serine hydroxymethyltransferase catalyzes the reversible interconversion of L-serine and glycine with transfer of one-carbon groups to and from tetrahydrofolate. Active site residue Thr254 is known to be involved in the transaldimination reaction, a crucial step in the catalytic mechanism of all pyridoxal 5'-phosphate- (PLP-) dependent enzymes, which determines binding of substrates and release of products. In order to better understand the role of Thr254, we have expressed, characterized, and determined the crystal structures of rabbit cytosolic serine hydroxymethyltransferase T254A and T254C mutant forms, in the absence and presence of substrates. These mutants accumulate a kinetically stable *gem*-diamine intermediate, and their crystal structures show differences in the active site with respect to wild type. The kinetic and crystallographic data acquired with mutant enzymes permit us to infer that conversion of *gem*-diamine to external aldimine is significantly slowed because intermediates are trapped into an anomalous position by a misorientation of the PLP ring, and a new energy barrier hampers the transaldimination reaction. This barrier likely arises from the loss of the stabilizing hydrogen bond between the hydroxymethyl group of Thr254 and the  $\epsilon$ -amino group of active site Lys257, which stabilizes the external aldimine intermediate in wild type SHMTs.

## 1. Introduction

Serine hydroxymethyltransferase (SHMT; EC 2.1.2.1) is a ubiquitous pyridoxal 5'-phosphate- (PLP-) dependent enzyme that catalyzes the reversible interconversion of L-serine and glycine, coupled to the formation and breakdown of 5,10-methylenetetrahydrofolate (5,10-CH<sub>2</sub>-H<sub>4</sub>PteGlu) [1, 2]. Because of its essential role in one-carbon units metabolism, SHMT has been often indicated as a potential target of chemotherapeutic agents [3–5]. It also catalyzes the conversion of 5,10-methenylene- to 5-formyl-H<sub>4</sub>PteGlu [6], the transamination and racemization of D- and L-alanine [7], the retro-aldol cleavage of *erythro* and *threo* isomers of both L-threonine and L- $\beta$ -phenylserine [8], and the decarboxylation of aminomalonate [9]. PLP-dependent

enzymes exist in complexes that absorb in the 310 nm to 500 nm range as the result of a conjugated  $\pi$ -electron system. These absorption properties have played an important role in elucidating the mechanisms of PLP addition and catalysis, since several intermediates on the reaction pathway have unique structural and absorbance characteristics [10, 11]. SHMT is distinctive among the PLP-dependent enzymes in the number of these absorbing complexes that can be observed, and these have been exploited to determinate kinetic rates for their interconversion by stopped-flow and temperature jump spectroscopy [11–13].

In PLP-dependent enzymes, the 4'-aldehyde of PLP is bound as an aldimine to the  $\epsilon$ -amino moiety of an active site Lys residue in what is called the "internal aldimine." For those PLP-dependent enzymes that catalyze reactions involving



SCHEME 1: Mechanism of transaldimination reaction of SHMT.

substrate amino acids, the initial step in the catalytic reaction is the formation of the “geminal diamine” (*gem*-diamine) between the C4' aldehyde of PLP and the amino group of the substrate. The orientation of the substrate in the active site with respect to the plane of PLP, to which it is covalently linked through its amino group, in turn determines which of the three substituent bonds on C $\alpha$  of the substrate will be cleaved. In 1966, Dunathan [14] provided a unifying concept for the specific selection of the substrate scissile bond in PLP-dependent enzymes, which has been confirmed in solution and structural studies. In his proposal, all bonds broken and made on the catalytic pathway are the nearest perpendicular to the conjugated  $\pi$  system of the PLP ring. The resulting carbanion at C $\alpha$  of the substrate amino acid is stabilized by resonance with the  $\pi$ -electron system in the pyridine ring of PLP. This intermediate on the catalytic pathway is referred to as the “quinonoid” complex and absorbs near 500 nm (Scheme 1). Solution studies have shown that SHMT passes through several ordered, spectrophotometrically identifiable intermediates that reflect changes in the electron system of the PLP cofactor [12, 15] and are consistent with Dunathan's proposal.

Prior to the availability of crystallographic structure information on SHMT, it was noted that the amino acid sequences of SHMTs from diverse species have a conserved run of 4 threonine residues terminating 2 residues upstream of the active site lysine: V-V-T-T-T<sup>254</sup>-T-H-K<sup>257</sup>(PLP)-T (numbering is that for rabbit cytosolic serine hydroxymethyltransferase (rcSHMT)) [16]. To determine the possible roles of this conserved sequence in SHMT catalysis, each threonine of this active site stretch was mutated in ecSHMT to an alanine, and the effects of the changes on the spectral and kinetic properties were investigated [17]. It was found that

only the T226A mutant of ecSHMT (Thr226 in ecSHMT numbering is equivalent to rcSHMT Thr254) had significant spectral and kinetic differences from the wild type enzyme. There was a 32-fold lower  $k_{cat}$  in the conversion of L-serine to glycine, and the T226A mutant was virtually inactive toward cleavage of L-allo-threonine compared to wild type ecSHMT. Furthermore, in the presence of L-serine the T226A mutant exhibited a large spectral absorbance peak at 343 nm, which is characteristic of a *gem*-diamine intermediate and only a small peak at 425 nm characteristic of the external aldimine. Stopped-flow analysis showed that the 343 nm peak was formed rapidly, but its conversion to the 425 nm absorbing peak was slow [17]. Since the *gem*-diamine is generally a short-lived intermediate on the reaction pathways of PLP-dependent enzymes, this T226A ecSHMT mutant offered the opportunity to investigate the structural changes that apparently slowed the conversion of the *gem*-diamine intermediate to the external aldimine. We were unable to obtain crystals for the T226A mutant of ecSHMT. However, we were able to crystallize the homologous T254A and T254C mutants of rcSHMT. We report here the kinetic properties and crystal structures of the T254 mutants of rcSHMT and their glycine and L-serine complexes. In addition, we have increased the resolution of the structure of wild type rcSHMT to 2.1 Å as an aid in examining details of the *gem*-diamine structures.

## 2. Results and Discussion

**2.1. Spectroscopic Studies.** Wild type rcSHMT exhibits a characteristic major single absorption band with maximum intensity at 430 nm, due to the protonated internal aldimine between enzyme and cofactor. Also, a minor band is observed

at 340 nm (Scheme 1). The addition of saturating concentrations of glycine results in a decrease of the major absorption band, with a slight blue shift at 426 nm and the appearance of a well-defined band at 343 nm. A small band centered at 498 nm is also visible. It is well established that these absorption bands correspond to the formation of the external aldimine, the *gem*-diamine, and the quinonoid intermediates, respectively [1, 12, 18]. All absorption bands of wild type and mutant enzymes are shown in Figure 1.

Like the wild type, the T254A mutant form exhibits a 430 nm absorption band (although much less intense than wild type), indicative of the presence of an internal aldimine, and also shows an important band at around 340 nm that may represent either the enolimine form or the carbinolamine, a hydrated form of the internal aldimine in which the water molecule mimics the substrate nucleophilic attack and the *gem*-diamine formation. As shown in Figure 1, this band is usually present in very low concentration in the freshly purified wild type enzyme. The addition of a saturating concentration of glycine to T254A mutant results in the almost complete loss of absorbance at 430 nm, with a concomitant increase of absorbance at 343 nm. This effect was also observed with *E. coli* SHMT T226A mutant (residue Thr226 of *ec*SHMT corresponds to residue Thr254 in *rc*SHMT). Kinetic studies on the latter mutant showed that the complex absorbing at 343 nm is formed in a bimolecular step providing strong evidence that it is indeed the *gem*-diamine intermediate [17]. The addition of  $H_4PteGlu$  to glycine-saturated wild type SHMT results in the increase of the 498 nm absorbing band, corresponding to the quinonoid intermediate. The large increase in absorbance below 400 nm is the absorbance of the excess  $H_4PteGlu$ . Instead, when the T254A mutant was saturated with glycine, even in the presence of  $H_4PteGlu$ , it did not show any 498 nm absorbing band. The effects of the addition of a saturating concentration of L-serine to T254A *rc*SHMT mutant enzyme are similar to those observed for glycine, with a decrease of the 430 nm absorbing band and a concomitant increase of the 343 nm absorbing species. In contrast, when wild type *rc*SHMT is saturated with L-serine, there are a marked increase and a blue shift of the major absorbing band, centered now at 426 nm, but no absorbance is observed at around 340.

The spectral features of the unliganded T224C mutant are largely similar to those of the wild type enzyme. However, the 340 nm band is slightly more intense. If compared to the T254A mutant, the relative intensities of the 430 nm and 340 nm bands are reversed. Spectral changes upon substrates addition are similar to the ones observed with the T254A mutant, except that a residual absorbance is shown in the 420–430 nm region.

**2.2. Kinetics Studies.** The spectral properties of the *rc*SHMT T254A and T254C mutant enzymes described above suggest that the *gem*-diamine intermediate accumulates upon substrate addition. The purified mutant enzymes were tested for catalytic activity using L-serine and L-allo-threonine as substrates (Table 1). For L-serine, both mutant enzymes showed slightly increased  $K_m$  values (about 2-fold) when compared to wild type *rc*SHMT;  $k_{cat}$  values decreased 46-fold

for the Thr to Ala mutant and 531-fold for the Thr to Cys mutant. Similarly,  $K_m$  values for L-allo-threonine were found to be only slightly higher than wild type (less than 2-fold for both mutants), whereas  $k_{cat}$  values showed a 9- to 29-fold decrease for T254A and T254C mutants, respectively.

To better understand the role of Thr254 in the formation and breakdown of the *gem*-diamine intermediate and thus on the transaldimination reaction, the rate of the spectral changes occurring when L-serine and glycine were added to the enzyme was determined at different pH values by means of stopped-flow measurements. The  $k_{on}$  and  $k_{off}$  values for the rate of formation and breakdown of the enzyme-substrate complex absorbing at 343 nm were determined from a plot of  $k_{obs}$  versus substrate concentration, after linear regression of data and extrapolation of the slope and intercept values (Table 2). For both mutants and for both substrates at each pH value,  $k_{obs}$  was a linear function of substrate concentration, as expected for a second-order reaction. The second-order rate constants for substrate addition and *gem*-diamine formation ( $k_{on}$ ) were corrected for the concentration of the amino acid anionic form at each pH value and are listed as  $k'_{on}$ . The anionic form of the  $\alpha$ -amino group is assumed to be the true substrate for the transaldimination reaction. In the pH range used in the experiments (6.4–8.0), the concentration of the anionic form of the amino acid substrates increases about 40 times. The  $k_{on}$  values increased with pH and varied from  $3.3 \cdot 10^4$  to  $10.7 \cdot 10^4 \text{ s}^{-1} \cdot \text{M}^{-1}$  when L-serine was used as substrate and from  $0.8 \cdot 10^4$  to about  $4.4 \cdot 10^4 \text{ s}^{-1} \cdot \text{M}^{-1}$  when glycine was used as substrate;  $k_{on}$  values were very similar for both T254 mutant forms. After correction for the concentration of anionic substrate,  $k'_{on}$  values showed a 10-fold decrease as pH increased from 6.4 to 8.0 and ranged from  $20 \cdot 10^6$  to  $1.8 \cdot 10^6 \text{ s}^{-1} \cdot \text{M}^{-1}$  with L-serine and from  $13 \cdot 10^6$  to  $1.8 \cdot 10^6 \text{ s}^{-1} \cdot \text{M}^{-1}$  with glycine. The sigmoidal dependence of  $k'_{on}$  on pH suggests the titration of a group at the active site involved in a general acid catalysis, with a  $pK_a$  around 6.8 (Figure 2). If the internal aldimine of the mutant enzymes is mostly in the carbinolamine form, as inferred from the absorption spectra shown in Figure 1, it must be dehydrated (through the protonation of the hydroxyl group followed by the elimination of water) in order to be converted into the ketoenamine that is able to react with the incoming amino group of the substrates. Importantly, we have observed that the ratio of the 428 nm and 340 nm bands changes with pH in a similar manner, with the ketoenamine form being favored at higher pH values (data not shown). A possible candidate for this acid catalysis is Tyr73, which is involved in a cation- $\pi$  interaction with Arg263. It has been shown that Tyr residues involved in cation- $\pi$  interactions may have their  $pK_a$  lowered by 1 to 3 pH units (the normal  $pK_a$  of tyrosine residue is about 9.5) [19]. Furthermore, this residue points toward the protein region where the transaldimination reaction takes place, and its phenolic hydroxyl is located in close proximity to C4' (see Figure 6). When L-serine was used as substrate,  $k_{off}$  values showed a decreasing trend as pH was increased and ranged from 10.3 to  $3.1 \text{ s}^{-1}$  for the T254A mutant form and from 39 to  $23 \text{ s}^{-1}$  for T254C. In contrast, when glycine was used as substrate,  $k_{off}$



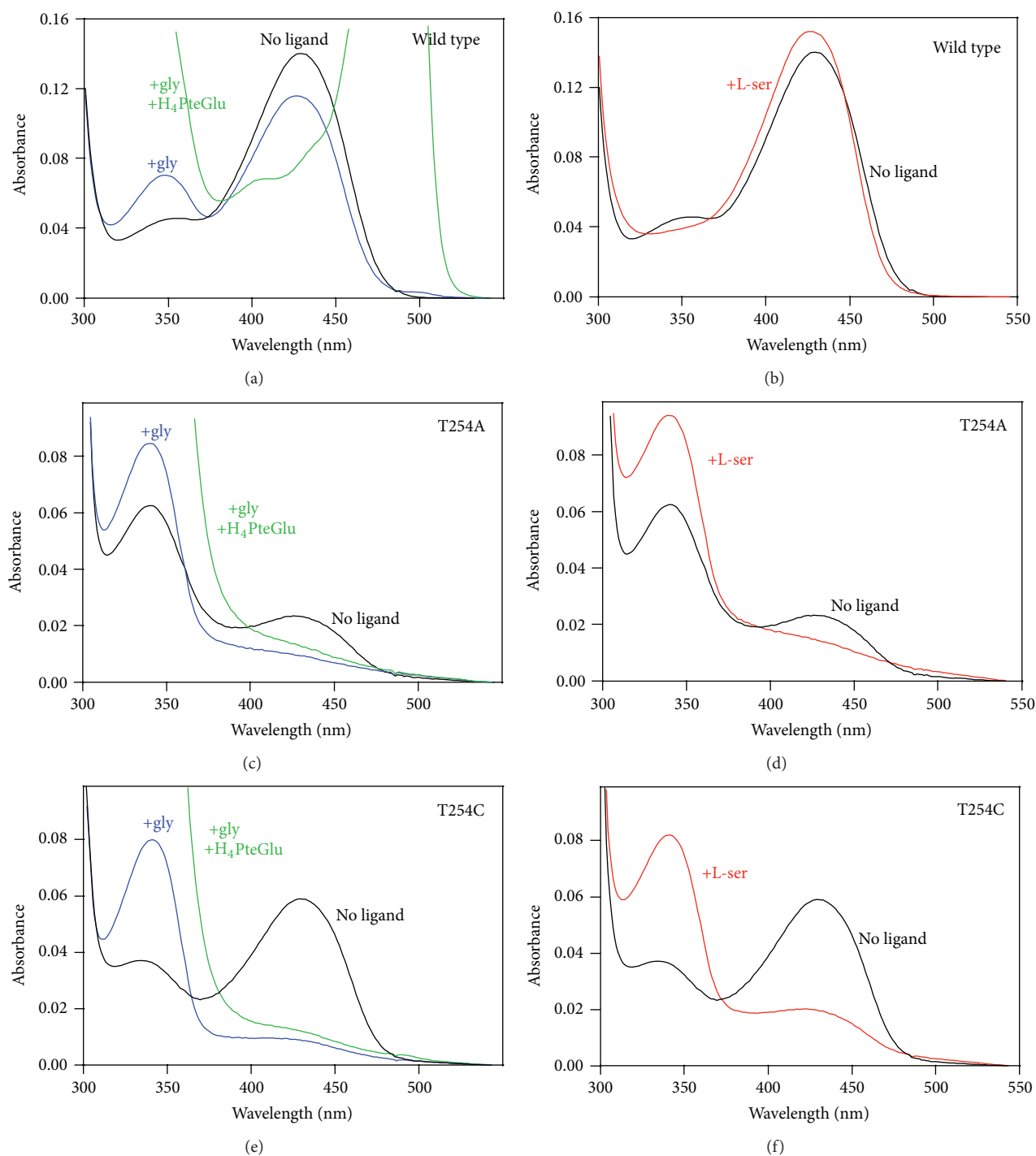


FIGURE 1: Absorption spectra of wild type and mutant rcSHMT in the absence and presence of substrates. Left panels show the absorption spectra of wild type, T254A and T254C rcSHMTs at 30°C before (black lines) and after the addition of 90% saturating glycine (blue lines). Green lines are spectra taken after the addition of 100  $\mu$ M H<sub>4</sub>PteGlu to the samples containing glycine. Right panels show the absorption spectra of the same enzymes before (black lines) and after the addition of 90% saturating L-serine (red lines).

values slightly increased with pH, ranging from 1 to 2.9 s<sup>-1</sup> for the T254A mutant form and from 5.1 to 7.0 s<sup>-1</sup> for T254C.

Stopped-flow studies done many years ago at pH 7.3 for wild type rcSHMT [12] gave a comparable  $k_{on}$  value to the values for the T254A and T254C mutants. On the other hand,

the  $k_{off}$  values determined with the mutant enzymes are about 2 orders of magnitude lower than the wild type. These data suggest that the mutations have not significantly affected the rate of formation of the *gem*-diamine intermediate but have a more significant effect on the rate of its breakdown.

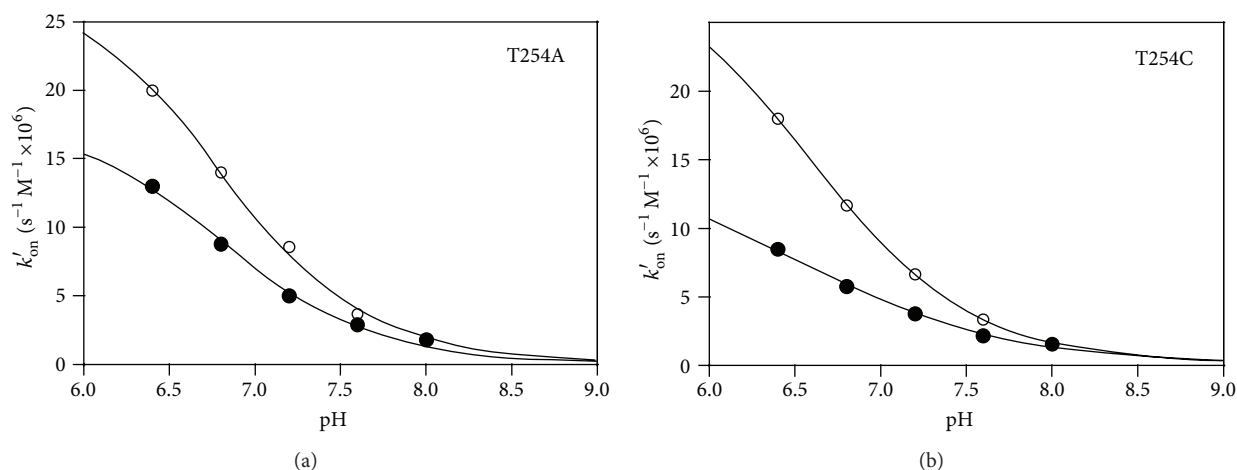


FIGURE 2: Dependence of  $k'_{on}$  values determined from stopped-flow experiments on pH, for T254A and T254C rcSHMT mutants. Open circles correspond to data obtained with L-serine, while closed circles correspond to data obtained with glycine. The continuous lines through the experimental points were obtained through a least square minimization process using the equation for a sigmoidal curve (the software used was GraphPad, Prism).

TABLE 1: Kinetic constants for the hydroxymethyltransferase and retro-aldol cleavage reactions catalyzed by wild type and T254 mutant rcSHMT forms.

Substrate	Kinetic constant	Form of rabbit cytosolic SHMT		
		Wild type	T253A	T253C
L-Serine	$K_m$ (mM)	0.3	0.6	0.5
	$k_{cat}$ ( $min^{-1}$ )	850	18.5	1.6
L-allo-Threonine	$K_m$ (mM)	1.5	2.5	2.6
	$k_{cat}$ ( $min^{-1}$ )	130	14.3	4.5

If the rapid spectroscopic changes occurring when the enzyme was mixed with saturating concentration of substrates were followed for a longer period of time (up to 50 seconds), a slow first-order increase was observed at 426 nm. For the T254A mutant with saturating concentration of L-serine, the rate constant was determined to be  $10 min^{-1}$ . This value is in agreement with previous studies on the T226A mutant of *ecSHMT* [17]. It is interesting to notice that this rate constant is very close to the  $k_{cat}$  measured for both hydroxymethyltransferase and retro-aldol cleavage reactions catalyzed by this mutant. This shows that for the T254A mutant the conversion of the *gem*-diamine into the external aldimine intermediate has become the rate-limiting step.

The spectral and kinetic studies both strongly suggest that removing the hydroxymethyl group of Thr254 by replacing it with either an Ala or a Cys residue greatly slows the conversion of the *gem*-diamine intermediates to the external aldimine. This may be the result of either blocking the conversion of *gem*-diamine I to *gem*-diamine II or of slowing conversion of *gem*-diamine II to the external aldimine. Therefore, the slowing of the catalytic cycle could be explained by either the mutant *gem*-diamine complexes being in a more stable form (in an energy well) compared to the wild type enzyme or by an increased energy barrier to pass to the

external aldimine. These two hypotheses are not mutually exclusive and could be applied at the same time.

**2.3. Crystal Structures.** We determined the crystal structures of the T254A and T254C mutant enzymes and the complex of each with glycine and L-serine, and the structure of wild type rcSHMT to a higher resolution than had previously been attained [20]. Table 3 lists the crystallographic and refinement data for the new rabbit cytosolic SHMT structures determined and described in this work. All structures except for the T254C-glycine complex were solved in space group  $P4_1$  with a tetramer of 4 independently determined subunits per asymmetric unit. The T254C-glycine complex was solved in space group  $P4_12_12$  with a dimer per asymmetric unit. The oligomeric structure of rcSHMT consists of two tight dimers each made of identical monomers. These tight dimers are loosely associated to form a so-called dimer of dimers. Disordered density recurred in the insert segment around residue 272 and at the amino termini of all monomer subunits, as observed in previously determined SHMT structures, but these disordered residues are not close to the regions of the enzyme around the PLP and substrate binding site, which are the subject of this study.

**2.3.1. Differences in Structure of Unliganded Wild Type and T254 Mutants.** Except for the small differences in the active site described herein, all structures are virtually identical (rmsd  $< 0.4 \text{ \AA}$  in all cases). The interactions of the PLP cofactor with the protein in the wild type and T254 mutants are almost identical. The distance of the Asp228 carboxylate to N1 of the pyridine ring is unchanged in the mutants as are the noncovalent bond constraints on the phosphoryl group of the PLP tail and the coplanarity of the His148 imidazole with the PLP ring. The active sites of all subunits of the wild type have phosphate or MES buffer anions bound where the carboxylate moiety of the amino acid substrate binds

TABLE 2: Kinetic constants for the rate of formation and breakdown of the *gem*-diamine complex for mutant rcSHMT forms with glycine and L-serine substrates.

Substrate	pH	T253A			T253C		
		$k_{on} (s^{-1} M^{-1} \cdot 10^4)$	$k'_{on} (s^{-1} M^{-1} \cdot 10^6)$	$k_{off} (s^{-1})$	$k_{on} (s^{-1} M^{-1} \cdot 10^4)$	$k'_{on} (s^{-1} M^{-1} \cdot 10^6)$	$k_{off} (s^{-1})$
L-Serine	6.4	3.3	20	10.3	2.9	18	39
	6.8	5.8	14	8.3	4.0	10	36
	7.2	8.7	8.6	5.8	6.8	6.7	32
	7.6	9.5	3.7	5.3	8.7	3.4	27
	8.0	10.7	1.8	3.1	9.4	1.5	23
Glycine	6.4	0.8	13	1.0	0.5	8.5	5.1
	6.8	1.3	8.0	1.3	0.7	4.5	6.7
	7.2	2.1	5.0	1.9	1.5	3.8	6.9
	7.6	3.0	2.9	2.4	2.1	2.2	7.0
	8.0	4.4	1.8	2.9	3.7	1.6	6.8

in SHMT-substrate complexes (see next paragraph). In the T254A mutant, this site is occupied by phosphate ions in one dimer and by MES in the other dimer. In the T254C mutant this anionic site is occupied by water in three subunits and by an apparent phosphate in the fourth subunit (Table 4).

There are significant differences between the wild type and the T254 mutants in the conformation of the PLP methylene phosphate tail although these are seen to a different extent in different subunits (Figure 3). These differences correlate with the absence of the C $\beta$  methyl group in the Ala254 and Cys254 side chains in the mutants. In the wild type structure, this methyl group of Thr254 projects toward the methylene phosphate tail. Replacement of the side chain by Ala or Cys opens a small space that allows the cofactor tail to assume a different conformation, moving the C5' towards this cavity. This is the most evident change observed in the mutants. The fact that not all of the T254A and C subunits show this change to the same extent suggests that there is a low barrier to this switch of conformations and that the crystallization process is selecting out an asymmetric distribution. As a consequence of the elbow-like rotation of the methylene phosphate PLP tail in the mutant T254 forms, the PLP ring orientation also diverges from that of the wild type. Moreover, in the mutant enzyme structures with the largest PLP tail conformational differences, the aldimine linkage between C4' and the  $\epsilon$ -amino group of the active site lysine (Lys257) is far from being in the plane of the PLP ring (Figure 3(d)), as required by the double bond conjugation present in the ketoenamine form of the internal aldimine. As the aldimine linkage is driven away from this plane, its conjugation with the  $\pi$ -electron system of the pyrimidine ring is diminished, and the maximum absorbance is shifted to lower wavelengths [21], as observed for the mutant enzymes in solution (Figure 1). As discussed above, we cannot exclude that the 340 nm absorbing band of the unliganded mutant enzymes may correspond to the hydrated form of the internal aldimine (carbinolamine; Scheme 1). In the internal aldimine form of the T254C mutant, the conformational change of the methylene phosphate tail and the displacement of the PLP ring are less evident (data not shown). This correlates with the observation that, in the absorption spectrum of this mutant

in solution, the amount of the canonical 428 nm ketoenamine band is higher than in the T254A mutant.

**2.3.2. The Glycine and L-Serine Complexes of T254A and T254C Mutants.** The structures of the T254A and T254C mutants with glycine and L-serine substrate ligands are all in the *gem*-diamine form (Table 4), showing both the amino group of the substrate and the  $\epsilon$ -amino group of Lys257 forming bonds to C4' of PLP. In all subunits of both mutants and with both substrates, the orientation of the PLP ring and the conformation of the methylene phosphate tail are very similar. Interestingly, the inhomogeneity seen in the internal aldimine structures of the mutant enzymes has disappeared upon binding of substrates. For example, Figure 4 shows a comparison between the active site structures of the T254A mutant with either L-serine (a) or glycine (b) bound to C4' of PLP in the *gem*-diamine form and the internal aldimine. The comparison is made with the subunit of the unliganded mutant enzyme in which the internal aldimine shows the largest difference with respect to wild type (Figure 3(d)). It can be seen that, in both *gem*-diamine structures, the orientation of the PLP ring and the conformation of the methylene phosphate tail and of the active site lysine (Lys257) are very similar to those of the internal aldimine form and therefore differ significantly from the wild type internal aldimine structure. The carboxylate group of substrates is oriented to form dual hydrogen bonds with Arg402 and also with Y83. Residues Ser203 and His231 make hydrogen bonds with the O3' of PLP, as already observed in all other SHMT structures. In the L-serine *gem*-diamine complex, the hydroxyl group of the substrate makes H-bond interactions with Glu75 and Tyr83, as also observed in the crystal structure of the *Bacillus stearothermophilus* SHMT-L-serine complex [22].

Wild type rcSHMT enzyme cocrystallized with glycine and 5-CHO-H<sub>4</sub>PteGlu showed two of the enzyme subunits in the *gem*-diamine form [19] (Table 4). No external aldimines were present, as the other two subunits were in the internal aldimine form. It is worth noting that structural variation among subunits in ligand binding site occupancy and type of intermediate complex is also found in other eukaryotic and

TABLE 3: Crystallographic data collection and refinement statistics for rcSHMT structures determined in this work.

	Wild type	T254A	T254A + gly.	T254A + L-ser.	T254C	T254C + gly.	T254C + L-ser.
Cell/space group	115.6,115.6,156.0 P <sub>4</sub> <sub>1</sub>	115.1,115.1,157.4 P <sub>4</sub> <sub>1</sub>	115.0,115.0,156.8 P <sub>4</sub> <sub>1</sub>	115.5,115.5,156.3 P <sub>4</sub> <sub>1</sub>	114.0,114.0,154.7 P <sub>4</sub> <sub>1</sub>	114.6,114.6,156.9 P <sub>4</sub> <sub>1</sub> ,2,2	114.0,114.0,155.6 P <sub>4</sub> <sub>1</sub>
Resolution	119.0–2.10 (2.16–2.10)	111.8–2.55 (2.62–2.55)	20.0–2.65 (2.72–2.65)	115–2.40 (2.46–2.40)	111.8–2.40 (2.46–2.40)	90.0–2.65 (2.72–2.65)	111.8–2.55 (2.62–2.55)
Completeness (%)	98.5 (98.2)	92.2 (87.9)	99.6 (99.8)	88.3 (85.8)	90.1 (86.9)	69.6 (62.0)	90.9 (76.9)
R <sub>work</sub>	.199 (.248)	.201 (.306)	.203 (.292)	.197 (.247)	.195 (.242)	.221 (.333)	.202 (.284)
R <sub>free</sub>	.242 (.316)	.271 (.432)	.277 (.399)	.258 (.318)	.256 (.346)	.305 (.414)	.263 (.362)
N <sub>work</sub>	105631 (7668)	55295 (3849)	52905 (3769)	63363 (4478)	62364 (4393)	19976 (1244)	52787 (5963)
N <sub>free</sub>	11736 (845)	6204 (426)	5968 (406)	7156 (510)	7009 (470)	1654 (96)	5963 (375)
$\langle B_{\text{protein}} \rangle$	30.8	44.8	34	37.3	39.4	36.6	38
$\langle B_{\text{water}} \rangle$	39.8	43.8	34.6	37.3	41.9	NA	40.1
RMSD from ideal							
Bond lengths	0.008	0.007	0.007	0.006	0.006	0.006	0.007
Bond angles	1.3	1.24	1.22	1.13	1.13	1.08	1.16
Ramachandran plot							
Favored	1460	1424	1403	1425	1435	702	1427
Additionally allowed	123	142	142	146	133	69	128
Generously allowed	13	8	9	12	15	6	12
Forbidden	3	7	9	5	5	7	10
MolProbity score	1.73 (93%)	2.04 (96%)	2.04 (97%)	1.88 (96%)	1.81 (97%)	2.24 (93%)	2.00 (96%)



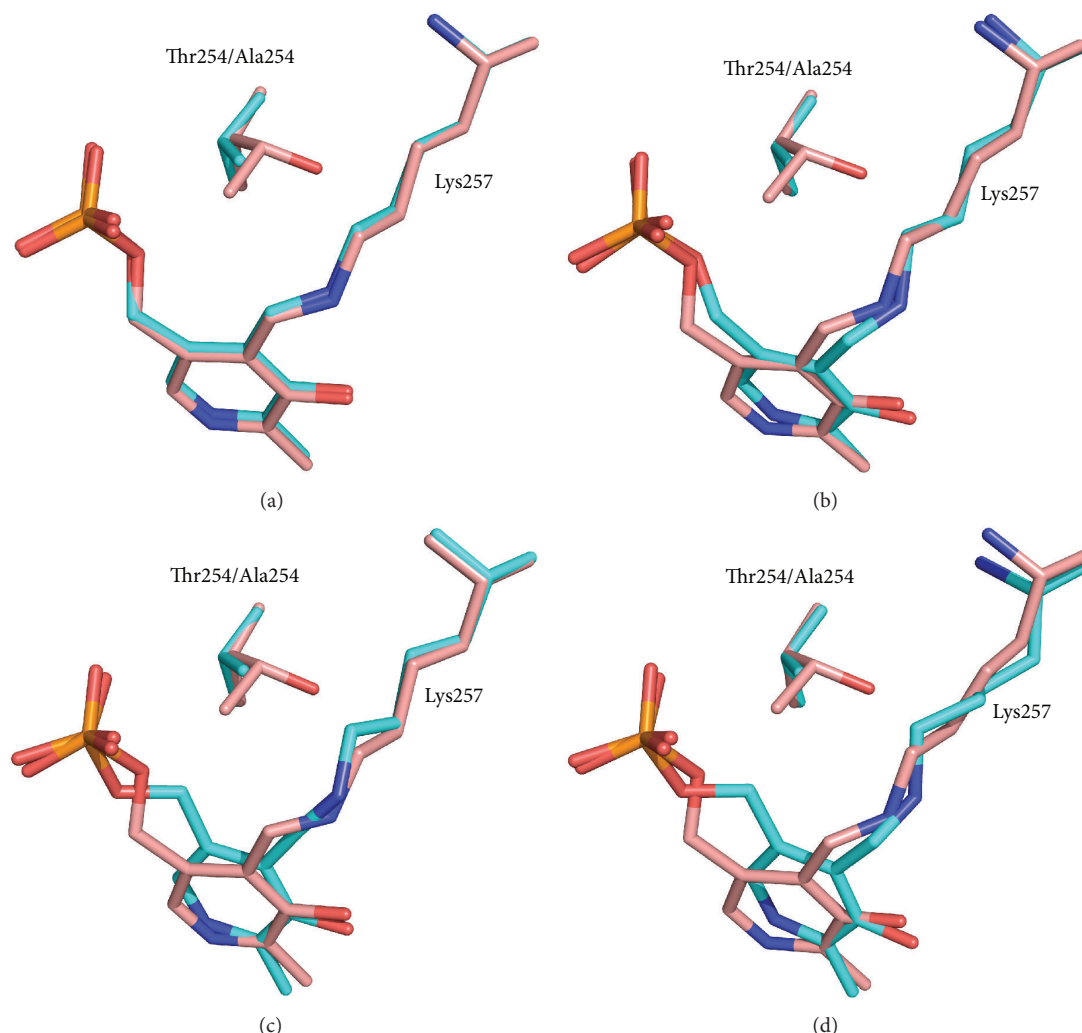


FIGURE 3: Superposition of the active site structures of rcSHMT wild type (salmon) and T254A (cyan) in the internal aldimine form. Panels (a) to (d) correspond to different subunits of the tetramer.

prokaryotic SHMTs [22–26]. The above wild type rcSHMT-glycine-5-CHO- $H_4$ PteGlu ternary complex structure and that of mouse cytosolic SHMT (which was also cocrystallized with glycine and 5-CHO- $H_4$ PteGlu [25]) are the only wild type SHMT structures in which *gem*-diamine intermediates can be seen.

When wild type and T254A rcSHMT-glycine *gem*-diamine structures are superimposed, some striking differences can be noticed (Figure 5). The methylene phosphate tail conformation and the orientation of the PLP ring are significantly different. The carboxylate group of glycine in wild type rcSHMT *gem*-diamine, although still interacting with Y83 and Arg402 through one of its oxygen atoms, is no more oriented to interact optimally with Arg402, and the other oxygen points away from it. Moreover, the position of the two amino groups in the *gem*-diamine is different between wild type and mutant (see arrows in Figure 5). In particular, the hydrogen atoms of the amino groups point away from Tyr73, which might be involved in the proton

exchange required to interconvert the two *gem*-diamine intermediates (see below for discussion).

In the wild type *gem*-diamine, the bond between the substrate amino group and C4' of PLP lies roughly perpendicular to the cofactor ring, indicating a strong similarity to *gem*-diamine I intermediate, in which the amino group of the substrate has attacked the C4' Schiff base of the cofactor with a trajectory that is perpendicular to the pyridine ring (Scheme 1). It appears that the wild type rcSHMT in the crystal has been trapped as a *gem*-diamine I intermediate that barely accumulates in solution. On the other hand, the *gem*-diamine forms found in T254 mutants seem to be in an aberrant position. The best way to appreciate this is to superimpose the structures of wild type *gem*-diamine (Figure 6(a)) or T254 mutant *gem*-diamine (Figure 6(b)) with wild type internal and external aldimines. In SHMTs, as PLP reacts with the substrate and the internal aldimine is converted into the external aldimine, the pyridine ring rotates by about 25°, primarily around the C2-C5 axis. This is also

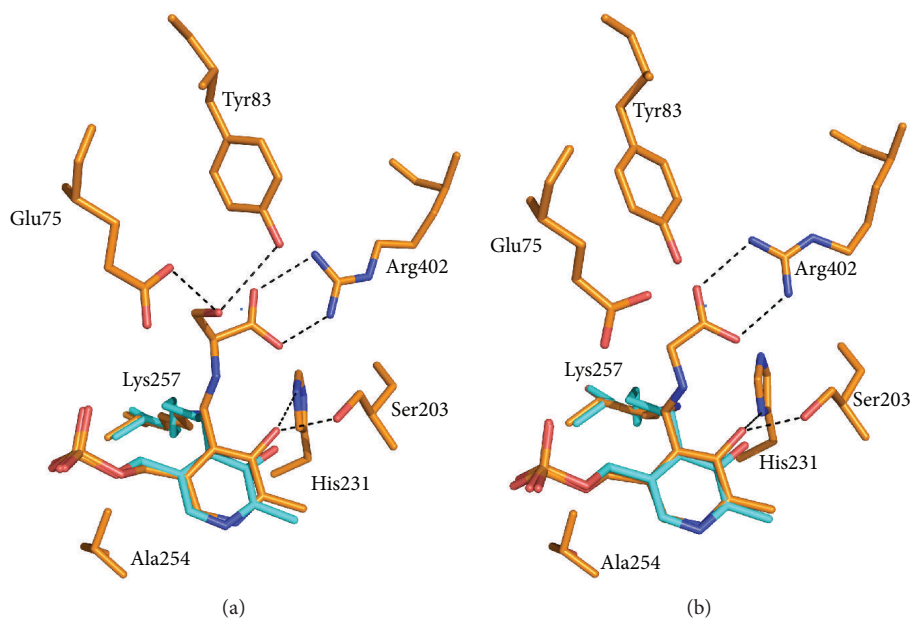


FIGURE 4: Superposition of the active site structures of the T254A mutant in the internal aldimine form (cyan) and as a *gem*-diamine complex (orange) with either L-serine (a) or glycine (b).

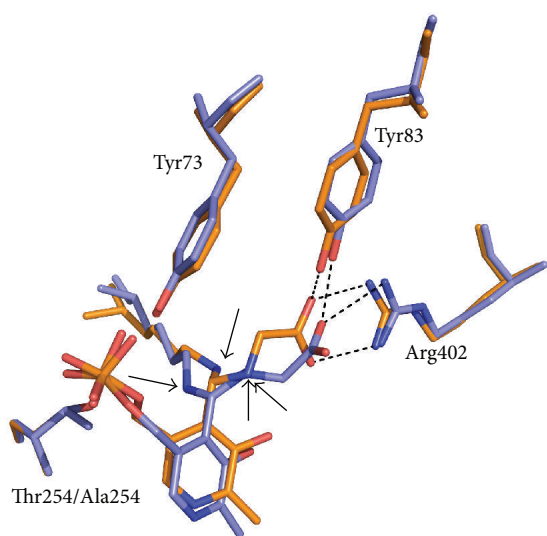


FIGURE 5: Superposition of the active site structures of the wild type (slate) and T254A mutant form (orange) of rcSHMT as *gem*-diamine complexes with glycine (pdb 1ls3). The arrows in the figure point towards the amino groups of the *gem*-diamine complexes.

observed in prokaryotic *B. stearotherophilus* SHMT with both glycine and L-serine as substrates and in the ternary complex with glycine and 5-CHO-H<sub>4</sub>PteGlu [22]. In the wild type rcSHMT *gem*-diamine, the PLP ring lies between the positions observed in the internal and external aldimines. Strikingly, in the mutant T254 *gem*-diamine the cofactor ring has a different orientation, which is unlikely to correspond to that occurring in the transaldimination reaction. This is obviously a consequence of the mutation, since this position

of the PLP ring is also observed in the unliganded forms of T254A and T254C rcSHMT structures. The *gem*-diamine structures of the mutant enzyme appear to be close to the *gem*-diamine II intermediate (Scheme 1), and the angle of the bond from C4' of the PLP ring to the  $\epsilon$ -amino group of K257 being close to the 90° predicted for this intermediate II, in which the amino group of Lys257 has to be eliminated in order to form the external aldimine intermediate. Moreover, the carboxylate group of the substrate makes optimal dual hydrogen bonds with Arg402 (Figure 6(b); structure in orange), as is observed in the external aldimine form of wild type SHMT-glycine complex (Figure 6(b); structure in magenta).

These observations suggest that in the T254 rcSHMT crystals, the PLP-substrate complex is blocked in the form of an anomalous and stable *gem*-diamine intermediate. As mentioned above, it is noteworthy that in the T254 mutant *gem*-diamine intermediates the position and orientation of the two amino groups point away from Tyr73 compared to the wild type *gem*-diamine structure. Tyrosine 73 was shown in *E. coli* and *bs*SHMT to have an important role in the transaldimination process and was proposed to act as proton exchanger between *gem*-diamines I and II. Interestingly, Tyr to Phe mutants of this residue also accumulate the *gem*-diamine intermediate [18, 27].

An additional remarkable variation in the T254 mutant structures compared to wild type is observed in the peptide bond between His256 and Lys257. Among the determined mutant structures, this peptide bond adopts two distinct orientations, one similar to the wild type rcSHMT and the other differing by up to 180°. The local variation in conformation of the His256-Lys257 peptide bond may be linked to the rcSHMT T254 mutations, since, in the internal

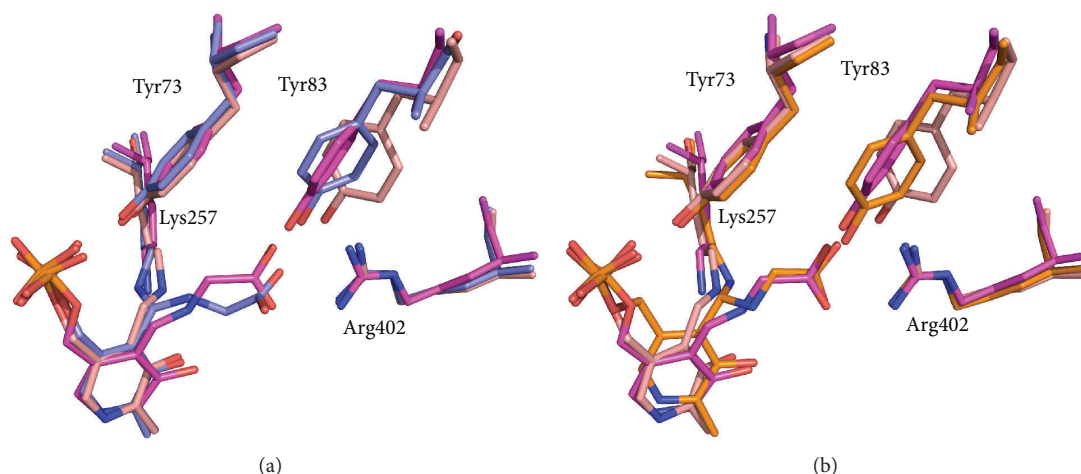


FIGURE 6: Superposition of wild type structures corresponding to the internal aldimine (salmon; rcSHMT) and external aldimine (magenta; mcSHMT, pdb 1eji) forms of the cofactor with the glycine *gem*-diamine form of the wild type (slate) and T254A mutant (orange).

aldimine of wild type rcSHMT, the carbonyl oxygen of His256, which is flipped in some mutant structures, makes a hydrogen bond through a water molecule to the Thr254 side chain. The lack of uniformity in structure among the subunits of the T254 mutants in the conformation of the PLP methylene phosphate tail, the position of the PLP ring, and the orientation of the His256-Lys257 peptide bond suggest that mutation of T254 relaxes some local structural constraints around the active site.

### 3. Conclusions

The T254A and T254C mutations have created a small empty space in the active site of rcSHMT due to the absence of the threonine methyl group. This has allowed the methylene phosphate tail of PLP to adopt a stable, uncharacteristic conformation that is in turn responsible for an aberrant positioning of the PLP ring. This clearly affects the transaldimination step of the SHMT reaction, making it the rate-limiting step in the catalytic cycle. In these mutants, when either L-serine or glycine is added to the enzyme, *gem*-diamine intermediates greatly accumulate. This may be the result of either blocking the conversion of *gem*-diamine I to *gem*-diamine II, slowing the conversion of *gem*-diamine II to the external aldimine, or both.

Conversion of the *gem*-diamine II into the external aldimine requires that the  $\epsilon$ -amino group of Lys257 is protonated and that it leaves perpendicularly from the *si* face of C4' of PLP. In Scheme 1 this is shown as a direct proton transfer from the substrate amino group in *gem*-diamine I to the leaving amino group of Lys257 in *gem*-diamine II. However, this proton transfer almost certainly does not occur directly but through shifts of protons in a network of acid-base groups at the active site. It is possible, based on the wild type and T254 mutant structures, that protonation of the Lys257 amine of the *gem*-diamine is mediated by Tyr73. The position of the *gem*-diamine amino groups relative to the Tyr73 side chain

varies in the mutants. These local structure changes in T254 mutants could be responsible for a perturbation of the proton transfer chain which slows the transaldimination reaction.

Available external aldimine SHMT structures (such as, *E. coli* SHMT as ternary complex with glycine and 5-CHO-H<sub>4</sub>PteGlu (pdb 1dfo) and *bs*SHMT with glycine and L-serine (pdb 1kl1 and 1kkp, resp.)) all show a good hydrogen bond between the Lys257  $\epsilon$ -amino group and the hydroxyl group of the Thr254 side chain, as originally suggested by Pascarella et al. [16]. The nucleophilicity of the  $\epsilon$ -amino group and the NH<sub>2</sub> of the substrate must be balanced so that transaldimination can occur rapidly from either direction. The hydrogen bond between Thr254 and the Lys257  $\epsilon$ -amino group is likely to be a critical determinant of this balance. In the T254A and T254C mutants, which lack the hydroxyl group, this H-bond cannot be formed. We suggest that the loss of this hydrogen bond destabilizes the external aldimine of the T254 mutants relative to the *gem*-diamine intermediates and results in the trapping of the latter.

PLP-dependent enzymes typically catalyze the reversible transaldimination reaction between the internal and external aldimines very rapidly, within the dead time of stopped-flow measurements, and do not accumulate *gem*-diamine intermediates. This is a crucial step in the catalytic mechanism of all PLP-dependent enzymes because it determines binding of substrates and release of products. Our studies show that a single, semiconservative mutation of an active site residue can be critical for the transaldimination in SHMT.

### 4. Materials and Methods

**4.1. Materials.** All chemicals, coenzymes, antibiotics, and buffers were from Sigma-Aldrich (St. Louis, MO, USA) or FisherScientific (Pittsburgh, PA, USA). (6S)-H<sub>4</sub>PteGlu and (6S)-5-CHO-H<sub>4</sub>PteGlu were gifts from Merck Eprova AG (Schaffhausen, Switzerland). Crystallization buffers were from Hampton Research (Laguna Niguel, CA, USA).

TABLE 4: Rabbit cytosolic SHMT structures compared in this study. The table shows the cofactor form and the ligand present in each subunit of the structures.

Enzyme	Chain	Form	Ligand
Unliganded wild type	A	i.a.	PO <sub>4</sub> <sup>2-</sup>
	B	i.a.	PO <sub>4</sub> <sup>2-</sup>
	C	i.a.	MES
	D	i.a.	MES
Unliganded T254A	A	i.a.	PO <sub>4</sub> <sup>2-</sup>
	B	i.a.	PO <sub>4</sub> <sup>2-</sup>
	C	i.a.	PO <sub>4</sub> <sup>2-</sup>
	D	i.a.	PO <sub>4</sub> <sup>2-</sup>
T254A + glycine	A	g.d.	Gly.
	B	g.d.	Gly.
	C	g.d.	Gly.
	D	g.d.	Gly.
T254A + L-serine	A	g.d.	L-Ser.
	B	g.d.	L-Ser.
	C	g.d.	L-Ser.
	D	g.d.	L-Ser.
Unliganded T254C	A	i.a.	H <sub>2</sub> O
	B	i.a.	H <sub>2</sub> O
	C	i.a.	H <sub>2</sub> O
	D	i.a.	PO <sub>4</sub>
T254C + glycine	A	g.d.	Gly.
	B	g.d.	Gly.
T254C + L-serine	A	g.d.	L-Ser.
	B	g.d.	L-Ser.
	C	g.d.	L-Ser.
	D	g.d.	L-Ser.
Wild type + glycine + 5-CHO-H <sub>4</sub> PteGlu <sub>3</sub>	A	g.d.	Gly.
	B	i.a.	—
	C	g.d.	Gly.
	D	i.a.	—

i.a.: internal aldimine.

g.d.: *gem*-diamine.

MES: 2-(N-morpholino)ethanesulfonate.

5-CHO-H<sub>4</sub>PteGlu<sub>3</sub>: triglutamic form of 5-formyltetrahydrofolate.

**4.2. Mutagenesis, Expression, and Purification of SHMT.** Mutants were made using the QuikChange site-directed mutagenesis kit from Stratagene (La Jolla, CA, USA) on rcSHMT cDNA in the pET22b vector [28]. The T254A and T254C mutant forms were produced using the primers 5'-CGTGGTGACCACCGCGACCCACAAGACGC-3' and 5'-CGTGGTGACCACCTGCACCCACAAGACGC-3', respectively, and their complementary oligonucleotides (the mutated codons are underlined). Each mutation was confirmed by sequencing the cDNA insert in both directions. Oligonucleotides synthesis and DNA sequencing were performed by Eurofins MWG Operon (Ebersberg, Germany). Each mutant protein was expressed in an *E. coli* HMS174(ΔDE3), and purification was done by the same procedure published previously [23] and resulted in high

yields of >95% pure enzymes that exhibited the size of wild type rcSHMT.

**4.3. Spectra and Kinetic Studies.** All spectra and steady state kinetic studies were performed in a cell with a path length of 1 cm with an Agilent 8354 spectrophotometer at 30°C, in a 20 mM potassium phosphate buffer, pH 7.3, containing 5 mM 2-mercaptoethanol and 0.2 mM ethylenediaminetetraacetic acid. Kinetic assays were performed as previously reported [23]. Briefly, catalytic assay for L-serine and H<sub>4</sub>PteGlu was measured by coupling the product CH<sub>2</sub>-H<sub>4</sub>PteGlu to methylenetetrahydrofolate dehydrogenase with the concomitant reduction of NADP to NADPH. To determine the *K<sub>m</sub>* for L-serine, H<sub>4</sub>PteGlu was maintained at 0.15 mM, and the L-serine concentration was varied between 0.05 mM and 5 mM. The concentration of mutant rcSHMT in these assays was 10 μM. The rate of L-allo-threonine cleavage was assayed by coupling the reduction of the product acetaldehyde with NADH and alcohol dehydrogenase. Kinetic constants values were determined from double-reciprocal plots of the decrease in absorbance at 340 nm with L-allo-threonine concentrations varied between 0.5 and 50 mM.

**4.4. Rapid Reaction Studies.** Stopped-flow absorbance experiments were performed with an Applied Photophysics SX18 apparatus (Leatherhead, UK) equipped with a 1 cm optical path observation chamber. Temperatures were held at either 8°C by a circulating water bath. Each study was an average of 4–6 traces.

The rate of formation of the *gem*-diamine intermediate was measured by following the increase at 343 nm for the first 0.4 seconds after mixing enzyme and substrate solutions. The effect of substrate concentration was determined by varying L-serine and glycine concentrations in a 0.5–5 mM range. The curves for absorbance variation versus time were fit by a single-exponential curve. For each concentration of substrate, both the first-order rate constant, *k<sub>obs</sub>*, and the amplitude of the spectra change were determined. Rate constants and amplitudes for each individual reaction varied less than 10% from the average values for each reaction:

For calculation of *k<sub>on</sub>* and *k<sub>off</sub>* the following equation was applied, assuming the reaction to be pseudo-first toward [E], and [S] equal to free substrate concentration:

$$k_{\text{obs}} = k_{\text{on}} [S] + k_{\text{off}} \quad (1)$$

The values of *k<sub>on</sub>* and *k<sub>off</sub>* for the rate of formation and breakdown of the enzyme-substrate complex absorbing at 343 nm can be then determined from the slope and *y*-axis intercept of the *k<sub>obs</sub>* versus [S] graph. A double-reciprocal plot of absorbance changes at 343 nm versus substrate concentration gives a linear fit with an *x*-axis intercept representing *K<sub>d</sub>*. The enzyme concentration was held constant at 40 μM. The buffer used was a mix of 20 mM potassium 2-(N-morpholino) ethanesulfonic acid (MES), 20 mM N,N-bis[2-hydroxyethyl]-2-aminoethane sulfonate (BES), and 20 mM 4-(2-hydroxyethyl)-1-piperazineethanesulfonic acid (HEPES) brought to pH 6.4, 6.8, 7.2, 7.6, and 8.0. The concentrations of the anionic forms of amino acids were



calculated using the Henderson-Hasselbalch equation and pK values of 9.6 and 9.2 for the amino groups of glycine and L-serine, respectively.

**4.5. Crystallization.** All forms of the rcSHMT (50 mg/mL) and its mutants and complexes were crystallized as previously reported [20] from 2-3% PEG4000, 20 mM  $K_2HPO_4/KH_2PO_4$ , and 50 mM potassium MES or sodium HEPES (pH 7.0) in hanging drops or in 0.5 mL Eppendorf tubes at room temperature. The complexes with glycine and serine had 60 mM of the amino acid in the crystallization drop.

**4.5.1. Data Collection and Structure Determination.** Crystals were transferred to a stabilization solution of 4.8% polyethylene glycol 4000 in the same buffer for 1 hour, then transiently (<30 sec) placed in a cryoprotectant of 30% polyethylene glycol 400 and 6% polyethylene glycol 4000 in 50 mM potassium MES (pH 7.0) and flash-frozen in liquid  $N_2$  for data collection. Data for a  $100^\circ$  sector were collected on a RAxisII with Osmics confocal optics at 60 kV and 150 mA. Oscillation frames were integrated with Denzo and merged with Scalepack [29]. Merged intensity data were converted to structure factor amplitudes using Truncate re mac5 [30]. All crystals except the T254C-glycine were indexed in space group  $P4_1$  with a tetramer per asymmetric unit; T254C-glycine was indexed in space group  $P4_12_12$  with one dimer per asymmetric unit. Structures were solved by molecular replacement using a rabbit cytosolic SHMT dimer from pdb entry 1CJ0 as a search model and refined using alternating cycles of manual fitting into SigmaA weighted  $2mF_o - dF_c$  maps in COOT [31] and computational refinement in CNS [32] and re mac5 [30]. Structure factors and coordinates are being deposited to the RCSB protein databank.

## Abbreviations

SHMT:	Serine hydroxymethyltransferase
rc:	Rabbit cytosolic
mc:	Mouse cytosolic
ec:	<i>Escherichia coli</i>
bs:	<i>Bacillus stearothermophilus</i>
PLP:	Pyridoxal 5'-phosphate
gem-diamine:	Geminal diamine
$H_4$ PteGlu:	Tetrahydrofolate (tetrahydropteroylglutamate)
5,10- $CH_2$ - $H_4$ PteGlu:	5,10-Methylenetetrahydrofolate
5,10- $CH^+$ = $H_4$ PteGlu:	5,10-Methenyltetrahydrofolate
5-CHO- $H_4$ PteGlu:	5-Formyltetrahydrofolate.

## Acknowledgments

This work was supported by the National Institutes of Health through a Grant (Grant No. CA 16059-28) to the Massey Cancer Center of Virginia Commonwealth University in support of the structural biology resources used in this study and by grants from the Italian Ministero dell'Istruzione,

dell'Università e della Ricerca, and from Finanziamento Progetti di Ricerca 2011 of Sapienza University of Rome.

## References

- [1] V. Schirch, *Mechanism of Folate-Requiring Enzymes in One-Carbon Metabolism*, vol. 1, Academic Press, San Diego, Calif, USA, 1998.
- [2] R. Florio, M. L. Di Salvo, M. Vivoli, and R. Contestabile, "Serine hydroxymethyltransferase: a model enzyme for mechanistic, structural, and evolutionary studies," *Biochimica et Biophysica Acta*, vol. 1814, no. 11, pp. 1489–1495, 2011.
- [3] A. Amadasi, M. Bertoldi, R. Contestabile et al., "Pyridoxal 5'-phosphate enzymes as targets for therapeutic agents," *Current Medicinal Chemistry*, vol. 14, no. 12, pp. 1291–1324, 2007.
- [4] F. Daidone, R. Florio, S. Rinaldo et al., "In silico and in vitro validation of serine hydroxymethyltransferase as a chemotherapeutic target of the antifolate drug pemetrexed," *European Journal of Medicinal Chemistry*, vol. 46, no. 5, pp. 1616–1621, 2011.
- [5] M. L. di Salvo, R. Contestabile, A. Paiardini, and B. Maras, "Glycine consumption and mitochondrial serine hydroxymethyltransferase in cancer cells: the heme connection," *Medical Hypotheses*, vol. 80, pp. 633–636, 2013.
- [6] P. Stover and V. Schirch, "Enzymatic mechanism for the hydrolysis of 5,10-methenyltetrahydropteroylglutamate to 5-formyltetrahydropteroylglutamate by serine hydroxymethyltransferase," *Biochemistry*, vol. 31, no. 7, pp. 2155–2164, 1992.
- [7] M. L. di Salvo, R. Florio, A. Paiardini, M. Vivoli, S. D'Aguzzo, and R. Contestabile, "Alanine racemase from *Tolypocladium inflatum*: a key PLP-dependent enzyme in cyclosporin biosynthesis and a model of catalytic promiscuity," *Archives of Biochemistry and Biophysics*, vol. 529, pp. 55–65, 2013.
- [8] R. Contestabile, A. Paiardini, S. Pascarella, M. L. Di Salvo, S. D'Aguzzo, and F. Bossa, "L-Threonine aldolase, serine hydroxymethyltransferase and fungal alanine racemase: a subgroup of strictly related enzymes specialized for different functions," *European Journal of Biochemistry*, vol. 268, no. 24, pp. 6508–6525, 2001.
- [9] V. Schirch and D. M. E. Szebenyi, "Serine hydroxymethyltransferase revisited," *Current Opinion in Chemical Biology*, vol. 9, no. 5, pp. 482–487, 2005.
- [10] G. Giardina, R. Montioli, S. Gianni et al., "Open conformation of human DOPA decarboxylase reveals the mechanism of PLP addition to Group II decarboxylases," *Proceedings of the National Academy of Sciences of the United States of America*, vol. 108, no. 51, pp. 20514–20519, 2011.
- [11] F. Malerba, A. Bellelli, A. Giorgi, F. Bossa, and R. Contestabile, "The mechanism of addition of pyridoxal 5'-phosphate to *Escherichia coli* apo-serine hydroxymethyltransferase," *Biochemical Journal*, vol. 404, no. 3, pp. 477–485, 2007.
- [12] L. Schirch, "Serine transhydroxymethylase: relaxation and transient kinetic study of the formation and interconversion of the enzyme glycine complexes," *Journal of Biological Chemistry*, vol. 250, no. 5, pp. 1939–1945, 1975.
- [13] C.-F. Cheng and J. L. Haslam, "A kinetic investigation of the interaction of serine transhydroxymethylase with glycine," *Biochemistry*, vol. 11, no. 19, pp. 3512–3518, 1972.
- [14] H. C. Dunathan, "Conformation and reaction specificity in pyridoxal phosphate enzymes," *Proceedings of the National Academy of Sciences of the United States of America*, vol. 55, no. 4, pp. 712–716, 1966.

- [15] L. Schirch, "Serine hydroxymethyltransferase," *Advances in Enzymology and Related Areas of Molecular Biology*, vol. 53, pp. 83–112, 1982.
- [16] S. Pascarella, S. Angelaccio, R. Contestabile, S. Delle Fratte, M. Di Salvo, and F. Bossa, "The structure of serine hydroxymethyltransferase as modeled by homology and validated by site-directed mutagenesis," *Protein Science*, vol. 7, no. 9, pp. 1976–1982, 1998.
- [17] S. Angelaccio, S. Pascarella, E. Fattori, F. Bossa, W. Strong, and V. Schirch, "Serine hydroxymethyltransferase: origin of substrate specificity," *Biochemistry*, vol. 31, no. 1, pp. 155–162, 1992.
- [18] M. Vivoli, F. Angelucci, A. Ilari et al., "Role of a conserved active site cation- $\pi$  interaction in *Escherichia coli* serine hydroxymethyltransferase," *Biochemistry*, vol. 48, no. 50, pp. 12034–12046, 2009.
- [19] P. Baiocco, L. J. Gourlay, F. Angelucci et al., "Probing the Mechanism of GSH Activation in *Schistosoma haematobium* Glutathione-S-transferase by Site-directed Mutagenesis and X-ray Crystallography," *Journal of Molecular Biology*, vol. 360, no. 3, pp. 678–689, 2006.
- [20] J. N. Scarsdale, G. Kazanina, S. Radaev, V. Schirch, and H. T. Wright, "Crystal structure of rabbit cytosolic serine hydroxymethyltransferase at 2.8 Å resolution: mechanistic implications," *Biochemistry*, vol. 38, no. 26, pp. 8347–8358, 1999.
- [21] J. M. Goldberg, J. Zheng, H. Deng, Y. Q. Chen, R. Callender, and J. F. Kirsch, "Structure of the complex between pyridoxal 5'-phosphate and the tyrosine 225 to phenylalanine mutant of *Escherichia coli* aspartate aminotransferase determined by isotope-edited classical Raman difference spectroscopy," *Biochemistry*, vol. 32, no. 32, pp. 8092–8097, 1993.
- [22] V. Trivedi, A. Gupta, V. R. Jala et al., "Crystal structure of binary and ternary complexes of serine hydroxymethyltransferase from *Bacillus stearothermophilus*. Insights into the catalytic mechanism," *Journal of Biological Chemistry*, vol. 277, no. 19, pp. 17161–17169, 2002.
- [23] D. M. E. Szebenyi, F. N. Musayev, M. L. Di Salvo, M. K. Safo, and V. Schirch, "Serine hydroxymethyltransferase: role of Glu75 and evidence that serine is cleaved by a retroaldol mechanism," *Biochemistry*, vol. 43, no. 22, pp. 6865–6876, 2004.
- [24] T.-F. Fu, J. N. Scarsdale, G. Kazanina, V. Schirch, and H. T. Wright, "Location of the pteroylpolyglutamate-binding site on rabbit cytosolic serine hydroxymethyltransferase," *Journal of Biological Chemistry*, vol. 278, no. 4, pp. 2645–2653, 2003.
- [25] D. M. E. Szebenyi, X. Liu, I. A. Kriksunov, P. J. Stover, and D. J. Thiel, "Structure of a murine cytoplasmic serine hydroxymethyltransferase quinonoid ternary complex: evidence for asymmetric obligate dimers," *Biochemistry*, vol. 39, no. 44, pp. 13313–13323, 2000.
- [26] R. Contestabile, S. Angelaccio, F. Bossa et al., "Role of tyrosine 65 in the mechanism of serine hydroxymethyltransferase," *Biochemistry*, vol. 39, no. 25, pp. 7492–7500, 2000.
- [27] B. S. Bhavani, V. Rajaram, S. Bisht et al., "Importance of tyrosine residues of *Bacillus stearothermophilus* serine hydroxymethyltransferase in cofactor binding and l-allo-Thr cleavage: crystal structure and biochemical studies," *FEBS Journal*, vol. 275, no. 18, pp. 4606–4619, 2008.
- [28] M. L. Di Salvo, S. D. Fratte, D. De Biase, F. Bossa, and V. Schirch, "Purification and characterization of recombinant rabbit cytosolic serine hydroxymethyltransferase," *Protein Expression and Purification*, vol. 13, no. 2, pp. 177–183, 1998.
- [29] M. Otwinowski, "Processing of X-ray diffraction data collected in oscillation mode," in *Methods in Enzymology*, W. Charles and J. Carter, Eds., Macromolecular Crystallography Part A, pp. 307–326, Elsevier, 1997.
- [30] "The CCP4 suite: programs for protein crystallography," *Acta Crystallographica D*, vol. 50, pp. 760–763, 1994.
- [31] P. Emsley and K. Cowtan, "Coot: model-building tools for molecular graphics," *Acta Crystallographica D*, vol. 60, no. 12, pp. 2126–2132, 2004.
- [32] A. T. Brünger, P. D. Adams, G. M. Clore et al., "Crystallography & NMR system: a new software suite for macromolecular structure determination," *Acta Crystallographica D*, vol. 54, no. 5, pp. 905–921, 1998.

## Review Article

# Extremophilic SHMTs: From Structure to Biotechnology

**Sebastiana Angelaccio**

*Dipartimento di Scienze Biochimiche "A. Rossi Fanelli," "Sapienza" Università di Roma, Piazzale Aldo Moro 5, 00185 Roma, Italy*

Correspondence should be addressed to Sebastiana Angelaccio; [sebastiana.angelaccio@uniroma1.it](mailto:sebastiana.angelaccio@uniroma1.it)

Received 14 April 2013; Accepted 30 May 2013

Academic Editor: Alessandro Paiardini

Copyright © 2013 Sebastiana Angelaccio. This is an open access article distributed under the Creative Commons Attribution License, which permits unrestricted use, distribution, and reproduction in any medium, provided the original work is properly cited.

Recent advances in molecular and structural biology have improved the availability of virtually any biocatalyst in large quantity and have also provided an insight into the detailed structure-function relationships of many of them. These results allowed the rational exploitation of biocatalysts for use in organic synthesis. In this context, extremophilic enzymes are extensively studied for their potential interest for many biotechnological and industrial applications, as they offer increased rates of reactions, higher substrate solubility, and/or longer enzyme half-lives at the conditions of industrial processes. Serine hydroxymethyltransferase (SHMT), for its ubiquitous nature, represents a suitable model for analyzing enzyme adaptation to extreme environments. In fact, many SHMT sequences from Eukarya, Eubacteria and Archaea are available in data banks as well as several crystal structures. In addition, SHMT is structurally conserved because of its critical metabolic role; consequently, very few structural changes have occurred during evolution. Our research group analyzed the molecular basis of SHMT adaptation to high and low temperatures, using experimental and comparative *in silico* approaches. These structural and functional studies of SHMTs purified from extremophilic organisms can help to understand the peculiarities of the enzyme activity at extreme temperatures, indicating possible strategies for rational enzyme engineering.

## 1. Introduction

Studies on protein stability represented an important issue in the past forty years, owing to the central role these macromolecules play in maintaining life and their involvement in many diseases affecting humans. The comparison of structural and functional features of proteins among thermophilic/psychrophilic organisms and their homologs from mesophilic counterparts can provide insights into the ability of extremophiles to function at their extreme habitat temperatures and may give clues to better define the forces that stabilize proteins. In case of adaptations to extremes of pH, salinity, and pressure, membrane components and protective small molecules often play an important role and have been studied quite extensively [1–3]. For temperature adaptation, however, environmental stress generally cannot be avoided by compensatory mechanisms, and thus the cellular components themselves, specifically the proteins, have to achieve a certain level of stability at extreme temperatures, at which most of living species cannot grow because of their inability

to maintain adequate metabolic fluxes. For this reason, much interest has been directed to understand how proteins from thermophilic/psychrophilic organisms retain their structure and function at high or low temperatures, respectively. In particular, enzymes perform important tasks in all biological systems, and they do so by maintaining a specific globular conformation. This functional state, called the native state, is stabilized in a balancing act of opposing forces. The players in this act have long been identified [4], although their relative contributions have been debated [5–9]. The major stabilizing forces include the hydrophobic effect and hydrogen bonding, while conformational entropy favors the unfolded state. The crystal structures of extremophilic enzymes unambiguously indicate a continuum in the molecular adaptations to temperature. For example, from psychrophiles (living at low temperatures close to 0°C) to mesophiles (living at intermediate temperatures close to 37°C) and to thermophiles (living at high temperatures above to 37°C), there is a clear increase in the number and strength of all known weak interactions and structural factors, such as hydrophobicity,

polar surface area of the molecules, involved in protein stability [10–13]. Therefore, the same mechanism of molecular adaptation is involved in response to two distinct selective pressures, that is, the requirement for stable protein structure and activity in thermophiles and the requirement for high enzyme activity in psychrophiles. This of course suggests intricate and still controversial relationships between activity and stability in these naturally evolved enzymes. It seems that each extremophilic enzyme adopts its own adaptive strategy. In this contest, SHMT, for its ubiquitous nature and its critical metabolic role, represents a paradigm to study enzymes' adaptations to extreme environments.

The discovery of new extremophilic microorganisms and their enzymes had a great impact on the field of biocatalysis. The industrial application of enzymes that can withstand harsh conditions has greatly increased over the past decade. Recent advances in the study of extremozymes point to the acceleration of this trend. Much of the biotechnological interest in enzymes from extremophilic organisms stems from their surprising properties. In general, it has been found that psychrophilic enzymes can help to enhance yields of heat-sensitive products, halophilic enzymes, that are stable in high salt concentrations, serve as models for biocatalysis in low-water media, and thermophilic enzymes are highly resistant to proteases, detergents, and chaotropic agents, which may also afford resistance to the effects of organic solvents [14, 15]. Table 1 lists extremophiles by habitat and some applications of their enzymes.

## 2. SHMT

Serine hydroxymethyltransferase (SHMT; EC 2.1.2.1) is a ubiquitous and extensively studied pyridoxal 5'-phosphate- (PLP dependent-) enzyme that catalyzes the reversible transfer of  $C\beta$  of L-serine to tetrahydropteroylglutamate ( $H_4PteGlu$ ), with formation of glycine and 5,10-methylene- $H_4PteGlu$ . This reaction is a primary source of the one-carbon units required for the synthesis of thymidylate, purines, and methionine. Moreover, SHMT shows an exceptionally broad substrate and reaction specificity *in vitro*. In fact, with the appropriate substrate analogues, SHMT catalyzes  $H_4PteGlu$ -independent transamination, racemisation, decarboxylation, condensation, and retroaldol cleavage reactions [16, 17]. The rate of the cleavage of a number of 3-hydroxy-amino acids to glycine and the corresponding aldehyde, in some case, approaches and even exceeds the rate of serine cleavage [18, 19]. The increasing availability of solved crystal structures of the enzyme from various prokaryotic and eukaryotic sources [20–24] contributed to clarify a number of observations previously acquired with classical biochemical studies. SHMT belongs to the fold type I group (or aspartate aminotransferase family), which includes many of the best characterized PLP-dependent enzymes. An evolutionary analysis of the fold type I enzymes revealed that SHMT and l-threonine aldolase may actually belong to a subgroup of closely related proteins [25]; fungal alanine racemase, an extremely close relative of l-threonine aldolase, also appears to be a member of the same subgroup [26]. As

for the other members of this group, each enzyme subunit, which associates into dimers in prokaryotes and tetramers in eukaryotes, folds into two domains. The active site is located at the interface of the domains and is delimited by amino acid residues contributed by both subunits of the dimer. Several mechanisms have been proposed for the hydroxymethyl transfer [16, 27]. Although the reported crystal structures have provided a wealth of information regarding the architecture of the enzyme, the active site, and the residues involved in substrate binding and catalysis, several aspects of SHMT catalytic mechanism remain uncertain [28]. The currently accepted mechanism for the hydroxymethyltransferase reaction consists of a modified folate-dependent retroaldol cleavage via direct nucleophilic attack of N5 of  $H_4PteGlu$  to  $C\beta$  of L-serine, which results in the elimination of the quinonoid intermediate [28, 29] (Scheme 1).

The type of reaction catalyzed by SHMT with different substrate analogues is apparently determined by the structure of the amino acid substrate. With L-serine or glycine, SHMT catalyzes none of the alternative reactions. The currently accepted model attributes this reaction specificity to the existence of an "open" and a "closed" active site conformation, as observed in other members of this family [30]. The physiological substrates trigger the closed conformation, whereas alternative substrates react, while the enzyme remains in the open conformation, which permits alternative reaction paths [31]. The folding mechanism of *Escherichia coli* SHMT has been also investigated and understood in detail [32–34]. It may be divided into two phases and terminates with PLP binding. In the first step, the large and small domains rapidly assume their native state, forming a folding intermediate that is not able to bind PLP. In the second, slower phase, the enzyme folds into the native structure, acquiring the capability to bind the cofactor. Although the crystallographic data have provided a framework for a better understanding of folding studies [35], the key events required for the transition from the first to the second phase remain unclear. Most work on SHMT has focused on enzymes from mesophilic bacteria and eukaryotic organisms. Insights into a better understanding of the structural and functional properties of SHMT could be derived from the studies of the extremophilic enzymes, due to their amazing catalytic characteristics.

SHMT is one of the very few PLP-dependent enzymes that can be found in all living organisms [36], and as it plays a central role in cellular metabolism, it has been repeatedly hailed as a potential target for the development of anticancer and antimicrobial agents [37–39].

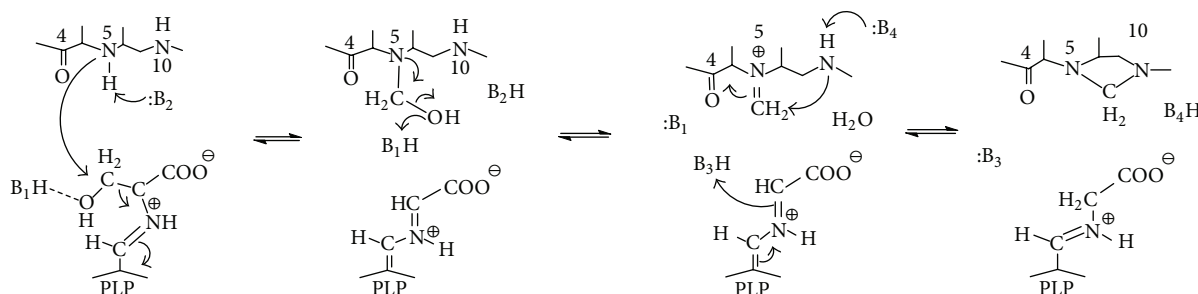
## 3. Thermophilic SHMTs

The thermophilic SHMTs, so far investigated, are present in organisms which belong to the two different kingdoms of life: Archaea and Eubacteria. In Eukarya and Eubacteria,  $H_4PteGlu$  functions as a carrier of C1 units in several oxidation states, which are used in the biosynthesis of important cellular components, such as purines and thymidylate, and in the regeneration of methionine from homocysteine. The



TABLE 1: Industrial applications of enzymes isolated from extremophiles.

Extremophiles	Habitat	Enzymes	Representative applications
Thermophile	High temperature	Amylases	Production of glucose, fructose for sweeteners
		Xylanases	Paper bleaching
		Proteases	Used in baking, brewing, and as detergent additive
		DNA polymerases	Genetic engineering
Psychrophile	Low temperature	Proteases	Cheese maturation
		Dehydrogenases	Biosensors
		Amylases	Polymer degradation in detergents
Acidophile	Low pH	Sulfur oxidation	Desulfurization of coal
Alkalophile	High pH	Cellulases	Polymer degradation in detergent



SCHEME 1: Proposed mechanism for folate-dependent conversion of L-serine to glycine, based on structural information, stereochemical studies, and properties of site mutants. B<sub>1</sub>H is believed to be Glu75 of eSHMT [28]. The other catalytic groups are not identified.

reaction catalyzed by SHMT represents in these organisms one of the major loading routes of C1 units onto the folate carrier [27]. In methanogens and several other Archaea, C1 fragments from formyl to methyl oxidation levels are carried by tetrahydromethanopterin (H<sub>4</sub>MPT), a pterin-containing compound involved in methanogenesis [40]. Although H<sub>4</sub>PteGlu and H<sub>4</sub>MPT are structurally similar (Figure 1) and are employed in analogous reactions, most of the H<sub>4</sub>PteGlu-specific and H<sub>4</sub>MPT-specific enzymes are phylogenetically not related. H<sub>4</sub>MPT does not appear to be suited to most of the biosynthetic functions of H<sub>4</sub>PteGlu. Moreover, the biosynthetic pathways of the two carriers have few, if any, homologies, suggesting the possibility of separate evolutionary origins. In the metabolism of folates, SHMT represents a unique link between Archaea and the rest of living beings, in the sense that while all SHMTs clearly share a common evolutionary origin [41], other enzymes which use H<sub>4</sub>MPT as cofactor do not show any significant similarity to their eukaryotic and eubacterial counterparts [40]. Although a gene encoding SHMT is present in all archaeal genomes so far sequenced, little information is available on the catalytic properties, and metabolic role of the enzyme in these organisms. Modified folates are not commercially available and this has clearly hindered a satisfactory characterization of archaeal SHMTs. Moreover, the purification of the enzymes from Archaea which thrive in extreme environments is complicated by the difficulty of growing these organisms in a laboratory.

Regarding enzymes derived from archaeal organisms, two reports of purified SHMT activity, from *Methanobacterium thermoautotrophicum*, renamed *Methanothermobacter marburgensis* [42], and from *Sulfolobus solfataricus* [43],

with limited structural and functional characterization, have been made. In the first report, the enzyme was proposed to function *in vivo* in the direction of L-serine biosynthesis. Both works provided evidence that SHMT was selective towards the modified folates used by the source organisms: H<sub>4</sub>MPT, for *M. marburgensis* and sulfopterin for *S. solfataricus* [40, 44]. More recently, SHMT from the hyperthermophilic methanogen *Methanococcus jannaschii* has been expressed in *E. coli*, purified, and characterized [45]. The results reported in that work suggested that the active site structure and the mechanism of *M. jannaschii* SHMT exhibit no significant differences with respect to their bacterial and eukaryotic counterparts, although the enzyme is characterized by the ability to bind and use the modified folate H<sub>4</sub>MPT as substrate and by an elevated thermal stability. For a better understanding of the functional characteristics of archaeal SHMTs, maybe it would be useful to have the same more structural information, such as the three-dimensional structures of the proteins. Concerning the eubacterial thermophilic SHMTs, two three-dimensional structures are available in Protein Data Bank: one from *Thermus thermophilus* (PDB ID: 2DKJ) and the other from *Bacillus stearothermophilus* (PDB ID: 1KKJ). So far, the best characterized thermophilic SHMT is the enzyme purified from *Bacillus stearothermophilus* (bstSHMT), a Gram-positive bacterium, which is able to grow within a temperature range of 30–75°C [46]. The crystal structures of this enzyme have been determined in its internal aldimine form, in binary complex with serine and glycine (external aldimine form), and in ternary complex with glycine and 5-formyltetrahydrofolate (FTHF) [21]. The different structures presented by the authors and the comparison with the other SHMT structures from

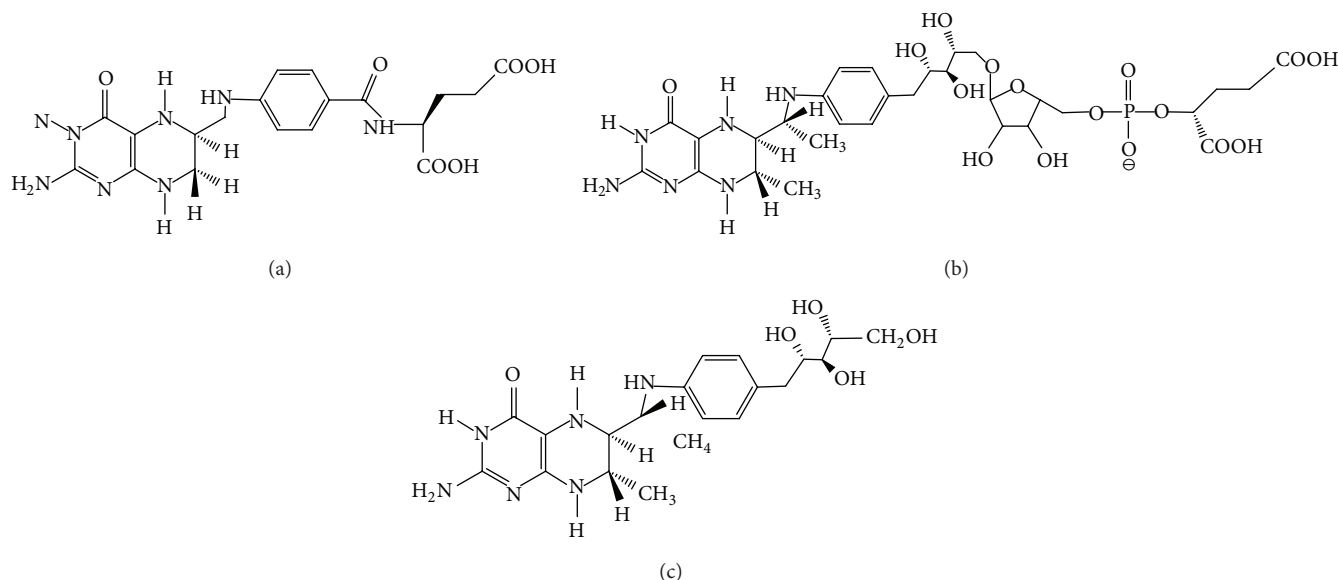


FIGURE 1: Structures of tetrahydropteroylglutamate (a), tetrahydromethanopterin (b), and sulfopterin (c).

different sources provide interesting structural information in the reaction mechanism of SHMT. The *bst*SHMT-L-serine complex does not show any significant conformational change compared with the enzyme without bound substrate, contrary to that expected for a conversion from an “open” to “closed” form of the enzyme. However, the ternary complex with FTHF and glycine shows the reported conformational changes. In Figure 2, where active site regions in the internal and external aldimine structures (ternary complex) of *bst*SHMT are depicted, it is possible to see the rotation of PLP ring and the conformational changes of the same active site residues. These small but significant conformational changes are similar to that observed in the structures of the murine cytoplasmic SHMT and *E. coli* SHMT [22, 23].

In contrast to the *E. coli* enzyme, this complex shows asymmetric binding of the FTHF to the two monomers within the dimer in a way similar to the murine SHMT. A detailed analysis of *bst*SHMT structures and a comparison with previously reported structures allow an accurate determination of conformational changes in protein structure, orientation of the PLP ring, and key amino acid residues during different stages of catalysis. An analysis of these results provides structural evidence for a direct transfer mechanism for the SHMT catalyzed reaction (Scheme 1). Further studies on kinetic and structural properties of many *bst*SHMT active-site mutants confirmed these results [47–49].

Moreover, an extensive characterization of the structural and functional changes of the *bst*SHMT during unfolding has been carried out [50, 51]. The unfolding properties of the thermophilic enzyme were compared with that of the mesophilic homologues, *Bacillus subtilis* SHMT (*bs*SHMT), with which it shares 77% amino acid sequence identity and with that reported for *E. coli* aspartate aminotransferase (*eAAT*), a mesophilic protein which belongs to the same structural

family even sharing a low level of amino acid sequence identity (about 14%) [52]. The results suggest that the *bst*SHMT follows an unfolding mechanism very different from that followed by the *bs*SHMT, despite the high degree of sequence amino acid identity of the two proteins. Instead, the unfolding mechanism of *bs*SHMT is similar to the one followed by the mesophilic aspartate aminotransferase. In fact, *bs*SHMT and *eAAT* undergo a noncooperative unfolding with stabilization of intermediates during the unfolding process, whereas the *bst*SHMT undergoes a highly cooperative unfolding with dissociation of the two monomers and unfolding of native dimer occurring in a single step. Interestingly, preliminary unfolding experiments carried out in our laboratory using the *M. jannaschii* SHMT seem to indicate the same unfolding pathway as the *bst*SHMT (unpublished results).

It would be interesting to compare the kinetic parameters for the folate-dependent and folate-independent reactions of SHMTs from organisms adapted to different temperature. As shown in Table 2, the thermophilic enzyme does not show any enzymatic activity which is significantly different from that shown by the mesophilic enzyme. On the contrary, the kinetic parameters shown by the psychrophilic SHMT, especially that for the folate-independent reactions, suggest that the cold-adapted enzyme is a more suitable catalyst with respect to the mesophilic one (see next paragraph).

#### 4. Psychrophilic SHMTs

Whereas many theoretical and experimental studies have been devoted to clarify the molecular basis of the adaption of thermophilic enzymes to high temperatures, comparing single thermophilic proteins with their mesophilic counterparts and systematically examining different properties for families of proteins [10, 55, 56], molecular mechanisms of cold adaptation are still relatively unknown. Because of their higher

TABLE 2: Comparison of the kinetic parameters of the reactions catalyzed by different SHMTs.

Substrate	<i>E. coli</i> SHMT <sup>a</sup>		SHMT <sup>a</sup> <i>P. ingrahamii</i>		<i>B. stearothermophilus</i> SHMT <sup>b</sup>	
	$K_m$ (mM)	$k_{cat}$ (min <sup>-1</sup> )	$K_m$ (mM)	$k_{cat}$ (min <sup>-1</sup> )	$K_m$ (mM)	$k_{cat}$ (s <sup>-1</sup> )
L-Threonine	43 <sup>d</sup>	4.3 <sup>d</sup>	20.2 <sup>f</sup>	6.6 <sup>f</sup>	ND <sup>c</sup>	ND <sup>c</sup>
L-Threo-phenylserine	19 <sup>d</sup>	167 <sup>d</sup>	17.2 <sup>f</sup>	852 <sup>f</sup>	ND <sup>c</sup>	ND <sup>c</sup>
L-Allo-threonine	1.5 <sup>e</sup>	30 <sup>e</sup>	1.6 <sup>f</sup>	107 <sup>f</sup>	0.9 <sup>g</sup>	0.47 <sup>g</sup>
L-Serine	0.3 <sup>e</sup>	640 <sup>e</sup>	0.4 <sup>f</sup>	555 <sup>f</sup>	0.9 <sup>g</sup>	3.9 <sup>g</sup>

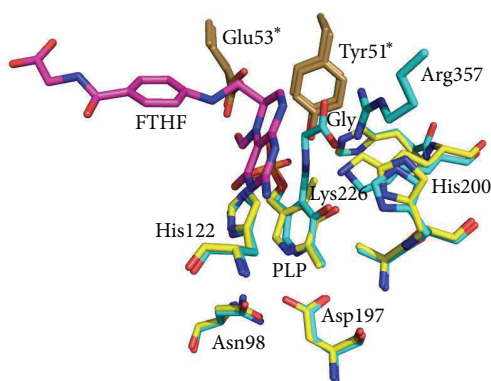
<sup>a</sup> Reactions were carried out at 30°C<sup>b</sup> Reactions were carried out at 37°C<sup>c</sup> Not determined<sup>d</sup> From [25]<sup>e</sup> From [53]<sup>f</sup> From [54]<sup>g</sup> From [48].

FIGURE 2: Superimposition of SHMT internal and external aldimine structures. Active site structures of *B. stearothermophilus* SHMT (internal aldimine form: PDB ID 1kkj) and *B. stearothermophilus* SHMT in complex with glycine and 5-formyl-H<sub>4</sub>PteGlu (PDB ID 1kl2) are displayed as yellow and cyan sticks, respectively. The 5-formyl-H<sub>4</sub>PteGlu molecule (FTHF) is displayed as magenta sticks. Side chains from the other subunits are rendered as brown sticks, and the corresponding labels are marked with asterisks. The picture was generated using PyMOL.

catalytic efficiency at low temperatures, enzymes extracted from psychrophilic organisms have significant potential for biotechnological applications, in particular in industrial processes as energy savers and in detergent industry as additives [57, 58]. The structural adaptation of SHMT synthesized by microorganisms adapted to low temperatures was first investigated using an *in silico* comparative approach, with the aim to detect significant variations of physicochemical properties in SHMTs [59]. Subsequently, the enzyme from psychrophilic microorganism *Psychromonas ingrahamii* was expressed in *Escherichia coli*, purified, and characterized with respect to its spectroscopic, catalytic, and thermodynamic properties [54]. The properties of the psychrophilic enzyme have been contrasted with the homologous counterparts from *E. coli*, which has been extensively, structurally, and functionally characterized [53]. As shown in Table 2, *P. ingrahamii* SHMT (*pi*SHMT) displays higher turnover numbers with respect to *E. coli* SHMT (*e*SHMT), in particular

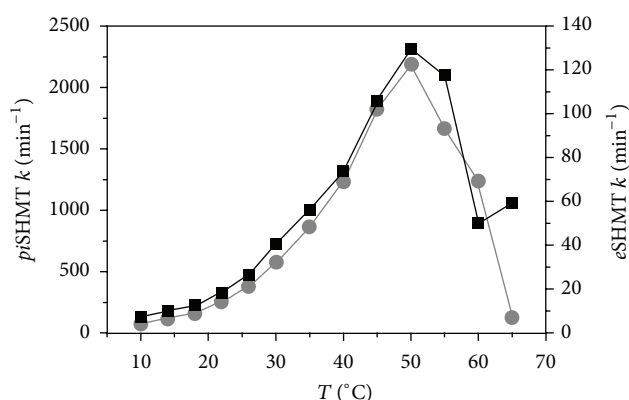


FIGURE 3: Temperature dependence of enzyme activity of *pi*- (gray dots and left axis scale) and *e*- (black squares and right axis scale) SHMTs. Activities were measured for the retroaldol cleavage of L-threo-phenylserine. The picture is adapted from [54].

for the side reactions where many substrates, typically  $\beta$ -hydroxy- $\alpha$ -amino acids, represent important compounds in pharmaceuticals, agrochemicals, and food additives [60]. Most of the comparative studies have been focused on thermal stability. Heat inactivation experiments indicated that *pi*SHMT activity is heat labile, and the apparent melting temperature of the protein is 62°C, which is lower than that of the *e*SHMT [61] (Table 3).

Interestingly, the difference of the apparent  $T_m$  values between the apoform and the holoform of the psychrophilic enzyme is about 20 degrees (Table 3). This observation suggests that the intrinsic instability of the active site is partly compensated by the interaction with the cofactor. The instability and the consequent flexibility of the active site may be functionally relevant also for the conformational transitions it must undergo during the low temperature transfer of the PLP to its binding site within the apoenzyme [34, 62]. Noteworthy, the optimal temperature of enzyme activity of *pi*SHMT is 50°C, which is the same value shown by the *e*SHMT, although the *pi*SHMT activity is at least tenfold higher than *e*SHMT activity (Figure 3).

TABLE 3: Apparent melting temperatures (Tm) of different SHMTs.

	Tm of apoenzymes (°C)	Tm of holoenzymes (°C)	Tm in presence of L-Serine (°C)	Reference
<i>E. coli</i> SHMT	58.8	69.5	73.0	[61]
<i>P. ingrahamii</i> SHMT	42.0	62.0	ND <sup>a</sup>	[54]
<i>B. stearothermophilus</i> SHMT	ND <sup>a</sup>	65.0	74.0	[48]

<sup>a</sup>Not determined.

The relatively high activity characterizing psychrophilic enzymes is the main adaptive parameter to low temperatures and seems to be achieved by the destabilization of the active site or of the entire protein structure, allowing the catalytic center to be more flexible at low temperatures. In this way, the enzyme should be able to reach the transition complex with lower requirement of energy, generally not abundant in a low temperature environment [63]. Recently, articles aimed at finding common structural determinants for cold adaptation have been published (e.g., [11, 13]). Compared with their mesophilic and thermophilic counterparts, cold-adapted enzymes have been reported to share common features such as reduction of the number of Arg, Pro, and Glu and increase in the number of Asn, Gln, Ser, and Met; low Ala/Leu ratio, and lower fraction of larger aliphatic residues expressed by the (Ile+Leu)/(Ile+Leu+Val) ratio; lowered Arg/(Arg+Lys) ratio; reduction in the hydrophobicity of the enzyme; increase of negative charge which facilitates interaction with the solvent; more polar and less hydrophobic residues; fewer hydrogen bond, aromatic interactions, and ion pairs; additional surface loops with more polar residues and lower Pro content. However, no structural feature is present in all cold-adapted enzymes, and no structural feature always correlates with cold adaptation [64]. *pi*SHMT could represent an attractive and interesting enzyme to highlight the structural characteristics coupled to the adaptation to low temperatures, since its structure is very conserved during evolution. Moreover, for its particular catalytic properties, this enzyme is very promising in biotechnological applications (see next paragraph).

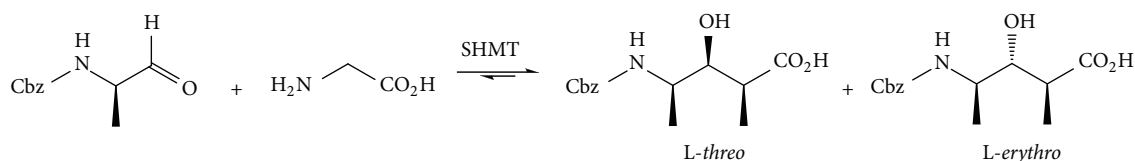
## 5. Extremophilic SHMTs as a Valuable Tool for Biotechnological Applications

With the steady growth of the importance of enantiomerically pure or enriched compounds in pharmaceuticals, agrochemicals, and food additives, the so-called “chiral market” has become an expanding area of the fine chemicals industry [65]. In particular,  $\beta$ -hydroxy- $\alpha$ -amino acids are an important class of natural products that have recently received much attention due to their biological activity on their own and as constituents of many naturally occurring complex compounds, such as antibiotics and immunosuppressants. For example, L-*threo*- $\beta$ -(3,4-dihydroxyphenyl) serine is a special remedy in the Parkinson's disease treatment as an agent for norepinephrine precursor therapy [66], L-*threo*- $\alpha$ -(4-methylthiophenyl) serine is an intermediate for the production of antibiotics, such as florfenicol and thiamphenicol [67, 68], 4-hydroxy-L-threonine is a precursor of

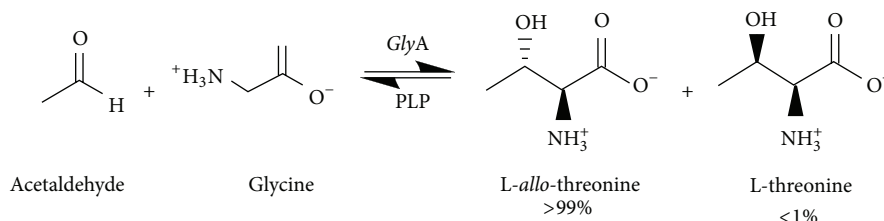
rhizobitoxine, and 3,4,5-trihydroxy-L-aminopentanoic acid is a key component of polyoxins [69]. Furthermore, the  $\beta$ -hydroxy- $\alpha$ -amino acids, as polyfunctional compounds, might be useful for building blocks for peptidomimetics and other nonproteinogenic peptide-like molecules of biological interest.  $\beta$ -hydroxy- $\alpha$ -amino acids can be obtained through the asymmetric chemical synthesis. Hayashi and Belokon carried out a series of fundamental and creative research in this field; for example, they have investigated asymmetric aldol reactions of isocyanoacetic derivatives with fluoroaryl aldehydes, benzaldehydes, and aryl ketones catalyzed by gold (I) or silver(I)/triethylamine [70, 71]. In addition to asymmetric synthesis,  $\beta$ -hydroxy- $\alpha$ -amino acids are mainly produced through chemical synthesis processes, followed by chiral resolution [72]. These processes however have some drawbacks, such as the following: chiral resolution is time-consuming and inefficient, and the overuse of organic solvents results in environmental problems. Accordingly, the development of an efficient and clean enzymatic resolution process is desirable. As discussed previously, SHMT catalyzes the cleavage of several C3-OH amino acids varying in substituent and stereochemistry at C3, with most research focusing on threonine and  $\beta$ -phenylserine [18, 19]. None of these reactions requires H<sub>4</sub>PteGlu as a cosubstrate, and the rates approach or exceed the rate of H<sub>4</sub>PteGlu-dependent serine cleavage. Therefore, SHMT represents a good tool for biotechnological applications. Extensive studies have been carried out on the biotransformation activity of serine hydroxymethyltransferase from different species. The SHMTs extracted from *H. methylovorum* and from *E. coli* were found to have a wide substrate specificity. Regarding the degradation of the  $\beta$ -hydroxy- $\alpha$ -amino acids,  $\beta$ -*threo*-phenylserine, L-serine, *allo*-threonine, *threo*-3,4-dihydroxy-phenylserine, and L-threonine were good substrates [53, 73]. SHMT also showed potential as a biocatalyst for the stereoselective synthesis of  $\beta$ -hydroxy- $\alpha$ -amino acids. In [74] the authors described the aldol addition of glycine to nonnatural aldehydes, such as benzyloxycetaldehyde and (R)-N-Cbz-alaninal (Cbz = benzyloxycarbonyl) to corresponding  $\beta$ -hydroxy- $\alpha$ -aminoacid diastereoisomers catalyzed by the recombinant SHMT derived from the *Streptococcus thermophilus* YKA-184 strain. The reaction described in that work shows a moderate stereospecificity concerning the  $\beta$ -carbon, with diastereomeric ratio of 80:20 between the L-*threo* isomer versus L-*erythro* isomer (Scheme 2).

In [75], the authors investigated the effect of reaction variables, such as temperature, reaction media, and glycine concentration on this aldol addition reaction and the diastereomeric ratio, with the aim to obtain a better enzymatic reaction performance and to further exploit the synthetic





SCHEME 2: SHMT-catalyzed aldol addition of glycine to (R)-N-Cbz-alaninal.



SCHEME 3: GlyA-catalyzed aldol reaction of glycine and acetaldehyde in the presence of the cofactor PLP.

utility of this enzyme. In particular, it has been shown that temperature is an important parameter. In fact, at low temperatures, the retroaldol activity is strongly inhibited, whereas a high synthetic capacity is maintained. Thus, it might be synthetically useful to work at low temperatures. Moreover, in [76], it has been reported the diastereospecific formation of L-allo-threonine catalyzed by an *E. coli* strain harbouring serine hydroxymethyltransferase gene (*glyA* gene) (Scheme 3).

These results show that SHMT could be a promising biocatalyst for the stereoselective synthesis of  $\beta$ -hydroxy- $\alpha$ -amino acids. Such industrial processes would benefit from the employ of SHMTs that function at extreme temperature. Generally, thermophilic enzymes offer economic advantages such as increased rates of reactions, a higher substrate solubility, and/or longer enzyme half-lives at the conditions of industrial processes. On the other hand, psychrophilic enzymes provide other important benefits through energy savings: they exhibit increased reaction yields in cold environments, a high level of stereospecificity, an increased thermal lability for rapid and easy enzyme inactivation when required and minimization of undesirable chemical reactions that can occur at higher temperatures. In particular, the structural and functional properties of the cold-adapted SHMT from *Psychromonas ingrahamii* described in [54] are especially promising for biotechnological applications. This enzyme, in fact, is a more efficient biocatalyst compared to the other SHMTs, especially for the side reactions involving  $\beta$ -hydroxy- $\alpha$ -amino acids as substrates. However, further investigations are required for a better understanding of the catalytic properties and, in particular, the stereospecificity of *pi*SHMT. Stereospecificity in cold-adapted enzymes has been poorly investigated. It has been reported [77] that psychrophilic enzymes seem to be more stereoselective with respect to meso/thermophilic homologs, although it is not completely clear how the high flexibility of their molecules can be related to this peculiarity.

## 6. Conclusions

The synthesis of polymer precursors, pharmaceuticals, specialty chemicals, and agrochemicals is often hampered by

expensive processes that suffer from low selectivity and undesired byproducts. Mesophilic enzymes are often not well suited for the harsh reaction conditions required in industrial processes because of the lack of enzyme stability. The recent advances in the study of the stable enzymes from extremophiles have resulted in their increased use for applications in the organic synthesis. Our understanding of the biochemical and structural properties of the extremophilic SHMTs, coupled to enzyme modification by rational protein engineering or directed evolution, could lead to improved catalytic and physical properties and the development of novel catalytic functions.

## Abbreviations

- H<sub>4</sub>PteGlu: Tetrahydrofolate or tetrahydropteroylglutamate  
H<sub>4</sub>MPT: Tetrahydromethanopterin  
FTHF: 5-Formyl tetrahydrofolate  
PLP: Pyridoxal 5'-phosphate  
*e*SHMT: *Escherichia coli* serine hydroxymethyltransferase  
*pi*SHMT: *Psychromonas ingrahamii* serine hydroxymethyltransferase  
*bst*SHMT: *Bacillus stearothermophilus* SHMT  
*bs*SHMT: *Bacillus subtilis* SHMT  
*e*AAT: *Escherichia coli* aspartate aminotransferase.

## Acknowledgments

The author gratefully acknowledges Professor Stefano Pascarella for constant support provided during the studies and for his helpful advice and Dr. Martino Luigi Di Salvo for critical reading of the paper and fruitful discussions.

## References

- [1] R. Jaenicke, "Protein stability and molecular adaptation to extreme conditions," *European Journal of Biochemistry*, vol. 202, no. 3, pp. 715–728, 1991.

- [2] P. H. Yancey, M. E. Clark, S. C. Hand, R. D. Bowlus, and G. N. Somero, "Living with water stress: evolution of osmolyte systems," *Science*, vol. 217, no. 4566, pp. 1214–1222, 1982.
- [3] J. L. C. M. Van de Vossenbergh, A. J. M. Driessen, and W. N. Konings, "The essence of being extremophilic: the role of the unique archaeal membrane lipids," *Extremophiles*, vol. 2, no. 3, pp. 163–170, 1998.
- [4] W. Kauzmann, "Some factors in the interpretation of protein denaturation," *Advances in Protein Chemistry*, vol. 14, no. C, pp. 1–63, 1959.
- [5] K. A. Dill, "Dominant forces in protein folding," *Biochemistry*, vol. 29, no. 31, pp. 7133–7155, 1990.
- [6] L. Itzhaki and P. Wolynes, "Erratum to 'Nature and nurture in protein folding and binding' [Curr Opin Struct Biol 2010, 20:1–2]," *Current Opinion in Structural Biology*, vol. 20, no. 3, p. 397, 2010.
- [7] G. D. Rose and R. Wolfenden, "Hydrogen bonding, hydrophobicity, packing, and protein folding," *Annual Review of Biophysics and Biomolecular Structure*, vol. 22, pp. 381–415, 1993.
- [8] C. N. Pace, B. A. Shirley, M. McNutt, and K. Gajiwala, "Forces contributing to the conformational stability of proteins," *FASEB Journal*, vol. 10, no. 1, pp. 75–83, 1996.
- [9] B. Honig, "Protein folding: from the levinthal paradox to structure prediction," *Journal of Molecular Biology*, vol. 293, no. 2, pp. 283–293, 1999.
- [10] C. Vieille and G. J. Zeikus, "Hyperthermophilic enzymes: sources, uses, and molecular mechanisms for thermostability," *Microbiology and Molecular Biology Reviews*, vol. 65, no. 1, pp. 1–43, 2001.
- [11] G. Gianese, F. Bossa, and S. Pascarella, "Comparative structural analysis of psychrophilic and meso- and thermophilic enzymes," *Proteins*, vol. 47, no. 2, pp. 236–249, 2002.
- [12] N. J. Russell, "Toward a molecular understanding of cold activity of enzymes from psychrophiles," *Extremophiles*, vol. 4, no. 2, pp. 83–90, 2000.
- [13] A. O. Smalås, H.-K. S. Leiros, V. Os, and N. P. Willassen, "Cold adapted enzymes," *Biotechnology Annual Review*, vol. 6, pp. 1–57, 2000.
- [14] A. Siglioccolo, A. Paiardini, M. Piscitelli, and S. Pascarella, "Structural adaptation of extreme halophilic proteins through decrease of conserved hydrophobic contact surface," *BMC Structural Biology*, vol. 11, no. article 50, 2011.
- [15] G. A. Sellek and J. B. Chaudhuri, "Biocatalysis in organic media using enzymes from extremophiles," *Enzyme and Microbial Technology*, vol. 25, no. 6, pp. 471–482, 1999.
- [16] R. G. Matthews and J. T. Drummond, "Providing one-carbon units for biological methylations: mechanistic studies on serine hydroxymethyltransferase, methylenetetrahydrofolate reductase, and methyltetrahydrofolate-homocysteine methyltransferase," *Chemical Reviews*, vol. 90, no. 7, pp. 1275–1290, 1990.
- [17] M. Sinnott, *Comprehensive Biological Catalysis: A Mechanistic Reference*, Academic Press, San Diego, Calif, USA, 1998.
- [18] R. J. Ulevitch and R. G. Kallen, "Purification and characterization of pyridoxal 5'-phosphate dependent serine hydroxymethylase from lamb liver and its action upon  $\beta$ -phenylserines," *Biochemistry*, vol. 16, no. 24, pp. 5342–5350, 1977.
- [19] R. J. Ulevitch and R. G. Kallen, "Studies of the reactions of substituted D,L-erythro- $\beta$ -phenylserines with lamb liver serine hydroxymethylase. Effects of substituents upon the dealdolization step," *Biochemistry*, vol. 16, no. 24, pp. 5355–5363, 1977.
- [20] S. B. Renwick, K. Snell, and U. Baumann, "The crystal structure of human cytosolic serine hydroxymethyltransferase: a target for cancer chemotherapy," *Structure*, vol. 6, no. 9, pp. 1105–1116, 1998.
- [21] V. Trivedi, A. Gupta, V. R. Jala et al., "Crystal structure of binary and ternary complexes of serine hydroxymethyltransferase from *Bacillus stearothermophilus*. Insights into the catalytic mechanism," *Journal of Biological Chemistry*, vol. 277, no. 19, pp. 17161–17169, 2002.
- [22] D. M. E. Szebenyi, X. Liu, I. A. Kriksunov, P. J. Stover, and D. J. Thiel, "Structure of a murine cytoplasmic serine hydroxymethyltransferase quinonoid ternary complex: evidence for asymmetric obligate dimers," *Biochemistry*, vol. 39, no. 44, pp. 13313–13323, 2000.
- [23] J. N. Scarsdale, S. Radaev, G. Kazanina, V. Schirch, and H. T. Wright, "Crystal structure at 2.4 Å resolution of *E. coli* serine hydroxymethyltransferase in complex with glycine substrate and 5-formyl tetrahydrofolate," *Journal of Molecular Biology*, vol. 296, no. 1, pp. 155–168, 2000.
- [24] J. N. Scarsdale, G. Kazanina, S. Radaev, V. Schirch, and H. T. Wright, "Crystal structure of rabbit cytosolic serine hydroxymethyltransferase at 2.8 Å resolution: mechanistic implications," *Biochemistry*, vol. 38, no. 26, pp. 8347–8358, 1999.
- [25] R. Contestabile, A. Paiardini, S. Pascarella, M. L. Di Salvo, S. D'Aguzzo, and F. Bossa, "L-Threonine aldolase, serine hydroxymethyltransferase and fungal alanine racemase: a subgroup of strictly related enzymes specialized for different functions," *European Journal of Biochemistry*, vol. 268, no. 24, pp. 6508–6525, 2001.
- [26] M. L. di Salvo, R. Florio, A. Paiardini, M. Vivoli, S. D'Aguzzo, and R. Contestabile, "Alanine racemase from *Tolypocladium inflatum*: a key PLP-dependent enzyme in cyclosporin biosynthesis and a model of catalytic promiscuity," *Archives of Biochemistry and Biophysics*, vol. 529, pp. 55–65, 2013.
- [27] V. Schirch, "Mechanism of folate-requiring enzymes in one-carbon metabolism," in *Comprehensive Biological Catalysis*, M. L. Sinnott, Ed., pp. 211–252, Academic Press, New York, NY, USA, 2nd edition, 1998.
- [28] V. Schirch and D. M. E. Szebenyi, "Serine hydroxymethyltransferase revisited," *Current Opinion in Chemical Biology*, vol. 9, no. 5, pp. 482–487, 2005.
- [29] D. M. E. Szebenyi, F. N. Musayev, M. L. Di Salvo, M. K. Safo, and V. Schirch, "Serine hydroxymethyltransferase: role of Glu75 and evidence that serine is cleaved by a retroaldol mechanism," *Biochemistry*, vol. 43, no. 22, pp. 6865–6876, 2004.
- [30] G. Giardina, R. Montioli, S. Gianni et al., "Open conformation of human DOPA decarboxylase reveals the mechanism of PLP addition to Group II decarboxylases," *Proceedings of the National Academy of Sciences of the United States of America*, vol. 108, no. 51, pp. 20514–20519, 2011.
- [31] V. Schirch, K. Shostak, M. Zamora, and M. Gautam-Basak, "The origin of reaction specificity in serine hydroxymethyltransferase," *Journal of Biological Chemistry*, vol. 266, no. 2, pp. 759–764, 1991.
- [32] K. Cai and V. Schirch, "Structural studies on folding intermediates of serine hydroxymethyltransferase using fluorescence resonance energy transfer," *Journal of Biological Chemistry*, vol. 271, no. 44, pp. 27311–27320, 1996.
- [33] K. Cai and V. Schirch, "Structural studies on folding intermediates of serine hydroxymethyltransferase using single tryptophan mutants," *Journal of Biological Chemistry*, vol. 271, no. 6, pp. 2987–2994, 1996.

- [34] K. Cai, D. Schirch, and V. Schirch, "The affinity of pyridoxal 5'-phosphate for folding intermediates of *Escherichia coli* serine hydroxymethyltransferase," *Journal of Biological Chemistry*, vol. 270, no. 33, pp. 19294–19299, 1995.
- [35] T.-F. Fu, E. S. Boja, M. K. Safo, and V. Schirch, "Role of proline residues in the folding of serine hydroxymethyltransferase," *Journal of Biological Chemistry*, vol. 278, no. 33, pp. 31088–31094, 2003.
- [36] R. Singh, F. Spyarakis, P. Cozzini, A. Paiardini, S. Pascarella, and A. Mozzarelli, "Chemogenomics of pyridoxal 5'-phosphate dependent enzymes," *Journal of Enzyme Inhibition and Medicinal Chemistry*, vol. 28, pp. 183–194, 2013.
- [37] A. Amadasi, M. Bertoldi, R. Contestabile et al., "Pyridoxal 5'-phosphate enzymes as targets for therapeutic agents," *Current Medicinal Chemistry*, vol. 14, no. 12, pp. 1291–1324, 2007.
- [38] F. Daidone, R. Florio, S. Rinaldo et al., "In silico and in vitro validation of serine hydroxymethyltransferase as a chemotherapeutic target of the antifolate drug pemetrexed," *European Journal of Medicinal Chemistry*, vol. 46, no. 5, pp. 1616–1621, 2011.
- [39] M. L. di Salvo, R. Contestabile, A. Paiardini, and B. Maras, "Glycine consumption and mitochondrial serine hydroxymethyltransferase in cancer cells: the heme connection," *Medical Hypotheses*, vol. 80, pp. 633–636, 2013.
- [40] H. Maden, "Tetrahydrofolate and tetrahydromethanopterin compared: functionally distinct carriers in C1 metabolism," *Biochemical Journal*, vol. 350, no. 3, pp. 609–629, 2000.
- [41] A. Paiardini, G. Gianese, F. Bossa, and S. Pascarella, "Structural plasticity of thermophilic serine hydroxymethyltransferases," *Proteins*, vol. 50, no. 1, pp. 122–134, 2003.
- [42] A. Wasserfallen, J. Nöling, P. Pfister, J. Reeve, and E. C. De Macario, "Phylogenetic analysis of 18 thermophilic *Methanobacterium* isolates supports the proposals to create a new genus, *Methanothermobacter* gen. nov., and to reclassify several isolates in three species, *Methanothermobacter thermautotrophicus* comb. nov., *Methanothermobacter wolfei* comb. nov., and *Methanothermobacter marburgensis* sp. nov.," *International Journal of Systematic and Evolutionary Microbiology*, vol. 50, no. 1, pp. 43–53, 2000.
- [43] S. D. Fratte, R. H. White, B. Maras, F. Bossa, and V. Schirch, "Purification and properties of serine hydroxymethyltransferase from *Sulfolobus solfataricus*," *Journal of Bacteriology*, vol. 179, no. 23, pp. 7456–7461, 1997.
- [44] R. H. White, "Distribution of folates and modified folates in extremely thermophilic bacteria," *Journal of Bacteriology*, vol. 173, no. 6, pp. 1987–1991, 1991.
- [45] S. Angelaccio, R. Chiaraluce, V. Consalvi et al., "Catalytic and thermodynamic properties of tetrahydromethanopterin-dependent serine hydroxymethyltransferase from *Methanococcus jannaschii*," *Journal of Biological Chemistry*, vol. 278, no. 43, pp. 41789–41797, 2003.
- [46] H. Ide, K. Hamaguchi, S. Kobata et al., "Purification of serine hydroxymethyltransferase from *Bacillus stearothermophilus* with ion-exchange high-performance liquid chromatography," *Journal of Chromatography*, vol. 596, no. 2, pp. 203–209, 1992.
- [47] S. Bhavani, V. Trivedi, V. R. Jala et al., "Role of lys-226 in the catalytic mechanism of *Bacillus stearothermophilus* serine hydroxymethyltransferase—crystal structure and kinetic studies," *Biochemistry*, vol. 44, no. 18, pp. 6929–6937, 2005.
- [48] V. Rajaram, B. S. Bhavani, P. Kaul et al., "Structure determination and biochemical studies on *Bacillus stearothermophilus* E53Q serine hydroxymethyltransferase and its complexes provide insights on function and enzyme memory," *FEBS Journal*, vol. 274, no. 16, pp. 4148–4160, 2007.
- [49] V. R. Pai, V. Rajaram, S. Bisht et al., "Structural and functional studies of *Bacillus stearothermophilus* serine hydroxymethyltransferase: the role of Asn341, Tyr60 and Phe351 in tetrahydrofolate binding," *Biochemical Journal*, vol. 418, no. 3, pp. 635–642, 2009.
- [50] A. N. Bhatt, K. Prakash, H. S. Subramanya, and V. Bhakuni, "Different unfolding pathways for mesophilic and thermophilic homologues of serine hydroxymethyltransferase," *Biochemistry*, vol. 41, no. 40, pp. 12115–12123, 2002.
- [51] A. N. Bhatt, V. Bhakuni, A. Kumar, M. Y. Khan, and M. I. Siddiqi, "Alkaline pH-dependent differential unfolding characteristics of mesophilic and thermophilic homologs of dimeric serine hydroxymethyltransferase," *Biochimica et Biophysica Acta*, vol. 1804, no. 6, pp. 1294–1300, 2010.
- [52] M. Herold and K. Kirschner, "Reversible dissociation and unfolding of *Aspartate aminotransferase* from *Escherichia coli*: characterization of a monomeric intermediate," *Biochemistry*, pp. 1907–1913, 1990.
- [53] V. Schirch, S. Hopkins, E. Villar, and S. Angelaccio, "Serine hydroxymethyltransferase from *Escherichia coli*: purification and properties," *Journal of Bacteriology*, vol. 163, no. 1, pp. 1–7, 1985.
- [54] S. Angelaccio, R. Florio, V. Consalvi, G. Festa, and S. Pascarella, "Serine hydroxymethyltransferase from the cold adapted microorganism *Psychromonas ingrahamii*: a low temperature active enzyme with broad substrate specificity," *International Journal of Molecular Sciences*, vol. 13, no. 2, pp. 1314–1326, 2012.
- [55] A. Razvi and J. M. Scholtz, "Lessons in stability from thermophilic proteins," *Protein Science*, vol. 15, no. 7, pp. 1569–1578, 2006.
- [56] E. Maugini, D. Tronelli, F. Bossa, and S. Pascarella, "Structural adaptation of the subunit interface of oligomeric thermophilic and hyperthermophilic enzymes," *Computational Biology and Chemistry*, vol. 33, no. 2, pp. 137–148, 2009.
- [57] C. Gerday, M. Aittaleb, M. Bentahir et al., "Cold-adapted enzymes: from fundamentals to biotechnology," *Trends in Biotechnology*, vol. 18, no. 3, pp. 103–107, 2000.
- [58] N. J. Russell, "Molecular adaptations in psychrophilic bacteria: potential for biotechnological applications," *Advances in Biochemical Engineering/Biotechnology*, vol. 61, pp. 1–21, 1998.
- [59] A. Siglioccolo, F. Bossa, and S. Pascarella, "Structural adaptation of serine hydroxymethyltransferase to low temperatures," *International Journal of Biological Macromolecules*, vol. 46, no. 1, pp. 37–46, 2010.
- [60] G.-H. Zhao, H. Li, W. Liu et al., "Preparation of optically active  $\beta$ -hydroxy- $\alpha$ -amino acid by immobilized *Escherichia coli* cells with serine hydroxymethyl transferase activity," *Amino Acids*, vol. 40, no. 1, pp. 215–220, 2011.
- [61] M. Vivoli, F. Angelucci, A. Ilari et al., "Role of a conserved active site cation- $\pi$  interaction in *Escherichia coli* serine hydroxymethyltransferase," *Biochemistry*, vol. 48, no. 50, pp. 12034–12046, 2009.
- [62] F. Malerba, A. Bellelli, A. Giorgi, F. Bossa, and R. Contestabile, "The mechanism of addition of pyridoxal 5'-phosphate to *Escherichia coli* apo-serine hydroxymethyltransferase," *Biochemical Journal*, vol. 404, no. 3, pp. 477–485, 2007.

- [63] A. Siglioccolo, R. Gerace, and S. Pascarella, "Cold spots in protein cold adaptation: insights from normalized atomic displacement parameters (B<sub>f</sub>-factors)," *Biophysical Chemistry*, vol. 153, no. 1, pp. 104–114, 2010.
- [64] A. Hoyoux, V. Blaise, T. Collins et al., "Extreme catalysts from low-temperature environments," *Journal of Bioscience and Bioengineering*, vol. 98, no. 5, pp. 317–330, 2004.
- [65] M. T. Reetz, "Combinatorial and evolution-based methods in the creation of enantioselective catalysts," *Angewandte Chemie*, vol. 40, pp. 284–310, 2001.
- [66] W. Maruyama, M. Naoi, and H. Narabayashi, "The metabolism of L-DOPA and L-threo-3,4-dihydroxyphenylserine and their effects on monoamines in the human brain: analysis of the intraventricular fluid from parkinsonian patients," *Journal of the Neurological Sciences*, vol. 139, no. 1, pp. 141–148, 1996.
- [67] M. Apley, "Ancillary therapy of bovine respiratory disease," *The Veterinary Clinics of North America*, vol. 13, no. 3, pp. 575–582, 1997.
- [68] M. Apley, "Antimicrobial therapy of bovine respiratory disease," *The Veterinary clinics of North America. Food animal practice*, vol. 13, no. 3, pp. 549–556, 1997.
- [69] V. P. Vassilev, T. Uchiyama, T. Kajimoto, and C. H. Wong, "L-threonine aldolase in organic synthesis: preparation of novel  $\beta$ -hydroxy- $\alpha$ -amino acids," *Tetrahedron Letters*, vol. 36, no. 23, pp. 4081–4084, 1995.
- [70] V. A. Soloshonok, Y. N. Belokon, N. A. Kuzmina et al., "Asymmetric synthesis of phosphorus analogues of dicarboxylic  $\alpha$ -amino acids," *Journal of the Chemical Society*, vol. 1, no. 12, pp. 1525–1529, 1992.
- [71] V. A. Soloshonok, V. P. Kukhar, S. V. Galushko et al., "General method for the synthesis of enantiomerically pure  $\beta$ -hydroxy- $\alpha$ -amino acids, containing fluorine atoms in the side chains. Case of stereochemical distinction between methyl and trifluoromethyl groups. X-ray crystal and molecular structure of the nickel(II) complex of (2S,3S)-2-(trifluoromethyl)threonine," *Journal of the Chemical Society*, vol. 1, no. 24, pp. 3143–3155, 1993.
- [72] T. R. Burke Jr., M. Knight, B. Chandrasekhar, and J. A. Ferretti, "Solid-phase synthesis of viscosin, a cyclic depsipeptide with antibacterial and antiviral properties," *Tetrahedron Letters*, vol. 30, no. 5, pp. 519–522, 1989.
- [73] S. S. Miyazaki, S. Toki, Y. Izumi, and H. Yamada, "Further characterization of serine hydroxymethyltransferase from a serine producing methylotroph, *Hyphomicrobium-methylovorum*," *Agricultural and Biological Chemistry*, vol. 51, pp. 2587–2589, 1987.
- [74] L. Vidal, J. Calveras, P. Clapés, P. Ferrer, and G. Caminal, "Recombinant production of serine hydroxymethyl transferase from *Streptococcus thermophilus* and its preliminary evaluation as a biocatalyst," *Applied Microbiology and Biotechnology*, vol. 68, no. 4, pp. 489–497, 2005.
- [75] M. L. Gutierrez, X. Garrabou, E. Agosta et al., "Serine hydroxymethyl transferase from *Streptococcus thermophilus* and L-threonine aldolase from *Escherichia coli* as stereocomplementary biocatalysts for the synthesis of beta-hydroxy-alpha,omega-diamino acid derivatives," *Chemistry*, vol. 14, no. 15, pp. 4647–4656, 2008.
- [76] S. Makart, M. Bechtold, and S. Panke, "Towards preparative asymmetric synthesis of  $\beta$ -hydroxy- $\alpha$ -amino acids: l-allo-Threonine formation from glycine and acetaldehyde using recombinant GlyA," *Journal of Biotechnology*, vol. 130, no. 4, pp. 402–410, 2007.
- [77] K. Velonia, I. Tsigos, V. Bouriotis, and I. Smonou, "Stereospecificity of hydrogen transfer by the NAD<sup>+</sup>-linked alcohol dehydrogenase from the Antarctic psychrophile *Moraxella* sp. TAE123," *Bioorganic and Medicinal Chemistry Letters*, vol. 9, no. 1, pp. 65–68, 1999.



## Research Article

# Interaction of Human Dopa Decarboxylase with L-Dopa: Spectroscopic and Kinetic Studies as a Function of pH

Riccardo Montioli, Barbara Cellini, Mirco Dindo, Elisa Oppici, and Carla Borri Voltattorni

Section of Biological Chemistry, Department of Life Sciences and Reproduction, University of Verona, Strada Le Grazie 8, 37134 Verona, Italy

Correspondence should be addressed to Carla Borri Voltattorni; [carla.borrivoltattorni@univr.it](mailto:carla.borrivoltattorni@univr.it)

Received 18 April 2013; Accepted 8 May 2013

Academic Editor: Alessandro Paiardini

Copyright © 2013 Riccardo Montioli et al. This is an open access article distributed under the Creative Commons Attribution License, which permits unrestricted use, distribution, and reproduction in any medium, provided the original work is properly cited.

Human Dopa decarboxylase (hDDC), a pyridoxal 5'-phosphate (PLP) enzyme, displays maxima at 420 and 335 nm and emits fluorescence at 384 and 504 nm upon excitation at 335 nm and at 504 nm when excited at 420 nm. Absorbance and fluorescence titrations of hDDC-bound coenzyme identify a single  $pK_{\text{spec}}$  of  $\sim 7.2$ . This  $pK_{\text{spec}}$  could not represent the ionization of a functional group on the Schiff base but that of an enzymic residue governing the equilibrium between the low- and the high-pH forms of the internal aldimine. During the reaction of hDDC with L-Dopa, monitored by stopped-flow spectrophotometry, a 420 nm band attributed to the 4'-N-protonated external aldimine first appears, and its decrease parallels the emergence of a 390 nm peak, assigned to the 4'-N-unprotonated external aldimine. The pH profile of the spectral change at 390 nm displays a  $pK$  of 6.4, a value similar to that ( $\sim 6.3$ ) observed in both  $k_{\text{cat}}$  and  $k_{\text{cat}}/K_m$  profiles. This suggests that this  $pK$  represents the  $\text{ESH}^+ \rightarrow \text{ES}$  catalytic step. The assignment of the  $pK$ s of 7.9 and 8.3 observed on the basic side of  $k_{\text{cat}}$  and the PLP binding affinity profiles, respectively, is also analyzed and discussed.

## 1. Introduction

Dopa decarboxylase (DDC; EC 4.1.1.28) is a pyridoxal 5'-phosphate- (PLP-) dependent enzyme which catalyzes the irreversible decarboxylation of L-Dopa and L-5-hydroxytryptophan (5-HTP), thus producing the neurotransmitters dopamine and serotonin. The enzyme accepts other catechol- or indole-related L-amino acids and has been therefore also named L-aromatic amino acid decarboxylase (AADC). Like other PLP enzymes [1–7], DDC is of clinical interest since it is involved either in Parkinson's disease, a degenerative disorder of the central nervous system resulting from the death of dopamine-generating cells in the *substantia nigra*, or in AADC deficiency, a rare inherited neurometabolic disease due to mutations on the AADC gene leading to deficit of catecholamines and serotonin in the central nervous system and periphery [8]. Thus, the elucidation of the structural and functional features of the enzyme is relevant for the development of treatment strategies for both disorders. In this regard, a structure-based design search aimed at identifying

inhibitors of peripheral DDC more selective than those currently administered to patients with Parkinson's disease has been recently reported [9]. Moreover, the molecular basis of AADC deficiency analyzed by comparing the characteristics of normal human DDC (hDDC) with those of some pathogenic variants in their recombinant purified form has allowed not only to unravel their molecular defects but also to suggest appropriate therapeutic treatments for patients bearing the examined mutations [10, 11].

Progress in understanding the structure/function relationships operating in DDC has been obtained by means of kinetic, spectroscopic, and structural studies on the pig kidney and rat liver enzymes, either in the naturally occurring [12–17] or in the recombinant purified [18–26] forms, as well as, more recently, on recombinant purified hDDC [9–11, 27]. The crystal structure of pig kidney holo DDC alone and in complex with carbidopa (a substrate analog endowed with a hydrazinic group) has been solved at 2.6 and 2.5 Å resolutions, respectively [28]. The overall structure of the protein is a tightly associated dimer in which the active site is buried

in the central part. Each monomer is composed of a large domain and a C-terminal domain, typical of the aspartate aminotransferase family (Fold Type I), as well as an N-terminal domain characteristic of Group II decarboxylases. Several other features of DDC are evident in these structures: (i) the way in which PLP is anchored to the enzyme involving His302 and His192, two highly conserved residues in  $\alpha$ -decarboxylases [29]; (ii) how the inhibitor binds; and (iii) which amino acid residues might be involved in the catalytic activity. Unexpectedly, the crystal structure of hDDC in the apo form reveals that it exists in an open conformation in which the dimer subunits move 20 Å apart and the two active sites become solvent exposed. Moreover, by varying the PLP concentration in the crystals of the open DDC, two more structures have been solved, thus allowing to identify the structural determinants of the conformational change occurring upon PLP binding [27].

Although DDC enzymes share similar absorption spectra, that is, absorption maxima at 420 and 335 nm, pig kidney and rat liver enzymes display different PLP emission fluorescent properties, possibly due to the presence, even if to a different degree, of a species absorbing at 335 nm and emitting fluorescence at 390 nm in their apoenzyme forms [15, 24, 25]. These findings, together with the fact that the coenzyme absorbing bands show a modest pH dependence, do not allow to unequivocally assign the 335 nm absorbing band to a form of the internal aldimine and to understand how the equilibrium between the 420 and 335 nm species is governed. Moreover, although previous spectroscopic analyses of the reaction of both pig kidney and rat liver DDC with L-Dopa provided evidence for the appearance of two intermediates absorbing at 420 and 385 nm, the assignment of these species is conflicting. These absorbance bands have been attributed to 1-N-protonated-4'-N-protonated and 1-N-protonated-4'-N-unprotonated Schiff bases shown by the low- and high-pH forms of the external aldimine [13, 17]. On the other hand, other authors suggested that these species were formed during the course of the decarboxylation reaction, being the 420 nm and the 385 nm either the adsorption complex and the external aldimine with L-Dopa, respectively [25, 26], or two different external aldimines [30].

The present study presents a detailed investigation of the pH dependence of the bound coenzyme absorbance and fluorescence features and of the steady-state kinetic parameters of hDDC. Additionally, changes of the absorbance bands of hDDC upon L-Dopa binding as a function of pH have been monitored by rapid scanning stopped-flow experiments. Taken together, the results allow us to identify three observable ionizations in hDDC and to propose their involvement in the structures of the bound coenzyme and in the intermediates along the decarboxylation pathway.

## 2. Material and Methods

**2.1. Chemicals.** L-Dopa, PLP, 2,4,6-trinitrobenzene-1-sulfonic acid, isopropyl- $\beta$ -D-thiogalactopyranoside, and protease inhibitor cocktail were purchased from Sigma-Aldrich. Bis-Tris-propane at a final concentration of 50 mM was used

over the pH range 6–8.8. The other chemicals were of the highest purity available.

**2.2. Enzyme Preparation.** The conditions used for expression and purification of hDDC were as previously described [11]. The apo form was prepared as previously reported [11].

**2.3. Binding Affinity of hDDC for PLP.** The equilibrium dissociation constant for PLP,  $K_{D(PLP)}$ , was determined by measuring the quenching of the intrinsic fluorescence of the apoenzyme (0.15  $\mu$ M) in the presence of PLP at a concentration range of 0.01–20  $\mu$ M. The experiments were carried out in 50 mM Bis-Tris-propane in the pH range 6–8.8. The  $K_{D(PLP)}$  values were obtained by fitting the data to the following equation:

$$Y = Y_{\text{MAX}} \frac{[E]_t + [PLP]_t + K_{D(PLP)} - \sqrt{([E]_t + [PLP]_t + K_{D(PLP)})^2 - 4[E]_t[PLP]_t}}{2[E]_t}, \quad (1)$$

where  $[E]_t$  and  $[PLP]_t$  represent the total concentrations of hDDC dimer and PLP, respectively,  $Y$  refers to the intrinsic fluorescence quenching changes at a PLP concentration,  $[PLP]$ , and  $Y_{\text{max}}$  refers to the aforementioned changes when all enzyme molecules are complexed with the coenzyme.

**2.4. Enzyme Assay.** The decarboxylase activity toward L-Dopa was measured by the spectrophotometric assay described by Sherald et al. [31], and it was modified by Charteris and John [32]. Measurements were performed in the presence of 10  $\mu$ M PLP. Data of enzymatic activity as a function of substrate concentration were fitted to Michaelis-Menten equation.

**2.5. Spectral Measurements.** Absorption spectra were made with a Jasco V-550 spectrophotometer at a protein concentration of 10  $\mu$ M. Fluorescence spectra were taken with an FP750 Jasco spectrofluorometer using 5 nm excitation and emission bandwidths at a protein concentration of 10  $\mu$ M. The enzyme solution was drawn through a 0.2  $\mu$ m filter to reduce light scattering from the small amount of precipitate. Spectra of blanks, that is, samples containing all components except hDDC, were taken immediately before the measurements of samples containing protein.

**2.6. pH Studies.** Absorbance and fluorescence data were fitted to (2) and (3):

$$A = \frac{A_1 - A_2}{1 + 10^{pH - pK_{\text{spec}}}} + A_2, \quad (2)$$

$$A = \frac{A_1 - A_2}{1 + 10^{pK_{\text{spec}} - pH}} + A_2, \quad (3)$$

where  $A_1$  and  $A_2$  are the higher and the lower absorbance limits at a particular wavelength, respectively.

The  $\log K_{D(PLP)}$ ,  $\log k_{cat}$ ,  $\log k_{cat}/K_m$ , and values for hDDC versus pH were fitted to the following appropriate equations:

$$\log Y = \log \frac{Y_L + Y_H (H/K_1)}{1 + H/K_1}, \quad (4)$$

$$\log Y = \log \frac{C}{1 + H/K_A + K_B/H}, \quad (5)$$

$$\log Y = \log \frac{C}{1 + H/K_A}, \quad (6)$$

where  $K_A$  and  $K_B$  represent the ionization constants for enzyme or reactant functional groups,  $Y$  is the value of the parameter observed as a function of pH,  $C$  is the pH-independent value of  $Y$ ,  $H$  is the hydrogen ion concentration, and  $Y_L$  and  $Y_H$  are constant values at low and high pH, respectively.

**2.7. Pre-Steady-State Kinetic Analysis by UV-Vis Stopped-Flow Spectroscopy.** hDDC was mixed using a Biologic SFM300 mixer with an equal volume of 2 mM L-Dopa in 50 mM Bis-Tris-propane at pH ranging from 6.0 to 8.0. Coenzyme absorbance changes were monitored with a TC-100 (path length of 1 cm) quartz cell coupled to a Biokine PMS-60 instrument. The dead time was 3.8 ms at a flow velocity of 8 mL/sec. Absorbance scans (800) from 300 to 600 nm were collected on a logarithmic time scale with a J&M Tidas 16256 diode array detector (Molecular kinetics, Pullman, WA). Data were analyzed using either SPECFIT (Spectrum Software, Claix, France) or Biokine 4.01 (Biologic, Claix, France) to determine the observed rate constants. Single-wavelength time courses were fit to an equation of the following general form:

$$A_t = A_{\infty} \pm \sum A_i \exp(-k_{obs} t), \quad (7)$$

where  $A_t$  is the absorbance at time  $t$ ,  $A_i$  is the amplitude of each phase,  $k_{obs}$  is the observed rate constant for each phase, and  $A_{\infty}$  is the final absorbance.

### 3. Results

**3.1. pH Dependence of the Internal Aldimine and Coenzyme Binding Affinity.** Apo hDDC completely lacks absorbance in the visible region, while the holo form is characterized by absorbance bands at 420 and 335 nm associated with positive dichroic signals at the same wavelengths [11]. The absorbance spectrum of hDDC in the holo form changes as a function of pH over the range 6–8.5 (Figure 1): the 335 nm band increases with pH, while the 420 nm band decreases. The spectra do not show a clear isosbestic point, thus suggesting the presence of multiple species. When we fitted the data to curves with one, two, or three ionizations, we found that they fit best to a model with one ionization ((2) and (3)): the  $pK_{spec}$  values obtained were  $7.2 \pm 0.1$  and  $7.3 \pm 0.1$  for the absorbance at 420 and 335 nm, respectively (Figure 1, inset) (Table 1).

Excitation of hDDC at 420 nm results in an emission band at 504 nm, whose intensity decreases as pH increases below

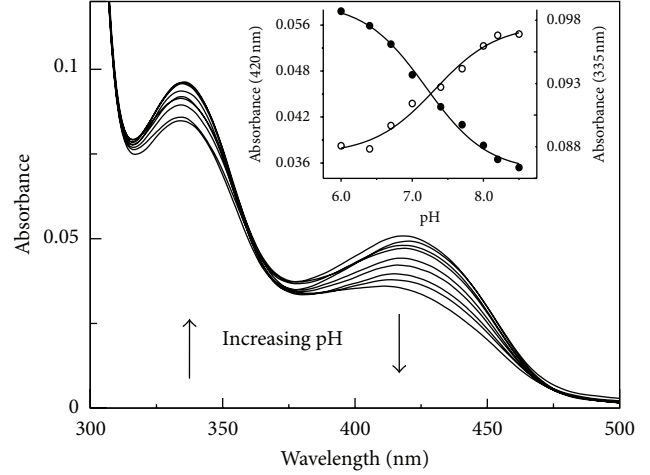


FIGURE 1: pH dependence of the visible spectra of hDDC. Absorbance spectra of 10  $\mu$ M hDDC were acquired in 50 mM Bis-Tris-propane at pH 6.0, 6.4, 7.0, 7.4, 7.7, 8.0, 8.2, and 8.5. The inset shows the pH dependence of the absorbance at 420 ( $\bullet$ ) and 335 nm ( $\circ$ ). The solid lines represent the theoretical curves according to (2) and (3).

TABLE 1: Summary of  $pK_a$  values for hDDC.

Parameter	pH-independent value	$pK_1$	$pK_2$
$k_{cat}$	$5.1 \pm 0.4 \text{ s}^{-1}$	$6.3 \pm 0.1$	$7.9 \pm 0.1$
$k_{cat}/K_m$	$174 \pm 3 \text{ mM}^{-1}\text{s}^{-1}$	$6.1 \pm 0.1$	
Absorbance at 420 nm pH titration			$7.2 \pm 0.1$
Absorbance at 335 nm pH titration			$7.3 \pm 0.1$
Emission fluorescence pH titration (exc. 335 nm)			
emis. <sub>384 nm</sub>			$7.3 \pm 0.1$
emis. <sub>504 nm</sub>			$7.2 \pm 0.1$
Emission fluorescence pH titration (exc. 420 nm)			
emis. <sub>504 nm</sub>			$7.2 \pm 0.1$
Amplitude ext. ald. 390 nm		$6.4 \pm 0.3$	
$K_{D(PLP)}$			$8.3 \pm 0.2$

a single  $pK$  of  $7.2 \pm 0.1$  (Figure 2(a) and inset). Moreover, hDDC emits at 384 and 504 nm upon excitation at 335 nm. Emission fluorescence intensity at 384 nm increases with increasing pH, while that at 504 nm decreases (Figure 2(b)). As shown in the inset of Figure 2(b), the pH profile for the 384 nm emission intensity increases above a single  $pK$  of  $7.3 \pm 0.1$ , while that at 504 nm decreases below a single  $pK$  of  $7.1 \pm 0.1$  (Table 1). When emission was observed at 384 nm, the excitation spectrum exhibits a maximum at 337 nm, whereas at 500 nm, the excitation spectrum displays maxima at 341 and 410 nm.

The  $K_{D(PLP)}$  value for hDDC at pH 7.4 is  $0.2 \mu$ M, and it increases as the pH increases. The pH dependence of  $K_{D(PLP)}$

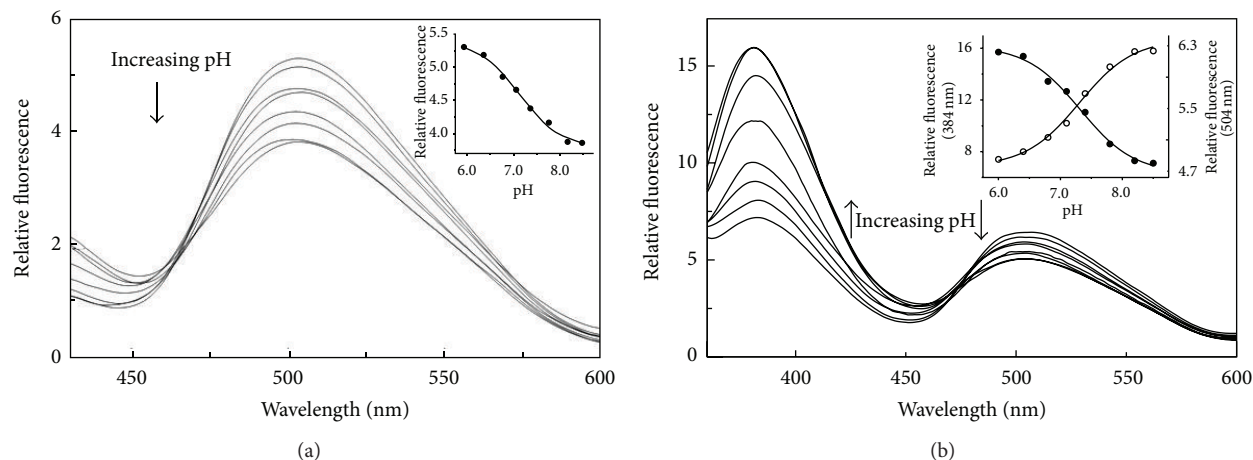


FIGURE 2: pH dependence of the internal aldimine emission fluorescence of hDDC. Emission fluorescence spectra of 10  $\mu\text{M}$  hDDC in 50 mM Bis-Tris-propane at pH 6.0, 6.4, 6.8, 7.1, 7.4, 7.8, 8.2, and 8.5 upon excitation at 420 nm (a) and 335 nm (b). The inset of (a) shows the pH dependence of the emission intensity at 504 nm ( $\bullet$ ), while that of (b) shows the pH dependence of the emission intensity at 504 nm ( $\circ$ ) and 384 nm ( $\circ$ ). The solid lines represent the theoretical curves according to (2) and (3).

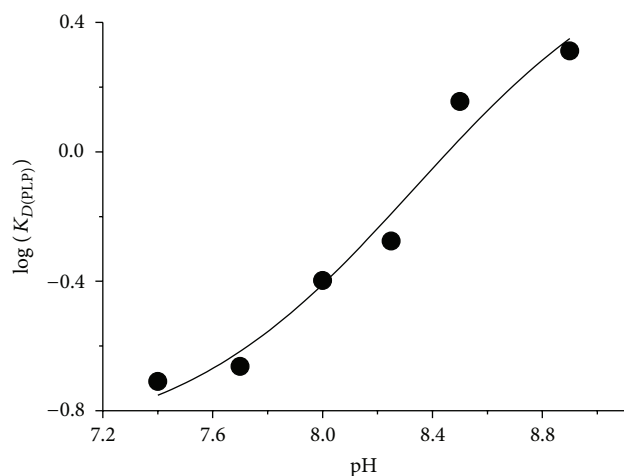


FIGURE 3: pH dependence of  $K_{D(\text{PLP})}$  of hDDC.  $K_{D(\text{PLP})}$  values were determined in 50 mM Bis-Tris-propane at the indicated pH as described under "Section 2". The points shown are the experimental values (expressed in  $\mu\text{M}$ ), while the curve is from fit to the data using (4).

fits well (4), giving a  $\text{p}K_{D(\text{PLP})}$  value of  $8.3 \pm 0.2$  (Figure 3, Table 1).

**3.2. pH Dependence of Kinetic Parameters for hDDC.** The pH dependence of the kinetic parameters for hDDC toward L-Dopa was determined, and the results are shown in Figures 4(a) and 4(b). The variation with pH of  $\log k_{\text{cat}}$  gives rise to a bell-shaped profile: fitting the data to (5) and (6) yields  $\text{p}K$  values of  $6.3 \pm 0.1$  and  $7.9 \pm 0.1$ ;  $\log k_{\text{cat}}/K_m$  decreases below a  $\text{p}K$  of  $6.1 \pm 0.1$  (Table 1).

**3.3. pH Dependence of External Aldimine with L-Dopa.** To obtain information about the identity of intermediates in the

reaction of hDDC with L-Dopa we carried out rapid-kinetic spectroscopic studies over the pH range 6–8. Upon mixing the enzyme with L-Dopa at a saturating concentration, a biphasic spectral change was observed. In the first phase, a rapid increase in the absorbance at 420 nm and a decrease in the 335 nm band were observed within 50 ms, followed by a second phase, in which the absorbance at 420 nm decreases and concomitantly a new absorbance band appears at 390, occurring with a rate of  $31 \text{ s}^{-1}$  (Figure 5). The amplitude of the absorbance changes at 390 nm increases with pH above a single  $\text{p}K$  of  $6.4 \pm 0.3$  (Figure 6) (Table 1). It should be also noted that at pH higher than 6.4 the appearance of the 390 nm band is accompanied by that of a shoulder absorbing at  $\sim 440 \text{ nm}$ . Considering that the enzyme-dopamine complex absorbs at  $\sim 400 \text{ nm}$  and that only a modest amount of dopamine ( $20 \mu\text{M}$ ) is formed at the end of the second phase, the shoulder cannot be attributed to the enzyme-dopamine complex. A likely attribution might be a quinonoid species, which, according to Metzler et al. [33], could absorb at wavelengths lower than 500 nm.

In order to establish if the intermediate absorbing at 420 nm represents a Michaelis complex or an external aldimine, its rate of formation as a function of L-Dopa concentration was measured. We decided to carry out these measurements at  $15^\circ\text{C}$  and at pH 6.0, that is, under experimental conditions in which the decarboxylation reaction is slow enough so that its kinetics can be measured. As shown in Figure 7, upon addition of L-Dopa to hDDC, an increase in the 420 nm band with a concomitant decrease in the 335 nm signal can be seen. The apparent first-order rate constant of the appearance of the 420 nm band,  $k_{\text{obs}}$ , shows a hyperbolic dependence on L-Dopa concentration in the range 0.08–1 mM (inset of Figure 7). The  $k_{\text{obs}}$  data were fitted to the following equation:

$$k_{\text{obs}} = k_{+2} \frac{[\text{L-Dopa}]}{K_1 + [\text{L-dopa}]} + k_{-2}, \quad (8)$$



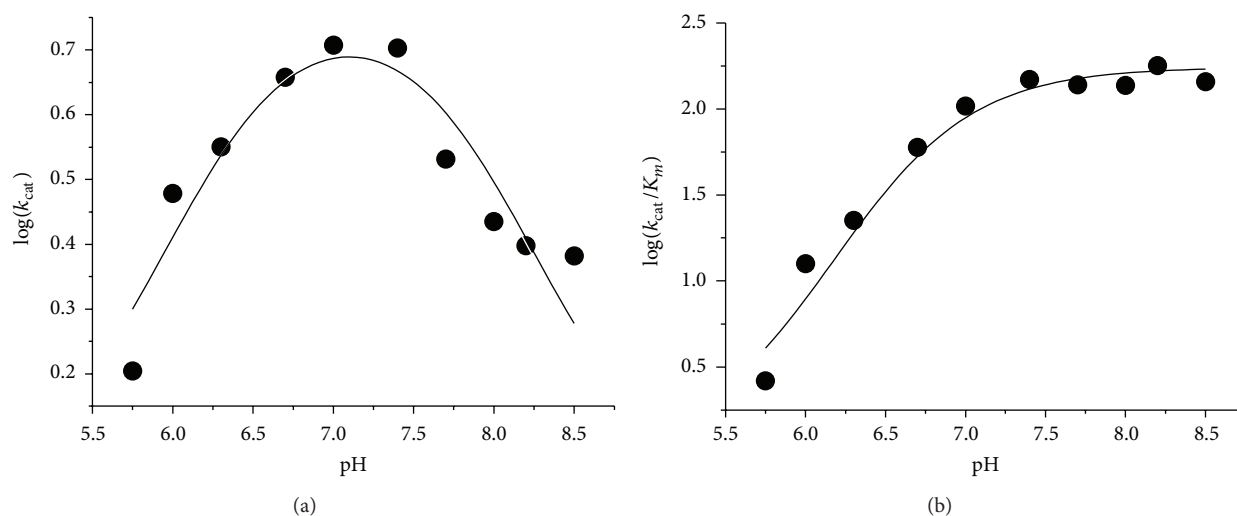


FIGURE 4: pH dependence of the kinetic parameters for the decarboxylase activity of hDDC toward L-Dopa. (a)  $\log k_{\text{cat}}$  profile and (b)  $\log k_{\text{cat}}/K_m$  profile. The assays were performed at 25°C in 50 mM Bis-Tris-propane at the indicated pH using 50 nM enzyme concentration in the presence of 10  $\mu\text{M}$  exogenous PLP. The points shown are the experimental values, while the curves are from fits to the data using (5) for  $\log k_{\text{cat}}$  and (6) for  $\log k_{\text{cat}}/K_m$ .

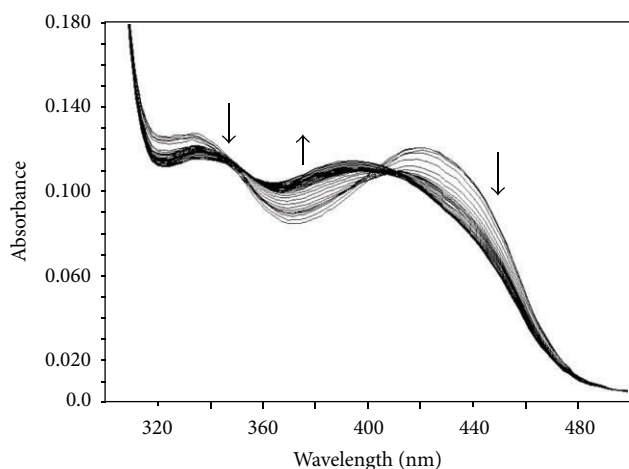
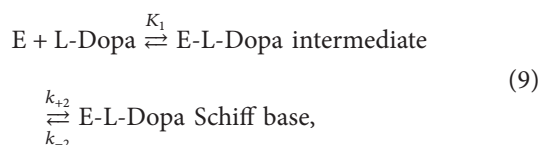


FIGURE 5: Time-resolved spectra for the reaction of hDDC with L-Dopa. Rapid scanning stopped-flow spectra obtained upon reaction of hDDC (20  $\mu\text{M}$ ) with L-Dopa (2 mM) in Tris-Bis-propane, pH 7.4, at 25°C. Spectra were taken between 1 and 100 ms at 1 ms intervals and between 101 and 200 ms at 10 ms intervals.

which describes the following two-step binding model assuming that the first step is rapid:



where  $K_1$  is the dissociation constant for the intermediate (Michaelis complex or geminal diamine) formed prior to the formation of the Schiff base species, and  $k_{+2}$  and  $k_{-2}$  are first-order rate constants for an interconversion between the intermediate and the Schiff base. Estimated values of  $k_{+2}$  and

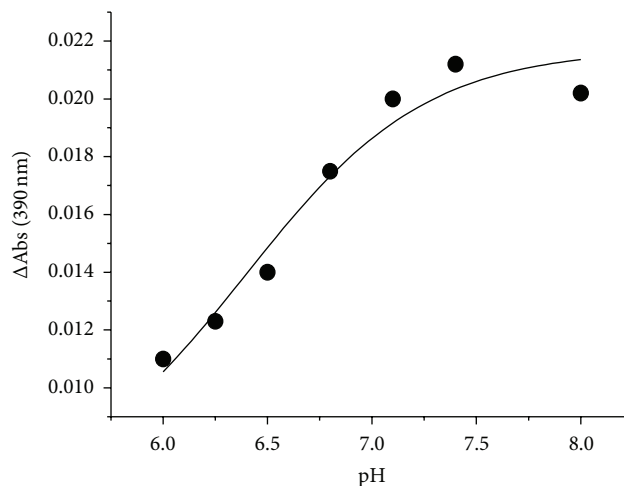


FIGURE 6: pH dependence of the amplitude of the change of the 390 nm absorbance band in the reaction of hDDC with L-Dopa. Amplitude of the 390 nm absorbance band monitored by rapid scanning stopped-flow spectra upon reaction of hDDC (20  $\mu\text{M}$ ) and L-Dopa (2 mM) in Tris-Bis-propane, at 25°C at the indicated pH. The points shown are the experimental values, while the curve is from fit to the data using (3).

$K_1$  based on the data in the inset of Figure 7 are  $124 \pm 3 \text{ s}^{-1}$  and  $0.32 \pm 0.02 \text{ mM}$ , respectively, while the  $k_{-2}$  value is nearly zero. The  $K_1$  value is consistent with the  $K_m$  value at pH 6.0 ( $0.23 \pm 0.03 \text{ mM}$ ) measured under steady-state conditions, thus strongly suggesting that the intermediate absorbing at 420 nm represents a 1-N-4'-N-protonated external aldimine. It follows that the rate of formation of the Schiff base at 25°C can be estimated to be around  $250 \text{ s}^{-1}$  using the empirical rule of a 2-fold reduction for a 10°C reduction in temperature. This value is considerably higher (~80-fold) than the  $k_{\text{cat}}$

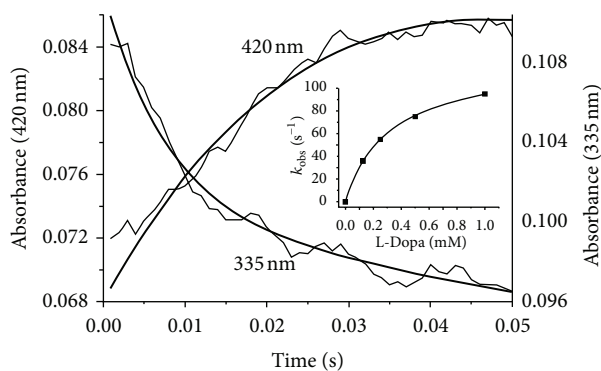


FIGURE 7: Single-wavelength stopped-flow measurements of the reaction of hDDC with L-Dopa at pH 6.0 and 15°C. Reaction of hDDC (20  $\mu$ M) with L-Dopa (1 mM) was carried out at 15°C in 50 mM Bis-Tris-propane (pH 6.0). Time courses at 420 and 335 nm are reported. The solid lines are from fits to (7). The inset shows the dependence of  $k_{\text{obs}}$  for the increase in the intensity of the 420 nm band as a function of the final concentrations of L-Dopa after mixing. The points shown are the experimental values, while the curve is from fit to the data using (8).

value at 25°C at pH 6.0 ( $3 \text{ s}^{-1}$ ), thus indicating that one of the catalytic steps after the external Schiff base formation, including the decarboxylation step, is rate determining in the entire catalytic reaction [34]. All together, these data indicate the consecutive formation of two external aldimines, one absorbing at 420 nm and the other at 390 nm, whose structures are presented in Figure 8.

#### 4. Discussion

The pH dependence of catalysis and spectral features has been studied in details for only a few PLP-dependent enzymes [35–39]. This allowed to elucidate how ionizations control their activities. Up to date, such analyses have been hampered for DDC for the following reasons: (i) a large portion of the coenzyme covalently bound is present in both pig kidney and rat liver enzymes in an inactive form and shows absorbance and PLP emission fluorescence similar to those of the corresponding holoenzymes and (ii) both pig kidney and rat liver DDC enzymes show little absorbance changes with altering pH.

Unlike the apo form of pig kidney and rat liver DDC, the apo hDDC does not display any absorbance in the 330 nm region and does not exhibit PLP emission fluorescence. Thus, we decided to perform a detailed investigation of the pH dependence of the spectroscopic properties of hDDC in its internal and external aldimine forms, of the PLP binding affinity as well as of the steady-state kinetic parameters. The following discussion attempts to assign the  $pK$  values observed in these analyses.

The titration of hDDC-bound coenzyme absorbance and fluorescence over the pH range 6–8.5 is consistent with a deprotonation event with a  $pK_a$  value of  $\sim 7.3$ , which could be the result of the deprotonation of the internal aldimine. However, there is no red shift in the 335 nm band at pH values

higher than the apparent  $pK$ , as would be expected for the unprotonated aldimine absorbing at 360 nm. Structures which could account for an increase in the 330 nm region at high pH have been postulated to arise either from the formation of an adduct upon addition of a deprotonated nucleophilic or a hydroxyl group to the imine double bond or from the conversion from the ketoenamine to the enolimine tautomer. The attribution of the 335 nm absorbance band to a substituted aldimine is in contrast with the following data: (i) when hDDC is treated with  $\text{NH}_2\text{OH}$ , the absorbance bands at 420 and 335 nm are completely lost, and the resultant apoenzyme lacks the PLP emission fluorescence, (ii) binding of L-Dopa causes the disappearance of the 335 absorbance band, (iii) upon excitation at 335 nm, the 384 nm fluorescence emission remains at low pH where the substituted aldimine would be destabilized by protonation, and (iv) the fluorescence excitation spectrum at the emission wavelength of 384 nm shows that the absorbance band that gives the excited state is seen at 341 nm, which is apparently longer than the wavelength generally observed for substituted aldimine structures, 330–335 nm. Thus, it should be taken in consideration the possibility that the 335 nm band could be attributed to the enolimine tautomer of the Schiff base. Both 384 and 504 nm emission maxima are seen upon excitation of hDDC at 335 nm, and acid promotes the 504 nm emission at the expense of the 384 nm emission. Honikel and Madsen have shown that the enolimine can emit either solely at  $\sim 400$  or  $\sim 500$  nm, or at a combination of both wavelengths, depending on the polarity and acidity of the solvent. Fluorescence emission at  $\sim 400$  nm versus 500 nm is determined by a competition between (i) proton transfer from the enolimine structure at the excited state to the aldimine nitrogen of the ketoenamine in the singlet excited state and (ii) radiative decay of the excited to the ground state [40]. On the basis of all these considerations, we can conclude that the 384 nm fluorescence emission of hDDC results from the excited state of the enolimine tautomer of the Schiff base before it has tautomerized to the ketoenamine excited state. A similar explanation has been proposed for the pH-dependent spectral changes observed for dialkylglycine decarboxylase [37], serine glyoxylate aminotransferase [38], histidine decarboxylase [41], and glutamate decarboxylase [42]. Examination of the absorbance titration curves indicates that at pH values much lower than the apparent  $pK$  ( $\sim 7.2$ ) some 335 nm is still present and that at pH values higher than  $pK$  some 420 nm absorbing species remains. Thus, one might expect from our results that the pyridine nitrogen in hDDC is not fully protonated, as it is usually assumed for PLP enzymes having an aspartate residue interacting with the pyridine nitrogen. Accordingly, the model depicted in Scheme 1 is proposed: the N-protonated (I) and N-unprotonated (II) ketoenamine forms absorb at 420 nm, while the N-protonated (III) and N-unprotonated (IV) enolimine tautomers absorb at 335 nm. At pH values less than  $pK$  I and III will be present, while II and IV represent the forms at pH much higher than the  $pK$ . Ring nitrogen protonation state governs the two equilibria between I and II absorbing at 420 nm as well as between III and IV absorbing at 335 nm, that is, between species spectroscopically indistinguishable. Thus, the most likely

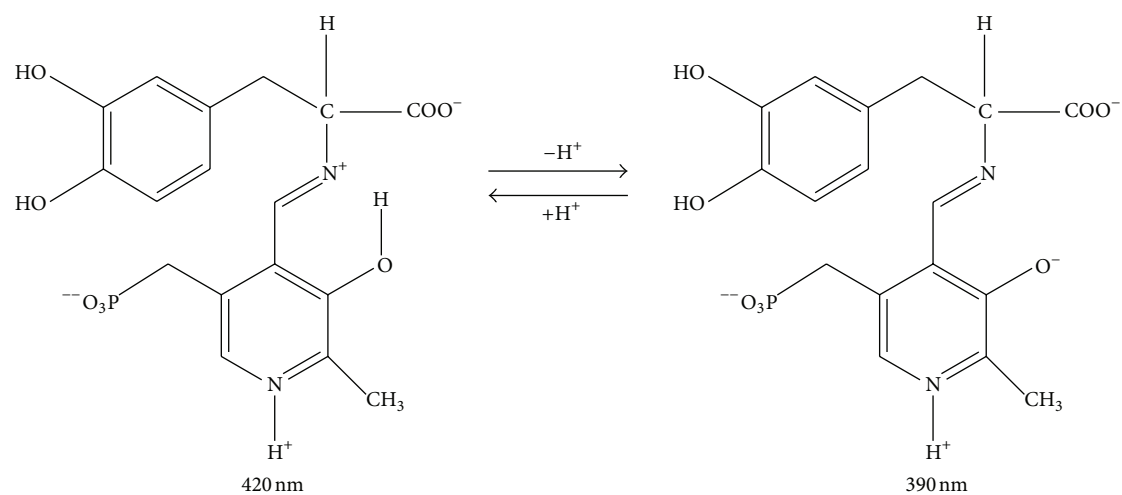
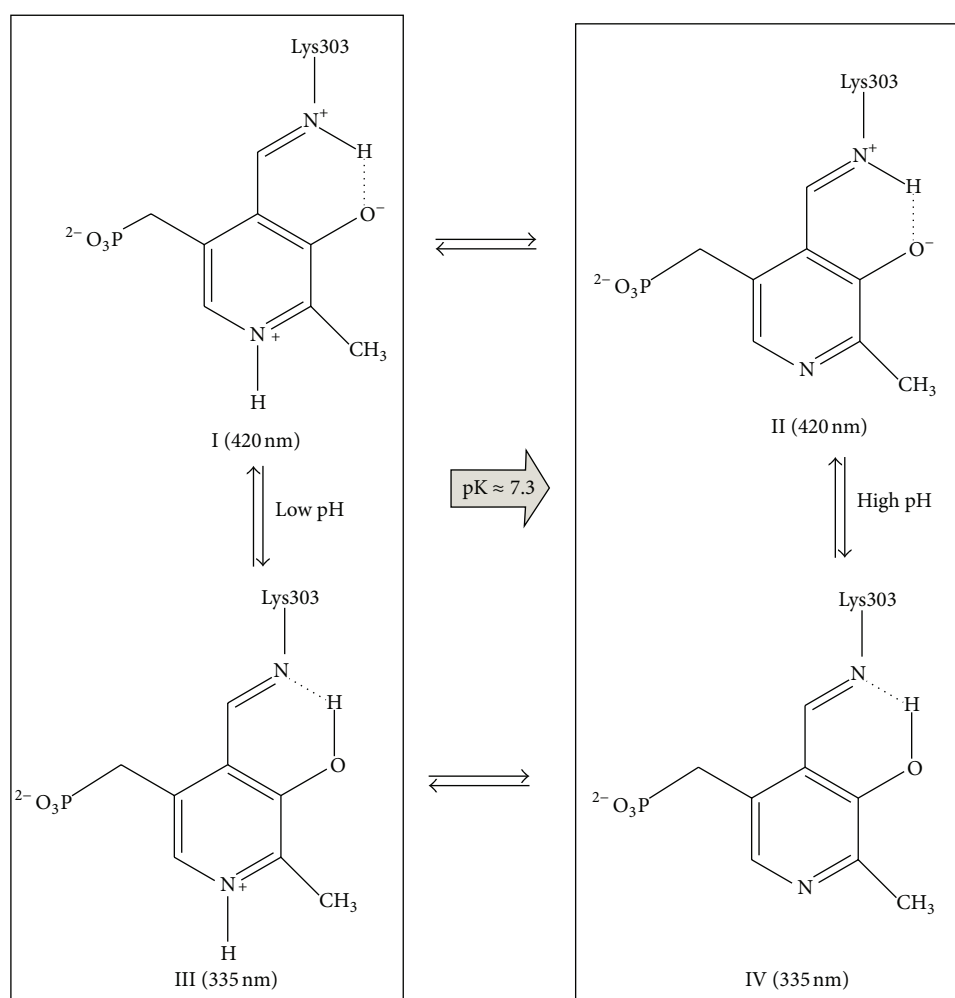


FIGURE 8: Structures of the coenzyme-L-Dopa complexes absorbing at 420 nm and 390 nm.



SCHEME 1: Putative model for the pH dependence of the internal aldimine.

explanation that accounts for the pH titration of coenzyme absorbance and fluorescence is that the ionization observed is not associated with any functional group on the Schiff base itself. Rather, it is an active site residue in close proximity to the coenzyme whose ionization alters the ratio between the two tautomers that absorb at 420 and 395 nm.

The  $k_{\text{cat}}$  profile of the decarboxylation reaction catalyzed by hDDC toward L-Dopa displays two pKa values at about 6.3 and 7.9, thus suggesting that one group is required to be unprotonated and a second group protonated to achieve maximum velocity. The pKa on the acidic side of the profile is similar to that seen in the  $k_{\text{cat}}/K_m$  profile, and, thus, it can be concluded that this group is involved in catalysis but not in binding. Since it has been proven that in pig kidney DDC  $\text{CO}_2$  release is rate limiting,  $k_{\text{cat}}$  must report on ionization(s) of the external aldimine. Thus, the spectral changes taking place in the bound coenzyme upon addition of L-Dopa have been analyzed as a function of pH by rapid scanning stopped-flow spectroscopy. The kinetic analyses of the reaction of hDDC with L-Dopa clearly demonstrate the presence of two intermediates absorbing at 420 and 390 nm. The 420 nm absorbing species is formed first, followed by formation of the second intermediate absorbing at 390 nm. The amplitude of the signal change at 390 nm increases with increasing pH above a single pK of  $\sim 6.4$ . The finding that the rate of appearance of the 420 nm band measured at pH 6.0 shows that a hyperbolic dependence on the concentration of L-Dopa is consistent with the assignment of this absorbance band to a 4'-N-protonated external aldimine. The time and pH dependence of the conversion of the 420 to the 390 nm absorbance band strongly suggest that the 390 nm band could be attributed to a 4'-N-unprotonated external aldimine. Even in the absence of the spectra of these intermediates, Minelli et al. [30] have predicted the presence of the step  $\text{ESH}^+ \rightarrow \text{ES}$ , corresponding to the 420  $\rightarrow$  390 nm conversion, along the reaction pathway of the decarboxylation of L-Dopa. Our results validate this proposal, thus ruling out that the 420 nm intermediate represents Michaelis complex, as previously suggested [25, 26]. The pK of this spectral transition (6.4) roughly coincident with those observed in both  $k_{\text{cat}}$  and  $k_{\text{cat}}/K_m$  profiles strengthens the argument that this ionization is associated with a catalytic event.

There is no evidence to support an assignment of the pK (7.9) observed on the basic side of the  $k_{\text{cat}}$  profile to a specific group. It is likely the same one seen in the pH profile for  $K_{\text{D(PLP)}}$  (8.3). Its presence on the  $K_{\text{D(PLP)}}$  profile could suggest that the phosphate ester of the coenzyme phosphate group is the likely origin of this pK, which has a value similar to that observed for the coenzyme phosphate group in *Treponema denticola* cystalysin [35]. In hDDC the effect of this ionization could be the loss of the hydrogen bond between the hydroxyl group of Ser149 and the coenzyme phosphate group oxygen. Considering the large conformational change accompanying the transition from the apo to the holo form of hDDC [27], it can be speculated that the loss of hydrogen bond not only decreases the PLP binding affinity but also could hamper a correct apo  $\rightarrow$  holo conversion resulting in a less catalytically competent conformation as the pH increases above 8. Nonetheless, it cannot be ruled out that the pK observed in

$K_{\text{D(PLP)}}$  does not coincide with the pK of the  $k_{\text{cat}}$  profile. In this case, the effect on the  $k_{\text{cat}}$  could be exerted by the ionization of a residue that, although remote from the active site, could affect the active site. A good candidate could be Tyr332 for which a role in C $\alpha$  protonation of the quinonoid along the decarboxylation pathway has been identified [22]. Although this assignment should be taken with caution, it is not in contrast with the detection at pH higher than pK of a  $\sim 440$  nm absorbing shoulder attributable to a quinonoid species. Taken together, these results indicate that the maximum  $k_{\text{cat}}$  value of hDDC is achieved when the deprotonation of the external aldimine and that of an unidentified residue take place.

In the light of these data, the absence of a band absorbing at 390 nm in the reaction with L-Dopa of four DDC variants responsible for AADC deficiency, an inherited rare neurometabolic disease, should be reconsidered. In these variants, mutations concerning amino acid residues that interact directly or indirectly with PLP and/or its microenvironment, cause a perturbation of the active site [11]. It can be postulated that in these variants the external aldimine absorbing at 420 nm is not in a proper position and/or orientation to transfer the proton at 4'-N of the Schiff base. Taking into account that, according to Minelli et al. [30], the 390 nm form is about 5-fold more reactive than the 420 nm one, it can be speculated that their reduced catalytic activity could be ascribable, at least in part, to the lack of the 420  $\rightarrow$  390 nm conversion.

## 5. Conclusions

A detailed investigation of the pH dependence of the steady-state kinetic parameters, of the spectroscopic titrations of the internal and external aldimine, as well as of the PLP binding affinity allows us to identify three observable ionizations in hDDC. The following tentative assignments for these have been made: pK<sub>1</sub> (6.3-6.4), the deprotonation of the 4'-N-protonated external aldimine occurring during the decarboxylation pathway, pK<sub>2</sub> ( $\sim 7.2$ ), a residue governing the equilibrium between the low- and the high-pH forms of the internal aldimine, and pK<sub>3</sub> (7.9, 8.3), two distinct groups (the coenzyme phosphate ester of the internal aldimine and a residue involved in the catalysis) or a unique residue affecting both PLP binding affinity and  $k_{\text{cat}}$  value: additional studies will be needed to sort out the various possibilities.

## Abbreviations

hDDC: Human Dopa decarboxylase  
 PLP: Pyridoxal 5'-phosphate  
 AADC: L-Aromatic amino acid decarboxylase  
 $K_{\text{D(PLP)}}$ : Equilibrium dissociation constant for PLP.

## Acknowledgments

This work was supported by grants from M.I.U.R and the Consorzio Interuniversitario per le Biotecnologie CIB (IT) to C. B. Voltattorni and B. Cellini.



## References

- [1] A. Amadasi, M. Bertoldi, R. Contestabile et al., "Pyridoxal 5'-phosphate enzymes as targets for therapeutic agents," *Current Medicinal Chemistry*, vol. 14, no. 12, pp. 1291–1324, 2007.
- [2] B. Cellini, A. Lorenzetto, R. Montioli, E. Oppici, and C. B. Voltattorni, "Human liver peroxisomal alanine:glyoxylate aminotransferase: different stability under chemical stress of the major allele, the minor allele, and its pathogenic G170R variant," *Biochimie*, vol. 92, no. 12, pp. 1801–1811, 2010.
- [3] B. Cellini, E. Oppici, A. Paiardini, and R. Montioli, "Molecular insights into primary hyperoxaluria type 1 pathogenesis," *Frontiers in Bioscience*, vol. 17, pp. 621–634, 2012.
- [4] M. L. di Salvo, R. Contestabile, A. Paiardini, and B. Maras, "Glycine consumption and mitochondrial serine hydroxymethyltransferase in cancer cells: the heme connection," *Medical Hypotheses*, vol. 80, pp. 633–636, 2013.
- [5] A. E. Pegg, L. M. Shantz, and C. S. Coleman, "Ornithine decarboxylase as a target for chemoprevention," *Journal of Cellular Biochemistry*, vol. 58, no. 22, pp. 132–138, 1995.
- [6] N. A. Rao, R. Talwar, and H. S. Savithri, "Molecular organization, catalytic mechanism and function of serine hydroxymethyltransferase—a potential target for cancer chemotherapy," *International Journal of Biochemistry and Cell Biology*, vol. 32, no. 4, pp. 405–416, 2000.
- [7] P. Storici, G. Capitani, D. De Biase et al., "Crystal structure of GABA-aminotransferase, a target for antiepileptic drug therapy," *Biochemistry*, vol. 38, no. 27, pp. 8628–8634, 1999.
- [8] B. Cellini, R. Montioli, E. Oppici, and C. B. Voltattorni, "Biochemical and computational approaches to improve the clinical treatment of dopa decarboxylase-related diseases: an overview," *Open Biochemistry Journal*, vol. 6, pp. 131–138, 2012.
- [9] F. Daidone, R. Montioli, A. Paiardini et al., "Identification by virtual screening and in vitro testing of human DOPA decarboxylase inhibitors," *PLoS ONE*, vol. 7, no. 2, Article ID e31610, 2012.
- [10] R. Montioli, E. Oppici, B. Cellini, A. Roncador, M. Dindo, and C. B. Voltattorni, "S250F variant associated with aromatic amino acid decarboxylase deficiency: molecular defects and intracellular rescue by pyridoxine," *Human Molecular Genetics*, vol. 22, no. 8, pp. 1615–1624, 2013.
- [11] R. Montioli, B. Cellini, and C. Borri Voltattorni, "Molecular insights into the pathogenicity of variants associated with the aromatic amino acid decarboxylase deficiency," *Journal of Inherited Metabolic Disease*, vol. 34, pp. 1213–1224, 2011.
- [12] B. Maras, P. Dominici, D. Barra, F. Bossa, and C. Borri Voltattorni, "Pig kidney 3,4-dihydroxyphenylalanine (Dopa) decarboxylase. Primary structure and relationships to other amino acid decarboxylases," *European Journal of Biochemistry*, vol. 201, no. 2, pp. 385–391, 1991.
- [13] C. B. Voltattorni, A. Minelli, and P. Dominici, "Interaction of aromatic amino acids in D and L forms with 3,4-dihydroxyphenylalanine decarboxylase from pig kidney," *Biochemistry*, vol. 22, no. 9, pp. 2249–2254, 1983.
- [14] C. B. Voltattorni, A. Minelli, and C. Turano, "Spectral properties of the coenzyme bound to DOPA decarboxylase from pig kidney," *FEBS Letters*, vol. 17, no. 2, pp. 231–235, 1971.
- [15] C. B. Voltattorni, A. Minelli, and P. Vecchini, "Purification and characterization of 3,4-dihydroxyphenylalanine decarboxylase from pig kidney," *European Journal of Biochemistry*, vol. 93, no. 1, pp. 181–187, 1979.
- [16] P. Dominici, B. Tancini, D. Barra, and C. B. Voltattorni, "Purification and characterization of rat-liver 3,4-dihydroxyphenylalanine decarboxylase," *European Journal of Biochemistry*, vol. 169, no. 1, pp. 209–213, 1987.
- [17] A. Fiori, C. Turano, and C. Borri Voltattorni, "Interaction of L DOPA decarboxylase with substrates. A spectrophotometric study," *FEBS Letters*, vol. 54, no. 2, pp. 122–125, 1975.
- [18] M. Bertoldi and C. Borri Voltattorni, "Reaction of dopa decarboxylase with L-aromatic amino acids under aerobic and anaerobic conditions," *Biochemical Journal*, vol. 352, no. 2, pp. 533–538, 2000.
- [19] M. Bertoldi, B. Cellini, B. Maras, and C. B. Voltattorni, "A quinonoid is an intermediate of oxidative deamination reaction catalyzed by Dopa decarboxylase," *FEBS Letters*, vol. 579, no. 23, pp. 5175–5180, 2005.
- [20] M. Bertoldi, B. Cellini, R. Montioli, and C. B. Voltattorni, "Insights into the mechanism of oxidative deamination catalyzed by DOPA decarboxylase," *Biochemistry*, vol. 47, no. 27, pp. 7187–7195, 2008.
- [21] M. Bertoldi, P. Frigeri, M. Paci, and C. B. Voltattorni, "Reaction specificity of native and nicked 3,4-dihydroxyphenylalanine decarboxylase," *Journal of Biological Chemistry*, vol. 274, no. 9, pp. 5514–5521, 1999.
- [22] M. Bertoldi, M. Gonsalvi, R. Contestabile, and C. B. Voltattorni, "Mutation of tyrosine 332 to phenylalanine converts dopa decarboxylase into a decarboxylation-dependent oxidative deaminase," *Journal of Biological Chemistry*, vol. 277, no. 39, pp. 36357–36362, 2002.
- [23] P. Dominici, P. S. Moore, S. Castellani, M. Bertoldi, and C. B. Voltattorni, "Mutation of cysteine III in Dopa decarboxylase leads to active site perturbation," *Protein Science*, vol. 6, no. 9, pp. 2007–2015, 1997.
- [24] P. S. Moore, P. Dominici, and C. Borri Voltattorni, "Cloning and expression of pig kidney dopa decarboxylase: comparison of the naturally occurring and recombinant enzymes," *Biochemical Journal*, vol. 315, no. 1, pp. 249–256, 1996.
- [25] H. Hayashi, H. Mizuguchi, and H. Kagamiyama, "Rat liver aromatic L-amino acid decarboxylase: spectroscopic and kinetic analysis of the coenzyme and reaction intermediates," *Biochemistry*, vol. 32, no. 3, pp. 812–818, 1993.
- [26] H. Hayashi, F. Tsukiyama, S. Ishii, H. Mizuguchi, and H. Kagamiyama, "Acid base chemistry of the reaction of aromatic L-amino acid decarboxylase and dopa analyzed by transient and steady-state kinetics: preferential binding of the substrate with its amino group unprotonated," *Biochemistry*, vol. 38, no. 47, pp. 15615–15622, 1999.
- [27] G. Giardina, R. Montioli, S. Gianni et al., "Open conformation of human DOPA decarboxylase reveals the mechanism of PLP addition to Group II decarboxylases," *Proceedings of the National Academy of Sciences of the United States of America*, vol. 108, no. 51, pp. 20514–20519, 2011.
- [28] P. Burkhard, P. Dominici, C. Borri-Voltattorni, J. N. Jansonius, and V. N. Malashkevich, "Structural insight into Parkinson's disease treatment from drug-inhibited DOPA decarboxylase," *Nature Structural Biology*, vol. 8, no. 11, pp. 963–967, 2001.
- [29] R. Singh, F. Spyraakis, P. Cozzini, A. Paiardini, S. Pascarella, and A. Mozzarelli, "Chemogenomics of pyridoxal 5'-phosphate dependent enzymes," *Journal of Enzyme Inhibition and Medicinal Chemistry*, vol. 28, no. 1, pp. 183–194, 2013.

- [30] A. Minelli, A. T. Charteris, C. B. Voltattorni, and R. A. John, "Reactions of DOPA (3,4-dihydroxyphenylalanine) decarboxylase with DOPA," *Biochemical Journal*, vol. 183, no. 2, pp. 361–368, 1979.
- [31] A. F. Sherald, J. C. Sparrow, and T. R. F. Wright, "A spectrophotometric assay for *Drosophila* dopa decarboxylase," *Analytical Biochemistry*, vol. 56, no. 1, pp. 300–305, 1973.
- [32] A. Charteris and R. John, "An investigation of the assay of dopamine using trinitrobenzenesulphonic acid," *Analytical Biochemistry*, vol. 66, no. 2, pp. 365–371, 1975.
- [33] C. M. Metzler, A. G. Harris, and D. E. Metzler, "Spectroscopic studies of quinonoid species from pyridoxal 5'-phosphate," *Biochemistry*, vol. 27, no. 13, pp. 4923–4933, 1988.
- [34] M. Bertoldi and C. B. Voltattorni, "Multiple roles of the active site lysine of Dopa decarboxylase," *Archives of Biochemistry and Biophysics*, vol. 488, no. 2, pp. 130–139, 2009.
- [35] B. Cellini, M. Bertoldi, R. Montioli, and C. B. Voltattorni, "Probing the role of Tyr 64 of *Treponema denticola* cystalysin by site-directed mutagenesis and kinetic studies," *Biochemistry*, vol. 44, no. 42, pp. 13970–13980, 2005.
- [36] G. A. Hunter, J. Zhang, and G. C. Ferreira, "Transient kinetic studies support refinements to the chemical and kinetic mechanisms of aminolevulinate synthase," *Journal of Biological Chemistry*, vol. 282, no. 32, pp. 23025–23035, 2007.
- [37] X. Zhou and M. D. Toney, "pH Studies on the mechanism of the pyridoxal phosphate-dependent dialkylglycine decarboxylase," *Biochemistry*, vol. 38, no. 1, pp. 311–320, 1999.
- [38] W. E. Karsten, T. Ohshiro, Y. Izumi, and P. F. Cook, "Initial velocity, spectral, and pH studies of the serine-glyoxylate aminotransferase from *Hyphomicrobium methylovorum*," *Archives of Biochemistry and Biophysics*, vol. 388, no. 2, pp. 267–275, 2001.
- [39] D. M. Kiick and P. F. Cook, "pH studies toward the elucidation of the auxiliary catalyst for pig heart aspartate aminotransferase," *Biochemistry*, vol. 22, no. 2, pp. 375–382, 1983.
- [40] K. O. Honikel and N. B. Madsen, "Comparison of the absorbance spectra and fluorescence behavior of phosphorylase b with that of model pyridoxal phosphate derivatives in various solvents," *Journal of Biological Chemistry*, vol. 247, no. 4, pp. 1057–1064, 1972.
- [41] M. T. Olmo, F. Sánchez-Jiménez, M. A. Medina, and H. Hayashi, "Spectroscopic analysis of recombinant rat histidine decarboxylase," *Journal of Biochemistry*, vol. 132, no. 3, pp. 433–439, 2002.
- [42] W. C. Chu and D. E. Metzler, "Enzymatically active truncated cat brain glutamate decarboxylase: expression, purification, and absorption spectrum," *Archives of Biochemistry and Biophysics*, vol. 313, no. 2, pp. 287–295, 1994.